The application of the passive sampling technique diffusive gradients in thin-films (DGT) to the measurement of uranium in natural waters.

Geraldine Sarah Clinton Turner

December 2013

The thesis is submitted in partial fulfilment of the requirements for the award of the degree of Doctor of Philosophy of the University of Portsmouth.

In collaboration with the Atomic Weapons Establishment (AWE)

Declaration:

Whilst registered as a candidate for the above degree, I have not been registered for any other research award. The results and conclusions embodied in this thesis are the work of the named candidate and have not been submitted for any other academic award.

Abstract

This thesis describes the application of a passive sampler, Diffusive Gradient in Thin Films (DGT), to the measurement of uranium in natural waters. Four resins (Chelex-100, manganese dioxide [MnO_2], Diphonix® and Metsorb™) were trialled with the DGT device. In freshwater environments, the Metsorb™ accumulated uranium in line with the DGT equation for 7 d with an acuracy of 75%; Chelex-100 did not accumulate uranium past 2 d; MnO_2 accumulated up to 75% of that predicted by the DGT equation for 4 d; and the Diphonix® accumulated uranium for 7 d with an accuracy of ~100%. None of the resins tested in this study accumulated uranium in a marine setting in line with DGT predicted values past 2 d.

The application of DGT to regulatory environmental monitoring schemes was investigated with Metsorb™. The Metsorb™ DGT devices were deployed for 7 days at a time over a 6 month period at two freshwater field sites. Fluctuations in water chemistry were monitored and the size of the diffusive boundary layer (DBL) was measured. The uranium accumulated by the Metsorb™ DGT showed close agreement with the grab samples. The size of the DBL was found to be significant, particularly in low flow conditions.

This study showed that DGT could be used as a tool to both monitor radioncludes in the environment, and to obtain information on the speciation and organic interactions. The lability of uranium-humic acid complexes was also examined in this study. Initial data shows that the uranyl-humic complex is labile in low pH environments, but becomes increasingly kinetically limited the higher the pH and the higher the humic acid:uranium ratio. Data is also presented on the penetration parameter of the uranyl ion into the resin gel layer, and how this can be used to indicate lability. Lability is important in determining bioavailability and potential toxicity of uranium.

Table of Contents

List of Figures

List of Tables

Abbreviations

ALARA	As low as is reasonably practicable
AWE	Atomic Weapons Establishment
BAT	Best available technologies
CRM	Certified reference material
DGT	Diffusive gradients in thin films
DOC	Dissolved organic carbon
EDTA	Ethylenediaminetetraacetic acid
EU	European Union
FA	Fulvc acid
HEDPA	1-hydroxyethylidene-1,1-diphosphonic acid
H_2O_2	Hydrogen peroxide
HA	Humic acid
HNO_3	Nitric acid
HCl	Hydrochloric acid
HS	Humic substances
ICP-MS	Inductively coupled plasma mass spectrometry
LoD	Limit of detection
MnO_2	Manganese dioxide
MQ	Milli-Q or ultrapure water
mz	Mass to charge ratio
NICA	Nica-Donnan Model
NaOH	Sodium hydroxide
NORM	Naturally occurring radioactive material
NTA	Nitrilotriacetic Acid
PAM	Polyacrylamide
RSD	Relative standard deviation

SHM	Stockholm Humic Acid Model
Sv	Sievert
TENORM	Technologically enhanced naturally occurring radioactive material
TiO_2	Titanium dioxide
TRU	Trans-uranic
U	Uranium
WHO	World Health Organisation

Units

α	alpha decay
β	beta decay
m	milli 1×10^{-3}
μ	micro 1×10^{-6}
n	nano 1×10^{-9}
p	pico 1×10^{-12}
f	femto 1×10^{-15}
a	atto 1×10^{-18}
ppm	parts per million
ppb	parts per billion
w/v	weight/volume
v/v	volume/volume
g	gram
kg	kilogram
ml	milli-litre
L	litre
cm	centimetre
m	metre

h	hour
d	day
y	year
M	mole
Bq	becquerel
dpm	disintegration per minute
^{o}C	degree Celsius

Acknowledgements

I would like to thank the supporting institutions, the University of Portsmouth and the Atomic Weapons Establishment, for funding this research, and my supervisors for their guidance throughout this process. I would like to thank Susan Atkins for her laboratory and practical support. I would also like to thank the Centre for Hydrology and Ecology (CEH), in particular Dr Mike Bowes and Dr Gareth Old, for providing this project with a freshwater field site (the River Lambourn) and for the water quality results; and the Wasings Estate Ltd. for access to the River Enborne; and the National Oceanography Centre for providing access to the marine field site.

I would like to thank Triskem International for the provision of the Diphonix® resin used in this study, and for the pre-filter material required to manufacture the MnO_2 resin. I would also like to acknowledge Graver Technologies Ltd for the provision of the Metsorb™ resin and to thank Pete Teasdale and Will Bennett at Griffiths University for sending the Metsorb™.

I would not have been able to complete this project if it were not for the moral support of my family, and in particular Andrew Bailey, who has been there for me and stuck by me through the weekends and late night working, and the emotional highs and lows.

Finally I would like to dedicate this work to my grandfather, Sidney Clinton-Abel, who sadly never saw the completion of this thesis.

'Tis all a Chequer-board of Nights and Days
Where Destiny with Men for Pieces plays:
Hither and thither moves, and mates, and slays,
And one by one back in the Closet lays.

Rubaiyat of Omar Khayyam, verse 49, translation by Edward FitzGerald.

Chapter 1: Introduction

1.1 Aims of the project

The aim of the project was to develop a robust passive sampler for the measurement of the actinides uranium (^{238}U, ^{235}U, ^{234}U), plutonium (^{238}Pu, $^{239+240}$Pu), thorium (^{232}Th, ^{230}Th) and americium (^{241}Am) in a number of natural waters ranging from surface waters to ground waters and marine environments. The project focused on uranium to ensure rigorous investigation of the diffusive gradients in thin films (DGT) applications to one actinide, with the potential of including the other listed actinides in futuer research. Uranium was chosen because of the complicated aqueous chemistry and because at the concentrations required for the experimental sections of this study, it could be handled in an un-supervised laboratory. Americium and plutonium require more rigorous laboratory controls due to higher specific activities than natural uranium, and thorium readily sorbs to most surfaces making laboratory method development and verification problematic.

It was necessary to test out various resins to combine with the DGT device that may be able to measure the dissolved or bioavailable fraction of uranium. As the research developed it became clear that dissolved and bioavailable could potentially have different meanings, and so work was undertaken to kinetically and mathematically establish the kinetic limitations and the contribution of partially labile fluxes of uranium to the DGT available fraction of the metal. Using this information, various radioisotopes of uranium were also measured using this technique in order to provide an indication of the contribution of anthropogenic uranium to a system against the natural uranium inputs.

This project was co-sponsored by the Atomic Weapons Establishment (AWE) who routinely undertake environmental monitoring of radionuclides.

1.2 Research training

As part of the doctoral training included in a Ph.D. the following courses were completed:

- Post-graduate research skills: passed with distinction. This module introduced important aspects of research such as abstract writing, proposal writing, health and safety in the laboratory, and literature searches and reviews.

- Graduate students professional development programme: units completed include teaching in large and small groups; demonstrating for graduate students; and effective feedback.

1.3 Dissemination of research

To date the research from this project has been presented at 14 national and international conferences. The platform presentation delivered on 14th April 2010 won second place at the Royal Society of Chemistry Radiochemistry Group Young Researchers Meeting.

Table 1.1 Table of conference contributions

Conference	Presentation type	Date	Title	Authors
Conference on DGT and the Environment (Lancaster, UK)	Platform	09/07/13-11/07/13	Evaluation of DGT as a long-term monitoring tool in natural waters using uranium as a case study	**Turner G.S.C.**, Fones, G.R.*, Mills G., Burnett J.L. and Amos S
6th International Passive Sampling Workshop and Symposium (Bordeaux, France).	Poster	26/06/13-29/06/13	Evaluation of DGT as a long-term monitoring tool in natural waters using uranium as a case study	**Turner G.S.C.**, Fones, G.R., Mills G.*, Burnett J.L. and Amos S
Society of Environmental Toxicology and Chemistry, UK: Royal Society of Chemistry Toxicology Group Joint Meeting Bioavailability: Linking complex Environmental Chemistry with Environmental Response	Platform	17/09/12-18/09/12	Evaluating the diffusive gradients in thin-films technique for the measurement of dissolved uranium in natural waters.	**Turner G.S.C.**, Fones, G.R., Mills G., Burnett J.L. and Amos S.
Coordinating Group on Environmental Radioactivity Annual Meeting (Portsmouth, UK).	Poster	02/04/12-04/04/12	Evaluating the passive sampling technique "Diffusive Gradients in Thin Films" for long term environmental monitoring of uranium in aquatic systems.	**Turner G.S.C.**, Fones, G.R., Mills G., Burnett J.L. and Amos S.
Challenger Society for Marine Science: Marine biogeochemistry: observations from near and far (Portsmouth, UK).	Poster	07/09/11-09/09/11	Evaluating the diffusive gradients in thin-films technique for the measurement of dissolved uranium in seawater.	**Turner G.S.C.**, Fones, G.R., Mills G., Burnett J.L. and Amos S.
Coordinating Group on Environmental Radioactivity Annual Meeting (Stirling, UK).	Platform	04/07/11-06/07/11	Evaluating the diffusive gradients in thin-films technique for the measurement of dissolved uranium in natural waters.	**Turner G.S.C.**, Fones, G.R., Mills G., Burnett J.L. and Amos S.
IPSW 2011 4th International Passive Sampling Workshop and Symposium (Krakow, Poland).	Platform	11/05/11-14/05/11	The application of passive sampler technology to the *in situ* measurement of uranium in natural waters.	**Turner G.S.C.**, Fones G.R., Mills G., Burnett J. and Amos S.
	Poster		Measuring silver in marine environments using Chemcatcher®.	**Turner G.S.C.**, Fones, G., Mills G., Burnett J.L. and Amos S.

Conference	Presentation type	Date	Title	Authors
AWE Materials Science Research Division poster session (Aldermaston, UK).	Poster	02/11/10	The *in situ* measurement of dissolved uranium in natural waters using Diffusive Gradient in Thin Films: initial results.	**Turner G.S.C.**, Fones G.R, Mills G., Burnett J.L. and Amos S.
Royal Society of Chemistry 11th International Symposium on Environmental Radiochemical Analysis (Chester, UK).	Poster	15/09/10-17/09/10	The *in situ* measurement of dissolved uranium in natural waters using Diffusive Gradient in Thin Films: initial results.	**Turner G.S.C.**, Fones G.R., Mills G., Burnett J.L. and Amos S.
Triskem Resin Users Meeting (Chester, UK).	Platform	14/09/10	Using passive samplers to measure dissolved uranium: choosing a receiving phase.	**Turner G.S.C.**, Fones, G.R., Mills G., Burnett J.L. and Amos S.
RSC Environmental Chemistry Group and the Environmental Mineralogy Group. Geochemical speciation & bioavailability of trace elements: progress, challenges & future trends (Lancaster, UK).	Poster	07/09/10-08/09/10	The *in situ* measurement of dissolved uranium in natural waters using Diffusive Gradient in Thin Films: initial results.	**Turner G.S.C.**, Fones, G.R., Mills G., Burnett J.L. and Amos S.
Challenger: The 14th Biennial Challenger Conference for Marine Science (Southampton, UK).	Platform	06/09/10-06/09/10	The use of Chemcatcher® to measure silver in marine environments.	**Turner G.S.C.**, Fones, G.R.*, Burnett J.L. and Amos S.
Royal Society of Chemistry Radiochemistry Group Young Researchers Meeting (London, UK).	Platform	14/04/10	The application of passive sampler technology for the *in-situ* measurement of actinides in natural waters.	**Turner G.S.C.**, Fones, G.R., Mills G., Burnett J.L. and Amos S.
Coordinating Group on Environmental Radioactivity Annual Meeting (Lancaster, UK).	Platform	29/03/10–31/03/10	The application of passive sampler technology for the *in-situ* measurement of actinides in natural waters.	**Turner G.S.C.**, Fones, G.R., Mills G., Burnett J.L. and Amos S.

* denotes s different presenter

One paper has been published using results presented in Chapter 4 in this thesis:

Turner G.S.C., Fones G.R., Mills G.A., Teasdale P., Burnett J.L., Amos S. (2012) Evaluation of DGT technique for measuring inorganic uranium species in natural waters: Interferences, deployment time and speciation. *Analytica Chimica Acta* 739, 37-46.

One further paper has been accepted using the results presented in Chapter 5 and submitted to 'Environmental Science: Impacts and Processes':

Turner G.S.C., Fones G.R., Mills G.A., Teasdale P., Burnett J.L., Amos S. (2013) Evaluation of DGT as a long-term monitoring tool in natural waters using uranium as a case study.

Two further publications are planned from this project:

Monitoring actinides in natural waters (Chapter 2), to be submitted to 'Trends in Analytical Chemistry'.

Evaluation of the sorbent Diphonix® with DGT for measuring dissolved uranium in natural waters (Chapter 6), to be submitted to 'Analytica Chimica Acta'.

1.4 Organisation of thesis

Due to the publications arising from the thesis, each chapter is treated as a discrete body of work, each organised using a paper template (introduction, materials and methods, results and discussion, conclusions).

Chapter 2: Monitoring actinides in natural waters

2.1 Introduction

The open testing of nuclear weapons testing has introduced approximately 2 x 10^{20} Bq of radioactivity into the environment. Other sources such as accidental releases from nuclear reactors contribute only about 0.3% of this figure [1, 2]. Environmental monitoring of aqueous systems for the presence of radionuclides is a regulatory requirement imposed on all nuclear facilities in the UK by the 'Environmental Permitting (England and Wales) Regulations (2010)' (formerly the Environment Agency Radioactive Substances Act 1993) [3]. Actinides lie in the periodic table between atomic numbers 89 (actinium) and 104 (rutherfordium). The most commonly occurring natural and anthropogenic actinides are americium (Am), plutonium (Pu), thorium (Th), and uranium (U), for which a number of sophisticated extraction procedures and instrumental analytical techniques have been developed for their measurement in a range of environmental samples, including natural waters. Monitoring of actinides in the aquatic environment is challenging because they have a complex chemistry and speciation pattern, in part due to their wide range of oxidation states [5]. The species of the metal present in the environment is important in determining its bioavailability and potential toxicity. In addition actinides can form complexes with other ligands (e.g. carbonates, phosphates, humic substances) that are also present in natural waters [6]. The formation of these complexes is dependent on the oxidation state of the element and pH of the water [1, 6, 7]. These factors also control their solubility and mobility in the environment. All these different factors have to be taken into account when developing quantitative monitoring strategies for these elements. Historically, these monitoring techniques have relied on taking discrete, high volume, bottle or spot samples of water for subsequent analysis using methods such as alpha spectrometry [8] or mass spectrometry. More recently, there has been interest in using alternative *in situ* methods such as bio-monitors, passive samplers and sensors.

This chapter reviews the sources, environmental chemistry and concentrations of actinides in natural waters, methods for their extraction, instrumental analysis and finally the different sampling strategies that are currently used. This is linked to the aims and objectives of this project, which explores the application of passive sampling for environmental monitoring of U in natural waters. This review will show that U is the largest natural contributor to activity and concentrations of actinides in the aquatic environment and therefore not only important to monitor, but important to distinguish

from anthropogenic activity, so a true representation of any source of pollution is achieved and naturally occurring contributions are identified separately.

2.2 Regulatory monitoring and aqueous discharge limits

It is important to understand current regulatory monitoring requirements in order to ensure any sampling methods or strategies are capable of satisfying these. Regulatory monitoring in the UK requires that waste producers continually monitor aqueous discharges, and seek to apply 'best available technology' (BAT) principles [9] in order to ensure that radiological risks are 'as low as is reasonably practicable' (ALARA). BAT also includes economic feasibility in assessments and the cost/benefit of a particular technology i.e. diminishing returns with increasing costs. The UK's Environment Agency uses the application of BAT in the consideration and review of permits; for instance, the Atomic Weapons Establishment's (AWE) environmental permit issued by the Environment Agency under the Environmental Permitting Regulation (2010) [10] requires samples to be taken, measurements, test, surveys, analyses and calculations to be conducted, and that BAT principles be applied to all these monitoring facets [10].

Each discharger of nuclear materials has a unique aqueous discharge authorisation calculated from dose pathways and annual doses to critical groups, historical discharges, current site use and risk to human health. The Environment Agency, when setting discharge limits, accounts for maximum doses to the pubic of no more than 0.3 mSv y^{-1} from any source from which radioactive discharges are made, or 0.5 mSv y^{-1} from the discharges from any single site [11]. AWE's environmental permit [10] allows the aqueous discharges from the site to the public sewers, with an annual limit of 10 MBq of total alpha activity (with the quarterly notification level set at 2 MBq) and an annual limit of 20 MBq of total beta activity (with quarterly notification levels set to 4 MBq). This is in contrast to the Sellafield site, which has different environmental pathways and exposure routes. The annual alpha aqueous discharge limit to the sea from Sellafield is 1000 GBq per annum, and beta gamma is 225 000 GBq per annum. A report [12] detailing BAT at Sellafield recommends a maximum dose to the critical group of no more than 20 μSv y^{-1}, in line with the objective of the UK's Discharge Strategy (which is less than the maximum of 0.5 mSv y^{-1} used by the Environment Agency). The report also recommends that for surface, marine and drinking water, there is a requirement to understand and monitor the behaviour of radionuclides through quarterly to annual spot monitoring, and to continuously monitor

these environments in order to detect abnormal or unauthorised releases. It is therefore important to understand the contributing radionuclides to the total activities in order to understand if the radioactivity is from naturally occurring radioactive materials (NORM) or is of anthropogenic origin. This is also important in instances where activity limits may be breached, particularly where NORM activities are the principle contributors to the regulatory breach. The radionuclides that Sellafield is permitted to releases to the aqueous environment (the Ribble Estuary) include the isotopes ^{230}Th, ^{232}Th, ^{237}Np, U (total, 238, 235 and 234) and transuranic radionuclides [13]. Current monitoring around the Sellafield site has shown that environmental concentrations are responsive to on-site activities. For instance discharges of U into the Ribble Estuary increased in 2012 due to an increase in processing of legacy uranic residues, while ^{234}Th discharges decreased following an end to the Uranium Ore Concentrate purification process [13]. The Sellafield nuclear site is not solely responsible for discharges of radionuclides in the local marine environment, thereby making it important to distinguish the origin of the pollution via isotopic fingerprinting. A previous incident near Whitehaven, Cumbria involved the discharge of liquid slurry containing Th and U into the Irish Sea from a phosphate plant. Localised monitoring detected an increase in Technologically Enhanced Naturally Occurring Radioactive Materials (TENORM), with levels 10 years later still slightly elevated above background levels [13].

The importance of regulatory monitoring of radioactivity and the actinides is also highlighted within the EU. Under article 35 of the Euratom Treaty all EU Member states must monitor levels of radioactivity in the air, water and soil. The main industries within the EU that are required to monitor for environmental radioactivity under article 35 are:

1. Reprocessing plants
2. Mining, milling etc. of U and Th
3. Enrichment of U
4. Fabrication of nuclear fuel
5. Nuclear power stations
6. Large research establishments (including research reactors)
7. Industrial processing, including radiopharmaceuticals
8. Radioactive waste facilities
9. Facilities processing natural radioactive materials
10. Medical facilities
11. Small research establishments
12. Industries producing Th compounds
13. Thermal phosphorus production
14. Producers of phosphorus fertilizers
15. Producers of phosphoric acid
16. Oil and gas industries.
17. Defence

Article 35 also states that the materials that are most likely to incorporate radionuclides from NORM industries are fly ash, phosphogypsum, and phosphorus slag. The largest contributors to aqueous discharges of radionuclides in the UK are likely to be defence, nuclear fuel production and reprocessing, research establishments, radiochemical production and waste disposal.

Environmental monitoring of actinide concentrations is equally as important as radioactivity monitoring because of the hazards the contaminants pose to human health. The only actinide to have a drinking water limit [14] assigned by the World Health Organisation (WHO) was U, which was designated 30 μg L^{-1}, based upon the renal toxicity of U. U in drinking water varies between geographical areas, and is a factor of the underlying bedrock type, and local anthropogenic activities that may affect U concentrations. For instance in a study of 130 sites supplying drinking water in Ontario, Canada, the average U concentration was 0.4 μg L^{-1} with a range of 0.05 – 4.21 μg L^{-1} [14]. There are also incidences where U has been detected in private drinking water supplies at concentrations up to 700 μg L^{-1} [14]. A study of drinking water by Bacquart *et al*. [15] also found that Th was detectable in some drinking water supplies. Th does not have a WHO drinking water limit and could therefore pose a risk to human health as it is not monitored.

The determination of actinides in surface waters is important, as surface waters not only provide a source of drinking water, but are also involved in food supply (i.e. fishing), and are used for irrigation and leisure. The WHO sets out drinking water limits (activities) for pollutants in its 'Guidelines for drinking water' [16]. A recommended monitoring scheme is shown in Figure 2.1. Where gross alpha (α) and beta (β) activities are found to exceed a threshold activity of > 0.5 Bq L^{-1} gross α or > 1 Bq L^{-1} gross β, further radiochemical analysis is required to determine the source (natural or anthropogenic) of the elevated activity [16]. Table 2.1 below lists some of the WHO drinking water limits (Bq L^{-1}) for radionuclides [16]. These have been converted to μg L^{-1} using $A=N\lambda$ (where A is activity (Bq), N is the number of atoms (which can be converted to Moles using Avogadro's number) and λ is the decay constant unique to each radionuclide ($Ln(2)/t_{½}$)), so that the results from this study can be compared to a benchmark concentration. This benchmark helps to determine the usefulness of the technique for regulatory monitoring of radionuclides in the aquatic environment.

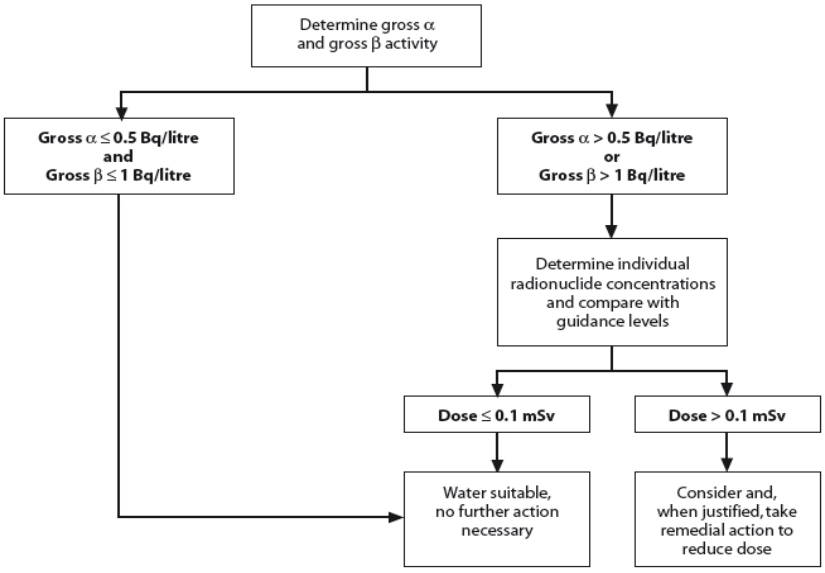

Figure 2.1 World Health Organisation recommended radiological screening of drinking water [16].

Table 2.1 World Health Organisation drinking water limits on selected actinides [16].

Radionuclides	**Drinking water limit**	
	Bq L^{-1}	**µg L^{-1}**
^{227}Th	10	8.75 x10^{-9}
^{228}Th	1	3.29 x 10^{-8}
^{229}Th	0.1	1.26 x 10^{-5}
^{230}Th	1	1.31 x 10^{-2}
^{231}Th	1000	5.08 x 10^{-8}
^{232}Th	1	2.47 x 10^{2}
^{234}Th	100	1.17 x 10^{-7}
^{231}Pa	0.1	5.72 x 10^{-4}
^{233}Pa	100	1.30 x 10^{-7}
^{233}U	1	2.80 x 10^{-3}
^{234}U	1	4.35 x 10^{-3}
^{235}U	1	1.25x 10^{1}
^{236}U	1	4.18 x 10^{-1}
^{238}U*	10	8.04 x 10^{2}
^{237}Np	1	3.83 x 10^{-2}
^{239}Np	100	1.17 x 10^{-8}
^{236}Pu	1	4.57 x 10^{-8}
^{238}Pu	1	1.58 x 10^{-6}
^{239}Pu	1	4.35 x 10^{-4}
^{240}Pu	1	1.19 x 10^{-4}
^{241}Pu	10	2.62 x 10^{-6}
^{242}Pu	1	6.86 x 10^{-3}
^{244}Pu	1	1.49
^{241}Am	1	7.89 x 10^{-6}
^{243}Am	1	1.36 x 10^{-4}
^{242}Cm	10	8.16 x 10^{-8}
^{243}Cm	1	5.33 x 10^{-7}
^{244}Cm	1	3.32 x 10^{-7}
^{245}Cm	1	1.57 x 10^{-4}
^{246}Cm	1	8.74 x 10^{-5}

Radionuclides	Drinking water limit	
	Bq L^{-1}	µg L^{-1}
^{247}Cm	1	2.99×10^{-1}
^{248}Cm	0.1	6.37×10^{-7}
^{249}Bk	100	1.58×10^{-6}
^{248}Cf	10	1.71×10^{-7}
^{249}Cf	1	6.61×10^{-6}
^{250}Cf	1	2.48×10^{-7}
^{251}Cf	1	1.67×10^{-5}
^{252}Cf	1	5.03×10^{-8}
^{253}Es	10	1.07×10^{-8}
^{254}Es	10	1.45×10^{-7}

*The drinking water limit for uranium is set at 30 µg L^{-1} due to renal toxicity.

2.3 The actinides

2.3.1 Sources and distributions of the actinides

The source of the actinide is important as they are not often in thermodynamic equilibrium upon entering the environment [1]. This affects the solubility and speciation in aquatic systems; for instance actinides formed in high temperature nuclear explosions are highly refractory [17] and therefore chemically inert and are not incorporated into bottom sediments of lakes, rivers or oceans [18]. The toxicity of highly refractory radionuclides is therefore dominated by their radiological properties due to decreased bioavailability. Table 2.2 details the source of the actinides. It can be seen that the transuranic elements are artificial. Elements such as mendelevium (Md), nobelium (No) and lawrencium (Lr) are formed in reactors and have not been released into the environment. Berkelium (Bk), californium (Cf), einsteinium (Es) and fermium (Fm) are also of little environmental concern due to very low environmental levels, most of which were released into the environment during atmospheric weapons testing, which ceased in 1980. They have short half lives and are generally very particle reactive quickly becoming incorporated into sediments thereby further reducing their dissolved concentrations. Curium (Cm) is a produced through transmutation reactions in U ores and successive neutron capture and beta decays from U and Pu in nuclear fuel and nuclear explosions, but is not considered to be of concern in the aquatic environment as it occurs in very low concentrations. Curium oxide is the most common form in the environment. Cm is typically quite insoluble and adheres very tightly to soil particles; the concentration of Cm in sandy soil particles is estimated to be about 4,000 times higher than in interstitial water (in pore spaces between soil particles), and it binds even more tightly to loam soil where concentration ratios are even higher (18,000) [19, 20]. Atmospheric testing of nuclear weapons would have also generated a small amount of environmental Cf; but fallout levels are extremely low. Cf is typically quite insoluble

and adheres well to soil, with the concentration in soil particles estimated to be about 500 times higher than in interstitial water [19]. It is for this reason (particle affinity) and low environmental discharges that there is a paucity of dissolved concentrations of Cm and Cf in the open literature.

Actinides heavier than Cf are formed through bombardment predominantly in particle accelerators and are therefore not discharged to the environment. There are no reviews on the environmental behaviour of these elements as they are of little concern at present. For these reasons the actinide elements actinium (Ac) to Am have been the focus when examining aquatic environmental distributions, seen in Table 2.3.

The most abundant actinide that occurs in the dissolved form in the environment is U. Uranium can enter aquatic systems through erosion and weathering of bedrock containing naturally occurring U (such as granites) [14], or through anthropogenic activities. The most common use for U is as a fuel in nuclear power stations, however much of the U is well contained in these establishments with very little environmental contamination as a result of accidental or planned discharges. Other sources of U into the environment are through diffuse sources such as deposition during the combustion of fossil fuels and the application of contaminated fertilisers, or more localised inputs into the environment such as mine tailings [14].

U is a known contaminant in phosphate fertilisers and has been shown to be a contaminant through surface run off of top soils treated with phosphatic fertilisers. Up to 95% of the World's total phosphate rock production is used in agriculture (fertilisers, pesticides and animal feeds) [21]. This diffuse source of U can lead to increases in U concentrations in local rivers, for instance in a review by Spalding and Sackett [22], U runoff due to the application of phosphate fertilisers was attributed to the increased concentrations of U in North American rivers by ~0.7-0.9 ug L^{-1} [14]. In New Zealand top soils, Taylor [23] found an increase of U by 0.033 ± 0.008 µg g^{-1} y^{-1} most likely as a result of the application of phosphate fertilizers.

Th is another naturally occurring radionuclide, but due to the very low solubility of ThO_2, it exists in soluble form in very low concentrations in aqueous environments. It is however, very particle reactive and is used extensively in the study of vertical and horizontal transport, particle cycling and sediment dynamics [24].

There have been numerous studies of Pu in the marine environment, due to increased inventories as a result of atmospheric testing of nuclear weapons. Pu is mainly associated with particulates and sediments, however, in areas which were directly affected by nuclear weapons testing, such as in Pacific Atoll sediments, it has been

shown that the Pu is continuously mobilised from the sediment into the water column and so providing a continual source [25]. Figure 2.2 below shows the inventory of $^{239+240}$Pu in oceans across the world. It can be seen that high contamination levels are localised around areas with higher and more continual discharges, such as the Irish Sea. The sites of historic contamination, such as in the Equatorial and South Pacific regions have some of the lowest water column Pu activities on average most likely due to particle reactivity and subsequent settling.

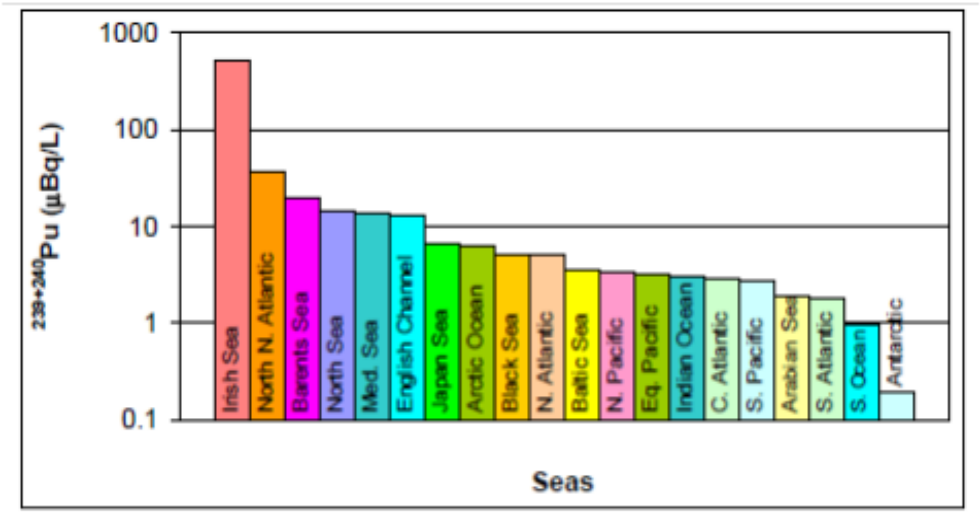

Figure 2.2 $^{239+240}$Pu activities (µBq L^{-1}) in marine environments across the world (taken from [25]).

Am levels in the marine environment are of growing concern as it is a decay product of Pu, however, in oxic waters, Am exits in the 3+ state which is even more particle reactive than Pu. This may however present an increasing risk to filter feeders and sediment dwelling organisms, resulting in bioaccumulation through the food chain.

Table 2.3 shows a selection of environmental distributions of the actinides Ac to Am (the actinides previously identified as being more environmentally important). What can be seen is that most studies are focused on the sediment accumulation of the actinides (due to their particle reactivity) or oceanic concentrations (where due to higher pH and carbonates, some of the actinides display a higher solubility). There is a paucity of data existing on dissolved (of primary importance for passive sampling) actinide concentrations in freshwater streams. As can be seen in this table, environmental concentrations vary dependent upon the location. For instance, freshwater concentrations of U are as low as 0.1 µg L^{-1} in typical freshwater streams, but if the stream is in a granitic area such as the Brahmaputra River system, India, the dissolved

concentrations can reach 8 μg L^{-1}. This is similar for Pu concentrations which in the open ocean are approximately 2.5 x 10^{-5} μg L^{-1}, but in the Irish Sea are 1.6 x 10^{-3} μg L^{-1}.

Table 2.2 Sources and formation of the actinides and the most commonly occurring isotopes.

Actinide	Isotopes	Half life	Predominant decay mode[1]	Specific activity (Bq g^{-1}) [2]	Origin or formation	Ref.
Actinium (Ac)	225	10 d	α	2.15×10^{15}	• Naturally occurring in the ^{232}Th and ^{235}U decay chains. • ^{227}Ac is in secular equilibrium with ^{231}Pa in the environment.	[20, 26]
	227*	21.7 y	β^-	2.69×10^{12}		
	228*	6.5 h	β^-	7.82×10^{16}		
Thorium (Th)	227*	0.051 y	α	1.14×10^{15}	• ^{232}Th is a primordial isotope. • Th is naturally abundant in the Earth's crust at 10^4 to 1.2×10^4 µg kg^{-1}, with the principle ore monazite sand, found in India, Brazil, Ceylion, former Soviet Union and USA. • The Oceanic abundance is ~ 6×10^{-4} µg L^{-1}. • ^{227}Th is in the ^{235}U decay chain. • ^{228}Th is in the ^{232}Th decay chain. • ^{229}Th is in the ^{232}Th decay series after neutron irradiation of ^{232}Th to form ^{233}Th: $^{232}_{90}Th(n,\gamma)^{233}_{90}Th \xrightarrow{\beta^-} {}^{233}_{91}Pa \xrightarrow{\beta^-} {}^{233}_{92}U \xrightarrow{\alpha} {}^{229}_{90}Th$ • ^{231}Th is in the ^{235}U decay series. • ^{230}Th and ^{234}Th are in the ^{238}U decay chain.	[19, 20, 26-28]
	228*	1.91 y	α	3.04×10^{13}		
	229	7.3×10^3 y	α	7.91×10^9		
	230	75.4 ky	α	7.63×10^8		
	231*	25.5 h	β^-	1.97×10^{16}		
	232*	1.41×10^{10} y	α	4.04×10^3		
	234*	24.1 d	β^-	8.57×10^{14}		
Protactinium (Pa)	231*	32.76 ky	α	1.75×10^9	• ^{234}Pa is in the ^{238}U decay series. • ^{231} Pa is in the ^{235}U decay series. • ^{233}Pa is in the ^{232}Th decay series (see ^{225}Ac formation above) and is an intermediate product in thorium reactors: $^{232}_{90}Th + {}^{1}_{0}n \rightarrow {}^{232}_{90}Th \xrightarrow{\beta^-} {}^{233}_{91}Pa \xrightarrow{\beta^-} {}^{233}_{92}U$	[19, 20, 28, 29]
	233	27 d	β^-	7.68×10^{14}		
	234*	6.75 h	β^-	7.34×10^{16}		

Actinide	Isotopes	Half life	Predominant decay mode[1]	Specific activity (Bq g^{-1}) [2]	Origin or formation	Ref.
Uranuim (U)	233 234* 235* 236 238*	1.59 x 10^5 y 2.46 x 10^5 y 7.04 x 10^8 y 2.34 x 10^7 y 4.47 x 10^9 y	α α α α α	3.57 x 10^8 2.30 x 10^8 8.00 x 10^4 2.40 x 10^6 1.24 x 10^4	• U is naturally occurring and the most abundant isotopes are ^{234}U, ^{235}U and ^{238}U, comprising 2.3 mg kg^{-1} of the earth's crust. Natural isotopic composition is 0.0054, 0.72 and 99.28 atom percent for ^{234}U, ^{235}U and ^{238}U respectively. The $^{235/238}$U ratio is constant in natural environments, but the $^{234/238}$U ratio can vary in for instance groundwater. The most abundant U ores are uraninate (UO_2) or pitchblend (U_3O_8) and carnotite ($K_2(UO_2)_2(VO_4)_2.3H_2O$), although there are approximately 200 U minerals in total. • ^{233}U can be produced via neutron irradiation of ^{232}Th in reactors ($^{232}_{90}Th(n,\gamma)^{233}_{90}Th \xrightarrow{\beta^-} {}^{233}_{91}Pa \xrightarrow{\beta^-} {}^{233}_{92}U$). ^{233}U is an important isotope because like ^{235}U, it is fissile. • ^{234}U is in secular equilibrium with ^{238}U in the environment: • ^{236}U forms as a result of bombardment if ^{235}U with fast neutrons in nuclear weapon reactions: $^{235}_{92}U(n,3n)^{236}_{92}U$	[19, 28]
Neptunium (Np)	237 239	2.14 x 10^6 y 2.356 d	α β^-	2.61 x 10^7 8.58 x 10^5	• Bombardment of $^{238}_{92}U$ with $^{1}_{0}n$: $(^{238}_{92}U(n,\gamma)^{239}_{92}U \xrightarrow{\beta^-} {}^{239}_{93}Np)$ $(^{238}_{92}U(n,2n)^{237}_{92}U \xrightarrow{\beta^-} {}^{237}_{93}Np)$ • Transmutation in uranium ores: $(^{235}_{92}U(n,\gamma)^{236}_{92}U(n,\gamma)^{237}_{92}U \xrightarrow{\beta^-} {}^{237}_{93}Np)$ • Alpha decay of ^{241}Am from ^{241}Pu decay: $(^{241}_{94}Pu \xrightarrow{\beta^-} {}^{241}_{95}Am \xrightarrow{\alpha} {}^{237}_{93}Np)$. • The main source of Np in the environment is the nuclear industry, and historically atmospheric testing of nuclear weapons (~2500 kg released).	[19, 20, 26, 30]
Plutonium (Pu)	236 238 239* 240 241 242 244	2.56 y 87.7 y 2.41 x 10^4 y 6.561 x 10^3 y 14.4 y 3.75 x 10^5 y 8.08 x 10^7 y	α α α α β^- α α	2.19 x 10^{13} 6.34 x 10^{11} 2.30 x 10^9 8.40 x 10^9 3.81 x 10^{12} 1.46 x 10^8 6.71 x 10^5	• ^{239}Pu formed through neutron capture by $^{238}_{92}U$and ^{240}Pu, ^{241}Pu and ^{242}Pu then results from subsequent beta decays ($^{238}_{92}U(n,\gamma)^{239}_{92}U \xrightarrow{\beta^-} {}^{239}_{93}Np \xrightarrow{\beta^-} {}^{239}_{94}Pu$). • Naturally occurring in small quantities dues to neutron capture by U in natural decay chains. • Anthropogenic inputs are as a bi-product of nuclear weapons, nuclear power and reprocessing plants. • Approximately 3500 kg of Pu was released into the environment from atmospheric weapons tests, and approximately 1000 kg by subsurface tests.	[2, 20, 26, 31, 32]

Actinide	Isotopes	Half life	Predominant decay mode[1]	Specific activity (Bq g^{-1}) [2]	Origin or formation	Ref.
Americium (Am)	241	433 y	α	1.27×10^{11}	• Biproduct of nuclear weapons explosion and nuclear reactions from nuclear power and reprocessing plants. Am, totalling about 95 kg is present from the decay of Pu and bombardment of $^{239}_{94}Pu$ with $^{1}_{0}n$. • Because of the decay of ^{241}Pu, the amount of ^{241}Am in the environment is increasing and will continue to do so over the next few decades	[19, 31-34]
	243	7.38×10^3 y	α	7.38×10^9		
Curium (Cm)	242	163 d	α	1.22×10^{14}	• Bombardment of $^{239}_{94}$Pu with $^{4}_{2}$He. • Transmutation reactions in U ores • Successive neutron captures and beta decays from U and Pu in nuclear fuel and nuclear explosions • ^{244}Cm and ^{242}Cm not an environmental concern due to very short half lives. • Atmospheric testing of nuclear weapons, which ceased worldwide by 1980, generated most environmental curium. Accidents and other releases from weapons production facilities have caused localised contamination.	[19, 20]
	243	29 y	α	1.88×10^{12}		
	244	18 y	α	3.01×10^{12}		
	245	8.5 ky	α	6.35×10^9		
	246	4.7 ky	α	1.14×10^{10}		
	247	16 my	α	3.35×10^6		
	248	340 ky	α	1.57×10^8		
	250	6.9 ky	α β^-	7.67×10^9		
Berkelium (Bk)	247	1.38 k y	α	3.88×10^{10}	• Bombardment of $^{241}_{95}$Am with $^{4}_{2}$He. • Transmutation reactions in uranium ores	[19]
	249	320 d	β-	6.06×10^{13}		
	250	3.212 h		1.44×10^{17}		
Californium (Cf)	248	0.91 y	α	5.86×10^{13}	• Bombardment of $^{242}_{96}$Cm with $^{4}_{2}$He. • Transmutation reactions in uranium ores	[19]
	249	351 y	α	1.51×10^{11}		
	250	13.1 y	α	4.04×10^{12}		
	251	878 y	α	6.00×10^{10}		
	252	2.64 y	α	1.99×10^{13}		
Einsteinium (Es)	252	472 d	α	4.06×10^{13}	• Neutron bombardment and capture by a heavy element followed by β particle emission. • Found in debris of first thermonuclear explosion in 1952. • Synthetic	[19]
	253	20.47 d	α	9.33×10^{14}		
	254	276 d	α	6.89×10^{13}		
	255	39.8 d	β^-	4.76×10^{14}		
Fermium (Fm)	257	100.5 d	α	1.87×10^{14}	• Neutron bombardment and capture by a heavy element followed by β particle emission. • Found in debris of first thermonuclear explosion in 1952. • Synthetic	[19]
Mendelevium (Md)	258	56 d	α	3.34×10^{14}	• Bombardment of $^{253}_{99}Es$ with $^{4}_{2}He$. • Synthetic	[19]

Actinide	Isotopes	Half life	Predominant decay mode[1]	Specific activity (Bq g^{-1}) [2]	Origin or formation	Ref.
Nobelium (No)	259	1 h	α EC	4.48 x 10^{17}	• Bombardment of $^{243}_{95}Am$ with $^{15}_{7}N$. • Synthetic	[19]
Lawrencium (Lr)	262	3.6 h	α	1.23 x 10^{17}	• Bombardment of mixed isotopes of $^{251}_{98}Cf$ with $^{10}_{5}B$, $^{11}_{5}B$, and of $^{243}_{95}Am$, $^{18}_{8}O$ • Synthetic	[19]

*Naturally occurring radioisotopes

[1]Radioactive decay mechanisms listed are α: ejection of $^{4}_{2}He$ from the nucleus; β^-: a neutron is converterd to a proton and an electron, the electron (plus an anti-neutrino) is ejected from the nucleus; EC (electron capture): capture of an inner core electron by the nucleus; SF: spontaneous fission.

[2]specific activity calculated using: $(Ln(2) \times N_A)/(t_{1/2} \times M_R)$ where is N_A Avogadro's number, $t_{1/2}$ is the radionuclide half life (s) and M_R is the molecular mass of the radionuclide.

Table 2.3 Examples of aquatic environmental concentrations of environmentally relevant actinides (this is not an exhaustive list but an indication of the magnitude of reported values).

Actinide	**Environment**		
	Marine and estuarine (dissolved concentrations, µg L^{-1})	**Freshwater (dissolved concentrations, µg L^{-1})**	**Sediment & groundwater (µg kg^{-1})**
Actinium (Ac)[1]	• Pacific Ocean: up to 0.02 x 10^{-9} close to sea floor (none in upper ocean) [35]. • Near-shore marine end-members range from 2.5 x 10^{-12} at the Gulf of Mexico to 0.02 x10^{-9} in the coastal waters of the Korean Strait [36]. • Gulf of Aquaba 0 – 0.06 x 10^{-9} [36], 0.6 x 10^{-12} in shallow open ocean and 0.6-9.3 x 10^{-12} in coastal waters [36]. • A North Sea Estuary had measurable concentrations up to 0.03 x 10^{-9} [36].	• Korean Straight fluvial input is ~0.035 x 10^{-9} [36].	• ^{227}Ac is in secular equilibrium with ^{231}Pa in marine sediments [37, 38] so the latter (the progenitor) is frequently used in ^{227}Ac concentration calculations. • Naturally occurring in pitchblend up to 1.7 pg [39]. • ^{227}Ac found in an equatorial Pacific sediment core 2.9 –8.5 x 10^{-6} [37].
Thorium (Th)	• Atlantic 3 – 3.5 ^{234}Th [40]. • 10 – 12 µg L^{-1} in surface Atlantic, 6 – 10 at depth (<600m) in Atlantic ^{232}Th [40]. • Southern Ocean > 250 m 19.6 x 10^{-12}[41]. • 1 x 10^{-6} deep pelagic average [42].	• European rivers average: 0.025 with the median value as 0.009[43]	• Ribble Estuary sediments: ^{228}Th 0.8 x 10^{-6}, ^{230}Th 39 x 10^{-3}, ^{232}Th 6 x 10^{3}, ^{234}Th 76 x 10^{-6} [44]. • Black Sea Bottom sediments: ^{232}Th 0.5 x 10^{3}, ^{230}Th 23 x 10^{-3}, ^{228}Th 0.69 x 10^{-6}, ^{227}Th 11 x 10^{-9} [45]. • General marine sediment concentrations: ^{232}Th 7.4 x 10^{-3}, ^{230}Th 48 x 10^{-3}, ^{228}Th 0.9 x 10^{-6} [46].
Protactinium (Pa)	1.17 x 10^{-8} (deep pelagic) [42]. 3.2 (ocean margin) [42].		• Abundant in deep sea sediments [36].
Uranuim (U)	• Total U ~3 [47]. • Atlantic ocean total U, 2-3.5 [40] • ^{238}U, Tampa Bay, Florida 2.38 [48].	• ^{238}U, Alafia River Florida, 1.96 [48]. • ^{238}U, Brahmaputra River system, India, 0.44 – 8.32 [49]	• Ribble Estuary, UK sediments: ^{238}U 1.6 x 10^{-3}, ^{234}U 0.1 [44]. • Black Sea Bottom sediments: ^{238}U 0.8 x 10^{-3}, ^{235}U 6.2, ^{234}U 43 x 10^{-3} [45]. • General marine sediment concentrations: ^{238}U 1.7

[1] ^{227}Ac only examined here because the half life of ^{228}Ac is only 6.5h, therefore environmental levels are very low.

Actinide	Environment		
	Marine and estuarine (dissolved concentrations, µg L^{-1})	**Freshwater (dissolved concentrations, µg L^{-1})**	**Sediment & groundwater (µg kg^{-1})**
			mg kg^{-1}, ^{235}U 0.3 x 10^{-3}[46]. • Sarzhal Wells, Kazakhstan: ^{234}U 9.3, ^{235}U 81 x 10^{-3}, ^{234}U 1.2 x 10^{-3}[50]. • Ocean margin sediment 2 x 10^{3} [42]
Neptunium (Np)	Has been of little interest in the environment due to its very low concentrations until recently. Planned future thorium reactors may have potential to release this radionuclide into the environment in greater quantities. Environmental concentrations thought to < 1 % Pu concentrations [51].		• Arctic marine sediments: 0.54 to 80.3 x 10^{-6} [52]
Plutonium (Pu)	• Open ocean 2.5 x 10^{-5} [1]. • Pacific surface water: $^{239/240}Pu$ 1.4 – 7.8 x 10^{-10}[5]. • Irish sea 4 x 10^{-4} – 1.6 x 10^{-3} [5].		• Ribble Estuary sediments: $^{239,240}Pu$ 32 x $10^{-3}$and ^{238}Pu 40 x 10^{-6}[44] • Black Sea Bottom sediments: ^{38}Pu 47 x 10^{-9}, $^{239+240}$ Pu 0.1 x 10^{-3}, ^{241}Pu 0.9 x 10^{-6}[45] • Arctic marine sediments:^{238}Pu x 10^{-9}, $^{239+240}Pu$ up to 0.2 x 10^{-3} [52]. • Sarzhal Wells, Kazakhstan: ^{238}Pu 1.3 x 10^{-9}, $^{239+240}Pu$ 7.3 x 10^{-6}[50].
Americium (Am)	• Dissolved concentrations 7.8 ag L^{-1} to 0.4 x 10^{-9}[53]		• Ribble Estuary sediments[44]: 1.76 x 10^{-3} • Sarzhal Wells, Kazakhstan[50] 0.12 x 10^{-6}

Note: all units quoted in the literature have been converted to mass units, generally from activities or atom numbers. To convert from activities to mass units, the following was used: A = λN, where N = number of atoms, A = activity in Bq (disintegrations per second) and λ=Ln2/t½ where t½ = the half life (s) of the radioisotope.

2.3.2 Environmental chemistry

This section briefly reviews the environmental chemistry of the actinides as the behaviour of the actinides in the environment has been cited as an important component to monitor [12]. This is because complexation, sedimentation and speciation are closely linked to the mobility of the actinides and dissolved concentrations.

2.3.2.1 Redox chemistry

Knowledge of the predominant chemical forms of the radionuclide in the system allows prediction of its likely behaviour, e.g. its solubility, volatility, bioavailability and particle reactivity. The chemistry of the actinides is controlled by the filling up of the 6d, 7s and f-orbitals (4f and 5f) by valence electrons [19, 54]. The oxidation states adopted by the actinides of interest are shown in Table 2.4 below. The large array of oxidation states displayed by the earlier actinides indicates that the valence electrons are less tightly bound thereby increasing their availability for bonding and complexing [19], with Pu often existing in multiple oxidation states in natural systems [55] such as the Irish Sea where it has been found to exist as (V) and (VI) in the dissolved phase, and as (III) and (IV) reduced onto particle surfaces [56].

Table 2.4 Oxidation states adopted the actinides. Bold type represents the most stable states in oxic solution [4, 17, 19, 55] .

Oxidation State	**Ac**	**Th**	**Pa**	**U**	**Np**	**Pu**	**Am**	**Cm**	**Bk**	**Cf**	**Es**	**Fm**	**Md**	**No**	**Lr**
+7					+	+									
+6				**+**	+	+	+								
+5			**+**	+	**+**	+	+								
+4		**+**	+	+	+	**+**	+	+	+	Solid only					
+3	**+**	+	+	+	+	+	**+**	**+**	**+**	**+**	**+**	**+**	**+**	+	**+**
+2							Solid only			Solid only	Solid only	+	+	**+**	

They appear in the oxidation states as the following forms:

+ III: An^{3+}

+ IV: An^{4+}

+ V: AnO^{2+}

+ VI: AnO_2^{2+}

} Formed as a product of hydrolysis. Only Pa, U, Np and Pu generally found in this form.

Th(III) is rapidly oxidised by water so this ion is predominantly found in the (IV) state in aqueous environments [57]. U exists in oxidation states in solution from (III) to (VI) as per Table 2.3; however (III) is readily oxidised by atmospheric contact, (IV) is only stable in very acidic solutions or solutions containing high concentrations of

a stabilising ligand, and (V) disproportionates. U(VI) as the uranyl ion (UO_2^{2+}) or its complexes is the most stable solution species in oxic solutions [19], although U(IV) is also found under reducing conditions [58].

The trivalent state of the actinides stabilises with increasing atomic number through the actinides, until Am whereby (III) is the preferred oxidation state [28, 59]. Am(IV) in solution requires high concentrations of a stabilising ligand, the (V) state is susceptible to disproportionation and the (VI) state is easily reduced. In environmental systems, Am is most likely to occur only in the (III) state in solution [28, 59]. Pu aqueous oxidation chemistry, in contrast is very complicated; Pu is capable of 5 oxidations states (III to VII) in aqueous systems [2], although (VII) only exists in very strong alkali solutions. Under reducing conditions the Pu(III) and Pu(IV) states will dominate and under oxic conditions the Pu(V) and Pu(VI) states dominate especially when stabilised with high carbonate concentrations [60]. Pu(VI) oxidation state most readily forms complexes; (IV) disproportionates to (III) and (VI), and (V) disproportionates to (IV) and (VI), which is an important mechanism for Pu sorption to mineral surfaces as (VI) is easily reduced [60].

The actinides Th, U, Pu and Am readily form compounds in high oxidation states and stable complexes with oxygen containing ligands such as chloride, sulphate, carbonate and acetate.

In addition to the redox potential of the aqueous environment, the actinides are continuously undergoing radioactive decay; alpha decay in particular acts as a strong reducing agent.

2.3.2.2 Speciation

It is important to understand how the actinides of interest behave or speciate in varying aquatic settings in order to understand their fate and toxicity [5]. Important in aqueous environments is the partitioning between the solid and the solution phases, which is mediated by chemical characteristics such as pH, redox potential, ionic strength, presence of complexing ligands (oxides, hydroxides, phosphates, carbonates, sulphates), surfactants or flocculating agents [58, 60-62]. These all act to influence the oxidation states of the radionuclides and will all affect reactions with other dissolved components and sediment-solution interactions. Actinide elements have similar complex chemistry, the complex formation constants generally being very similar for the elements U, Np, Pu, and Am of the same oxidation state [27]. Formation of organic complexes with humic acids (HA) and fulvic acids (FA) can significantly influence the

solution speciation of the actinides, with the trivalent oxidation states forming much more stable organic complexes than higher oxidation states.

Important processes for the interaction of the actinides with the aquatic environment include precipitation, complexation, sorption and colloid formation. Precipitation and sorption will retard actinide release and transport by limiting solution concentrations near the solid phase; complexation with inorganic ligands (such as CO_3^{2-}) will increase solubility and therefore mobility, whilst colloidal formation will enhance or retard mobility, depending on the nature of the colloid [1, 58, 62]. It is the oxidation state of the actinide that determines which of these processes predominates and therefore the solubility and mobility, and these processes will also show similarities across the actinides of a similar oxidation state [58]. The solubility will also be dominated by the presence of dissolved ligands [57]. Cooper [58] found that solubility of the actinides originating from nuclear sites in cationic form was low due to cation exchange with soil. Anionic forms of the actinides are highly mobile due to the poor anion exchange capacity of soil [58, 62].

To illustrate speciation and complexation in natural waters, Table **2.**2.5 shows complex formation constants for the actinides with a variety of ligands. As can be seen from Table 2.5, carbonate concentration is a major control on speciation of the (VI) valence (AnO_2^{2+}), found for the actinides in oxic waters. The stability or formation constant (log*K*) for (VI) valence actinides has been reported as 9.9 – 12 for CO_3^{2-}, 8.1 – 9.1 for OH^- and ~8.4 for HPO_4^{2-} (Table 2.5). The influence of each of these inorganic ligands will vary depending on the pH of the system. In lower carbonate concentrations or in systems with a lower pH, phosphate and other oxygen containing ligands will dominate complexation reactions.

Table 2.5 Complex formation constants for inorganic actinide complexes [27]

Ligand	**Log*K***			
	An^{3+}	**An^{4+} (excluding Th (IV))**	**AnO^{2+}**	**AnO_2^{2+}**
OH^-	5.7-6.3	12.5-13.7	4.0-5.1	8.1-9.1
CO_3^{2-}	4.6-6.3	-	5-5.9	9.9-12
HPO_4^{2-}	-	12-13	2.8-3.4	8.4
$H_2PO_4^-$	2.4*2.7	4.5-5	-	2.9-4
F^-	3.4-4.3	7.9-8.6	3.7	5.1-5.7
SO_4^{2-}	3.5-3.7	5.5-5.8	2	2.8-3.3
Cl^-	<1	<2	<0	<2

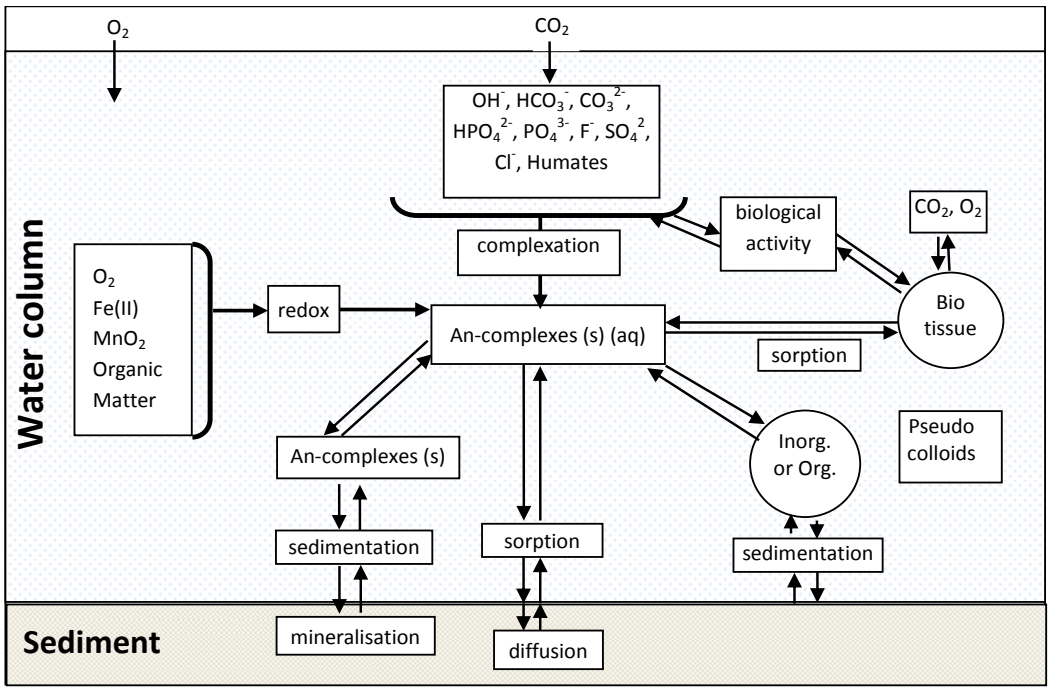

Figure 2.3 Diagram to illustrate possible pathways and reactions for the actinides (An) upon entering an aquatic environment. From Choppin [4].

Figure 2.3 above illustrates the speciation pathways available to the actinides in the aquatic environment. It is a complicated system and involves a number of pathways that also include organic carbon (humic and fulvic acids) interactions, biota, sediment-water interface and particulates and colloids. Some of these processes are discussed below, but due to the breadth of the field it has not been possible to discuss all actinide pathways and reactions in the aquatic environment. Only those reactions that may impact upon the passive sampling of the actinides have been discussed here.

2.3.2.3 Colloids and particulates

Colloids and particulates (for instance minerals) have been recognised as influencing the mobility of contaminants that are strongly sorbed to mineral surfaces [63, 64]. Hydrolysis is important in the formation of colloids [58, 65] as it is the primary step in polynucleation; for instance hydrolysis controls Pu speciation by resulting in positively charged to neutral colloidal hydrolysed molecules [66]. Mechanisms that control precipitation and adsorption processes are related to pH, ionic strength, the composition of the aqueous and solid phases [67], the nature of radionuclide binding to colloids and the stability and the size of colloids [68]. Retention of colloids is high at high ionic strength, low pH and in impermeable rock [64].

HA and FA may also interact with the mineral surfaces to provide strong binding sites for higher valence actinides. Lippold and Pipke [63] investigated the effect of humic matter on the adsorption of metals onto clay minerals as natural clay contains

humic-like organic compounds that can act as carriers for the actinides. They found that the adsorption of Terbium(III) was greatly enhanced in the presence of HA, particularly at pH > 5. Chen *et al.* [69] studied the sorption of Th(IV) to montmorillonite as a function of FA concentration and pH. It was found that Th sorption was strongly pH dependent and enhanced by the presence of FA, especially at lower pHs. Surface complexation, rather than cation exchange, was cited as the binding mechanism.

Colloids can also be present as HA rather than simply intermediaries as described above. Transport of actinides by humic colloids was studied by Artinger *et al.* [70] on two humic rich Gorleben (north-east Germany) groundwater-sediment systems. They found a strong dependency of radionuclide transport on the radionuclide concentration as the dissociation kinetics of the trace metals naturally associated with the HA is proportional to the radionuclides added. HA agglomeration has been shown by Geckeis *et al*. [68] and Geckeis and Rabung [64] through the use of flow-field flow fractionation to study colloid hydrodynamical size distributions. It was found that the degree of agglomeration depended on the metal ion charge. It is these agglomerations that may delay the dissociation of aged metal ion- HA/FA complexes [64], which is significant as radionuclide transport or mobility is reliant on the sorption / desorption processes occurring at mineral surfaces [71]. $^{239+240}$Pu and ^{241}Am were studied by Santschi *et al* [72] in storm runoff and pond discharge from the Rocky Flats Environmental Technology Site, US DOE. It was found in both studies that Pu and Am was transported in the particulate phase (≥ 0.45 μm; 40−90%) and colloidal phase (~2 nm or 3 kDa to 0.45 μm; 10−60%). They also found remobilization of Pu and Am was enhanced by the presence of FA and HA. A preference for complexation with FA and HA was found over the inorganic iron and manganese oxides.

Sorption mechanisms are important for predictive modelling of radionuclide migration, bioavailability of radionuclides in the natural environment [73] and biogeochemical cycling of particle-reactive nuclides [74]. Sorption to particle surfaces is pH dependent with cations having increased sorption in more alkaline conditions and anions increased sorption in more acidic conditions [57]. Tetravalent actinides are strongly sorbed by mineral colloids and have a strong tendency to form colloids. Th sorption is sensitive to carbonate alkalinity due to the formation of positively charged aqueous mixed hydroxyl-carbonate complexes. The solubility of ThO_2 increases with increasing ionic strength, potentially as a result of destabilisation and flocculation of colloidal particles, with the two important aqueous marine species of Th being $Th(OH)_3(CO_3)$ [75] and $Th(OH)_4$, which occur in approximately equal proportions [57].

As the oceans are chemically uniform, and Th is very particle reactive, this actinide is found in the dissolved phase in oxygenated systems in very low concentrations [74, 76]. As a result of its particle reactivity and its constant source from ^{238}U, Th (particularly ^{234}Th) is commonly used by oceanographers to quantify particulate transport through the ocean column [74, 76] , providing information on particle distribution and sinking rates [57]. The short half life of 24.1 d is used to provide flux information, such as was used by Buesseler *et al*. [76] during a study of particulate organic carbon (POC) fluxes in the Arabian Sea. Diatoms transport Th through the ocean column as it is bound within the frustules and to the exopolymeric polysaccharide rich gel that surrounds the sinking diatoms. This can be evidenced from the reduced Th concentrations in surface waters during diatom blooms [77].

Particulates associated with microbial assemblages can affect the redox conditions locally. Keith-Roach [61] found that microbial assemblages controlling biodegradation may play a major role in radionuclide speciation in natural waters. A study by Swarzenski et al. [78] also found that U was modified by microbial transformations across redox transition zones.

The role that particulates play in controlling actinide solubility is varied and dependent upon the environment, as the quantity of particulates can vary from high values in silt carrying rivers (Mississippi – 260 mg L^{-1}) to very low values in the ocean (0.5 mg L^{-1}) [2]. In addition to particulate loading of a system, the partition coefficient (K_D) between the solid and the liquid phase (solid concentration per unit mass / liquid concentration per unit mass) of the actinides is also important as this gives the affinity of the actinides to particulates. Some K_D's are given in Table 2.6 below for illustrative purposes. The higher the K_D, the more particle reactive the element is in a given system. What can be seen is that U has the lowest K_D in oceanic environments, as its chemistry is dominated by the carbonate in that system. Np has the next lowest K_D value, meaning it is also highly mobile in the marine environment, whilst the other actinides are all very particle reactive, with high K_D values.

Table 2.6 Typical K_D values of some actinides in oceanic and freshwater systems [42, 79].

Actinide	Open Ocean [42]	Ocean margin [42]	Freshwater [79]
Ac	2×10^6	2×10^6	-
Th	5×10^6	3×10^6	1.9×10^6
Pa	5×10^6	5×10^6	-
U	5×10^2	1×10^3	5×10^1
Np	1×10^3	1×10^3	1×10^1
Pu	1×10^5	1×10^5	-
Am	2×10^6	2×10^6	-
Cm	2×10^6	2×10^6	5×10^3
Bk	2×10^6	2×10^6	-
Cf	2×10^6	2×10^6	-

2.3.2.4 Sediment-water interface

Removal and remobilisation of metals and actinides at the sediment-water interface is well documented. Dunk [80] evaluated the U budget in the oceans and found that of the 53 Mmol a^{-1} U input into the oceans, predominantly via fluvial systems, approximately 11 Mmol a^{-1} is removed *via* salt marches and mangrove swamps. The three major sinks of U in the ocean are through the removal to oxygen depleted sediments (~26 Mmol a^{-1}), incorporation into biogenic carbonate (~13.3 Mmol a^{-1}) and through crustal sequestration during hydrothermal alteration and seafloor weathering (~5.7 Mmol a^{-1}).

Removal of actinides from aquatic systems is generally by processes described previously in this report, such as inorganic complexation with iron or organic matter flocculation. Sediment water interactions may also effectively remove the actinides from the water column via bacterially mediated biogeochemical cycling [81, 82]. This bacterial reduction in sediment, which follows the trend of terminal electron acceptors ($O_2 \rightarrow MnO_2 \rightarrow NO_3 \rightarrow FeO_2 \rightarrow SO_4$) in decreasingly thermodynamically favourable reactions, is dependent upon availability of the elements and organic matter, and creates a diffusive flux driving the metal into the sediment. These processes are being researched as solutions to the removal of radionuclide and heavy metal pollution, for instance reduction of U(VI) by sulphate reducing bacteria has been proposed as a new technology for the removal of U from groundwater [81]. A review was undertaken by Wilkins *et al.* [83] on the influence of iron reducing bacteria on U solubility and mobility in relation to radioactive wastes and how microbial activity could be used for bioremediation.

Reduction is not only microbially driven, but occurs as a result of minerals present in the sediment. In ocean column and sediments, the presence of iron (hydr)oxides can reduce metals [84]. Charette and Allen [85] reported that the Waquoit bay, Massachussetts, USA, subterranean estuary was a sink for U. The U-salinity

distribution displayed strong evidence of removal at intermediate salinity potentially due to anoxic conditions, with an average removal efficiency of 50% for U. This trend was also present in another study on the Amazon and Fly Rivers, Papua New Guinea [86]. Aquatic systems are regarded as a sink for Pu because reactions with particulates results in settling out [87, 88]. U distribution in the coastal and pore waters of Tampa Bay, Florida, were found to vary by Swarzenski and Baskaran [89] because of the fluid exchange processes across the sediment/water interface, inputting U from U rich phosphatic deposits. The estuarine distribution here in this case study indicates geologic control that is influenced by sediment/water interface providing enrichment through the U(IV) and U(VI) valence state transformations. Pore water profiles showed both flux into and out of bottom sediments consistent with Fe(II) and Mn(II) redox cycling.

Another sink for actinides in aquatic systems is incorporation into the food chain [90] *via* plankton. Sanchez-Cabeza *et al*. analysed plankton from the western Mediterranean Sea for plutonium and americium. Microplankton accounted for 50% of the Pu measured, with high $^{239,\ 240}$Pu activity due to contamination from the bottom sediments. Mesoplankton was also found to efficiently concentrate transuranic (TRU) elements, however in open waters the concentrations were much lower (up to five times) indicating a larger role in sediment transfer of elements.

Bioturbation within the sediments also has to be considered as this re-mobilises sediment sorbed metals by changing the Eh and pH of an environment. Cournane *et al*. [91] undertook a 40 day microcosm laboratory experiment to determine biological reworking of sediments by the ragworm *Nereis diversicolor* using particle-bound radionuclides (^{137}Cs) as tracers. Over the course of the experiment they found that up to 35% of the radio-labelled particulates deposited on the sediment surface had been redistributed to depth up to 11cm.

2.4 Analysis

Low concentrations of actinides can be challenging to detect directly using conventional elemental analytical techniques (e.g. ICP-MS) particularly when further dilution is required for complex matrices such as marine and estuarine waters. In addition to total actinide concentrations, isotopic ratios are required in order to assess the source (natural or anthropogenic) of the actinide. Most isotopes of dissolved actinides are in concentrations below conventional detection limits and therefore require a pre-concentration step using such techniques as precipitation, ion-exchange, solvent extraction or extraction chromatography [20]. Pre-concentration and radiochemical

separation usually require large volumes (for instance > 5 L [92] or 200 L [93]) grab samples of water, although this will depend on the actinide environmental concentrations and the sensitivity of the technique employed.

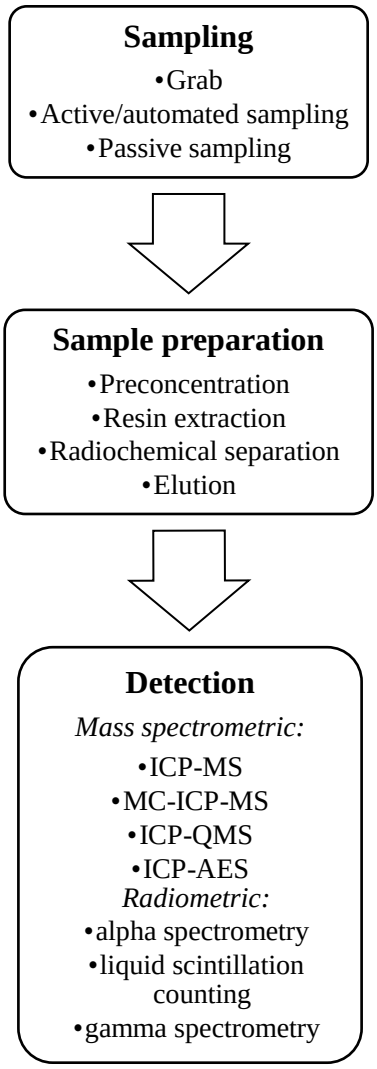

Figure 2.4 Diagram illustrating the measurement of actinides in the environment.

2.4.1 Pre-concentration

Pre-concentration can improve a limit of detection for a technique by increasing the sensitivity of a method by several orders of magnitude, which also enhances accuracy and precision. It also achieves the separation of the analyte from the environmental matrix. There are numerous pre-concentration techniques including ion exchange, liquid liquid extraction, chromatography, co-precipitation and solid phase extraction [94]. Most involve some kind of sorbent which extracts the actinide from the sample matrix by having a higher partition coefficient, followed by elution and measurement.

One of the most commonly applied methods of pre-concentration is through the use of co-precipitants such as ferrihydrite followed by a resin clean-up step, or directly using resins that act as sorbents, isolating the actinides from the sample matrix. Table 2.7 below details some of the resins that have been used to separate actinides from an environmental matrix.

Table 2.7 Examples of applications of selected resins in extraction and separation of actinides from environmental matrices.

Resin	Application examples
Manganese dioxide (MnO_2)	• Preconcentration of radionuclides [95] and radium [96] in seawater and natural waters [97, 98].; and U and Th from artificial freshwaters[99]. Has been found to be pH limited pH < 6 [99] due to phase change. • Co-precipitation to determine U and Pu isotopes in natural water , and Th in seawater [40] • Used with diffusive gradients in thin films (DGT) to measure U in natural waters [100].
Diphonix® (TrisKem)	• Actinide separation from environmental samples [101], waste streams[102] and acidic solutions [103]. • Application to the thin films technique [98, 104] to measure dissolved U.
Actinide Resin (TrisKem)	• Used for preconcentration of U and Pu from soils and large water samples [92, 105, 106].
Ferrihydrite	• Remediation of actinide contaminated waste streams [107]. • Used in coprecipitation of ^{233}Pa following acid dissolution of Arctic marine sediments [108].
Titanium Dioxide (TiO_2) Including Metsorb™	• Separation of U from seawater and complex matrices [109, 110]. • Used in geological disposal of radioactivie waste [111-116] to sorb radionuclides. • Used with DGT to measure uranium in natural waters [100]. • Soprtion of Th in presence of fulvic and humic acid [115]. • Sorption of Pu [117].
Chelex-100 (BioRad)	• Used with DGT to measure U [100, 118-121]
DE81 (DOW)	• Used by to measure U in artificial alkaline river water using DGT [118] .
Dowex (DOW)	• Used by to measure U in artificial alkaline river water using DGT [119] • Separation of U from groundwater [122]. • Used in radiochromatography used it to separate ^{239}Pu and ^{240}Pu from environmental samples [123].

2.4.2 Detection

Analytical tools available for measuring radionuclides in the environment can be divided into 2 broad categories: radiometric and mass spectrometric. Radiometric techniques are dependent on the decay mode of the nuclide of interest and can be difficult to quote detection limits for as they depend on the type of detector used, the

distance of the sample to the detector [124], sample matrix, the separation process used and the geometry of the sample (especially for gamma spectrometry). Generally, radionuclides require separation prior to measurement because of energy peak interferences in the case of radiometric techniques, and mass interferences in mass spectrometry.

Table 2.8 Summary of some measurement techniques selected from the literature

Detection	Analyte(s)	Extraction and pre-concentration techniques	LoD*	REF
		Mass spectrometric		
Inductively couple plasma atomic emission spectrometry (ICP-AES)	Total U & Th	Silica sorbent modified with 5-nitro-2-furaldehyde.	0.3 µg cm^{-3} sorbent	[125, 126]
Inductively couple plasma mass spectrometry (ICP-MS)	^{235}U, ^{238}U		^{235}U: 0.21 ng L^{-1} ^{238}U: 0.91 ng L^{-1}	[127]
	$^{240/239}$ Pu	SPE- serine type chitosin resin.		[128]
	^{238}U	No pre-concentration technique used. The sample was diluted x 10 and analysed directly in hydrogen mode.	0.49 ng L^{-1}	[129, 130]
ICP-MS using octopole reaction system	Total U (as ^{238} U)		0.25 – 0.3 ng L^{-1}	[129, 131],[132]
	^{238}U, ^{235}U	Samples pre-concentrated using Chelex-100, MnO_2, Metsorb^{TM} and Diphonix.	^{235}U: 4 ng L^{-1}; ^{238}U: 0.2 ng L^{-1}	
Multi-collector ICP-MS (MC-ICP-MS)	Pu, NP	Sediment samples acid digested and co-precipitated with LaOH, separated from the liquid, centrifuged and re-digested in HNO_3. Pu and Np then isolated using TEVA resin.	Isotopic ratios measured with 1-5% uncertainty	[133]
ICP-quadrupole mass spectrometry (ICP-QMS)	U, Th & Pu	Preconcentrated with $Ca(PO_4)_2$.	17 - 29 pg L^{-1}	[134]
	^{238}U	TRU resin.	0.3 ng L^{-1}	[129, 135]
		SPE-TRU resin	48 pg L^{-1}	[129, 136]
		SPE-Duolite XAD 761 adsorption resin	1.5 ng L^{-1}	[129, 137]
	Np	Sorption from acidic solutions by the resins AG1-X8, TEVA, U/TEVA and TRU	0.3-0.5 counts s^{-1}	[29]
Thermal ionisation mass spectrometry (TIMS)	^{234}U, ^{235}U, ^{236}U, ^{238}U, ^{239}Pu, ^{240}Pu, ^{241}Pu, ^{242}Pu	DOWEX 1X4 anion exchange resin was used to purify the Pu solutions in this study.	Used to quantify atom ratios between U & Pu only.	[138]

Detection	Analyte(s)	Extraction and pre-concentration techniques	LoD*	REF
	^{237}Np	Acid dissolution of sediments followed by anion separation.	78 fg ($5x10^5$atoms)	[52]
	$^{239+240}$Pu		80 ng (5×10^4atoms)	
Positive thermal ion isotope dilution mass spectrometry (PTI-ID-MS)	Total U & Th		1 ng kg^{-1} (U) 8 ng kg^{-1} (Th)	[139]
Multicollector ICP-MS	$^{240/239}$Pu	Isotopic ratios determined only in this study.	0.9662 ± 0.0011	[140]
	$^{242/239}$Pu		1.0253 ± 0.0019	
		Radiometric		
Alpha spectrometry	^{241}Am		0.3 fg L^{-1} (0.01Bq kg^{-1})	[141]
	Pu & U	Actinide^{TM} resin used as pre-concentrator, followed by a lithium metaborate fusion to back extract. Anion exchange and TEVA resins were used to separate the actindes.	0.3 ng L^{-1} (0.001 Bq L^{-1})	[92]
	^{227}Ac	MnO_2 impregnated polypropylene filter cartridges used to pre-concentrate seawater (545 – 2784 L pump through). Back eluted using with HNO_3, HF and N,N-hydroxylammonium.	background (<0.002 cpm)	[35]
Gamma spectrometry	^{241}Am	HPGe detector used for 3 day count		[141]
	^{227}Ac	Underground gamma chamber used to measure very low level gamma emitters.	Background reduction of 15 times.	[37]
	^{233}Pa	A 300 cm^3 well-type high purity Germanium detector used		[29]
	^{234}Th	Large volume (>200 L) seawater, pre-concentrated using MnO_2 cartridges.	Background was 0.02 cpm over a 24 h count time.	[41]
Liquid scintillation counting	^{233}Pa, ^{234}Th			[46]
	^{231}Pa	Separated from environmental matrix using acid dissolution and then coprecipitated with $Fe(OH)_3$, dissolved in 9M HCl and passed through an anion exchange column.		[108]

***Many of the limits of detection are dependent upon the conditions of the study (for instance count times for radiometric analysis) and the units quoted. Some uniformity of reported units has been undertaken where possible by conversion to mass units from activity or atom units. These are just examples of limits of detection and vary for every study and/or radioisotope analysed.*

Table 2.8 illustrates the breadth and scope of the analytical tools available for measuring radionuclides in the environment. These are just some examples of analytical techniques used for radionuclides. As stated, defining a limit of detection (LoD) for radiometric techniques that would normally be given for mass spectrometric techniques can be difficult. This is because the LoD for radiometric techniques depends on energy peak discrimination from background sources. Limits of detection for radiometric techniques generally lie in the fg kg^{-1} range, while for mass spectrometric, it is in the pico- to nanogram range. This is a function of count times or acquisition times which tend to be longer for radiometric technique. One of the major drawbacks to radiometric analysis is the time taken to process a sample, which from isotopic separation (for alpha emitters particularly) to counting can be upwards of 1 week. However, the choice of measurement technique is also dependent upon the half life of the radionuclide. Mass determinations are more sensitive for those radionuclides with longer half-lives, whereas activity determinations are more suited for short-lived radionuclides.

2.5 Monitoring/Sampling Methods

2.5.1 Grab sampling

Many water sampling strategies rely on spot sampling techniques followed by instrumental laboratory analysis [142], providing a snap shot of pollutants present at that point in time. Spot sampling is necessary for environmental monitoring, but during episodic events, or within fluctuating environments (such as estuaries [143, 144]) it could present as a source of inaccuracies when assessing long term trends in water quality [145]. Passive sampling overcomes these inaccuracies by measuring the mass of the analytes *in situ* and providing a simple method of obtaining a time weighted average (TWA) value. Spot sampling is used in many environmental monitoring schemes such as undertaken by Tosheva *et al.* [146] in assessing naturally occurring radionuclides in Luxembourg drinking waters, where samples from 316 outflows were collected twice for analysis over a three month period. There will be no data in between each of the sampling times, which is why regular, daily spot sampling for regulatory monitoring is required. Grab sampling for radionuclides generally required large volumes (for instance 5 L [92] for U and Pu preconcentration from freshwaters or 200 L for Th isotopic analyses of seawater [93]) of water followed by preconcentration, due to the very low levels of some radionuclides in natural waters.

2.5.2 Biomonitoring

Many anthropogenic pollutants are toxic to organisms in aquatic environments however, sub-lethal doses causing chronic diseases are more common than large pollution events that result in a large number of deaths. Due to the uptake of bio-available pollutants, biological indicators can be used to measure the presence and toxic effect of pollutants [147-150].

Biomonitoring techniques include correlating gill mass of fish with metal concentrations [149] as seasonal indicators of the presence of heavy metals, and plants [150], which can also be used to give a bioaccumulation factor corresponding to the level of heavy metals present in the aquatic environment [151]. Plants are excellent indicators of heavy metal concentrations as they incorporate the metals into their cellular structure. To this end they are also used in remedial techniques [152]. U and Th were evaluated by Zoriy *et al*. [153] at two former U mines and a U reprocessing factory in Aktau, Kazakhstan using a biomonitoring technique. Plant samples (*A. austriaca*) were taken from around the city from 2007 to 2008 and U and Th concentration distributions determined. Burger *et al* [154] used marine brown aglae and Ulva to measure levels of radionuclides for the Northern Pacific Ocean / Bering Sea (Aleutian Islands). Inter-specific differences in radionuclides were found, for instance *Ulva lactuca* had the highest levels of ^{241}Am, *Alaria fistulosa* the highest levels of $^{239+240}$Pu and *Fucus distichus* contained the highest levels of $^{234, 235, 238}$ U. However, all algae had levels of radionuclides close to the minimum detectable activity. The authors suggested that algae could be used to indicate low levels of radioactivity caused by for instance, seepage, as they bio-accumulate at very low levels.

An issue with biomonitoring, particularly with bioaccumulation which may occur over an extended period of time is that the cause of the accumulation of the radionuclide in the tissue cannot always be determined. Dependent on the organism, preferential uptake of particular isotopes may occur, which means that no isotopic fingerprinting of the pollutant could be undertaken to determine the source or point of discharge. There is also the issue of movement or migration of the organism, particularly in the marine environment with tidal movement. This again would make it difficult to identify the source of the pollution. This technique is only suitable to monitor long-term trends of actinides in the environment, rather than for routine regulatory environmental monitoring.

2.5.3 Sensors

Grate *et al*. [155] in a review of radionuclide sensors for environmental monitoring identified a major challenge as limits of detection for the very low concentrations of the analytes and separation from complex matrices. However, one of the advantages to *in situ* sensing is the elimination of sampling and laboratory procedures. They describe a preconcentration sensor that comprises a straight or coiled column of a solid phase (particles or beads) to preconcentrate the analyte of interest within a detection zone (i.e. between two photomultiplier tubes (PMT) if the solid phase is a scintillator, or colorimeters if the technique is optical). Flow injection and sequential injection systems suitable for large volumes of water or down to μL, have also been used for sampling aquatic radionuclides. One example are pre-concentrating mini-column sensors that contain a sorbent such as ion exchangers or complexing resins [156], that accumulate the analyte while a bulk solution is pumped through the column; thereby providing real time concentrations. The analyte can then be eluted from the resin and analysed. A renewable solid phase was also described, as an alternative to eluting the analyte from the solid phase [157]. Another sorbent was described by DeVol *et al* [155, 158] for the sorption of uranium uranium onto a CaF_2:Eu scintillator, which acts as both sorbent and scintillator. The detection efficiencies of this technique were (ratio of observed counts to decay events) 60%.

A different type of sensor, based on electrochemistry developed by the Boise State University and currently pending patent rights [159], was developed because of an existing gap in the availability of portable in-field sensors. It is a portable electrode coated with an actinyl-selective polymer, such as a chelate, that undergoes electrochemical changes with binding of the target analyte, which is directly proportional to the concentration of the analyte. The electrochemical changes are based on redox chemistry of the analyte-sorbent complex. Initial experiments shown in the patent application [159] demonstrate a linear response of the instrument to increasing analyte concentration, with a detection limit for Th and U of 0.1 ppb, with 3σ noise interference of 0.01 ppb.

Hayes *et al* [160] describe the development of a fibre optic sensor in conjunction with Isoamethurin, which is an actinide selective molecule that changes colour on complexation, for radiological detection in the aqueous phase to sub ppm levels. The sensor was found to respond rapidly to changes in U concentrations (< 5 s) with a detection limit of < 500 ppb at low cost. This type of sensor would only be useful

during pollution events rather than for regulatory monitoring due it the high limit of detection.

Despite a wide array of tools available for the detection of radionuclides in the environment, for alpha and beta emitting radionuclides, detection by sensors may not always be possible because of the very low limits of detection required. Three major obstacles have been identified that radiometric sensors would have to overcome [155], namely proximity of the analyte to the sensor due to the short wave length of the emitted radiation; energy discrimination problems and interferences; and large sample volumes required due to the low limit of detection.

2.5.4 Passive sampling

Passive sampling is important in aiding the understanding of chemical transformations and pathways in a variety of aquatic environments including pore-waters [161-164], marine environments [165, 166] and freshwater systems [118, 167], which have been described as important to understand for environmental monitoring. The ability to separate and size exclude complexed species provides vital information regarding lability, toxicity and bioavailability. Vrana *et al*. [168] conducted a literature survey on passive sampling techniques and their application in organic and inorganic pollutant monitoring. Passive sampling can be categorised as an *in situ* technique and is based on the free flow of analytes from the bulk solution to a receiving phase or sink [168]. Many current analytical methods rely on the removal of samples to a laboratory environment for processing, thereby changing physical and chemical parameters such as temperature, pressure and oxygen content, and acidification of the sample for preservation purposes. These alterations lead to inherent changes in the chemical makeup of the analytes of interest and will therefore not give direct information on the chemical forms present.

Current passive samplers are based on either permeation or diffusion and can be either kinetically driven or equilibrium based. Examples include semi-permeable membranes, passive *in situ* concentration/extraction samplers such as diffusive gradients in thin films (DGT) and solid phase micro-extraction devices [169].

2.5.4.1 Diffusive gradients in thin-films(DGT)

This method separates the analytes *in situ* by molecular size and kinetic availability (lability) [170]. The devices consist of multiple layers; the top layer being the protective film such as a filter membrane with a known pore size; the mid layer is the diffusive layer and comprises a polyacrylamide gel of known thickness and pore

size; and the bottom layer which is a resin or the receiving phase held in place by polyacrylamide gel. The technique operates using Fick's first law of diffusion to establish a steady-state diffusion coefficient between the bulk solution (the solution in which the devices are deployed) concentration, and the zero dissolved ion concentration at the resin layer interface [171]. At the end of the deployment the ions in the resin layer are eluted and measured using instrumental techniques (or in the case of beta analyses, directly submerged in liquid scintillation cocktail [172]).

Research into the potential contribution of DGT in the measurement of actinides in the environment is a relatively new area. Initial studies examined the possibility of using DGT to measure U, particularly in more challenging alkaline water environments [118, 167, 173] where it forms anionic carbonate species, with further studies examining the effects of speciation and ionic interferences. DGT has also been used to measure bioavailability or plant uptake of U [120, 121]. Many of these studies focused on finding a suitable resin or receiving phase for this technique. Li *et al*. [118] examined speciation of U in natural alkaline waters using two binding phases; DE 81 and Chelex-100. The device was tested in both synthetic and natural river water. DE 81 was found to out-perform Chelex-100 in higher ionic strength water. This study was taken forward [167] by comparing DE 81 and Chelex-100 resins to the anion exchange Dowex resin in natural and synthetic river water to investigate the performance differences. They found that because the three resins contain different functional groups and therefore bind to different uranyl complexes, when used together they provide more information on the speciation of the labile uranyl complexes than if used alone. More recent studies by Gregusova *et al*. [173], Hutchins *et al*. [100] used Spheron-Oxin and Metsorb^{TM} (a TiO_2 based resin) respectively to measure U in natural waters. These were all compared against the most commonly used resin with DGT, Chelex-100. All new resins were found to out-form the Chelex-100 in alkaline waters, but were comparable in neutral to acidic streams.

Vandenhove *et al.* [120] used DGT to assess the bioavailability of U to plants by testing the DGT devices in varying soil conditions to mimic the actions or uptake of the soluble fractions by the plants. This application of the DGT device did not prove to be a conclusive proxy for U bioavailability to plants. Duquene *et al*. [121] applied the DGT technique as a proxy for uptake or availability of U to plants, in comparison of the U present in the soil solution. Ryegrass was used and grown in a greenhouse on a range of U spiked soils and the DGT recovered U correlated with the U soil concentration. They found that the DGT technique did not provide any advantages over other conventional

methods to predict U uptake in soils and that the DGT method did not predict uptake in shoots.

Docekal and Gregusova [164] have recently used the Spheron-Oxin resin as the binding agent in DGT to examine U concentration and $^{235/238}$U isotopic ratio profiles in sediment pore-waters. Using DGT, they were able to assess immobilisation/remobilisation processes as a tool to examine the migration of contaminants.

The application of DGT as a monitoring tool for actinides has been shown to have potential, with longer deployment times than other techniques reviewed (e.g. 48 h Gaiasafe devices [174]) and better limits of detection than the sensors.

2.5.4.2 Solid phase extraction (SPE)

Solid phase extraction has been developed for the pre-concentration and separation of metal ions in solution, and is a proven method for the removal of matrix interferences [175]. Many SPE devices employ silica based resins that have many disadvantages including a narrow operating pH range (4-7) and poor adsorption/desorption kinetics due to its porous nature [175]. There are other SPE disks that have been developed in recent years that employ different materials in the construction of the disk base so that a wider range of sorbents can be used, making this technique more versatile and analyte specific.

Polyethylene terephthalate (PET, polyester) capillary-channelled polymer (C-CP) fibres have been described by Pittman *et al.* [175]. The surface of the fibres were modified by surface functionalisation with polyacrylic acid (PAA), chosen because the repeating acrylic acid monomeric unit containing a carboxylic acid, which have the ability to bind metal ions. The fibres were deployed in a micropipette tip, and uptake trials under various pHs and aqueous matrices were trialled for several metals (Cu^{2+}, Cu^{+}, Ni^{2+}, Fe^{3+}, UO_2^{2+}), which were eluted with extremely low concentrations of hydrochloric acid (1 ml of 0.005%), resulting in overall recoveries of greater than 88%.

2.5.4.3 Diffusive equilibrium in thin-films (DET)

Similar to diffusive gradients in thin films (DGT), DET comprise of a diffusion phase separating the receiving phase or the resin from the external water body (or bulk solution). The dissolved analytes diffuse though the diffusion layer (a hydrogel) to the resin, until the resin has the same concentration of analytes as the external waters (or it has reached equilibrium) [176]. These samplers have successfully been deployed to monitor pollutants in sediment pore waters as segmented probes [177, 178] to produce

fine scale depth profiles or to study early diagensis [179]. One of the major drawbacks with this technology is that some analytes may take extended periods of time to reach equilibrium due to the molecular size or the diffusion coefficient. A more recent application of DET has been in the measurement of U to establish historical redox conditions in sediments [180] and to measure fine scale U sediment redox processes [164].

2.5.4.4 Gaiasafe paper

Gaiasafe devices [174] are sorbent papers, such as filter paper, impregnated with a resin or analyte specific adsorber. The device has been developed to hold multiple receiving phases for broad deployment applications. Recent applications include the analysis of explosives [181] and actinides [174] in water. Using iron-oxide as the adsorber, laboratory experiments demonstrated an uptake after 48 h of up to 87% of U and Th in an acidic solution, with 65% sorbed within the first 8 h of exposure. The capacity of the Gaiasafe paper for U adsorption could be altered with the addition or removal of the iron oxide adsorbant; one iron atom was found to bind with 6.7 atoms of U in uranyl acetate form, 7.6 atoms of U in uranyl nitrate form and 5.2 Th atoms from thorium nitrate.

2.5.4.5 Scintillating sorptive membrane

A composite polymer membrane with liquid anion exchanger and scintillator molecules immobilized in it has been described by Das *et al*. [182] for the determination of anionic radionuclides. The membrane, after exposure, is removed from the bulk medium, washed, dried and mounted on the inside wall of a quartz cell for scintillation counting. Experiments run using TcO_4^- found that these ions were quantitively transferred to the membrane within a pH 2-8 operation range with an uptake efficiency of 95 ± 5%, and β counting efficiencies of 72%. This device has to date only been developed for β-emitters, and so may only be used for the isotopes ^{241}Pu, ^{231}Th and ^{234}Th, however, with a different scintillant, alpha scintillation could be possible. The high uptake efficiencies mean that this technique could be used in the determination of very low levels of actinides with further investigation into deployment housing. This type of membrane also has possibilities of being combined with another technique such as Chemcatcher® or DGT as it would provide an ideal receiving phase.

2.6 Conclusions and future work

The behaviour of actinide chemistry in aqueous environments is very complicated and requires further study. Much work, such as that undertaken by Allard and Rydberg [17, 27] has been undertaken on the behaviour Pu in natural waters for the purposes of waste stream characterisation from nuclear installations. U behaviour in natural waters is well documented in natural waters [80] in part due to its high natural abundance but also because of anthropogenic enrichment of particular isotopes during the nuclear fuel cycle. Th and Am are not as completely studied. Am, as a decay product of Pu, is generally included in studies of Pu behaviour, and Th as a highly particle reactive element with only one stable oxidation state is used as a tracer for particulate and biological fluxes in the natural environment [76]. Passive sampling techniques can provide a method to aid in a more complete assessment of actinide concentrations and speciation in natural waters, with Chemcatcher® and DGT most widely studied. Only preliminary studies have been undertaken combining passive sampling with actinide measurement [167, 183, 184] and have provided promising results. Future studies would include a more detailed analysis of optimum environmental operating conditions of resins in DGT and more field deployments. The evaluation of the Chemcatcher® and the application of SPE discs (such as the chelating or anion exchange discs provided by Empore) to the analysis of actinides in waters could further develop this technique. Due to the initial developmental work that has already been undertaken, the DGT technique would be the most suitable sampling method to progress further as an environmental monitoring tool.

2.7 References

[1] G.R. Choppin, Actinide speciation in aquatic systems, Marine Chemistry, 99 (2006) 83-92.

[2] B. Allard, J. Rydberg, behaviour of plutonium in natural waters, ACS Symposium Series, 216 (1983) 275-295.

[3] Environmental Permitting Regulations (England and Wales) 2010, in: 675, Department for Environment, Food and Agriculture, England and Wales, 2010, pp. 212.

[4] G.R. Choppin, Actinide speciation in the environment, Radiochimica Acta, 91 (2003) 645-649.

[5] J. Qiao, X. Hou, M. Miró, P. Roos, Determination of plutonium isotopes in waters and environmental solids: A review, Analytica Chimica Acta, 652 (2009) 66-84.

[6] K. Tagami, S. Uchida, Rapid uranium preconcentration and separation method from fresh water samples for total U and U-235/U-238 isotope ratio measurements by ICP-MS, Analytica Chimica Acta, 592 (2007) 101-105.

[7] C.C. May, P.J. Worsfold, M.J. Keith-Roach, Analytical techniques for speciation analysis of aqueous long-lived radionuclides in environmental matrices, Trac-Trends in Analytical Chemistry, 27 (2008) 160-168.

[8] M. Baskaran, G.H. Hong, P.H. Santschi Radionuclide Analysis in Seawater, in: O. Wurl (Ed.) Practical Guidelines for the Analysis of Seawater, CRC Press, Taylor and Francis Group, 2009, pp. 389.

[9] Environment Agency, Environmental Permitting Regulations, The Stationary Office, London, 2010, pp. 186.

[10] AWE Environmental Permit: Permit with introductory note, Environmental Permitting Regulations (2010), 2012, pp. 17.

[11] Environment Agency, Radioactive Substances Regulation – Environmental Principles, in: Radioactive Substances Regulation, Environment Agency, Bristol, 2010.

[12] G. Royston-Bishop, Environmental management: Best available techniques (BAT) case for Sellafield environmental monitoring programm., in, 2011, pp. 70.

[13] Environment Agency, Food Standards Agency, Northern Ireland Environment Agency, Scottish Environment Protection Agency, Radioactivity in Food and the Environment 2012, in, October 2013, pp. 258.

[14] Uranium in drinking water: background document for the development of WHO guidelines for drinking water quality, in, World Health Organisation, 2004, pp. 15.

[15] T. Bacquart, K. Bradshaw, S. Frisbie, E. Mitchell, G. Springston, J. Defelice, H. Dustin, B. Sarkar, A survey of arsenic, manganese, boron, thorium, and other toxic

metals in the groundwater of a West Bengal, India neighbourhood., Metallomics, 4 (2012) 653 - 659.
[16] Radiological Aspects, in: World Health Organisation Guidelines for drinking-water quality, incorporating 1st and 2nd addenda, Chapter 9, Geneva, 2008.
[17] G.R. Choppin, Actinide speciation in the environment, Journal of Radioanalytical Nuclear Chemistry, 273 (2007) 695-703.
[18] G.R. Choppin, B.E. Stout, Actinide behavior in natural-waters, Science of the Total Environment, 83 (1989) 203-216.
[19] N. Kaltsoyannis, P. Scott, The f elements, 1st ed., Oxford University Press, 2007.
[20] J. Lehto, X. Hou, Chemistry and analysis of radionuclides: laboratory techniques and methodology, Wiley-VCH, Weinheim, 2010.
[21] M. Ragheb, M. Khasawneh, Uranium fuel as a by-product of phosphate fertiliser production, in: 1st International Nuclear and Renewable Energy Conference (INREC), Amman, Jordan, 2010, pp. 1-15.
[22] R.F. Spalding, W.M. Sackett, Uranium runoff from the Gulf of Mexico: distribution province anomalous concentration, Science, 175 (1972) 629-631.
[23] M. Taylor, D., Accumulation of uranium in soils from impurities in phosphate fertilisers, Landbauforschung Volkenrode, 2 (2007) 133-137.
[24] T.J. Waples, C. Benitez-Nelson, N. Savoge, M.R. van der Loeff, M. Baskaran, O. Gustafsson, An introduction to the application and future use of Th-234 in aquatic systems, Marine Chemistry, 100 (2006) 166-189.
[25] A. Aarkog, K.O. Buesseler, R. Delfanti, K. Hirose, G. Hoon Hong, T. Ito, H.D. Livingston, H. Nies, V.E. Noshkin, P.P. Povinec, S. Shima, O. Togawa, Worldwide marine radioactivity studies (WOMARS): Radionuclide levels in oceans and seas, final report of a coordinated research project., in, IAEA, Vienna, 2005.
[26] R.L. Kathren, NORM sources and their origins, Applied Radiation and Isotopes, 49 (1998) 149-168.
[27] B. Allard, U. Olofsson, B. Torstenfelt, Environmental actinide chemistry, Inorganica Chimica Acta-F-Block Elements Articles and Letters, 94 (1984) 205-221.
[28] S. Cotton, The lanthanides and actinides, Macmillan Education Ltd, 1991.
[29] M. Mendes, J. Aupiais, C. Jutier, F. Pointurier, Determination of weight distribution ratios of Pa(V) and Np(V) with some extraction chromatography resins and the AG1-X8 resin, Analytica Chimica Acta, 780 (2013) 110-116.

[30] B.R. Harvey, L.M. Thurston, Analytical procedures for the determination of neptunium radionuclides in marine waters, sediments and biota., in, Centre of Food, Fisheries and the Aquatic Environment, Lowestoft, 1988.

[31] G.T. Seaborg, Overview of the actinide and lanthanide (the f) elements, Radiochimica Acta, 61 (1993) 115-122.

[32] G.T. Seaborg, A.C. Wahl, J.W. Kennedy, Radioactive element 94 from deuterons on uranium, Physical Review, 69 (1946) 367.

[33] J.W. Kennedy, G.T. Seaborg, E. Segrè, A.C. Wahl, Properties of 94(239), Physical Review, 70 (1946) 555.

[34] G.R. Choppin, Soluble Rare-Earth and Actinide Species in Seawater, Marine Chemistry, 28 (1989) 19-26.

[35] W. Geibert, M.M. Rutgers van der Loeff, C. Hanfland, H.J. Dauelsberg, Actinium-227 as a deep-sea tracer: sources, distribution and applications, Earth and Planetary Science Letters, 198 (2002) 147-165.

[36] W. Geibert, M. Charette, G. Kim, W.S. Moore, J. Street, M. Young, A. Paytan, The release of dissolved actinium to the ocean: A global comparison of different end-members, Marine Chemistry, 109 (2008) 409-420.

[37] P. van Beek, M. Souhaut, B. Lansard, M. Bourquin, J.L. Reyss, P. von Ballmoos, P. Jean, LAFARA: a new underground laboratory in the French Pyrénées for ultra low-level gamma-ray spectrometry, Journal of Environmental Radioactivity, 116 (2013) 152-158.

[38] Y. Nozaki, Excess ^{227}Ac in deep ocean water, Nature, 310 (1984) 486-488.

[39] D.R. Percival, D.B. Martin, Sequential determination of radium-226, radium-228, actinium-227, and thorium isotopes in environmental and process waste samples, Analytical Chemistry, 46 (1974) 1742-1749.

[40] S.A. Owens, K.O. Buesseler, K.W.W. Sims, Re-evaluating the ^{238}U-salinity relationship in seawater: Implications for the ^{238}U–^{234}Th disequilibrium method, Marine Chemistry, 127 (2011) 31-39.

[41] K.O. Buesseler, C. Benitez-Nelson, M. Rutgers van der Loeff, J. Andrews, L. Ball, G. Crossin, M.A. Charette, An intercomparison of small- and large-volume techniques for thorium-234 in seawater, Marine Chemistry, 74 (2001) 15-28.

[42] T. Cabianca, J. Carroll, N.S. Fisher, S.W. Fowler, P.J. Kershaw, Sediment distribution coefficients and concentration factors for biota in the marine environment, in: Technical Report Series, IAEA, Vienna, Austria, 2004, pp. 103.

[43] B. De Vivo, E.L. Ander, M. Bidovec, A. Lima, S. Pirc, S. Reeder, U. Sieqers, B. Smith, Distribution of elements in stream waters, in: W. De Vos, T. Tarvainen (Eds.) Geochemical atlas of Europe, Part 2, FOREGS, 2006, pp. 33-35.

[44] D.J. Assinder, S.M. Mudge, G.S. Bourne, Radiological assessment of the Ribble Estuary .1. Distribution of radionuclides in surface sediments, Journal of Environmental Radioactivity, 36 (1997) 1-19.

[45] A. Strezov, I. Yordanova, M. Pimpl, T. Stoilova, Natural radionuclide and plutonium content in Black Sea bottom sediments, Health Physics, 70 (1996) 70-80.

[46] R.F. Anderson, A.P. Fleer, Determination of natural actinides and plutonium in marine particulate material, Analytical Chemistry, 54 (1982) 1142-1147.

[47] G.R. Choppin, P.J. Wong, The chemistry of actinide behavior in marine systems, Aquatic Geochemistry, 4 (1998) 77-101.

[48] P.W. Swarzenski, M. Baskaran, Uranium distribution in the coastal waters and pore waters of Tampa Bay, Florida, Marine Chemistry, 104 (2007) 43-57.

[49] M.M. Sarin, S. Krishnaswami, B.L.K. somayajulu, W.S. Moore, Chemistry of uranium, thorium, and radium isotopes in the Ganga-Brahmaputra river system: Weathering processes and fluxes to the Bay of Bengal, Geochimica et Cosmochimica Acta, 54 (1990) 1387-1396.

[50] L.L. Vintro, P.I. Mitchell, A. Omarova, M. Burkitbayev, H.J. Napoles, N.D. Priest, Americium, plutonium and uranium contamination and speciation in well waters, streams and atomic lakes in the Sarzhal region of the Semipalatinsk Nuclear Test Site, Kazakhstan, Journal of Environmental Radioactivity, 100 (2009) 308-314.

[51] Argonne National Laboratory, Human Health Sheet: Neptunium, 2001.

[52] L.W. Cooper, J.M. Kelley, L.A. Bond, K.A. Orlandini, J.M. Grebmeier, Sources of the transuranic elements plutonium and neptunium in arctic marine sediments, Marine Chemistry, 69 (2000) 253-276.

[53] J. La Rosa, W. Burnett, S. Lee, I. Levy, J. Gastaud, P. Povinec, Separation of actinides, cesium and strontium from marine samples using extraction chromatography and sorbents, Journal of Radioanalytical and Nuclear Chemistry, 248 (2001) 765-770.

[54] J.J. Katz, G.T. Seaborg, L.R. Morss, The chemistry of the actinide elements, Chapman and Hall, 1986.

[55] D. Solatie, Development and comparison of analytical methods for the determination of uranium and plutonium in spent fuel and environmental samples., in: Faculty of Science, Department of Chemistry, Laboratory of Radiochemistry, University of Helsinki, Helsinki, 2002, pp. 54.

[56] P.I. Mitchell, J. Vives Batlle, T.P. Ryan, W.R. Schell, J.A. Sanchez-Cabeza, A. Vidal-Quadras, Studies on the speciation of plutonium, and americium in the Western Irish Sea, in: P.J. Kershaw, D.D. Woodhead (Eds.) Radionuclides in the study of marine processes, Springer, Netherlands, 1991, pp. 37-51.

[57] P.H. Santschi, J.W. Murray, M. Baskaran, C.R. Benitez-Nelson, L.D. Guo, C.C. Hung, C. Lamborg, S.B. Moran, U. Passow, M. Roy-Barman, Thorium speciation in seawater, Marine Chemistry, 100 (2006) 250-268.

[58] E.L. Cooper, M.K. Haas, J.F. Mattie, Studies of the speciation of plutonium and other actinides in natural groundwater using anion exchange resin, Applied Radiation and Isotopes, 46 (1995) 1159-1173.

[59] J.C. Laul, M.R. Smith, Disequilibrium Study of Natural Radionuclides in Groundwaters, Abstracts of Papers, American Chemical Society, 192 (1986) 99-Geoc.

[60] Q.H. Hu, M. Zavarin, T.P. Rose, Effect of reducing groundwater on the retardation of redox-sensitive radionuclides, Geochemical Transactions, 9 (2008).

[61] M.J. Keith-Roach, The speciation, stability, solubility and biodegradation of organic co-contaminant radionuclide complexes: A review, Science of the Total Environment, 396 (2008) 1-11.

[62] R.J. Silva, H. Nitsche, Actinide environmental chemistry, Radiochimica Acta, 70-1 (1995) 377-396.

[63] H. Lippold, J. Lippmann-Pipke, Effect of humic matter on metal adsorption onto clay materials: Testing the linear additive model, Journal of Contaminant Hydrology, 109 (2009) 40-48.

[64] H. Geckeis, T. Rabung, Actinide geochemistry: From the molecular level to the real system, Journal of Contaminant Hydrology, 102 (2008) 187-195.

[65] J.I. Kim, B. Kanellakopulos, Solubility products of plutonium (IV) oxide and hydroxide, Radiochimica Acta, 48 (1989) 145-150.

[66] D.I. Kaplan, E.L. Wilhite, Discovery of new plutonium chemistry and it's potential effect on LLW disposal at SRS, in, Westinghouse Savannah River Company, 2009.

[67] Z.Y. Tao, W.J. Li, F.M. Zhang, Y.Q. Ding, Z. Yu, Am(III) adsorption on oxides of aluminium and silicon: effects of humic substances, pH, and ionic strength, Journal of Colloid and Interface Science, 265 (2003) 221-226.

[68] H. Geckeis, T.N. Manh, M. Bouby, J.I. Kim, Aquatic colloids relevant to radionuclide migration: characterization by size fractionation and ICP-mass spectrometric detection, Colloids and Surfaces A. -Physicochemical Engineering Aspects, 217 (2003) 101-108.

[69] L. Chen, X.J. Yu, Z.D. Zhao, Y.H. Dong, The sorption of Th(IV) ions onto montmorillonite: the effect of pH, ionic strength and fulvic acid, Adsorption Science and Technology, 24 (2006) 301-310.
[70] R. Artinger, G. Buckau, P. Zeh, K. Geraedts, J. Vancluysen, A. Maes, J.I. Kim, Humic colloid mediated transport of tetravalent actinides and technetium, Radiochimica Acta, 91 (2003) 743-750.
[71] X.L. Tan, M. Fang, X.K. Wang, Sorption Speciation of Lanthanides/Actinides on Minerals by TRLFS, EXAFS and DFT Studies: A Review, Molecules, 15 (2010) 8431-8468.
[72] P.H. Santschi, K.A. Roberts, L.D. Guo, Organic mature of colloidal actinides transported in surface water environments, Environmental Science & Technology, 36 (2002) 3711-3719.
[73] A. Kowal-Fouchard, R. Drot, E. Simoni, J.J. Ehrhardt, Use of spectroscopic techniques for uranium (VI)/montmorillonite interaction modeling, Environmental Science & Technology, 38 (2004) 1399-1407.
[74] L. Guo, P.H. Santschi, M. Baskaran, Interactions of thorium isotopes with colloidal organic matter in oceanic environments, Colloids and Surfaces A: Physicochemical and Engineering Aspects, 120 (1997) 255-271.
[75] M.D. Siegel, C.R. Bryan, Environmental geochemistry of radioactive contamination, in: B.S. Lollar (Ed.) Environmental geochemistry, Elsevier, Oxford, 2005, pp. 631.
[76] K. Buesseler, L. Ball, J. Nadrews, C. Benitez-Nelson, R. Belastock, F. Chai, Y. Chao, Upper ocean export of particulate organic carbon in the Arabian Sea derived from throium-234, Deep Sea research II, 45 (1998) 2461-2487.
[77] K.O. Buesseler, C.R. Benitez-Nelson, S.B. Moran, A. Burd, M. Charette, J.K. Cochran, L. Coppola, N.S. Fisher, S.W. Fowler, W. Gardner, L.D. Guo, O. Gustafsson, C. Lamborg, P. Masque, J.C. Miquel, U. Passow, P.H. Santschi, N. Savoye, G. Stewart, T. Trull, An assessment of particulate organic carbon to thorium-234 ratios in the ocean and their impact on the application of Th-234 as a POC flux proxy, Marine Chemistry, 100 (2006) 213-233.
[78] P.W. Swarzenski, B.A. McKee, J.M. Skei, J.F. Todd, Uranium biogeochemistry across the redox transition zone of a permanently stratified fjord: Framvaren, Norway, Marine Chemistry, 67 (1999) 181-198.

[79] IAEA, Hanbook of parameter values for the prediction of radionuclide transfer in terrestrial and freshwater environments. Technical report series: 472., in, Vienna, 2010, pp. 208.
[80] R.M. Dunk, R.A. Mills, W.J. Jenkins, A reevaluation of the oceanic uranium budget for the Holocene, Chemical Geology, 190 (2002) 45-67.
[81] J.R. Lloyd, D.R. Lovley, Microbial detoxification of metals and radionuclides, Current Opinions in Biotechnology, 12 (2001) 248-253.
[82] Y. Zhengji, Microbial removal of uranyl by sulfate reducing bacteria in the presence of Fe (III) (hydr)oxides, Journal of Environmental Radioactivity, 101 (2010) 700-705.
[83] M.J. Wilkins, F.R. Livens, D.J. Vaughan, J.R. Lloyd, The impact of Fe(III)-reducing bacteria on uranium mobility, Biogeochemistry, 78 (2006) 125-150.
[84] M.A. Charette, W.S. Moore, W.C. Burnett, Chapter 5 Uranium- and Thorium-Series Nuclides as Tracers of Submarine Groundwater Discharge, in: S. Krishnaswami, J.K. Cochran (Eds.) Radioactivity in the Environment, Elsevier, 2008, pp. 155-191.
[85] M.A. Charette, M.C. Allen, Precision ground water sampling in coastal aquifers using a direct-push, shielded-screen well-point system, Ground Water Monitoring and Remediation, 26 (2006) 87-93.
[86] P. Swarzenski, P. Campbell, D. Porcelli, B. McKee, The estuarine chemistry and isotope systematics of U-234,U-238 in the Amazon and Fly Rivers, Continental and Shelf Research, 24 (2004) 2357-2372.
[87] W.G. Sutcliffe, R.H. Condit, W.G. Mansfield, D.S. Myers, D.W. Layton, P.W. Murphy, A perspective on the dangers of plutonium, in, Lawrence Livermore National Laboratory, 1995, pp. 14.
[88] J.M. Smoak, C. Benitez-Nelson, W.S. Moore, R.C. Thunell, Y. Astor, F. Muller-Karger, Radionuclide fluxes and particle scavenging in Cariaco Basin, Continental and Shelf Research, 24 (2004) 1451-1463.
[89] P.W. Swarzenski, M. Baskaran, Uranium distribution in the coastal waters and pore waters of Tampa Bay, Florida, Marine Chemistry, 104 (2007) 43-57.
[90] J.A. Sanchez-Cabeza, J. Merino, P. Masque, P.I. Mitchell, L.L. Vintro, W.R. Schell, L. Cross, A. Calbet, Concentrations of plutonium and americium in plankton from the western Mediterranean Sea, Science of the Total Environment, 311 (2003) 233-245.
[91] S. Cournane, L.L. Vintro, P.I. Mitchell, Modelling the reworking effects of bioturbation on the incorporation of radionuclides into the sediment column:

implications for the fate of particle-reactive radionuclides in Irish Sea sediments, Journal of Environmental Radioactivity, 101 (2010) 985-991.

[92] I.W. Croudace, P.E. Warwick, R.C. Greenwood, A novel approach for the rapid decomposition of Actinide^{TM} resin and its application to measurement of uranium and plutonium in natural waters, Analytica Chimica Acta, 577 (2006) 111-118.

[93] K.O. Buesseler, C. Benitez-Nelson, M.R. van der Loeff, J. Andrews, L. Ball, G. Crossin, M.A. Charette, An intercomparison of small- and large-volume techniques for thorium-234 in seawater, Marine Chemistry, 74 (2001) 15-28.

[94] T.P. Rao, P. Metilda, J.M. Gladis, Preconcentration techniques for uranium(VI) and thorium(IV) prior to analytical determination—an overview, Talanta, 68 (2006) 1047-1064.

[95] G. Koulouris, B. Slowikowski, R. Pilvio, T. Bostrom, M. Bickel, Pre-concentration of actinoids from waters: a comparison of various sorbents, Applied Radiation and Isotopes, 53 (2000) 279-287.

[96] W.S. Moore, D.F. Reid, Extraction of radium fro natural waters using manganese impregnated acrylic fibers Journal of Geophysical Research, 78 (1973) 8880-8886.

[97] D.S. Moon, W.C. Burnett, S. Nour, P. Horwitz, A. Bond, Preconcentration of radium isotopes from natural waters using MnO_2 Resin, Applied Radiation and Isotopes, 59 (2003) 255-262.

[98] J. Eikenberg, A. Tricca, G. Vezzu, S. Bajo, M. Ruethi, H. Surbeck, Determination of Ra-228, Ra-226 and Ra-224 in natural water via adsorption on MnO_2-coated discs, Journal of Environmental Radioactivity, 54 (2001) 109-131.

[99] J.L. Burnett, I.W. Croudace, P.E. Warwick, Pre-concentration of naturally occurring radionuclides and the determination of ^{212}Pb from fresh waters, Journal of Environmental Radioactivity, 102 (2011) 4.

[100] C.M. Hutchins, J.G. Panther, P.R. Teasdale, F. Wang, R.R. Stewart, W.W. Bennett, H. Zhao, Evaluation of a titanium dioxide-based DGT technique for measuring inorganic uranium species in fresh and marine waters, Talanta, 97 (2012) 550-556.

[101] R. Chiarizia, E.P. Horwitz, S.D. Alexandratos, M.J. Gula, Diphonix(R) resin: A review of its properties and applications, Separation Science Technology, 32 (1997) 1-35.

[102] N.C. Oboyle, G.P. Nicholson, T.J. Piper, D.M. Taylor, D.R. Williams, G. Williams, A review of plutonium(IV) selective ligands, Applied Radiation and Isotopes, 48 (1997) 183-200.

[103] E.P. Horwitz, R. Chiarizia, H. Diamond, R.C. Gatrone, S.D. Alexandratos, A.Q. Trochimczuk, D.W. Crick, Uptake of metal-ions by a new chelating ion-exchange resin. 1. Acid dependencies of actinide ions, Solvent Extraction and Ion Exchange, 11 (1993) 943-966.

[104] H. Surbeck, Alpha spectrometry sample preparation using selectively adsorbing thin films, Applied Radiation and Isotopes, 53 (2000) 97-100.

[105] E.P. Horwitz, R. Chiarizia, M.L. Dietz, DIPEX: A new extraction chromatographic material for the separation and preconcentration of actinides from aqueous solution, Reactional and Functional Polymers, 33 (1997) 25-36.

[106] P.J.M. Kwakman, M. Witte, Determination of gross alpha in drinking water and nuclear waste water using Actinide Resin^{TM} and LSC, in: P. Warwick (Ed.) Environmental Radiochemical Analysis, Royal Society Chemistry, Cambridge, 2003, pp. 354-359.

[107] J.D. Navratil, Wastewater treatment technology based on iron oxides, in: P. Misaelides, F. Macasek, T.J. Pinnavaia, C. Colella (Eds.) Natural Microporous Materials in Environmental Technology, Springer, Dordrecht, 1999, pp. 417-424.

[108] L. Saarinen, J. Suksi, Determination of uranium series radionuclides Pa-231 and Ra-226 by liquid scintillation counting, in, Nuclear Waste Commission of the Finnish Power Companies, Helsinki, 1992.

[109] T. Sasaki, Y. Komatsu, Y. Fujiki, Ion-exchange properties of hydrouse titanium dioxide with a fibrous form obtained from potassium dititanate, Solvent Extraction and Ion Exchange, 1 (1983) 775-790.

[110] C. Heitner-Wirguin, A. Albu-Yaron, Hydrous oxides and their cation exchange properties--II Structure and equilibrium experiments, Journal of Inorganic and Nuclear Chemistry, 28 (1966) 2379-2384.

[111] T.E. Payne, J.A. Davis, G.R. Lumpkin, R. Chisari, T.D. Waite, Surface complexation model of uranyl sorption on Georgia kaolinite, Applied Clay Science, 26 (2004) 151-162.

[112] A.M. Jakobsson, Measurement and modeling of Th sorption onto TiO_2, Journal of Colloid and Interface Science, 220 (1999) 367-373.

[113] Z.J. Guo, L.J. Niu, Z.Y. Tao, Sorption of Th(IV) ions onto TiO_2: Effects of contact time, ionic strength, thorium concentration and phosphate, Journal of Radioanalytical and Nuclear Chemistry, 266 (2005) 333-338.

[114] Z.J. Guo, Y.N. Niu, W.G. Zhang, M.Y. Tan, Liquid-liquid extraction of thorium(IV) and uranium(VI) with three ether-amide type tripodands, Journal of Radioanalytical and Nuclear Chemistry, 262 (2004) 331-337.
[115] X.L. Tan, X.K. Wang, C.L. Chen, A.H. Sun, Effect of soil humic and fulvic acids, pH and ionic strength on Th(IV) sorption to TiO_2 nanoparticles, Applied Radiation and Isotoes, 65 (2007) 375-381.
[116] J. Vandenborre, R. Drot, E. Simoni, Interaction mechanisms between uranium(VI) and rutile titanium dioxide: From single crystal to powder, Inorganic Chemistry, 46 (2007) 1291-1296.
[117] M. Olsson, A.M. Jakobsson, Y. Albinsson, Sorption of Pu(VI) onto TiO2, Journal of Colloid and Interface Science, 266 (2003) 269-275.
[118] W.J. Li, J.J. Zhao, C.S. Li, S. Kiser, R.J. Cornett, Speciation measurements of uranium in alkaline waters using diffusive gradients in thin films technique, Analytica Chimica Acta, 575 (2006) 274-280.
[119] W.J. Li, C.S. Li, J.J. Zhao, R.J. Cornett, Diffusive gradients in thin films technique for uranium measurements in river water, Analytica Chimica Acta, 592 (2007) 106-113.
[120] H. Vandenhove, K. Antunes, J. Wannijn, L. Duquene, M.V. Hees, Method of diffusive gradients in thin films (DGT) compared with other soil testing methods to predict uranium phytoavailability, Science of the Total Environment, 373 (2007) 542-555.
[121] L. Duquène, H. Vandenhove, F. Tack, M. Van Hees, J. Wannijn, Diffusive gradient in thin films (DGT) compared with soil solution and labile uranium fraction for predicting uranium bioavailability to ryegrass, Journal of Environmental Radioactivity, 101 (2010) 140-147.
[122] D.H. Phillips, B. Gu, D.B. Watson, C.S. Parmele, Uranium removal from contaminated groundwater by synthetic resins, Water Research, 42 (2008) 260-268.
[123] Y. Muramatsu, S. Yoshida, K. Tagami, S. Uchida, W. Ruhm, ICP-MS analysis of environmental plutonium, in: A. Kudo (Ed.) Plutonium in the Environment, Elsevier Science Bv, Amsterdam, 2001, pp. 63-77.
[124] D.D. Rao, V. Sudheendran, P.K. Sarkar, Optimization of parameters of alpha spectrometry with silicon detector for low level measurements of actinides in environmental samples, Applied Radiation and Isotopes, 70 (2012) 1519-1525.
[125] S.R. Yousefi, S.J. Ahmadi, F. Shemirani, M.R. Jamali, M. Salavati-Niasari, Simultaneous extraction and preconcentration of uranium and thorium in aqueous

samples by new modified mesoporous silica prior to inductively coupled plasma optical emission spectrometry determination, Talanta, 80 (2009) 212-217.
[126] S. Carter, A.S. Fisher, P.S. Goodall, M.W. Hinds, S. Lancaster, S. Shore, Atomic spectrometry update. Industrial analysis: metals, chemicals and advanced materials, Journal of Analytical Atomic Spectrometry, 25 (2010) 1808-1858.
[127] W.R. Kelly, B.S. MacDonald, W.F. Guthrie, Gravimetric approach to the standard addition method in instrument analysis. 1., Analytical Chemistry, 80 (2008) 8154-8158.
[128] R.N. Taylor, T. Warneke, J.A. Milton, I.W. Croudace, P.E. Warwick, R.W. Nesbitt, Multiple ion counting determination of plutonium isotope ratios using multi-collector ICP-MS, Journal of Analytical Atomic Spectrometry, 18 (2003) 480-484.
[129] J.S. Santos, L.S.G. Teixeira, W.N.L. dos Santos, V.A. Lemos, J.M. Godoy, S.L.C. Ferreira, Uranium determination using atomic spectrometric techniques: An overview, Analytica Chimica Acta, 674 (2010) 143-156.
[130] Y. Sohrin, S. Iwamoto, S. Akiyama, T. Fujita, T. Kugii, H. Obata, E. Nakayama, S. Goda, Y. Fujishima, H. Hasegawa, K. Ueda, M. Matsui, Determination of trace elements in seawater by fluorinated metal alkoxide glass-immobilized 8-hydroxyquinoline concentration and high-resolution inductively coupled plasma mass spectrometry detection, Analytica Chimica Acta, 363 (1998) 11-19.
[131] K. Oshita, M. Oshima, Y.H. Gao, K.H. Lee, S. Motomizu, Synthesis of novel chitosan resin derivatized with serine moiety for the column collection/concentration of uranium and the determination of uranium by ICP-MS, Analytica Chimica Acta, 480 (2003) 239-249.
[132] P. Leonhard, R. Pepelnik, A. Prange, N. Yamada, T. Yamada, Analysis of diluted sea-water at the ng L-1 level using an ICP-MS with an octopole reaction cell, Journal of Analytical Atomic Spectrometry, 17 (2002) 189-196.
[133] T.C. Kenna, F.L. Sayles, The distribution and history of nuclear weapons related contamination in sediments from the Ob River, Siberia as determined by isotopic ratios of plutonium and neptunium, Journal of Environmental Radioactivity, 60 (2002) 105-137.
[134] D. Beauchemin, Inductively coupled plasma mass spectrometry, Analytical Chemistry, 80 (2008) 4455 - 4486.
[135] J.H. Aldstadt, J.M. Kuo, L.L. Smith, M.D. Erickson, Determination of uranium by flow injection inductively coupled plasma mass spectrometry, Analytica Chimica Acta, 319 (1996) 135-143.

[136] M. Huang, H. Kojima, T. Shirasaki, A. Hirabayashi, H. Koizumi, Study on solvent-loading effect on inductively coupled plasma and microwave-induced plasma sources with a microliter nebulizer, Analytica Chimica Acta, 413 (2000) 217-222.
[137] F.A. Aydin, M. Soylak, Solid phase extraction and preconcentration of uranium(VI) and thorium(IV) on Duolite XAD761 prior to their inductively coupled plasma mass spectrometric determination, Talanta, 72 (2007) 187-192.
[138] K. Ramakumar, S. Jeyakumar, R. Rao, L. Gnanayyan, H. Jain, Simultaneous analysis of uranium and plutonium using thermal ionization mass spectrometry, Journal of Radioanalytical and Nuclear Chemistry, 190 (1995) 121-136.
[139] K.G. Heumann, Isotope-dilution mass-spectrometry, International Journal of Mass Spectrometry and Ion Processes, 118 (1992) 575-592.
[140] R.N. Taylor, T. Warneke, J.A. Milton, I.W. Croudace, P.E. Warwick, R.W. Nesbitt, Plutonium isotope ratio analysis at femtogram to nanogram levels by multicollector ICP-MS, Journal of Analytical Atomic Spectrometry, 16 (2001) 279-284.
[141] P.E. Warwick, I.W. Croudace, J.S. Oh, Radiochemical Determination of ^{241}Am and Pu in Environmental Materials, Analytical Chemistry, 73 (2001) 3410 - 3416.
[142] G.A. Mills, R. Greenwood, I.J. Allan, E. Lopuchin, J. Brummer, J. Knutsson, B. Vrana, Application of passive sampling techniques for monitoring the aquatic environment, in: J. Namiesnik, P. Szeter (Eds.) Analytical measurements in aquatic environments, CRC Press, 2009.
[143] R.J.K. Dunn, P.R. Teasdale, J. Warnken, M.A. Jordan, J.M. Arthur, Evaluation of the in situ, time-integrated DGT technique by monitoring changes in heavy metal concentrations in estuarine waters, Environmental Pollution, 148 (2007) 213-220.
[144] R.J.K. Dunn, P.R. Teasdale, J. Warnken, R.R. Schleich, Evaluation of the diffusive gradient in a thin film technique for monitoring trace metal concentrations in estuarine waters, Environmental Science & Technology, 37 (2003) 2794-2800.
[145] N. Montero, M.J. Belzunce-Segarra, J.L. Gonzalez, J. Larreta, J. Franco, Evaluation of diffusive gradients in thin-films (DGTs) as a monitoring tool for the assessment of the chemical status of transitional waters within the Water Framework Directive, Marine Pollution Bulletin, 64 (2012) 31-39.
[146] Z. Tosheva, H. Hofmann, A. Kies, Spatial distribution investigation of radioactivity of potable waters in Luxembourg, Journal of Radioanalytical and Nuclear Chemistry, 282 (2009) 501-505.
[147] J. Salanki, A. Farkas, T. Kamardina, K.S. Rozsa, Molluscs in biological monitoring of water quality, Toxicology Letters, 140 (2003) 403-410.

[148] Z. Kljakovic-Gaspic, I. Ujevic, T. Zvonaric, A. Baric, Biomonitoring of trace metals (Cu, Cd, Cr, Hg, Pb, Zn) in Mali ston bay (eastern Adriatic) using the Mediterranean blue mussel (1998-2005), Acta Adriatica, 48 (2007) 73-88.

[149] Z. Dragun, M. Podrug, B. Raspor, Combined use of bioindicators and passive samplers for the assessment of river water contamination with metals, Archives of Environmental Contamination and Toxicology, 57 (2009) 211-220.

[150] E.E. Ukpebor, J.E. Ukpebor, E. Aigbokhan, I. Goji, A.O. Onojeghuo, A.C. Okonkwo, Delonix regia and Casuarina equisetifolia as passive biomonitors and as bioaccumulators of atmospheric trace metals, Journal of Environmental Science, 22 (2010) 1073-1079.

[151] M. Rajfur, A. Klos, M. Waclawek, bioaccumulation of heavy metals in aquatic plants using the example of *Elodea canadensis Michx*, in: M. Waclawek (Ed.) Proceedings of Ecopole, Vol 4, No 1, Opole Univ, Opole, 2010, pp. 193-198.

[152] K.J. Appenroth, K. Krech, A. Keresztes, W. Fischer, H. Koloczek, Effects of nickel on the chloroplasts of the duckweeds Spirodela polyrhiza and Lemna minor and their possible use in biomonitoring and phytoremediation, Chemosphere, 78 (2010) 216-223.

[153] P. Zoriy, P. Ostapczuk, H. Dederichs, J. Hobig, R. Lennartz, M. Zoriy, Biomonitoring of environmental pollution by thorium and uranium in selected regions of the Republic of Kazakhstan, Journal of Environmental Radioactivity, 101 (2010) 414-420.

[154] J. Burger, M. Gochfeld, D.S. Kosson, C.W. Powers, S. Jewett, B. Friedlander, H. Chenelot, C.D. Volz, C. Jeitner, Radionuclides in marine macroalgae from Amchitka and Kiska Islands in the Aleutians: establishing a baseline for future biomonitoring, Journal of Environmental Radioactivity, 91 (2006) 27-40.

[155] J.W. Grate, O.B. Egorov, M.J. O'Hara, T.A. Devol, Radionuclide sensors for environmental monitoring: From flow injection solid-phase absorptiometry to equilibration-based preconcentrating minicolumn sensors with radiometric detection, Chemical Reviews, 108 (2008) 543-562.

[156] O.B. Egorov, M.J. O'Hara, J.W. Grate, Equilibration-based preconcentrating minicolumn sensors for trace level monitoring of radionuclides and metal ions in water without consumable reagents, Analytical Chemistry, 78 (2006) 5480-5490.

[157] O.B. Egorov, S.K. Fiskum, M.J. O'Hara, J.W. Grate, Radionuclide sensors based on chemically selective scintillating microspheres: Renewable column sensor for analysis of Tc-99 in water, Analytical Chemistry, 71 (1999) 5420-5429.

[158] T.A. DeVol, M.E. Keillor, L.W. Burggraf, Influence of radionuclide adsorption on detection efficiency and energy resolution for flow-cell radiation detectors, IEEE Transactions on Nuclear Science, 43 (1996) 1310-1315.
[159] D.D. Russell, W.B. Knowlton, Field portable electrochemical sensor for uranium and other actinides, in: U.P. Office (Ed.) Patent Application Publication, Boise State University, United States of America, 2006.
[160] N.W. Hayes, C.J. Tremlett, P.J. Melfi, J.D. Sessler, A.M. Shaw, Fibre optic system for detection of uranyl ions in the solution phase - art. no. 673917, in: G.W. Kamerman, O.K. Steinvall, K.L. Lewis, K.A. Krapels, J.C. Carrano, A. Zukauskas (Eds.) Electro-optical remote sensing, detection, and photonic technologies and their applications, Spie-International Society for Optical Engineering, Bellingham, 2007, pp. 73917-73917.
[161] M. Beck, O. Dellwig, K. Kolditz, H. Freund, G. Liebezeit, B. Schnetger, H.J. Brumsack, In situ pore water sampling in deep intertidal flat sediments, Limnology and Oceanography Methods, 5 (2007) 136-144.
[162] D. Robertson, P.R. Teasdale, D.T. Welsh, A novel gel-based technique for the high resolution, two-dimensional determination of iron (II) and sulfide in sediment, Limnology and Oceanography Methods, 6 (2008) 502-512.
[163] H. Zhang, W. Davison, R.J.G. Mortimer, M.D. Krom, P.J. Hayes, I.M. Davies, Localised remobilization of metals in a marine sediment, Science of the Total Environment, 296 (2002) 175-187.
[164] B. Docekal, M. Gregusova, Segmented sediment probe for diffusive gradient in thin films technique, Analyst, 137 (2012) 502-507.
[165] M. Schintu, B. Marras, L. Durante, P. Meloni, A. Contu, Macroalgae and DGT as indicators of available trace metals in marine coastal waters near a lead-zinc smelter, Environmental Monitoring and Assessment, 167 (2010) 653-661.
[166] J.E. Sherwood, D. Barnett, N.W. Barnett, K. Dover, J. Howitt, H. Ii, P. Kew, J. Mondon, Deployment of DGT units in marine waters to assess the environmental risk from a deep sea tailings outfall, Analytica Chimica Acta, 652 (2009) 215-223.
[167] W.J. Li, C.S. Li, J.J. Zhao, R.J. Cornett, Diffusive gradients in thin films technique for uranium measurements in river water, Analytica Chimica Acta, 592 (2007) 106-113.
[168] B. Vrana, G.A. Mills, I.J. Allan, E. Dominiak, K. Svensson, J. Knutsson, G. Morrison, R. Greenwood, Passive sampling techniques for monitoring pollutants in water, Trac-Trends in Analytical Chemistry, 24 (2005) 845-868.

[169] G. Ouyang, Y. Chen, J. Pawliszyn, Time-weighted average water sampling with a solid-phase microextraction device, Analytical Chemistry, 77 (2005) 7319-7325.
[170] H. Zhang, W. Davison, In situ speciation measurements. Using diffusive gradients in thin films (DGT) to determine inorganically and organically complexed metals, Pure and Applied Chemistry, 73 (2001) 9-15.
[171] W. Davison, H. Zhang, Progress in understanding the use of diffusive gradients in thin films (DGT) – back to basics, Environmental Chemistry, 9 (2012) 1-13.
[172] M.A. French, H. Zhang, J.M. Pates, S.E. Bryan, R.C. Wilson, Development and performance of the diffusive gradients in thin-films technique for the measurement of technetium-99 in seawater, Analytical Chemistry, 77 (2005) 4.
[173] M. Gregusova, B. Docekal, New resin gel for uranium determination by diffusive gradient in thin films technique, Analytica Chimica Acta, 684 (2011) 142-146.
[174] R. Haas, Pfeiffer, F. and Tsivunchyk, O., Purification of acitnide-containing water with Gaiasafe filter papers, Functional Materials, 10 (2003) 4.
[175] J.J. Pittman, V. Klep, I. Luzinov, R.K. Marcus, Extraction of metals from aqueous systems employing capillary-channeled polymer (C-CP) fibers modified with poly(acrylic acid) (PAA), Analytical Methods, 2 (2010) 461-469.
[176] W. Davison, Fones G., Harper, M., Teasdale, P. And Zhang, H, Dialysis, DET and DGT: *In situ* diffusional techniques for studying water, sediments and soils., in: J. Buffle, Horvai, G. (Ed.) *In situ* monitoring of aquatic systems: chemical analysis and speciation, John Wiley & Sons Ltd, 2000, pp. 74.
[177] Y. Gao, L. Lesven, D. Gillan, K. Sabbe, G. Billon, S. De Galan, M. Elskens, W. Baeyens, M. Leermakers, Geochemical behavior of trace elements in sub-tidal marine sediments of the Belgian coast, Marine Chemistry, 117 (2009) 88-96.
[178] D. Shi, S. Ding, D. Xu, X. Bai, C. Fan, Determination of soluble reactive phosphorus in porewaters of sediments using the technique of diffusive equilibration in thin films, Hupo Kexue, 21 (2009) 768-774.
[179] L. Lesven, Y. Gao, G. Billon, M. Leermakers, B. Ouddane, J.C. Fischer, W. Baeyens, Early diagenetic processes aspects controlling the mobility of dissolved trace metals in three riverine sediment columns, Science of the Total Environment, 407 (2008) 447-459.
[180] J. Morford, L. Kalnejais, W. Martin, R. François, I.-M. Karle, Sampling marine pore waters for Mn, Fe, U, Re and Mo: modifications on diffusional equilibration thin film gel probes, Journal of Experimental Marine Biology and Ecology, 285–286 (2003) 85-103.

[181] Haas, R., Pfeiffer, F., Water-Monitoring in an WWII explosive factory with Gaiasafe Passive Collectors, http://www.gaiasafe.de/popsclz.pdf.

[182] S. Das, S. Chakraborty, S. Sodaye, A.K. Pandey, A.V.R. Reddy, Scintillating adsorptive membrane for preconcentration and determination of anionic radionuclides in aqueous samples, Analytical Methods, 2 (2010) 728-733.

[183] H.Q. Liao, J. Zheng, F.C. Wu, M. Yamada, M.G. Tan, J.M. Chen, Determination of plutonium isotopes in freshwater lake sediments by sector-field ICP-MS after separation using ion-exchange chromatography, Applied Radiation and Isotopes, 66 (2008) 1138-1145.

[184] W.J. Li, J.J. Zhao, C.S. Li, S. Kiser, R.J. Cornett, Speciation measurements of uranium in alkaline waters using diffusive gradients in thin films technique, Analytical Chimica Acta, 575 (2006) 274-280.

Chapter 3: General experimental

The organisation of the thesis provides each chapter with a methodologies section. This chapter provides an overview for each technique used.

3.1 Diffusive gradients in thin films (DGT)

3.1.1 Principles and calculations

Diffusive gradients in thin films (DGT) was developed in 1993 (the year the patent was filed) by Hao and Davison [1] as a technique to measure dissolved metals in natural waters. It has since been applied to various environmental measurement fields such as environmental monitoring [2], speciation measurements [3], metal in pore-water measurements [4], nutrient measurement [5], bioavailability predictions [6, 7] and in assessing the ecological status of rivers [8]. DGT measures the labile dissolved fraction of analytes *in situ* over a defined deployment time to give a time weighted average (TWA) value that provides information of an average measurement of an analyte that accounts for fluctuations in concentrations [9]. This is particularly practical in highly fluctuating environments, such as estuaries [10] or rivers [11] where routine grab sampling may miss episodic concentration peaks or troughs, thereby over- or under-estimating bulk solution concentrations.

The device consists of three layers: (i) a binding agent, which contains a resin or functional groups selective to the target ions, held in a thin layer of hydrogel (binding gel); (ii) a layer of hydrogel of known thickness, which serves as the diffusive layer; and (iii) a protective outer membrane with a known pore size. A diffusive boundary layer (DBL) that forms on the exposed face of the device must also be accounted for and added to the diffusive layer. This is an effective extension of the diffusive layer. Figure 3.1 below illustrates the various layers of the DGT device.

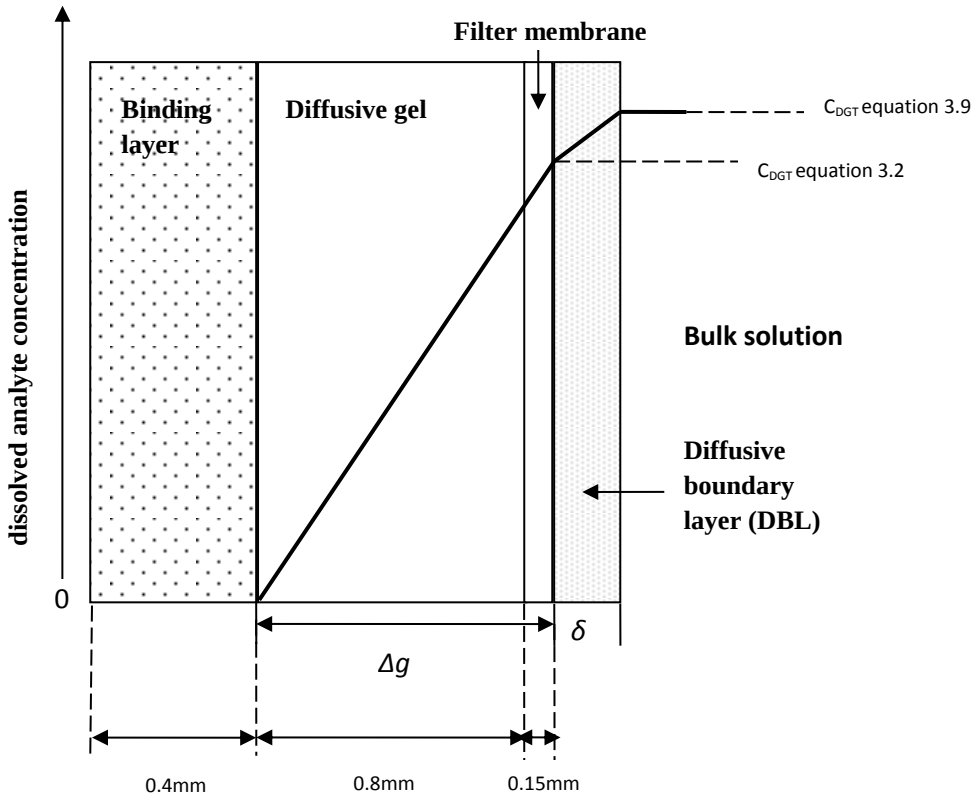

Figure 3.1 Schematic of DGT assembly showing the diffusive layers, concentration gradient and associated equations.

DGT is based on the establishment of a quasi steady state concentration gradient in a hydrogel used to separate an analyte specific resin from the bulk solution, according to Fick's first law of diffusion. It separates the target ions kinetically and is operational within a linear uptake phase of a passive sampler.

The flux (J) of the target ion(s) to the resin through the hydrogel at a particular rate (or diffusion coefficient D, $cm^2\ s^{-1}$) across a well defined diffusion distance (Δg) can be described by Fick's first law of diffusion where the flux is a function of the diffusion coefficient and the concentration gradient [12, 13]:

$$J = \frac{DC}{\Delta g} \qquad \text{Equation 3.1}$$

where C is the concentration of the diffusing species at the interface between the solution and the diffusion interface. Knowing the deployment time (t, s), the surface area over which the target ion is diffusing (A, cm^2), and assuming that the target ions are irreversibly bound to a resin or sorbent with an excess of binding sites (so that there is

no limitation or capacity issue) then a time weighted average value (C_{DGT}, µg L^{-1}) of a bulk solution concentration can be calculated over a defined deployment time using:

$$C_{DGT}=\frac{M\Delta g}{DtA} \quad \text{Equation 3.2}$$

where *M* is the absolute mass of the analyte accumulated on the resin phase. *M* can be calculated using equation 3.3, taking into account the gel volume (*Vg*, cm^3), the eluent volume (*Ve*, mL), the measured concentration of U in the eluent (*Ce*, ng mL^{-1}) and the elution factor (*fe*) [3].

$$M = \frac{Ce(Vg+Ve)}{fe} \quad \text{Equation 3.3}$$

After deployment, the resin layer is peeled from the diffusive layer and the metal ions accumulated in the resin layer are eluted and the concentration of the target ion (uranium (U) in this instance) is measured to give the U concentration (*Ce*). This project used the measurement method inductively coupled plasma mass spectrometry (ICP-MS) to give µg L^{-1} from the eluent (which in this case was multiplied by the dilution factor (×10)), although other techniques could be used, as discussed in Chapter 2.

The elution factor (*fe*) can be determined for the resin used by undertaking batch experiments and calculating the mass balance of the analyte between the solution and solid phase, or taken from literature values if this has already been determined for the analyte and resin specifically.

The uptake of U is found by exposing a known amount of the resin-gel to a known mass of U. A mass balance is calculated by measuring the mass of U in the exposure solution before and after exposure to the resin-gel: mass of U in solution prior to exposure to resin-gel minus mass of U in solution after exposure to resin-gel is equal to the mass of U taken up by resin-gel minus the blank measurement (mass of U sorbed to vessel walls). The elution factor is found by determining the mass of U eluted from the resin gel minus the blank measurement (mass of U eluted from resin-gel that has not been exposed to a solution containing U) as a ratio of the mass of U initially taken up by the resin-gel (from the mass balance calculations).

This project has determined the elution factors for all resins trialled rather than using a generic literature value. Chapter 4, section 4.2.4.1 ‘Uptake of U and elution efficiencies of the test resins’ details the method used to determine the elution

efficiencies of U for Chelex-100, Metsorb^{TM} and MnO_2 resins. Chapter 6, section 6.2.4.1 details the method used to determine the elution efficiency of the Diphonix® resin.

Diffusion coefficients (D, cm^2 s^{-1}) for U in the polyacrylamide gel were determined at various pH's by Hutchins *et al.* [14] from mass accumulation of U on to DGT devices over time during a laboratory tank deployment. The diffusion coefficient was calculated using the slope (α) of the linear regression of the mass of U (ng) accumulated in the Metsorb binding gel over time (s), the thickness of the diffusive layer (diffusive gel and filter membrane, Δg, cm), the area of the diffusive layer available for diffusion (A, cm^2) and the bulk concentration of the U of the deployment solution (C, ng mL^{-1}), as per equation 3.4:

$$D = \frac{\alpha \Delta g}{AC} \qquad \text{Equation 3.4}$$

The study by Hutchins *et al.* [14] measured the diffusion coefficients at 26^{o}C at pH values ranging from 3 to 8.1 (shown in Table 3.1 below). The uncertainties associated with each of the diffusion coefficient values represent the uncertainty of the slope (α) of the mass accumulation with time plots and the standard deviation of replicate measurements of the solution U concentration.

The diffusion coefficients (D) were corrected for temperature (T, ^{o}C) using the Stokes-Einstein equation (equation 3.5) [15] and the viscosity of water (η, mPa s) [16]:

$$\frac{D_1 \eta_1}{T_1} = \frac{D_2 \eta_2}{T_2} \qquad \text{Equation 3.5}$$

Diffusion coefficients used for sea water were 10% lower than fresh water [13], due to increased viscosity of higher ionic strength solutions.

Table 3.1 Diffusion coefficients of uranium in polyacrylamide gel (D_{gel}) in low ionic strength solutions (I = 0.01 M) across a range of pH values used in this study, from Hutchins *et al*. [14].

pH	**Diffusion coefficient at 26°C (x 10^{-6} cm^2 s^{-1})**
3.0	2.74 ± 0.14
3.5	3.22 ± 0.13
4.9	4.65 ± 0.27
6.0	3.71 ± 0.11
6.5	3.72 ± 0.27
7.0	3.11 ± 0.27
7.7	4.81 ± 0.54
8.1	4.44 ± 0.21

The diffusive boundary layer (δ) thickness was calculated using equation 3.6 after Warnken *et al.* [17] . Multiple devices with varying diffusive gel layer thickness (for instance 0.015 cm (filter only), 0.055 cm, 0.095 cm and 0.135 cm, including the filter membrane thickness of 0.015 cm) are deployed, and the reciprocal of the mass (*1/M*) accumulated by the devices plotted in straight line plot against the changing diffusive layer thickness (Δg). This plot of *1/M* vs Δg has a slope (m) of $1/(D_M^{gel} C_{DGT} At)$ and an intercept (b) of $\delta/(D_M^W C_{DGT} At)$, as per equation 3.7. The intercept (b) divided by the slope (m) of this plot gives the diffusive boundary layer thickness δ, as per equation 3.7, and also considers any discrepancy in diffusion coefficients of U in the gel (Δg) and the water (δ) where D_M^W and D_M^{gel} represent the diffusion coefficients of U in water and in the diffusive gel respectively.

$$\delta = \frac{b}{m}\left(\frac{D_M^W}{D_M^{gel}}\right) \qquad \text{Equation 3.6}$$

$$\frac{1}{M} = \frac{\Delta g}{D_M^{gel} C_{DGT} At} + \frac{\delta}{D_M^W C_{DGT} At} \qquad \text{Equation 3.7}$$

An alternative to equation 3.2 uses the slope (m) from the plot of equation 3.7. The C_{DGT} can is then calculated using equation 3.8 [18], which accounts for reciprocal of the slope from the linear regression of the plot of equation 3.7:

$$C_{DGT} = \frac{1}{M D_M^{gel} At} \qquad \text{Equation 3.8}$$

It is important to account for the discrepancy in the diffusion coefficients between the gel and the aqueous phases if the DBL is present. A recent study by Kerisit & Liu [19] has shown that U diffusion coefficients in aqueous solutions vary with U speciation [19]. Table 3.2 below details the self diffusion of uranyl carbonate and alkaline-earth uranyl carbonate species modelling at 25^{o}C, as detailed by Kerisit & Liu [19].

Table 3.2 Self diffusion coefficients of uranyl carbonate and alkaline-earth uranyl carbonate species, modelled at 25 ^{o}C, after Kerisit & Liu [19] unless specified.

Species	**Diffusion coefficient at 25^{o}C (x 10^{-6} cm^2 s^{-1})**
UO_2CO_3	6.67
$UO_2(CO_3)_2^{2-}$	5.52
$UO_2(CO_3)_3^{4-}$	5.52
$CaUO_2(CO_3)_3^{2-}$	5.06
$Ca_2UO_2(CO_3)_3$	4.60
UO_2^{2+}	7.59 [20]

It is not certain that diffusion coefficients for U in the diffusive gel do not change with U speciation. Hutchins *et al*. [14] only examined diffusion coefficients with changing pH, which only accounts for the carbonate and hydrolysed U species. The data presented by Kerisit & Liu [19] in Table 3.2 demonstrates that U diffusion coefficients change with alkaline-earth uranyl carbonate species. It stands to reason that U diffusion coefficients in the diffusive gel would also change with calcium-carbonate complexation. This is an area that requires further research.

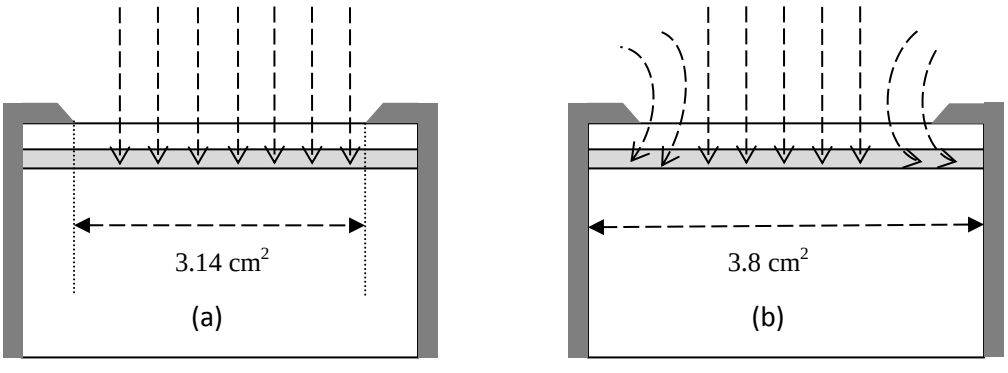

Figure 3.2 Schematic of DGT piston gel layers showing the diffusional pathways into the DGT devices (not accounting the presence of a DBL). (a) shows the physical geometric area of 3.14 cm^2 and is considered in equation 3.2; (b) allows for lateral diffusion at the edges of the window which should be used when considering a DBL as per equation 3.9.(after Davison and Zhang [21]).

The thickness of the DBL was included in the C_{DGT} calculations for the field trials. An effective sampling area (A_e) was found to be 3.8 cm^2 instead of the 3.14 cm^2 used in the laboratory trials, as described by Warnken *et al.* [17] to allow for lateral diffusion of the analyte at the edge of the diffusion window as per Figure 3.2 above. Under laboratory conditions, using the physical geometric area (3.14 cm^2) is acceptable as found by Warnken et al. [17]; when the DBL is very thin (i.e. ~0.23 mm) errors arising from not accounting for lateral diffusion are off-set by not accounting for the DBL.

To account for the effective sampling area (A_e), the difference in the diffusion coefficients between the water in the DBL and the gel phase ($\frac{D_M^W}{D_M^{gel}}$) and the DBL (δ), equation 3.2 can be re-written as equation 3.9 to calculate C_{DGT}, as described by Davison & Zhang [21]:

$$C_{DGT} = \frac{M(D_M^W \Delta g + D_M^{gel} \delta)}{D_M^W D_M^{gel} t A_e} \qquad \text{Equation 3.9}$$

Under laboratory conditions where the solution was well stirred and no significant DBL could form, equation 3.2 was used. The calculated TWA's for field deployments used equation 3.9, in conjunction with the information in Table 3.2. Equation 3.8 can only be used when the DBL has been measured. When the DBL is present but has not been measured (for instance when deploying continuously for 14 days and taking the initial DBL measured in the first 5 days as the average for the deployment period), the changes to the diffusion coefficient still require accounting for by using equation 3.9. When the diffusion coefficients in the DBL and the diffusive gel were similar, then equation 3.2 can be used and the DBL added to the diffusive distance (Δg).

3.1.2 Polyacrylamide gel fabrication

Polyacrylamide (PAM) diffusive gels (thickness 0.4, 0.8, 1.2 and 1.6 mm) were prepared according to Zhang and Davison [3] in a Class 100 laminar flow hood. The PAM gels were produced using a 10 mL quantity of gel solution containing 15% v/v acrylamide solution (Acros Organics, ThermoFisher, Loughborough, U.K.) and 0.3% v/v of patented agarose cross-linker (DGT Research Ltd., Lancaster, U.K.). To this 70 µL of freshly prepared solution of 10% ammonium persulfate (Acros Organics) was

added as the initiator, and 25 μL N,N,N',N'-tetramethylenediamine (TEMED, Acros Organics) was used as the catalyst for polymerisation. The solution was carefully (to avoid introducing air bubbles) mixed to fully distribute the initiator and catalyst to ensure even polymerisation throughout the gel, and cast between a pair of glass plates separated by a spacer of 0.5 mm to produce 0.8 mm thick gels. For the 0.4 mm thick gels a 0.25 mm spacer was used, and for the 1.2 mm thick gels a 0.75 mm spacer was used. The gel mixture in the glass plates were then left to polymerise at 42-46 ^{o}C for 1 h [15].

After polymerisation the gel sheets were rehydrated for 24 h in ultra-pure water, with a minimum of 4 changes of water to ensure that all polymerisation products were eliminated and potential charge effects reduced [21]. During the hydration period the gel volume expanded by 1.6 times to give a thickness of 0.8 mm. The pore size of the gel had a radius of ≥ 5 nm [22].

The properties of the PAM hydrogel used in this project can be seen in Table 3.3 below.

Table 3.3 Properties of the polyacrylamide (PAM) hydrogel used [15].

Property	**%**
Monomer	15.0
Crosslinker	0.3
T (total monomer concentration = acrylamide (g) + crosslinker (g)per 100 ml)	15.3
C (percentage cross linking = crosslinker (g)/T x100 %)	2.0

The diffusive gels were stored in either 0.01 M $NaNO_3$ or 0.4 M NaCl prior to either fresh water or sea water deployments, respectively. The gels are stored in solutions with an ionic strength $I > 0.01$ M and all experiments undertaken in solutions of at least $I = 0.01$ M because at very low ionic strength (< 0.1 mM), the diffusion coefficients have been shown to be affected, with a decrease of up to 50% because the diffusive gel develops a positive charge thereby creating a Donnan partitioning of cations at the gel surface [23].

The 0.4 mm thick PAM binding gels were prepared as above with either 2 g Chelex-100 resin (Na form, 75-150 μm particle size, BioRad Laboratories, Hemel Hempstead, U.K.), 1 g MnO_2 resin (prepared after Burnett *et al.* [24] by reducing a 2% w/v potassium permanganate solution onto pre-filtered material supplied by TrisKem International (Bruz, France)), 1 g Metsorb heavy metal removal powder (HMRP) (TiO_2

with an organic binder, < 50 µm; Graver Technologies, Glasgow, USA) or 1 g Diphonix® resin (TisKem International, Bruz, France) in 10 mL gel solution prior to polymerisation. The Chelex-100 gel was prepared according to Zhang and Davison [3]; and the MnO_2, the Metsorb™ and the Diphonix® gels were prepared according to the method described by Bennett *et al.* [25]. The Diphonix® resin is supplied with a high moisture content and therefore requires drying prior to fixation in the acrylamide.

DGT device mouldings were obtained from DGT Research Ltd. and washed for 24 h in 10% HNO_3, and then rinsed three times in Milli-Q water prior to use. The devices were assembled according to Davison *et al.* [13] and stored at 4°C in zip lock plastic bags, containing 1-2 mL of water (matrix matched to deployment site) to ensure the diffusion properties of the gels were not altered, and to prevent the gels drying out. A disk of (0.2 µm pore size) Supor polyethylene sulfone (Pall Corporation, Portsmouth, U.K.) was used as the outer membrane.

3.1.3 Deployment

Deployment techniques utilised in this project are described in each chapter. Typically, the devices were held between perspex plates (15 x 7 cm, 8 devices per plate) (see Figure 3.3 below) and attached to a rope, with a weight and float to keep the rope taught.

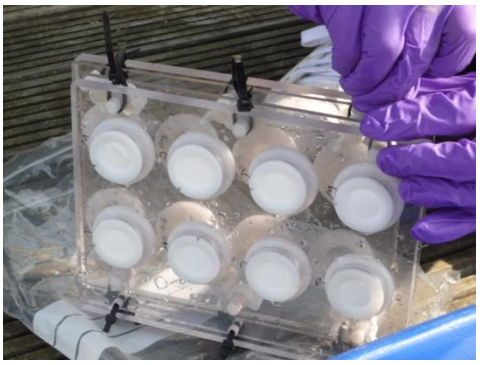

Figure 3.3 Photograph of the DGT devices held in a perspex plate for deployment. In this image two perspex plates are attached back to back to allow for multiple device deployment.

Three field sites were used in this project; two freshwater sites and one marine site. Freshwater site 1 (51.4469 N, -1.3838 W) was located on the River Lambourn at the village of Boxford, Berkshire, UK and site 2 (51.3792 N, -1.1855 W) on the River Enborne near Brimpton, Berkshire, UK. Both rivers are tributaries of the River Kennet. The River Lambourn has a Chalk catchment and is a fast flowing shallow channel with an average pH of 7.9-8 [26]. The River Enborne drains impermeable Tertiary sand, silt and clay deposits [27] and has a slow flowing deep channel with a pH ~7.8. The marine site was located adjacent to the National Oceanography Centre, Southampton, U.K.

(50.891313 N, -1.3938260 W). This site is a well mixed estuarine site with a salinity of 29 to 33 (dependent upon tidal fluctuations and freshwater inputs) and is a moderate flow site with tidal fluctuations agitating the water.

3.1.4 Treatment of data

Each DGT unit was deployed in the laboratory or the field in triplicate. This allows for the mean of each measurement to be calculated, in addition to the standard error. The standard error is the distribution of an estimate (the mean of triplicate measurements, of the slope of a linear regression) with respect to the normal curve (Gaussian distribution of results), or the extent to which an estimate can vary given a level of confidence. The standard error (*SE*) is calculated by dividing the standard deviation (*S*) of the triplicate results by the square root of the number of replicates (*n*), as per equation 3.10 below.

$$SE = \frac{S}{\sqrt{n}} \qquad \text{Equation 3.10}$$

In order to assess the uncertainty associated with the DBL measurements, the standard deviation of the error of the slope and intercept of *1/M* vs *Δg*, was used to find the proportion of the DBL that could be attributed to variation, as per equation 3.11, and is the square root of the sum of squared errors:

$$DBL\ uncertainty = \frac{\sqrt{\left(\frac{SE}{m}\right)^2 + \left(\frac{SE}{b}\right)^2}}{DBL} \qquad \text{Equation 3.11}$$

where *m* is the slope, *b* is the intercept of *1/M* vs *Δg*, and the standard error of the slope (SE_m) and the intercept (SE_b) found using equations 3.12 and 3.13 respectively.

$$SE_m = \frac{s}{\sqrt{\sum(x_i - \bar{x})^2}} \qquad \text{Equation 3.12}$$

where the standard deviation (*s*) is divided by the square root of the squared sum of each data point (x_i) minus the mean ($\bar{x}$) of all data points.

$$SE_b = s\sqrt{\frac{1}{n} + \frac{\bar{x}^2}{\sum(x_i - \bar{x})^2}} \qquad \text{Equation 3.13}$$

where the standard deviation (s) is multiplied by the square root of the mean ($\bar{x}$) divided by the squared sum of each data point (x_i) minus the mean ($\bar{x}$) of all data points, divided by the number of replicates or sample points (n).

3.2 Inductively coupled plasma mass spectrometry (ICP-MS)

An Agilent 7500*ce* ICP-MS (Agilent Technologies Inc., Japan) with an octopole reaction system was used for all U analysis in this thesis. The solution is nebulised through a sample introduction system fitted with a micromist nebuliser and U is measured under normal plasma conditions in 'no gas mode'. Bismuth (*m/z* = 209; 25 µg L^{-1}) was used as an internal standard to compensate for any potential instrument drift.

To ensure optimal instrument settings (including sample introduction, torch alignment and application of voltage to the lens stack, octopole and quadrupole), a tuning solution (Agilent Technologies Inc., Japan) containing 10 ppb Li, Y, Ce, Tl and Co with an addition of 10 ppb U in 0.2 wt % HNO_3 was used. The instrument was tuned to ensure maximum sensitivity and to reduce background counts each time analyses were performed. Typical tune settings used are detailed in Table 3.4. To ensure a good signal, the ICP-MS target tune settings were for < 2% doubly charged ions (*mz* Ce^{++} 70/140) and oxides (using CeO, *mz* 156/140) with a precision (RSD – relative standard deviation) better than 5%.

Table 3.4 Typical ICP-MS tune settings to analyse for U in no gas mode.

Tune parameter	**Range**	**Normal Settings**
Extraction Lens 1	0 –to 3 V	Better stability at 0 V
Extraction Lens 2	-120 to -80 V	-120 V (lower than this increased backgrounds)
Omega Bias-*ce*	-25 to 0 V	-20 V
Omega Lens-*ce*	-3 to 5 V	0 V
Cell Entrance	-40 to -15V	-30 V
QP (quadrupole) Focus	-2 to -5 V	2V
Cell Exit	-45 to -10 V	-30 V
Oct P (octopole) RF	150 to 200 V	180 V
Oct P Bias	-12 to -6 V	-6 V (3 V more negative than QP Bias)
QP Bias	-5 to -3 V	-3 V (3V more positive than Oct P Bias)

Some of the interferences commonly encountered when analysing for U using ICP-MS can be seen in Table 3.5, which can be avoided through robust tuning.

Table 3.5 Possible polyatomic interferences formed in the plasma that may interfere with uranium measurements using ICP-MS [28].

Polyatomic interferences	**m/z**
^{234}U	
$^{232}Th^{2}H$	234.05215
$^{203}Tl^{31}P$	233.94610
$^{202}Hg^{32}S$	233.94270
$^{201}Hg^{33}S$	233.94175
$^{200}Hg^{34}S$	233.93619
$^{199}Hg^{35}Cl$	233.93712
$^{198}Hg^{36}Ar$	233.93431
$^{198}Pt^{36}Ar$	233.93543
$^{197}Au^{37}Cl$	233.93246
$^{196}Pt3^{8}Ar$	233.92768
$^{194}Pt^{40}Ar$	233.92506
^{235}U	
$^{204}Pb^{31}P$	234.94680
$^{204}Hg^{31}P$	234.94724
$^{203}Tl^{32}S$	234.94441
$^{202}Hg^{33}S$	234.94209
$^{201}Hg^{34}S$	234.93816
$^{200}Hg^{35}Cl$	234.93717
$^{199}Hg^{36}Ar$	234.93582
$^{198}Hg^{37}Cl$	234.93266
$^{198}Pt^{37}Cl$	234.93378
$^{197}Au^{38}Ar$	234.92929
$^{195}Pt^{40}Ar$	234.92717
^{238}U	
$^{207}Pb^{31}P$	237.94965
$^{206}Pb^{32}S$	237.94653
$^{205}Tl^{33}S$	237.94587
$^{204}Pb^{34}S$	237.94091
$^{204}Hg^{34}S$	237.94135
$^{203}Tl^{35}Cl$	237.94119
$^{202}Hg^{36}Ar$	237.93818
$^{201}Hg^{37}Cl$	237.93619
$^{200}Hg^{38}Ar$	237.93105
$^{198}Hg^{40}Ar$	237.92914
$^{198}Pt^{40}Ar$	237.93026

To ensure that analysis is accurate, certified reference material (CRM) is used for comparison. The certified reference materials SLRS-5 (River Water Reference Material for Trace Metals) and NASS-5 (Seawater Reference Material for Trace Metals), both supplied by the National Research Council Canada, were used for quality control. The U in the SLRS-5 (with a U concentration of 0.1 μg L^{-1}) was analysed directly and the NASS-4 (with a U concentration of 2.6 μg L^{-1}) after a 20-fold dilution and were found to be within 1% of the stated values. Limits of detection for the ICP-MS

and the ICP-MS measured resin blanks can be seen in Table 3.6. Blank resin measurements were incorporated into every experiment and are described in each Chapter. The values detailed below represent the average values from this thesis.

Table 3.6 Figures of merit for the ICP-MS and the resins used in this project for each isotope of uranium studied (^{235}U and ^{238}U).

	238U ng L^{-1}	**RSD (%)‡**	**235U ng L^{-1}**	**RSD (%)‡**
Instrument blank*	6	< 3	6	< 3
Detection limit*	2	< 3	2	<3
Chelex-100 blank$	0.06	5	0.2	40
MnO_2 blank†	0.06	1.7	0.3	16.7
Metsorb™ blank†	0.03	66.6	0.3	33.3
Diphonix blank†	0.79	10.1	0.5	35.2

* as calculated using the Agilent Chemstation software: 3 σ x concentration of the standard solution/ s-b, where s is the counts of a 10ppb solution and b are the background counts.
† calculated from laboratory blanks.
‡ calculated using the (standard deviation of triplicate readings/average reading)*100.

$^{235/238}U$ isotopic ratios were measured using an Agilent microflow (100 µL min^{-1}) PTFE self aspirating nebuliser, to eliminate any signal pulses caused by the peristaltic pump when using the micromist concentric nebuliser. Isotopic ratios were determined with 3% standard deviation as low as 0.1 µg L^{-1} total U (0.000725 µg L^{-1} ^{235}U). The certified reference material U005a (New Brunswick Laboratories, DoE, Washington, USA) was analysed and was found to be within 99.5% of the isotopic value (0.0000342 $^{235/238}U$). The U005a was supplied to the project by AWE. To prepare U005a as an acidified solution (after the New Brunswick Laboratory procedure for the preparation of this standard [29]), 1 g of the uranium oxide (U_3O_8) powder was dissolved in Teflon beakers in trace analysis grade concentrated 50% HNO_3. After dissolution, the acidic solution was brought to dryness and re-dissolved in 100 mL ultra-pure 2% HNO_3. The stock mixture U005a CRM was 1mg L^{-1}, with further dilution (1 in 1000) to a working solution concentration of 1 µg L^{-1}. No isotopic fractionation was observed in the New Brunswick Laboratory Report [29], with an isotopic RSD of ± 0.1%, using a 95% confidence interval.

3.3 Water quality

Water quality parameters (listed in Table 3.7) were measured for the freshwater sites as part of the CEH Boxford Observatory Project and Thames Initiative by the Centre for Ecology and Hydrology.

Grab water samples were taken at weekly intervals from the main flow of the river at each monitoring site (the River Lambourn and the River Enborne). Sub-samples were immediately filtered (0.45 µm cellulose nitrate membrane, WCN grade:

Whatman Ltd., Maidstone, UK) for subsequent analysis of dissolved determinands. Unfiltered sub-samples were taken for the determination of chlorophyll-a, total phosphorus and suspended particulate matter. Samples for chlorophyll-a were filtered and processed within 24 h. Water samples (0.5 L) were passed through a GF/C grade filter paper (Whatman Ltd.) and the pigment extracted overnight using 90% acetone. The concentration of chlorophyll-a of the extract was determined spectrophotometrically [30]. Total phosphorus (TP) was determined by digesting an unfiltered water sample with acidified potassium persulphate in an autoclave at 121^{o}C for 40 min, then reacting with acid ammonium molybdate reagent to produce a molybdenum-phosphorus complex, which was quantified spectrophotometrically [31]. Soluble reactive phosphorus (SRP) was determined on a filtered sample, using the phosphomolybdenum blue colorimetry method of Murphy and Riley [32], as modified by Neal *et al*., [33]. Dissolved reactive silicon was determined by reaction with acid ammonium molybdate, to form yellow molybdosilicic acids. These were then reduced using an acidified tin (II) chloride solution to form intensely coloured silicomolybdenum blues, which were quantified spectrophotometrically using a Descrete Analyser (Auto Analyser 2; Seal Analytical, Fareham, UK) [34]. Total dissolved nitrogen and dissolved organic carbon were determined by thermal oxidation, (Elementar Isoprime). Nitrate, nitrite and major anion concentrations were analysed by ion chromatography (Dionex DX500). Major cations were analysed by ICP-MS (Perkin Elmer Optima 2100DV).

Table 3.7 Water quality parameters measured as part of the CEH Boxford Observatory Project and Thames Initiative.

Anions	**Cations**	**Particulates and organics**
Soluble reactive phosphate (SRP)	Sodium (Na^{+})	Chlorophyll *a* (Chl *a*)
Total dissolved phosphate (TDP)	Potassium (K^{+})	Dissolved organic carbon (DOC)
Total phosphate (TP)	Calcium (Ca^{+})	Suspended particulate material (SPM)
Ammonia (NH_4)	Magnesium (Mg^{+})	
Dissolved reactive silicon (Si)	Boron (B^{+})	
Total dissolved nitrate (TDN)	Iron (Fe^{+})	
Nitrate (NO_3^{-})	Manganese (Mn^{2+})	
Nitrite (NO_2^{-})	Zinc (Zn^{2+})	
Sulphate (SO_4^{2-})	Copper (Cu^{2+})	
Fluoride (F^{-})	Aluminium (Al^{3+})	
Chloride (Cl^{-})		
Bromide (Br^{-})		

3.4 Speciation modelling

All speciation distributions were calculated using Visual Minteq, version 3, beta (© 2010 KTH, Department of Land and Water Resources Engineering, Stockholm, Sweden). Constants used in the Visual Minteq model are derived from the US EPA's MinteqA2 code. This is a freely available programme that is able calculate metal speciation in natural waters. Table 3.8 below details the stability constants used by the model for uranium speciation calculations detailed in this project.

Table 3.8 Formation constants for U(VI) and U(IV) solution species used in the Visual Minteq calculation of U speciation (I = 0, t = 25°C).

Reaction	**log*K***
$UO_2^{2+} + H_2O \leftrightarrow UO_2OH^+ + H^+$	-5.2
$UO_2^{2+} + 2H_2O \leftrightarrow UO_2(OH)_{2(aq)} + 2H^+$	-12.2
$UO_2^{2+} + 3H_2O \leftrightarrow UO_2(OH)_3^- + 3H^+$	-20.2
$UO_2^{2+} + 4H_2O \leftrightarrow UO_2(OH)_4^{2-} + 4H^+$	-33.0
$UO_2^{2+} + H_2O \leftrightarrow (UO_2)_2OH_3^+ + H^+$	-2.7
$2UO_2^{2+} + 2H_2O \leftrightarrow (UO_2)_2(OH)_2^{2+} + 2H^+$	-5.62
$3UO_2^{2+} + 4H_2O \leftrightarrow (UO_2)_3(OH)_4^{2+} + 4H^+$	-11.9
$3UO_2^{2+} + 5H_2O \leftrightarrow (UO_2)_3(OH)_5^+ + 5H^+$	-15.55
$3\ UO_2^{2+} + 7H_2O \leftrightarrow (UO_2)_3(OH)_7^- + 7H^+$	-31.0
$4\ UO_2^{2+} + 7H_2O \leftrightarrow (UO_2)_4(OH)_7^+ + 7H^+$	-21.9
$UO_2^{2+} + CO_3^{2-} \leftrightarrow UO_2CO_{3(aq)}$	9.67
$UO_2^{2+} + 2CO_3^{2-} \leftrightarrow UO_2(CO_3)_2^{2-}$	16.61
$UO_2^{2+} + 3CO_3^{2-} \leftrightarrow UO_2(CO_3)_3^{4-}$	21.6
$3UO_2^{2+} + 6CO_3^{2-} \leftrightarrow (UO_2)_3(CO_3)_6^{6-}$	54.0
$2UO_2^{2+} + CO_3^{2-} + 3H_2O \leftrightarrow (UO_2)_2CO_3(OH)_3^- + 3H^+$	-0.86
$3UO_2^{2+} + CO_3^{2-} + 3H_2O \leftrightarrow (UO_2)_3CO_3(OH)_3^+ + 3H^+$	0.66
$11UO_2^{2+} + 6CO_3^{2-} + 12H_2O \leftrightarrow (UO_2)_{11}(CO_3)_6(OH)_{12}^{2-} + 12H^+$	36.43
$H^+ + CO_3^{2-} \leftrightarrow HCO_3$	10.329
$2H^+ + CO_3^{2-} \leftrightarrow H_2CO_3^* (\equiv CO_{2(aq)} + H_2O)$	16.683
$CO_2(g) + H_2O \leftrightarrow H_2CO_3^* (\equiv CO_{2(aq)} + H_2O)$	-1.472
$UO_2^{2+} + SO_4^{2-} \leftrightarrow UO_2SO_{4(aq)}$	3.15
$UO_2^{2+} + 2SO_4^{2-} \leftrightarrow UO_2(SO_4)_2^{2-}$	4.14
$SO_4^{2-} + H^+ \leftrightarrow HSO_4^-$	1.98
$UO_2^{2+} + PO_4^{3-} \leftrightarrow UO_2PO_4^-$	13.23
$UO_2^{2+} + PO_4^{3-} + H^+ \leftrightarrow UO_2HPO_{4(aq)}$	19.59
$UO_2^{2+} + PO_4^{3-} + 2H^+ \leftrightarrow UO_2H_2PO_4^+$	22.82
$UO_2^{2+} + PO_4^{3-} + 3H^+ \leftrightarrow UO_2H_3PO_4^{2+}$	22.46
$UO_2^{2+} + 2PO_4^{3-} + 4H^+ \leftrightarrow UO_2(H_2PO_4)_{2(aq)}$	44.04
$UO_2^{2+} + 2PO_4^{3-} + 5H^+ \leftrightarrow UO_2(H_2PO_4)(H_3PO_4)^+$	45.05
$PO_4^{3-} + H^+ \leftrightarrow HPO_4^{2-}$	12.35
$PO_4^{3-} + 2H^+ \leftrightarrow H_2PO_4^-$	19.562
$PO_4^{3-} + 3H^+ \leftrightarrow H_3PO_{4(aq)}$	21.702
$UO_2^{2+} + 4H^+ + 2e^- \leftrightarrow U^{4+} + 2H_2O$	8.89
$U^{4+} + 5CO_3^{-2} \leftrightarrow U(CO_3)_5^{6-}$	33.9
$U^{4+} + SO_4^{2-} \leftrightarrow USO_4^{2+}$	6.58
$U^{4+} + 4H_2O \leftrightarrow U(OH)_4 + 4H^+$	-12.0
$U^{4+} + H_2O \leftrightarrow UOH^{3+} + H^+$	-0.65
$UO_2^{2+} + 2Ca^{2+} + 3CO_3^{2-} \leftrightarrow Ca_2UO_2(CO_3)_3^0{}_{(aq)}$	5.34[35]
$UO_2^{2+} + Ca^{2+} + 3CO_3^{2-} \leftrightarrow CaUO_2(CO_3)_3^{2-}$	8.86[35]

The Stockholm Humic Acid Model (SHM) was used to model DOC in field samples as it is based upon the WHAM [36] and Model VI [37]. The SHM uses a model based on monodentate and bidentate binding of uranyl to the humic substance. In addition counter-ions are incorporated into the model to account for the cation attraction to the negative charges on the humic surfaces and any charge shielding this may cause. It has been used here for the field modelling because it does not distinguish between fulvic acid or humic acid, but between mono- and bidentate binding sites. The advantage to this in a non-specific system is that the dissolved organic carbon (DOC) in the field sites used in this study has not been characterised, and so the distribution of DOC between FA and HA is unknown. Table 3.9 details the formation constants used in this model for uranyl ion binding to organics. This model has also been used by other workers when modelling U interactions in fluvial systems [38, 39].

Table 3.9 Formation constants for U(VI) organic solution species used in the Visual Minteq Stockholm Humic Acid Model (SHM) DOC parameters (I = 0, t = 25^{o}C). Organic complexes are shown as FA2UO_2 which a bidentate complex (2:1, humic:uranyl); and FAUO_2^+ which is a 1:1 monodentate complex. Affixes of 'D' represent a weak electrostatic attraction.

Species	**log*K***	
FA2-UO_2	-6.93	organically bound uranyl
FA2-UO_2^+	0.79	
UO_2^{2+}D	0	weak electrostatic bonding from the counter ion database
UO_2OH^+D	-5.897	

When more detailed knowledge of speciation was required, such as for laboratory experiments when a known quantity of HA was added to DGT exposure tanks, the NICA Donan model was used. This model was also used to assess binding of uranyl to various phenolic and carboxylic sites in the kinetic laboratory experiments; the NICA Donan model was used here due to the NICA (non ideal competitive adsorption) models' ability to account for non-ideal binding to heterogeneous ligands [40], such as humic substances. Table 3.10 details the formation constants used in this model for uranyl ion binding to organics.

Table 3.10 Formation constants for U(VI) organic solution species used in the Visual Minteq Nica-Donan DOC parameters (I = 0, t = 25°C). HA/FA1 represent the carboxylic bonds, and HA/FA2 represent the phenolic bonds and +D is the electrostatic bond rather than covalent bond between the uranium and the organic. Each U-organic bond assumes a 1:1 bond.

Species	**log*K***
FA1-UO_2	9.06
FA2-UO_2	0.78
HA1-UO_2	4.81
HA1-UO_2	2.45
UO_2OH+D	-5.897

The use of speciation modelling is important in predicting the form of U, which in turn can be used to assess its bioavailability, and ultimately, fate, transport and environmental risk. However, the errors associated with using speciation models should be noted. These models use thermodynamic relationships to predict the equilibrium distribution of species in a system. This assumes that the system is in thermodynamic equilibrium, which is rare in natural systems [41, 42]. Models also assume that the formation and stability constants, mainly defined experimentally in simple laboratory solutions, are in equilibrium in the environment.

VanBriesen *et al.* [42] identified four main categories of speciation uncertainty:

1 – Decision rule uncertainty

This includes the operator decision as to whether or not to include certain species or processes in the model parameters. This may include humic complexation, changes in redox states or solid-phase adsorption, that may have a large impact but a minor contribution to the concentration values to be input into the model.

2 – Model uncertainty

This could include the choice of models used for the humic complexation or solid-phase adsorption.

3 – Parameter uncertainty

Uncertainty in the corrections of thermodynamic data for ionic strength, temperature and matrix interactions.

4 – Parameter variability

Models assume equilibrium has been achieved, and relies on the values of equilibrium constants that have been determined experimentally.

Speciation models rely on mass balance and thermodynamics to determine the concentration of each species in a given system. They also assume a rapid reaction takes

place particularly for aqueous based reactions as they are reversible. Most models (including Visual Minteq used here), are supplied with a database of thermodynamic data and generally offer only a single value for the overall formation reaction of each aqueous component. It has been shown that the use of a single formation value for an aqueous component can lead to increased uncertainty [42].

Denison and Garrier-LaPlace [41] examined the propagation of database parameter uncertainties (error 3 listed above) using Monte Carlo simulations, with particular reference to U(VI) aqueous species. They found that systems with a non-linear behaviour can lead to bimodal concentration output distributions, particularly close to equivalence point or solubility boundaries. It was also found that uncertainty in a model decreases for a particular species for which it is predicted to be dominant. As U has a complex aqueous chemistry, even minor uncertainties in the model input produced large output uncertainties.

3.5 References

[1] W. Davison, H. Zhang, G.W. Grime, Performance characteristics of gel probes used for measuring the chemistry of pore waters, Environmental Science & Technology, 28 (1994) 1623-1632.

[2] C. Murdock, M. Kelly, L.-Y. Chang, W. Davison, H. Zhang, DGT as an *in situ* tool for measuring radiocesium in natural waters, Environmental Science & Technology, 35 (2001) 4530-4535.

[3] H. Zhang, W. Davison, Direct in situ measurements of labile inorganic and organically bound metal species in synthetic solutions and natural waters using diffusive gradients in thin films, Analytical Chemistry, 72 (2000) 4447-4457.

[4] H. Zhang, W. Davison, R.J.G. Mortimer, M.D. Krom, P.J. Hayes, I.M. Davies, Localised remobilization of metals in a marine sediment, Science of the Total Environment, 296 (2002) 175-187.

[5] J.G. Panther, P.R. Teasdale, W.W. Bennett, D.T. Welsh, H.J. Zhao, Titanium dioxide-based DGT technique for *in situ* measurement of dissolved reactive phosphorus in fresh and marine waters, Environmental Science & Technology, 44 (2010) 9419-9424.

[6] L. Duquène, H. Vandenhove, F. Tack, M. Van Hees, J. Wannijn, Diffusive gradient in thin films (DGT) compared with soil solution and labile uranium fraction for predicting uranium bioavailability to ryegrass, Journal of Environmental Radioactivity, 101 (2010) 140-147.

[7] I. Ahumada, L. Ascar, C. Pedraza, V. Vasquez, A. Carrasco, P. Richter, S. Brown, Determination of the bioavailable fraction of Cu and Zn in soils amended with biosolids as determined by diffusive gradients in thin films (DGT), BCR sequential sxtraction, and ryegrass plant, Water Air and Soil Pollution, 219 (2011) 225-237.

[8] N. Roig, M. Nadal, J. Sierra, A. Ginebreda, M. Schuhmacher, J.L. Domingo, Novel approach for assessing heavy metal pollution and ecotoxicological status of rivers by means of passive sampling methods, Environment International, 37 (2011) 671-677.

[9] I.J. Allan, J. Knutsson, N. Guigues, G.A. Mills, A.M. Fouillac, R. Greenwood, Evaluation of the Chemcatcher and DGT passive samplers for monitoring metals with highly fluctuating water concentrations, Journal of Environmental Monitoring, 9 (2007) 672-681.

[10] R.J.K. Dunn, P.R. Teasdale, J. Warnken, R.R. Schleich, Evaluation of the diffusive gradient in a thin film technique for monitoring trace metal concentrations in estuarine waters, Environmental Science & Technology, 37 (2003) 2794-2800.
[11] I.J. Allan, J. Knutsson, N. Guigues, G.A. Mills, A.M. Fouillac, R. Greenwood, Chemcatcher (R) and DGT passive sampling devices for regulatory monitoring of trace metals in surface water, Journal of Environmental Monitoring, 10 (2008) 821-829.
[12] Ø.A. Garmo, K.R. Naqvi, O. Røyset, E. Steinnes, Estimation of diffusive boundary layer thickness in studies involving diffusive gradients in thin films (DGT), Analytical and Bioanalytical Chemistry, 386 (2006) 2233-2237.
[13] W. Davison, Fones G., Harper, M., Teasdale, P. And Zhang, H, Dialysis, DET and DGT: *In situ* diffusional techniques for studying water, sediments and soils., in: J.A.H. Buffle, G. (Ed.) *In situ* monitoring of aquatic systems: chemical analysis and speciation, John Wiley & Sons Ltd, 2000, pp. 74.
[14] C.M. Hutchins, J.G. Panther, P.R. Teasdale, F. Wang, R.R. Stewart, W.W. Bennett, H. Zhao, Evaluation of a titanium dioxide-based DGT technique for measuring inorganic uranium species in fresh and marine waters, Talanta, 97 (2012) 550-556.
[15] H. Zhang, W. Davison, Diffusional characteristics of hydrogels used in DGT and DET techniques, Analytica Chimica Acta, 398 (1999) 329-340.
[16] Tables of Physical & Chemical Constants in: 2.2.3 Viscosities, Kaye & Laby Online, 2005.
[17] K.W. Warnken, H. Zhang, W. Davison, Accuracy of the diffusive gradients in thin-films technique: diffusive boundary layer and effective sampling area considerations, Analytical Chemistry, 78 (2006) 3780-3787.
[18] K.W. Warnken, W. Davison, H. Zhang, Interpretation of *in situ* speciation measurements of inorganic and organically complexed trace metals in freshwater by DGT, Environmental Science & Technology, 42 (2008) 6903-6909.
[19] S. Kerisit, C. Liu, Molecular simulation of the diffusion of uranyl carbonate species in aqueous solution, Geochimica Et Cosmochimica Acta, 74 (2010) 4937-4952.
[20] G. Marx, H. Bischoff, Transport processes of actinides in electrolyte solutions, Journal of Radioanalytical Chemistry, 30 (1976) 567-581.
[21] W. Davison, H. Zhang, Progress in understanding the use of diffusive gradients in thin films (DGT) – back to basics, Environmental Chemistry, 9 (2012) 1-13.
[22] O.A. Garmo, W. Davison, H. Zhang, Interactions of trace metals with hydrogels and filter membranes used in DET and DGT techniques, Environmental Science & Technology, 42 (2008) 5682-5687.

[23] S. Scally, W. Davison, H. Zhang, Diffusion coefficients of metals and metal complexes in hydrogels used in diffusive gradients in thin films, Analytica Chimica Acta, 558 (2006) 222-229.

[24] J.L. Burnett, I.W. Croudace, P.E. Warick, Pre-concentration of naturally occurring radionuclides and the determination of ^{212}Pb from fresh waters, Journal of Environmental Radioactivity, 102 (2011) 4.

[25] W.W. Bennett, P.R. Teasdale, J.G. Panther, D.T. Welsh, D.F. Jolley, New diffusive gradients in a thin film technique for measuring inorganic arsenic and selenium(IV) using a titanium dioxide based adsorbent, Analytical Chemistry, 82 (2010) 7401-7407.

[26] H.P. Jarvie, C. Neal, M.D. Jürgens, E.J. Sutton, M. Neal, H.D. Wickham, L.K. Hill, S.A. Harman, J.J.L. Davies, A. Warwick, C. Barrett, J. Griffiths, A. Binley, N. Swannack, N. McIntyre, within-river nutrient processing in Chalk streams: The Pang and Lambourn, UK, Journal of Hydrology, 330 (2006) 101-125.

[27] R.M.S. Smith, D.J. Evans, H.S. Wheater, Evaluation of two hybrid metric-conceptual models for simulating phosphorus transfer from agricultural land in the river enborne, a lowland UK catchment, Journal of Hydrology, 304 (2005) 366-380.

[28] J.B. Truscott, P. Jones, B.E. Fairman, E.E. Hywel, Determination of actinide elements at femtogram per gram levels in environmental samples by on-line solid phase extraction and sector-field-inductively coupled plasma-mass spectrometry, Analytica Chimica Acta, 433 (2001) 245-253.

[29] New Brunswick Laboratory Progress Report, in, U.S. Department of Energy, Chicago Operations Office, Argonne, Illinois, September 1996, Report number 980S.

[30] A.F.H. Marker, E.A. Nusch, H. Rai, B. Riemann, The measurement of photosynthetic pigments in freshwaters and standardisation of methods: Conclusions and recommendations., Archiv für Hydrobiologie–BeiheftErgebnisse der Limnologie, 14 (1980) 91-106.

[31] S.J. Eisenreich, R.T. Bannerman, D.E. Armstrong, A simplified phosphorus analytical technique, Environmental Letters, 9 (1975) 45-53.

[32] J. Murphy, J.P. Riley, A modified single solution method for the determination of phosphorus in natural waters., Analytica Chimica Acta, 12 (1962) 31-36.

[33] C. Neal, M. Neal, H. Wickham, Phosphate measurement in natural waters: two examples of analytical problems associated with silica interference using phosphomolybdic acid methodologies, Science of the Total Environment, 251 (2000) 511-522.

[34] J.B. Mullin, J.P. Riley, The colourometric determination of silicate with special reference to sea and natural waters., Analytica Chimica Acta, 12 (1955) 31-36.

[35] W. Dong, S.C. Brooks, Determination of the formation constants of ternary complexes of uranyl and carbonate with alkaline earth metals (Mg^{2+}, Ca^{2+}, Sr^{2+}, and Ba^{2+}) using anion exchange method, Environmental Science & Technology, 40 (2006) 4689-4695.

[36] S. Lofts, E. Tipping, Assessing WHAM/Model VII against field measurements of free metal ion concentrations: model performance and the role of uncertainty in parameters and inputs, Environmental Chemistry, 8 (2011) 501-516.

[37] E. Tipping, Humic Ion-Binding Model VI: An Improved description of the interactions of protons and metal ions with humic substances, Aquatic Geochemistry, 4 (1998) 3-47.

[38] J. Zhao, I.I. Fasfous, J.D. Murimboh, T. Yapici, P. Chakraborty, S. Boca, C.L. Chakrabarti, Kinetic study of uranium speciation in model solutions and in natural waters using Competitive Ligand Exchange Method, Talanta, 77 (2009) 1015-1020.

[39] W.J. Li, J.J. Zhao, C.S. Li, S. Kiser, R.J. Cornett, Speciation measurements of uranium in alkaline waters using diffusive gradients in thin films technique, Analytica Chimica Acta, 575 (2006) 274-280.

[40] M.F. Benedetti, C.J. Milne, D.G. Kinniburgh, W.H. Van Riemsdijk, L.K. Koopal, Metal ion binding to humic substances: application of the Non-Ideal Competitive Adsorption Model, Environmental Science & Technology, 29 (1995) 446-457.

[41] F.H. Denison, J. Garnier-Laplace, The effects of database parameter uncertainty on uranium(VI) equilibrium calculations, Geochimica et Cosmochimica Acta, 69 (2005) 2183-2191.

[42] J.M. VanBriesen, S. Mitchell, C. Weber, J. Wilson, Modelling chemical speciation: thermodynamics, kinetics and uncertainty, in: G. Hanrahan (Ed.) Advanced topics in environmental science: modelling of pollutants in complex environmental systems, Volume 2, ILM Publications, St Albans, Hertfordshire, U.K., 2010, pp. 468.

Chapter 4: Evaluation of DGT techniques for measuring inorganic uranium species in natural waters: Interferences, deployment time and speciation

4.1 Introduction

Uranium (U) is a primordial radioactive element, originating from the three naturally occurring decay chains (^{235}U, ^{238}U and ^{232}Th), with three important isotopes (mass % shown in brackets): ^{238}U (99.276%), ^{235}U (0.718%) and ^{234}U (0.0056%) [1]. It is released into the environment *via* anthropogenic nuclear processes, such as nuclear power generation, nuclear weapons testing and accidental releases, or *via* natural processes such as weathering or erosion of rocks and sediments containing U. It is highly toxic and important to monitor due to its chemical and radiological properties [2].

U is predominantly found in the +6 state as the uranyl ion (UO_2^{2+}) at pH < 4 to 5, and at pH > 7 occurs as the stable uranyl carbonates $UO_2(CO_3)_2^{2-}$, $UO_2(CO_3)_3^{4-}$ or its complexes, although U(IV) is also found under reducing conditions [3]. Partitioning between the solid and the solution phases, which is mediated by chemical characteristics such as pH, redox potential, ionic strength, presence of complexing ligands (OH^- > CO_3^{2-} > HPO_4^{2-} > $H_2PO_4^-$ > F^- > SO_4^{2-} > Cl^-), surfactants or flocculating agents, is important in natural waters [4]. These all act to influence the oxidation states of the radionuclide and will affect reactions with other dissolved components and sediment-solution interactions.

Table 4.1 shows the concentration of U in a range of natural environments; typical marine concentrations are 3 µg L^{-1}, while estuarine concentrations can be as low as 0.3 µg L^{-1}, with typical fresh water values of 0.1–0.3 µg L^{-1}. The higher dissolved sea water concentrations are due to the formation of stable soluble uranyl carbonate complexes. The largest global sink for U is oceanic sediments, with oceanic carbonates solubilising fluvial and ground water inputs of U. The low environmental concentrations of U can be challenging to detect using conventional analytical techniques such as mass spectroscopy, particularly in complex matrices such as marine or estuarine waters. Isotopic ratios of $^{235}U/^{238}U$ are of interest as a tool to identify pollution sources. ^{235}U occurs in very low concentrations, even when enriched, and is normally below limits of detection without any form of pre-concentration by precipitation, ion-exchange, solvent extraction or extraction chromatography [5]. Pre-concentration and radiochemical separation require large volume (up to 5 L) [6] grab

samples of water. These approaches that use considerable sample processing can also introduce contamination and chemical transformations each time the sample is handled or during storage [7].

Table 4.1 Examples of U concentrations found in the aquatic environment

Environment	Concentration ($\mu g\ L^{-1}$)	Reference
Fluvial		
General	0.3 (dissolved) 3.0 (particulate)	[8]
Alafia River, Tampa Bay, Florida, USA	0.52	[8]
Euphrates River, Dhi Qar Province, Southern Iraq	1.5–4.3	[9]
River Fal, south-west England	0.19–1.34	[10]
Marine		
Open ocean	3.2	[8]
Sea surface	0.5-3.0	[11]
Estuarine		
Tampa Bay Estuary, Florida, USA	3.81	[8]
Gironde Estuary, SW France	0.32–3.37	[12]
Ground water/pore water		
Sarzal region of the Semispaltinsk nuclear test site, Kazakhsatn	1.1–95.5	[13]
Southern Nares Abyssal Plain, North Atlantic	0.1–0.5	[14]
Sediments		
Black Sea	0.5–1.2 ($g\ kg^{-1}$)	[15]
Ortigas River, Spain	0.001–0.01 ($g\ kg^{-1}$)	[16]

Alternative measurement approaches include bio-monitoring [17, 18], technologies based on the redox reactions between the analyte and a chelate [19], and fibre optical methods [20]. As many of these techniques have poor limits of detection they can be used only to indicate the presence of U or, during a pollution event where environmental concentrations are elevated. Passive sampling is another approach [21]. This method avoids many of the sources of error associated with grab sampling by pre-concentrating the analyte *in situ*. Furthermore, passive samplers can be used to measure time-weighted averaged (TWA) concentrations over the deployment period, which can be beneficial in investigations where concentrations are highly fluctuating [21, 22].

Diffusive gradients in thin films (DGT) are passive samplers that measure the labile, dissolved fraction of analytes *in situ* [23]. The device consists of three layers: (i) a binding agent, which contains a resin or functional groups selective to the target ions, held in a thin layer of hydrogel (binding gel); (ii) a layer of hydrogel of known thickness, which serves as the diffusive layer; and (iii) a protective outer membrane

with a known pore size. A diffusive boundary layer (DBL) that forms on the exposed face of the device must also be accounted for and added to the diffusive layer. After deployment, the metal ions accumulated in the resin layer are eluted (e.g. in nitric acid) and the extract analysed by sensitive instrumental techniques, e.g. ICP-MS.

U has been measured in artificial and natural waters using DGT in five reported studies [24-28]. Li *et al.* [24, 25] measured U uptake in artificial alkaline waters using a device that comprised a Whatman DE 81 membrane and Chelex-100 resin (BioRad; www3.bio-rad.com). In a later study they investigated the use of a Dowex 2 x 8-400 resin as the receiving phase [25]. Gregusova *et al.* [29] assessed a chelating ion-exchange resin, Spheron-Oxin® as a candidate binding phase, examining the effects of carbonate concentrations in artificial waters on the uptake of U. Vandenhove *et al.* [26] and Mihalik *et al*. [27] used a DGT containing Chelex-100 as a proxy for phyto-availability but did not undertake any further validation work. A recent study by Hutchins *et al.* [28] measured U in natural waters using a TiO_2-based resin, Metsorb (Graver Technologies; http://www.gravertech.com).

In this study comparisons are made between uptake of U using a DGT device containing either Chelex-100 resin, Metsorb resin, or manganese dioxide (MnO_2), as described by Burnett *et al.* [30]. MnO_2 is a natural scavenger of metals and radionuclides from waters and is stable in the presence of high radiation levels. It has applications in the remediation of nuclear aquatic waste and pre-concentration of radionuclides in sea water [31]. A MnO_2 precipitate has been used previously in passive samplers to study sediment redox profiles through remobilisation of the MnO_2 within the gels [32] and with DGT to measure ^{226}Ra [33, 34]. The performance of each resin in the presence of complexing agents such as HCO_3^-, PO_4^{3-} and SO_4^{2-} and common ionic interference Ca^{2+} were evaluated [35]. Experiments to assess the accumulation of U over time for artificial sea water and low ionic strength water were undertaken. Two 14-day field deployments in carbonate rich river water and in a marine harbour were used to validate laboratory results.

4.2 Experimental

Chemicals were of analytical grade or better and supplied by Fisher Scientific (Loughborough, U.K.), unless otherwise specified. Milli-Q (ultra-pure) water (> 18.2 MΩ cm, Millipore, Watford, U.K.) was used as the laboratory water. All U ICP-MS standards and experimental working solutions were prepared in low density polyethylene (LDPE) or polystyrene (PS) containers with polypropylene lids (PP) from a 1000 mg L^{-1} in 2% HNO_3 (Spex Certiprep, Fisher Scientific) U stock solution unless

otherwise stated. The ICP-MS internal standard was prepared from a 1000 mg L^{-1} in 2% HNO_3 (Spex Certiprep) bismuth stock solution. These solutions were adjusted to a given pH by addition of either 1 M HNO_3 or 1 M NaOH, and to a given ionic strength by addition of $NaNO_3$, with the pH monitored throughout experiments. Solutions were equilibrated with atmospheric CO_2 for 24 h before use unless otherwise specified. All readings were undertaken in triplicate with containers open to the atmosphere to ensure continuing equilibration with the atmospheric pCO_2 (i.e. to ensure a constant inorganic carbon concentration throughout the experiments). All plastic apparatus was soaked for 24 h in 10% HNO_3 and rinsed three times in Milli-Q water prior to use.

4.2.1 Preparation of DGT devices

Polyacrylamide (PAM) diffusive gels (thickness 0.4, 0.8, 1.2 and 1.6 mm) were prepared according to Zhang and Davison [36] and described in Chapter 3, section 3.1.1. The gels contained 15% v/v acrylamide solution (Acros Organics, ThermoFisher, Loughborough, U.K.) and 0.3% v/v of patented agarose cross-linker (DGT Research Ltd., Lancaster, U.K.). N,N,N',N'-tetramethylenediamine (TEMED, Acros Organics) was used as the catalyst and a freshly prepared solution of 10% ammonium persulfate (Acros Organics) was used as the initiator for polymerisation. The diffusive gels were stored in either 0.01 M $NaNO_3$ or 0.4 M NaCl prior to either fresh water or sea water deployments, respectively.

The 0.4 mm thick PAM binding gels were prepared with either 2 g Chelex-100 resin (Na form, 75-150 µm particle size, BioRad Laboratories, Hemel Hempstead, U.K.), 1 g MnO_2 resin (prepared after Burnett *et al.* [30] using pre-filtered material supplied by TrisKem International (Bruz, France) or 1 g Metsorb HMRP powder (TiO_2 with an organic binder, < 50 µm; Graver Technologies, Glasgow, USA) in 10 mL gel solution prior to polymerisation. The Chelex-100 gel was prepared according to Zhang and Davison [36], and the MnO_2 and the Metsorb gels were prepared according to the method described by Bennett *et al.* [37].

DGT device mouldings were obtained from DGT Research Ltd. and washed for 24 h in 10% HNO_3, and then rinsed three times in Milli-Q water prior to use. The devices were assembled according to Davison *et al.* [23] and stored at 4^{o}C in zip lock plastic bags, containing 1-2 mL of water (matrix matched to deployment site) to ensure the diffusion properties of the gels were not altered, and to prevent the gels drying out. A disk of (0.2 µm pore size) Supor polyethylene sulfone (Pall Corporation, Portsmouth, U.K.) was used as the outer membrane.

4.2.2 Analysis of DGT devices

After exposure, the Metsorb and MnO_2 binding gels were removed from the DGT devices and eluted (48 h) with 1 M H_2O_2/1 M HNO_3 (2 mL) solution (100 mL made by combining 90 mL 1.1 M HNO_3 and 10 mL H_2O_2). The Chelex-100 binding gels were eluted (48 h) with 2 M HNO_3 (2 mL). After the sea water deployments, the binding gels were first washed (5 mL) in Milli-Q water for 1 h to remove excess salts [37]. The eluents were then diluted 10 fold with Milli-Q water prior to instrumental analysis. U was determined in all solutions by ICP-MS using an Agilent 7500ce series instrument (Agilent Technologies Inc., Japan). Total U was measured under normal plasma conditions in 'no gas mode', with the sample introduction system fitted with a micromist nebuliser. The instrument blank for U was 6 ng L^{-1} while the limit of detection (calculated by the Agilent Chemstation software) for U was 2 ng L^{-1}, with a measurement standard deviation better than 3%. Laboratory blanks were undertaken in triplicate for each experiment and the average concentration per disk was determined for MnO_2 gel disks as 0.06 ± 0.001 ng and 0.3 ± 0.05 ng for ^{238}U and ^{235}U respectively; for the Chelex-100 gel disks as 0.06 ± 0.003 ng and 0.2 ± 0.08 ng for ^{238}U and ^{235}U respectively; and for the Metsorb gel disks as 0.03 ± 0.02 ng and 0.3 ± 0.1 ng for ^{238}U and ^{235}U respectively. Bismuth (*m/z* = 209; 25 µg L^{-1}) was used as an internal standard to compensate for any potential instrument drift. The certified reference materials SLRS-5 and NASS-4 (National Research Council Canada, Canada) were analysed directly for SLRS-5 and after a 20-fold dilution for NASS-4 and were found to be within 1% of the stated values.

$^{235/238}U$ isotopic ratios were measured using an Agilent microflow (100 µL min^{-1}) PTFE self aspirating nebuliser, to eliminate any signal pulses caused by the peristaltic pump when using the micromist concentric nebuliser. Isotopic ratios were determined with 3% standard deviation as low as 0.1 µg L^{-1} total U (0.000725 µg L^{-1} ^{235}U). The certified reference material U005a (New Brunswick Laboratories, DoE, Washington, USA) was analysed and was found to be within 99.5% of the isotopic value (0.00509 $^{235/238}U$).

4.2.3 Calculation of time-weighted average concentrations

The concentration of U measured by the ICP-MS in µg L^{-1} from the eluent was multiplied by the dilution factor (×10) to give the U concentration (*Ce*). The absolute mass (*M*) of the U in the resin gel was then calculated using equation 1, where *M* is calculated taking into account the gel volume (*Vg*, cm^3), the eluent volume (*Ve*, mL),

the measured concentration of U in the eluent (*Ce*, ng mL^{-1}) and the elution factor (*fe*) [36].

$$M = \frac{Ce(Vg+Ve)}{fe} \quad \text{Equation 4.1}$$

M from equation 4.1 is then used to calculated the TWA concentrations (equation 4.2) in the laboratory where the concentration (C_{DGT}, ng mL^{-1}) was calculated using the mass of the analyte in the binding gel (*M*, ng), the thickness of the diffusive path length (diffusive gel and filter membrane) (*Δg*, cm), the diffusion coefficient of the analyte (*D*, cm^2 s^{-1}) (as determined at different pHs for U by Hutchins *et al.* [28], detailed in Chapter 3), deployment time (*t*, s) and the area of the sample exposure window (*A*, cm^2).

$$C_{DGT} = \frac{M\Delta g}{DtA} \quad \text{Equation 4.2}$$

The diffusion coefficients (*D*) were corrected for temperature (*T*, ^oC) using the Stokes-Einstein equation (equation 4.3) [38] and the viscosity of water (*η*, mPa s) [39]. Diffusion coefficients used for sea water were 10% lower than fresh water [23], due to increased viscosity of higher ionic strength solutions.

$$\frac{D_1\eta_1}{T_1} = \frac{D_2\eta_2}{T_2} \quad \text{Equation 4.3}$$

The diffusion coefficients of uranyl carbonate ions in the diffusive gel and the water have been detailed in Chapter 3, section 3.1.1 and should be considered when calculating field DBLs and TWAs.

The diffusive boundary layer (δ) thickness was calculated using equation 4.4 after Warnken *et al.* [40] . A straight line plot of *1/M* vs *Δg* has a slope (*m*) of $1/(DC_{DGT}At)$ and an intercept (*b*) of $\delta/(DC_{DGT}At)$. The intercept (*b*) divided by the slope (*m*) of this plot gives the diffusive boundary layer thickness δ, also accounting for the discrepancies in diffusion coefficients of uranyl in the gel and water as described in Chapter 3, Section 3.1.1, and as per equation 4.5.

$$\frac{1}{M} = \frac{\Delta g}{DC_{DGT}At} + \frac{\delta}{DC_{DGT}At} \quad \text{Equation 4.4}$$

$$\delta = \frac{b}{m}\left(\frac{D_M^W}{D_M^{gel}}\right) \quad \text{Equation 4.5}$$

The thickness of the DBL was included in the C_{DGT} calculations for the field trials using equation 4.6. The effective sampling area (A_e) was 3.8 cm^2 instead of the 3.14 cm^2 used in the laboratory trials, as described by Warnken *et al.* [40].

Equation 4.6 as used where the DBL had to be accounted for in the calculations as described in section 3.1.1. The predominant uranyl species in the freshwater site ($Ca_2UO_2(CO_3)_3$) had a similar diffusion coefficient in water [41] as the diffusive gel (so$D_M^W : D_M^{gel} = 1$) and was therefore not accounted for here, meaning equation 4.2 could be used for the C_{DGT} calculations. The predominant uranyl species in seawater is $UO_2(CO_3)_2^{2-}$ which has a higher diffusion coefficient in water ($D_M^W : D_M^{gel} = 1.18$) [41] and was therefore accounted for in the C_{DGT} calculations using equation 4.6.

$$C_{DGT} = \frac{M(D_M^W \Delta g + D_M^{gel} \Delta g)}{t D_M^W D_M^{gel} A_e} \qquad \text{Equation 4.6}$$

The DGT equation (equation 4.2) was used in conjunction with the limits of detection for the ICP-MS to produce a matrix of minimum deployment times for varying diffusion coefficients (changes in temperature and pH) with changing solution concentration for fresh water deployments (Table 4.2). Marine deployments were calculated to take approximately 110% of the time required for fresh water deployments due to a reduction (10%) in the diffusion coefficient.

Table 4.2: Minimum deployment time (h) required to accumulate ICP-MS detectable concentrations of U in fresh water at various temperatures and pH values. Calculated using the DGT equation 4.2 and the diffusion coefficients from Hutchins *et al.* [28] (value shown next to pH), corrected for using the Stokes-Einstein equation 4.3. The non-linear change in diffusion coefficients with pH is discussed by Hutchins *et al.* [28]. It should be noted that very long deployment times (> 7 days or 168 h) are unfeasible for DGT as it is highly susceptible to biofouling due to the theoretical calibration used.

Bulk solution U concentration (µg L^{-1})	**Minimum deployment time (h)**			
	10°C	**15°C**	**20°C**	**25°C**
	pH 6 (D = 3.7 x 10^{-6} cm^2s^{-1})			
0.001	88.5	51.5	34	24
0.01	8.5	5	3.4	2.5
0.10	1	0.5	0.5	0.5
	pH 7 (D = 3.1 x 10^{-6} cm^2s^{-1})			
0.001	105	61.5	40.5	28.5
0.01	10.5	6	4	3
0.10	1	0.5	0.5	0.5
	pH 8.1 (D = 4.4 x 10^{-6} cm^2s^{-1})			
0.001	74.5	43	29	20
0.01	7.5	4	3	2
0.10	1	0.5	0.5	0.5

4.2.4 Comparison of the performance of Chelex-100, Metsorb, and MnO_2 resins

4.2.4.1 Uptake of U and elution efficiencies of the test resins

The uptake efficiencies of the three test resins for U were determined using a batch method. Disks (0.19 cm^3) of each resin gel were placed in Fisher brand PS vials (30 mL) and a solution (20 mL, 0.01 M $NaNO_3$ at pH 7 ± 0.2) containing 10, 25, 50 or 100 µg L^{-1} of U(VI) added. The vials were shaken (48 h) on a rotating table (IKA® KS 130 Basil, Sigma-Aldrich Ltd., Gillingham, U.K.) at a set speed of 240 revolutions min^{-1}. One mL aliquots were taken and acidified (using 20 µL 6 M HCl) before and after resin gel exposure to determine the mass balance and percentage uptake of U. To determine the elution efficiencies, the gels were removed from the solutions and placed into new PS vials containing 2 M HNO_3 (2 mL) for the Chelex-100 gels or 1 M HNO_3/1 M H_2O_2 (2 mL) for the Metsorb and MnO_2 gels. A 1 M $NaHCO_3$/1M H_2O_2 (2 mL) solution was also trialled for the Metsorb gels. The tubes were then agitated (48 h) on the rotating table and the resin gel removed. Control experiments containing 20 mL of 100 µg L^{-1} of U, 0.01 M $NaNO_3$ at pH 7 ± 0.2 with no resin gels showed no sorption of U to the vessel.

4.2.4.2 Effect of pH and ionic strength on uptake of U

A batch method was used as per section 4.2.4.1. A 0.19 cm^3 disk of each resin gel was placed in a PS vial (30 mL) and exposed to solutions (20 mL) containing 100 µg L^{-1} of U (VI) in 0.01 M $NaNO_3$ at pH 3, 4, 5, 7, 8 and 10 (to test the effect of pH) or 100 µg L^{-1} of U (VI) in 0.01, 0.1, 0.4, 0.7 and 1 M $NaNO_3$ at pH 7 (to test the effect of ionic strength). The vials were shaken (48 h) on a rotating table. One mL aliquots of the solution were taken and acidified (using 20 µL 6 M HCl) before and after resin gel exposure to determine the mass balance and percentage uptake of the U. Solutions were made up in the PS vials in triplicate for each pH value tested here with no addition of resin gels, to assess the sorption of U to the PS vials.

4.2.4.3 Mass accumulation of U over time

To measure the uptake of U over time, DGT devices were exposed (5 days) in square polypropylene tanks (5 L) to 0.01 M $NaNO_3$ (low ionic strength water) plus 0.983 mM $NaHCO_3^-$ to buffer the solution to pH 7.7 (a similar pH to the freshwater field test site) or an artificial sea water solution (prepared following [42]) containing 100 µg L^{-1} U. Devices were removed in triplicate at the time intervals of 4, 8, 12, 24, 48, 72, 96 and 120 h, and the resin gels eluted as per section 4.2.4.1. Two aliquots (1

mL) of the solution were taken daily from the exposure tank. One was filtered though a 0.2 µm filter and acidified (20 µL 6 M HCl), the other was acidified (20 µL 6 M HCl) with no filtration to ensure no precipitates were formed in the solution that may affect DGT uptake.

4.2.4.4 Effect of interferences and ligands on uptake of U

Effect of the presence of calcium (Ca^{2+}) as a potential interference in water and the complexants bicarbonate (HCO_3^-), phosphate (PO_4^{3-}) and sulphate (SO_4^{2-}) were tested for all three resin gels. Table 4.3 details the concentrations used, which exceed typical environmental concentrations to ensure any effect from an episodic event (e.g. heavy rain, or flooding) can be seen. The HCO_3^- and SO_4^{2-} concentrations are double those seen in some fluvial systems [43], with Ca^{2+} five times that found in the River Lambourn and approximately that found in sea water. The PO_4^{3-} concentrations were similar to sewage effluent inputs into the Lambourn [44, 45] and five times higher than a typical Thames tributary [46]. The higher PO_4^{3-} concentrations were used in order to clearly identify any effect outside of experimental errors on U uptake. An acid washed PP container (3 L) containing a 0.01 M $NaNO_3$, 100 µg L^{-1} U solution (3 L) plus either an interferent or ligand (concentrations detailed in Table 3) was equilibrated for 24 h at pH 6.5 ± 0.2 for the Ca^{2+}, SO_4^{2-} and PO_4^{3-} additions, and pH 8.1 ± 0.3 for the HCO_3^- additions. DGT devices containing each type of resin gel were then deployed (96 h) in triplicate, then removed and eluted as per section 4.2.4.1. One mL aliquots of the exposure tank solution were taken daily and acidified (using 20 µL 6 M HCl) to measure the concentration of U. Equation 4.2 was used to calculate the C_{DGT}, and this was compared to U concentrations in the grab samples. An agreement between these two measurements showed these devices to be working well.

In order to assess sorption of U to the polypropylene tank, a continuously stirred 5L solution containing 100 µg L^{-1} U, 0.01M $NaNO_3$ at pH 7 was left for 10 days with no DGT devices deployed. Two aliquots (1 mL) of the solution were taken daily from the exposure tank. One was filtered though a 0.2 µm filter and acidified (20 µL 6 M HCl), the other was acidified (20 µL 6 M HCl) with no filtration.

Table 4.3: Salt and concentration of ligands and interferences tested in this study.

Ligand (salt used)	**Salt concentrations tested in this study**					
Ca^{2+} ($CaCl_2.2H_2O$)	500 mg L^{-1}	250 mg L^{-1}	100 mg L^{-1}	1 mg L^{-1}	100 µg L^{-1}	50 µg L^{-1}
PO_4^{3-} (KH_2PO_4)	5 mg L^{-1}	1 mg L^{-11}	100 µg L^{-1}	50 µg L^{-1}	5 µg L^{-1}	
SO_4^{2-} (Na_2SO_4)	200 mg L^{-1}	20 mg L^{-1}	2 mg L^{-1}	200 µg L^{-1}	20 µg L^{-1}	
HCO_3^- ($NaHCO_3$)	500 mg L^{-1}	250 mg L^{-1}	100 mg L^{-1}	1 mg L^{-1}	100 µg L^{-1}	

4.2.5 Field deployments

Two field sites (fresh water and marine) were used in this study. The fresh water site (51.446933 N, -1.3838275 W) was located on the River Lambourn near Boxford, Berkshire, U.K. The river has a Chalk fed aquifer catchment and an average pH of 7.9-8 [44]. DGT devices were deployed between perspex plates (15 x 7 cm, 8 devices per plate) and attached to a rope and float and weighted to the river bed. The marine site was located adjacent to the National Oceanography Centre, Southampton, U.K. (50.891313 N, -1.3938260 W). This site is a well mixed estuarine site with a salinity of 29 to 33 (dependent upon tidal fluctuations and freshwater inputs) and is a moderate flow site with tidal fluctuations agitating the water. The devices were deployed as above at 1 m below the water surface. Ropes were used to attach the exposure plate to the dock pontoon.

Three DGT devices containing each resin gel were removed on days 2, 4, 7, 10 and 14. To assess the presence of the diffusive boundary layer, DGT devices containing the Metsorb gel were deployed for 5 days with diffusive layer PAM gel thicknesses (including 0.015 cm to account for the Supor membrane) of 0.015, 0.055, 0.095, 0.135 and 0.175 cm, as per Warnken *et al.* [40]. Diffusion coefficients calculated by Hutchins *et al.* [28] were used for the TWA calculations. Spot samples of water (20 mL) were collected at the exposure sites and were filtered (0.2 µm pore size Supor filters) and acidified *in situ* with 6 M HCl (40 µL). Water temperature and pH were recorded each time a device was removed so that diffusion coefficients could be corrected for variations in environmental conditions.

Procedural DGT blanks (3 per resin) were prepared along with the deployed devices and exposed to the field environment during deployment and retrieval of the sample devices. The blanks were then eluted and analysed with the samples as above.

4.3 **Results and discussion**

4.3.1 Uptake and elution efficiencies

Uptake and elution efficiencies were measured by exposing the Chelex-100, Metsorb and MnO_2 binding gels to known masses of U and then eluting the bound element. Uptake by Chelex-100 and MnO_2 was > 80% of the U in solution for a range of concentrations (10–100 µg L^{-1}), with the Metsorb resin accumulating > 90% of the U in solution. Using 2 M HNO_3 as the eluent, Chelex-100 had an elution efficiency of 80 ± 6%, which is higher than found by Li *et al.* [24] but comparable to other studies measuring trace metals using DGT with Chelex-100 resins [47]. Using 1 M HNO_3/1 M H_2O_2 as the eluent MnO_2 had an elution efficiency of 84 ± 4% and Metsorb 83 ± 3%. Using 1 M $NaHCO_3$/1 M H_2O_2 as eluent, Metsorb had an elution efficiency of 70 ± 3%. Hutchins *et al.* [28] used 1 M NaOH/1 M H_2O_2 solution to elute the U, with an efficiency of 95.2 ± 0.4 %. Sodium hydroxide was not used here as the sodium acts as a signal suppressor with the ICP-MS without further dilution. The low standard deviations for the elution step indicated that the procedure was reproducible.

4.3.2 Effect of pH and ionic strength on uptake

Over the range of ionic strengths tested there was consistent uptake of U by all three resins in line with the uptake efficiencies reported in section 4.3.1. However, when deployed in DGT devices containing Metsorb, that included a PAM layer, Hutchins *et al.* [28] observed a 24% decrease in U uptake in higher ionic strength solutions. The effect of increasing the ionic strength of a solution may act to hinder U diffusion through the PAM gel rather than uptake by the resin gel.

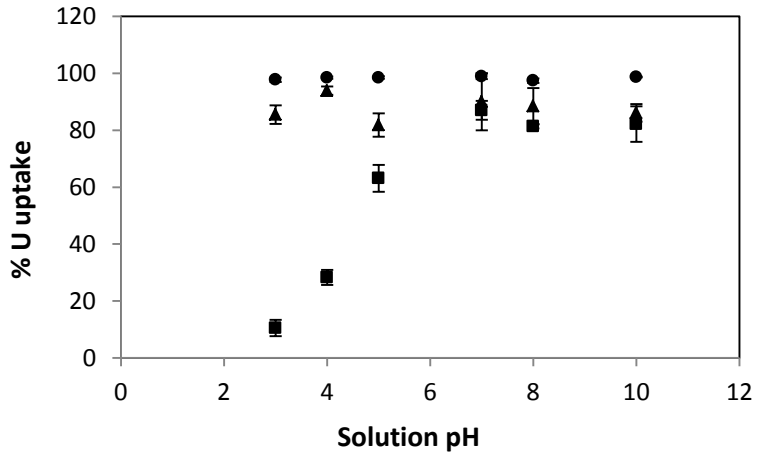

Figure 4.1 Uptake of U from a 100 µg L^{-1} solution by the three resin gels manganese dioxide (■), Metsorb (●) and Chelex-100 (▲) across a range of pH values. Error bars are the standard error of the mean of triplicate readings.

Figure 4.1 shows the effect of changing pH on U uptake by the Chelex-100, Metsorb and MnO_2 binding gels. There was found to be no sorption of the U to the PS vials observed in the experiments containing no resin gels. U accumulation by the MnO_2 resin decreased to ≈60% at pH 5, ≈30% at pH 4 and ≈10% at pH 3. As MnO_2 has a point of zero charge (pzc) at about pH 2.25 [48], and a negative charge throughout the pH range tested, a change in surface charge should not be causing this decrease above pH 3 as U exists as the uranyl cation over this pH range. At acidic pH values in which the E_h drops below +0.8 V the MnO_2 can form $Mn_2O_{3(s)}$ or even soluble Mn^{2+} therefore reducing the number of binding sites [30]. There were no obvious colour changes observed for the MnO_2 resin gels upon immersion in the pH 3 solution that would be indicative of a phase change of the manganese, however, Burnett *et al.* [30] observed a similar response of U uptake by MnO_2 at low pHs. Yao and Millero [49] identified the requirement for further work to fully characterise ion interactions with the MnO_2 surface.

Surface complexation and hydrolysis is the mechanism by which U is sorbed to Metsorb (TiO_2) [50, 51]. TiO_2 is amphoteric and has a pzc at pH 6 [48] to 7 [50, 52] and can therefore sorb both anions and cations on the positively and negatively charged surfaces respectively, allowing the Metsorb to operate over a wide range of pH values. The Chelex-100 resin was not adversely affected by changing pH, although previous studies have shown lower pH's inhibit U accumulation [24, 25]. Chelex-100 acts as a cation exchanger in solutions with a pH > 3-4, and an anion exchanger in solutions with a pH < 3-4 [53]. The predominant U species in this experiment were cationic uranyl UO_2^{2+} species with increasing anionic hydroxide or carbonate species present only at high pH values (> 7.5). Li *et al.* [24, 25] found that with pH < 5 the ability of the Chelex-100 to accumulate U decreased but this was not observed in our experiments. In the environmental pH range (5–8), there was no effect on U accumulation by either Chelex-100 or Metsorb.

4.3.3 Effect of interferences and ligands on uptake

All speciation distributions were calculated using Visual Minteq, version 3, beta (© 2010 KTH, Department of Land and Water Resources Engineering, Stockholm, Sweden) for each ligand tested. This was undertaken in order to support the experimental work outlined in section 4.2.4.4. The DGT concentration of the solution over the deployment period was calculated using equation 4.2, and compared as a ratio to the concentration measured directly by grab samples. A ratio of 1:1 shows that the

technique is working correctly and is unaffected by the ligand. All inorganic U complexes formed were initially assumed to be fully labile in this study.

Calcium ions were not calculated to form any complexes with U, except in the presence of atmospheric carbon dioxide at pH > 6.5, when calcium will form soluble $CaUO_2(CO_3)_3^{2-}$ and $Ca_2UO_2(CO_3)_3$ complexes [54, 55] (Figure 4.2). Increasing the Ca concentration increased U adsorption from 80% for Chelex-100 and 85% for Metsorb and MnO_2 at ln 4 (natural log 4), to 100% at ln 10 (natural log 10) for all three resin gels. The lower uptake at Ca concentration of ln 4 is commensurate with the uptake data discussed in section 4.3.1 in the absence of complexing ligands. The U species at this Ca concentration are predominantly hydroxide and carbonate. Using Visual Minteq 100% of the U was calculated to occur in the dissolved phase, so increases in U uptake by the Metsorb and MnO_2 maybe as a result of decreasing UO_2OH^+ and $UO_2(OH)_2$ which do not interact with these resins. As all three resins exhibited an increase in uptake in the presence of calcium, the $Ca_2UO_2(CO_3)_{3(aq)}$ and $CaUO_2(CO_3)_3^{2-}$ species that form may be more labile than the $UO_2CO_{3(aq)}$ and hydroxide species predominant at lower Ca concentrations, with $Ca_2UO_2(CO_3)_{3(aq)}$ being the more labile of the two. Yao and Millero [49] showed that anion uptake (PO_4^{3-}) by MnO_2 is enhanced in the presence of divalent cations (such as Ca^{2+} or Mg^{2+}) due to the surface charge of the MnO_2 being reversed by the exchange of H^+ for metal ions in solution, which may account for the increase in uptake of the U species by this resin with increasing Ca concentrations. As Chelex-100 also shows increasing U uptake with increasing Ca concentration it is unlikely that cation exchange is the sole uptake mechanism. The increase could be due also to chelation or cation assisted uptake, as with the MnO_2, or a combination of all three. The decrease in uptake observed at the very high Ca concentration (ln 13 or 500 µg L^{-1}) for all three resins, in particular MnO_2 for which there is a decrease from 100% to 70%, could be as a result of competition for binding sites between the U species and Ca, as at this concentration 97% of the Ca is predicted (using Visual Minteq) to occur as the free metal ion Ca^{2+}. The Metsorb uptake was above 0.8 (80%) at all Ca^{2+} concentrations.

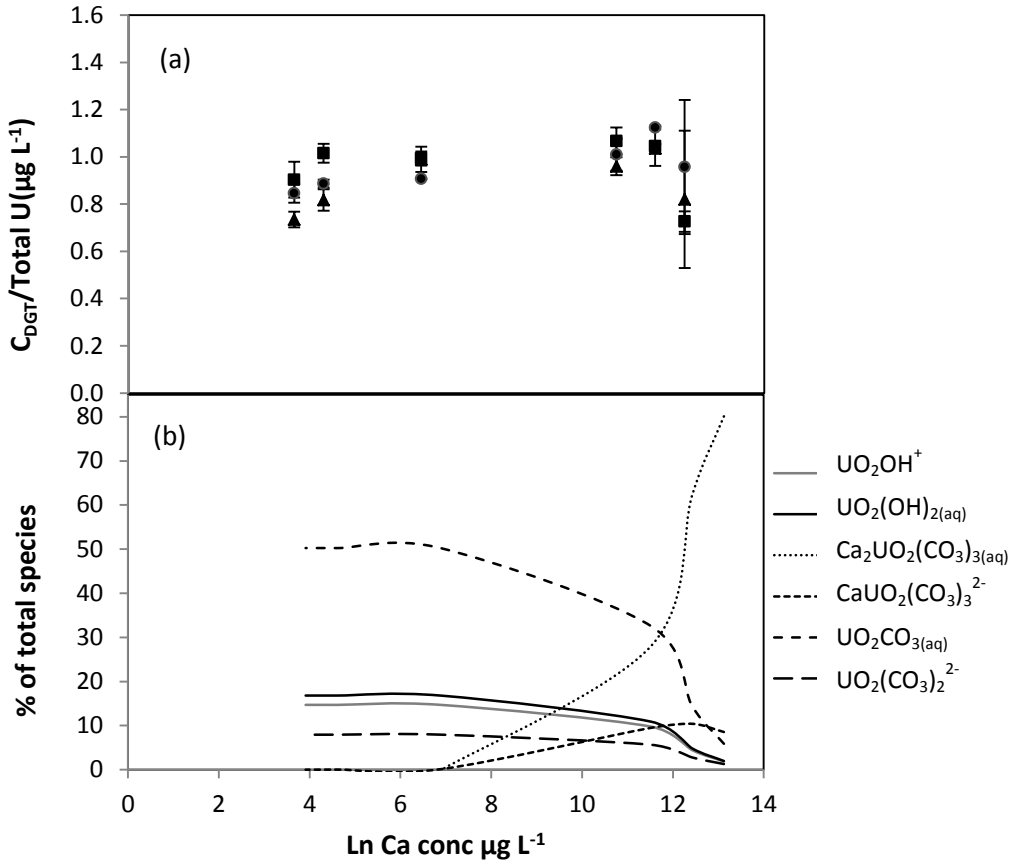

Figure 4.2 (a) Effect of Ca^{2+} on U uptake by manganese dioxide (■), Metsorb (●) and Chelex-100 (▲) resin gels. Concentration of U in DGT device (C_{DGT}) is shown as a ratio to the average concentration of the total U over the 96 h deployment period measured directly in the solution (C_{total}) across a range of Ca^{2+} concentrations from 50 µg L^{-1} to 500 mg L^{-1}; average pH 7, average temperature 18°C, calculated diffusion coefficient 1.9 x 10^{-6} cm^2 s^{-1}. 100% of the U was predicted to be in solution using Visual Minteq (version 3 beta). Error bars are the standard error of the mean of triplicate readings. (b) U species prediction calculated using Visual Minteq (version 3 beta) across Ca^{2+} concentrations from 50 µg L^{-1} to 500 mg L^{-1}, with a pH of 6.5, a U(VI) addition of 100µg L^{-1}, calculated ionic strength of 0.01 M, temperature of 18°C an atmospheric partial pressure of dissolved CO_2. Only major uranyl species are shown.

There was only a minor effect on U uptake with increasing SO_4^{2-} concentrations (Figure 4.3), with uranyl sulphate complexes only occurring at high SO_4^{2-} concentrations (> 20 mg L^{-1}) due to the preferential carbonate complexes formed with dissolved CO_2. SO_4^{2-} interaction with the resins may be increased by the presence of divalent cations in a more complex matrix [49], such as may occur in the field.

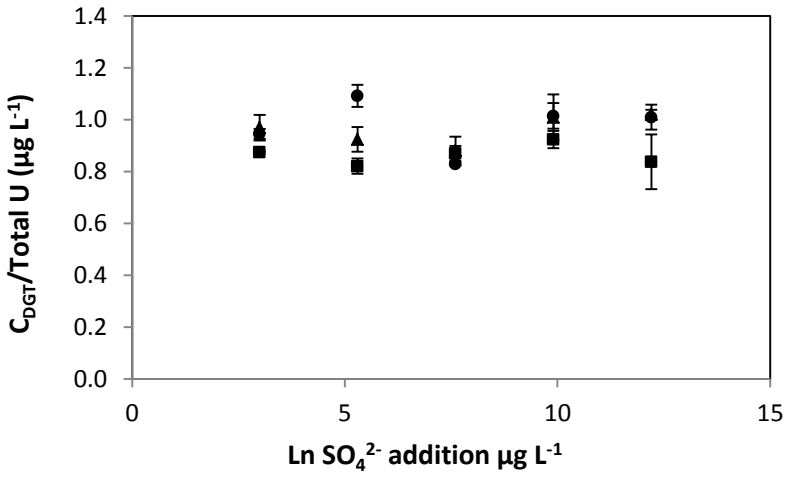

Figure 4.3. Effect of SO_4^{2-} on U uptake by manganese dioxide (■), Metsorb (●) and Chelex-100 (▲) resin gels. Concentration of U in DGT device (C_{DGT}) is shown as a ratio to the average concentration of the total U over the 96 h deployment period measured directly in the solution across a range of SO_4^{2-} concentrations from 20 µg L^{-1} to 200 mg L^{-1}; average pH 6.5 ± 0.2, average temperature 17°C, calculated diffusion coefficient 1.95 x 10^{-6} cm^2 s^{-1}. 100% of the U was predicted to be in solution using Visual Minteq (version 3 beta). Error bars are the standard error of the mean of triplicate readings.

PO_4^{3-} showed a significant influence on the distribution of U between the dissolved and precipitated phases (Figures 4.4a-c), with a marked decrease in dissolved U when the phosphate in this experiment was > 1 mg L^{-1}. This is the point at which the U hydroxide complexes become less dominant in the speciation distribution with the uranyl phosphate complexes $UO_2PO_4^-{}_{(s)}$ and $UO_2HPO_{4(aq)}$ (Figure 4.4c). PO_4^{3-} complexation with U becomes particularly important if the total phosphate:carbonate ratio is greater than 10^{-1} [56]; at 5 mg L^{-1} PO_4^{3-} addition in this experiment the total phosphate: total carbonate ratio is 0.3. Figure 4.4b shows that all three resins accumulated U at expected ratios similar to that of Figure 4.1 (0.8 to 1.0) in the presence of PO_4^{3-} concentrations up to and including 1 mg L^{-1}. At 5 mg L^{-1} the accumulation of U by the resins decreases to 60% for Chelex-100, 40% for the MnO_2 and 50% for the Metsorb. The decrease observed for the Metsorb [57] and the MnO_2 [49] is most likely as a result of direct competition for binding sites by the PO_4^{3-}, and Chelex-100 (which is the least affected by the phosphate additions) decrease can be attributed to the decrease in the cationic species UO_2OH^+ and UO_2^{2+}, and a concurrent increase in anionic $UO_2HPO_4^-$.

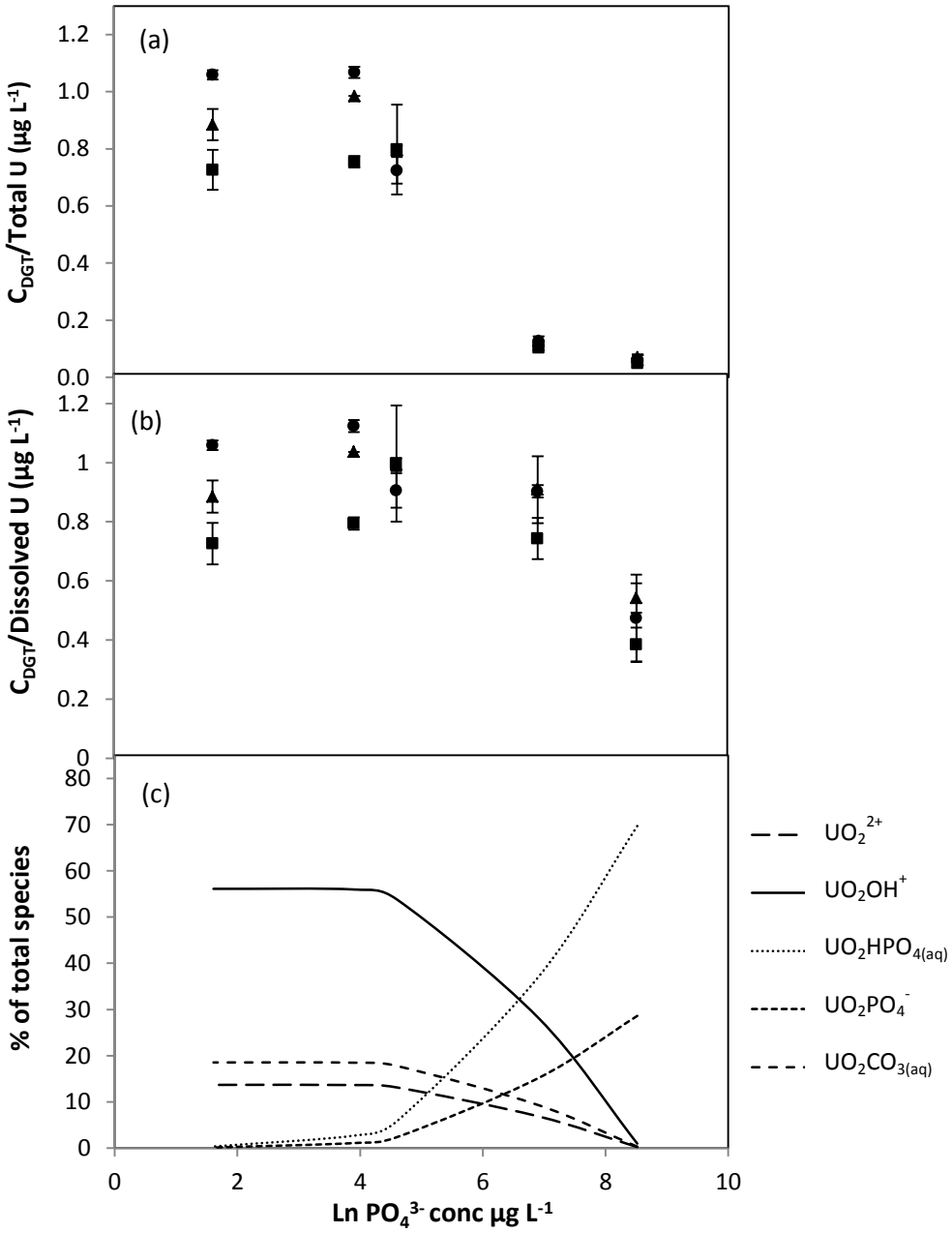

Figure 4.4 (a) Effect of PO_4^{3-} on U uptake by manganese dioxide (■), Metsorb (●) and Chelex-100 (▲) resin gels. Concentration of U in DGT device (C_{DGT}) is shown as a ratio to the average concentration of the total U over the 96 h deployment period measured directly across a range of PO_4^{3-} concentrations from 5 µg L^{-1} to 5 mg L^{-1}; average pH 6.5 ± 0.2, average temperature 17 ± 0.1°C, calculated diffusion coefficient 1.95 x 10^{-6} cm^2 s^{-1}. Error bars are the standard error of the mean of triplicate readings. (b) Effect of PO_4^{3-} on U uptake by manganese dioxide (■), Metsorb (●) and Chelex-100 (▲) resin gels. Concentration of U in DGT device (C_{DGT}) is shown as a ratio to the concentration of the dissolved U calculated from the total U measurements using Visual Minteq (version 3 beta) across a range of PO_4^{3-} concentrations from 5 µg L^{-1} to 5 mg L^{-1}; average pH 6.5 ± 0.2, average temperature 17°C, calculated diffusion coefficient 1.95 x 10^{-6} cm^2 s^{-1}. Error bars are the standard error of the mean of triplicate readings. (c) U species prediction calculated using Visual Minteq (version 3 beta) across PO_4^{3-} concentrations from 5 µg L^{-1} to 5 mg L^{-1}, with a pH of 6.5, a U(VI) addition of 100 µg L^{-1}, calculated ionic strength of 0.01 M, temperature of 17°C an atmospheric partial pressure of dissolved CO_2. Only major uranyl species are shown.

Carbonate speciation with the uranyl ion accounts for 90–100% of U in the oceans [58]. It is important to understand any impact complexation between U and carbonate may have on the uptake of the DGT devices used in this study. Gregusova *et al.* [29] conducted experiments to observe changes in U uptake with increasing HCO_3^- concentrations. For both the Chelex-100 and Spheron-Oxin® resins, a decrease in U uptake with increasing carbonate concentrations was observed, potentially as a result of the increasingly anionic species formed. In this study a similar decrease in DGT performance was noted with increasing bicarbonate concentration by the DGT devices containing Chelex-100, Metsorb and MnO_2 (Figure 4.5a). The MnO_2 sorbed less of the carbonate bound U than Metsorb or Chelex-100 and was particularly affected by increasing concentrations of the calculated uranyl carbonate species $UO_2(CO3)_3^{4-}$, as shown in Figure 4.5b. As stated previously, adsorption of anions by MnO_2 may be made possible through the presence of divalent cations, which were not present in this experiment. Gregusova *et al.* [29] observed that DGT devices containing Chelex-100 as the binding phase accumulated decreasing concentrations of U when the total carbonate concentration exceeded 30 mg L^{-1}. A similar decrease of U sorption by Chelex-100 has been observed in this experiment. Total carbonate concentrations higher than 30 mg L^{-1} yield more anionic species with the neutral uranyl carbonate species $UO_2(OH)_2$ and $UO_3CO_{3(aq)}$ decreasing, which will affect the ability of the U to bind to the Chelex-100. The Metsorb resin is affected by very high total carbonate concentrations only (≥ 100 mg L^{-1}). The decrease in adsorption of U may be as a result of competition with other anionic species present in the solution such as $NaCO_3^-$ and HCO_3^-.

The PP tank containing a 5 L 100 µg L^{-1} U solution with no DGT devices deployed showed a reduction in concentration of non-filterable U by 19% from 69 µg L^{-1} to 56 µg L^{-1}, and an initial reduction in 0.2 µm filtered U by 40% from 62 µg L^{-1} to 44 µg L^{-1} was observed, after which a stable concentration was attained. During the 10 day trial there was also a pH decrease by 0.25 units. The sorption of U observed between pH 6-7 is similar to that observed by Hutchins *et al.* [28] and was attributed to the neutral species more readily binding to the PP container. This decrease did not affect the results as an average concentration across the experimental period was used.

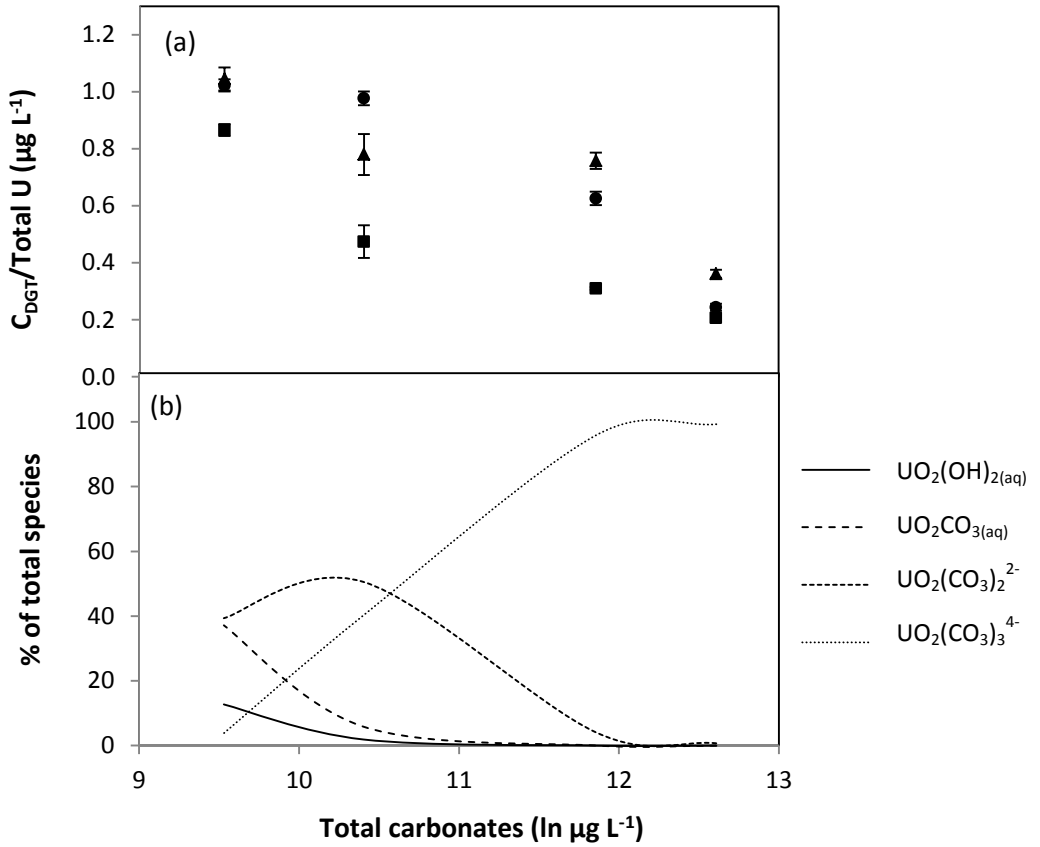

Figure 4.5 a) Effect of HCO_3^- on U uptake by manganese dioxide (■), Metsorb (●) and Chelex-100 (▲) resin gels. Concentration of U in DGT device (C_{DGT}) is shown as a ratio to the average concentration of the total U over the 96 h deployment period measured directly in the solution (C_{soln}) across a range of HCO_3^- concentrations from 100 µg L^{-1} to 500 mg L^{-1}; average pH 8.1 ± 0.3, average temperature 17 ± 0.2°C; calculated diffusion coefficient 2.31 x 10^{-6} cm^2 s^{-1}. Error bars are the standard error of the mean of triplicate readings. (b) U species prediction calculated using Visual Minteq (version 3 beta) across HCO_3^- concentrations from 100 µg L^{-1} to 500 mg L^{-1}, with a pH of 8.2, a U (VI) addition of 100µg L^{-1}, calculated ionic strength of 0.01 M, temperature of 17°C an atmospheric partial pressure of dissolved CO_2. Only major uranyl species are shown.

4.3.4 Mass accumulation over time

4.3.4.1 Laboratory deployments

DGT deployments for all three test resins in the low ionic strength solution (Figure 4.6) accumulated U as predicted by the DGT equation (equation 4.2). The predominant species present at pH 7.7 is $UO_2(CO_3)_2^{2-}$ with no significant precipitates forming and the filtered and non-filtered grab samples in close agreement. None of the devices appeared to be capacity limited under these experimental conditions. Using the DGT equation and taking into account the U depletion gives a DGT uptake: solution concentration ratio of 1:1 for the entire deployment period for Chelex-100 and Metsorb, with a slight decrease in U accumulation by the MnO_2 at 5 days. This means the MnO_2 may not be suitable for field deployments longer than 4 days, but that theoretically the

Chelex-100 and Metsorb™ DGT devices could be deployed in an alkaline freshwater system for 5 days or potentially longer.

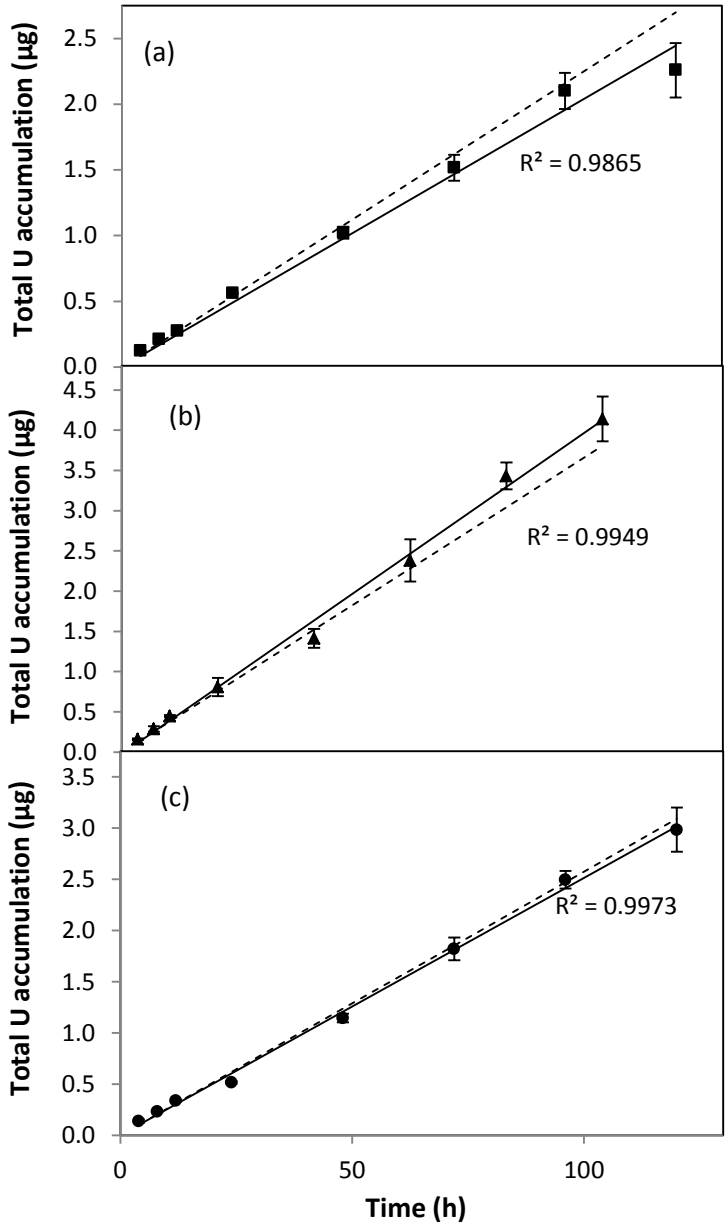

Figure 4.6: Mass accumulation with time in 0.01 M $NaNO_3$. Solution pH 7.7 ± 0.05 with 120 h deployment time: (a) manganese dioxide resin gel (■) average concentration 75 µg L^{-1}, average temperature 15°C, calculated diffusion coefficient 2.52 x 10^{-6} $cm^2 s^{-1}$; (b) Chelex-100 resin gel (▲), average concentration 83 µg L^{-1}, average temperature 20°C, calculated diffusion coefficient 3.21 x 10^{-6} $cm^2 s^{-1}$; (c) Metsorb resin gel (●) average concentration 75 µg L^{-1}, average temperature 18°C, calculated diffusion coefficient 2.74 x 10^{-6} $cm^2 s^{-1}$. The dashed line represents model U uptake calculated from DGT equation (equation 4.2) using the average solution concentration; and the solid line represents the linear regression of U uptake during the linear uptake phase. Error bars are the standard error of the mean of triplicate measurements.

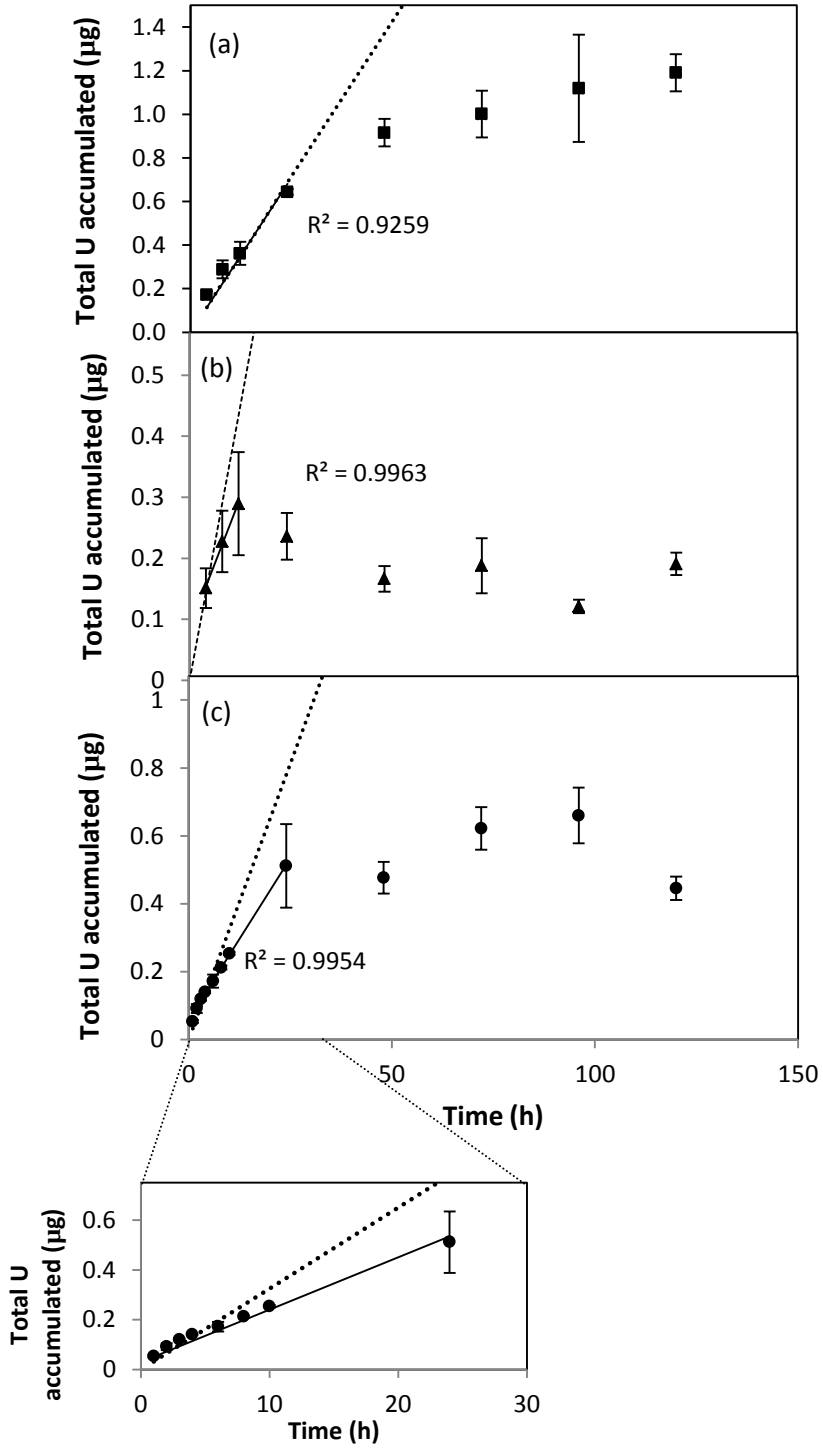

Figure 4.7: Mass accumulation with time in artificial sea water. Solution pH 8.2 with 120 h deployment time: (a) manganese dioxide resin gel (■), average U solution concentration 102 µg L^{-1}, average temperature 18°C, pH 8.1 calculated diffusion coefficient 2.26 x 10^{-6} cm^2 s^{-1}; (b) Chelex-100 resin gel (▲), average U solution concentration 115 µg L^{-1}, average temperature 18°C, pH 8.1, calculated diffusion coefficient 2.26 x 10^{-6} cm^2 s^{-1}; (c) Metsorb resin gel (●), average U solution concentration 103 µg L^{-1}, average temperature 20°C, pH 8.1, calculated diffusion coefficient 2.65 x 10^{-6} cm^2 s^{-1}. The dashed line represents model U uptake calculated from DGT equation (equation 4.2). Error bars are the standard error of the mean of triplicate measurements. Shorter time intervals have been measured here initially and shown in the inset graph.

Deployments in artificial sea water (Figure 4.7) showed that DGTs with the MnO_2 resin had a linear uptake of U as predicted by the DGT equation for 24 h up to 0.6 µg U. The DGT deployment time for the device with Metsorb resin was linear and in agreement with the DGT equation for about 10-12 h, with 0.25 µg U accumulated. The Chelex-100 was unable to accumulate U as predicted by the DGT equation past 4 h, accumulating 0.15 µg U, potentially due to ionic interferences and the anionic nature of the U species present. The Metsorb and Chelex results agree well with the findings of Hutchins *et al.* [28]. These results imply that the devices may not be capable of field deployments longer than 24 h, with Chelex-100 DGT devices unsuitable for the measurement of U in a marine environment.

4.3.4.2 Field deployments

The marine site had an average U concentration of 3 µg L^{-1} over the deployment period, which is similar to concentrations found at other marine sites (Table 4.1). The predominant uranium species in the marine environment are $UO_2(CO_3)_2^{2-}$ and $UO_2(CO_3)_3^{4-}$, with self diffusion coefficients of 5.52 x 10^{-6} cm^2 s^{-1} at 25°C (as described in section 3.1.1.) This gives a $D_M^W : D_M^{gel}$ ratio of 1.18 which is considered when calculating the DBL (equation 4.5). Figure 4.8a shows that the MnO_2 DGT accumulated U at the marine site in agreement with the DGT equation for 2 days. As the response for both the MnO_2 and TiO_2 resins is increasing over the deployment time, it is unlikely that saturation of either resin has been achieved and is affecting uptake. It is likely that biofouling (for instance a thin microbial layer) on the outer membrane inhibited accumulation in agreement with the DGT equation (equation 4.2) past 2 days, by retarding diffusion of the U, although this would be an area for further study. Fresh water inputs (salinity measurements varied throughout the deployment time from *salinity* = 27 to 32) to the marine site in this study could also have been responsible for the longer field deployment times than predicted in the laboratory trials due to decreased ionic competition, although a further marine field trial would be required for a 24 h period (the time period the uptake in the laboratory was in agreement with the DGT equation) to ascertain this. U in sea water exists predominantly as the soluble uranyl carbonate anion, $UO_2(CO_3)_2^{2-}$, which was taken up by all three resin gels under laboratory conditions, with MnO_2 being the most affected by increasing predominance of anionic U species The Chelex-100, as per laboratory experiments, did not accumulate U in agreement with the DGT equation.

Another explanation for the U accumulation past day 2 not agreeing with the DGT equation could be a reduction in available binding sites, as opposed to complete saturation. Competing ions in sea water (in particular in coastal waters where they occur in higher concentrations), could begin to fill the resin binding sites prior to U diffusing through the PAM. The diffusion coefficient of U is approximately half that exhibited by transition metals and other anions present such as phosphate (diffusion coefficient of PO_4^{3-} in water at 25°C, pH 6.5 is 6.05 x 10^{-6} cm^2 s^{-1} [57]; the U diffusion coefficient for equivalent conditions is 3.7 x 10^{-6} cm^2 s^{-1}[37]). This could lead to the binding sites on non-specific resins, such as the resins examined here, filling up faster in the presence of complex matrices such as sea water. The transition metals show an increase in the diffusion coefficients with increasing atomic mass, so it follows that as U has a high mass, it should have a higher rate of diffusion. As U does not continue the trend of increasing rate of diffusion with mass, the lower diffusion rates may in part be explained by steric effects of complexes formed and through interaction of the U with the PAM gel. Gregusova *et al.* [29] found that for up to 8 h, the DGT sampler underestimated the U concentration in solution. It was explained through a reaction between traces of acrylic acid groups in the gel formed during the polymerisation process, and the transient uranyl ions. Upon saturation (~ 200 ng per disk) of these weak binding sites within the gel, predicted uptake of the U was observed [59]. No such artefact was observed during this study; however, deployment times were longer.

The fresh water site had an average U concentration of 0.4 µg L^{-1} over the deployment period, which is similar to U concentrations found at other fresh water sites (Table 4.1). The predominant species of uranium in calcium carbonate dominated streams is $CaUO_2(CO_3)_3$ with a self diffusion coefficient of 4.6 x 10^{-6} cm^2 s^{-1} at 25°C (as described in section 3.1.1.) This gives a $D_M^W : D_M^{gel}$ ratio of 1.02 which is considered close enough to 1 to not impact upon the results. The results for the field fresh water deployments (Figure 4.8b) show that all three resins accumulated 80% of predicted U, as per the DGT equation for the first 2 days. The Metsorb device continued to accumulate U at 80% of predicted values until day 7, after which the accumulated U decreases to 60% of the predicted value until day 14. The Chelex-100 and MnO_2 devices accumulated decreasing concentrations of predicted U concentrations throughout the deployment. Li *et al.* [24, 25] showed that Chelex-100 was only able to measure ~50% of dissolved U concentrations as predicted by the DGT equation in alkaline waters for up to 3 days.

The DBL for each site was calculated according to Warnken *et al.* [40] (using diffusive layer thicknesses of 0.015, 0.055, 0.095, 0.135 to 0.175 cm) and found to be 0.066 ± 0.013 cm at the marine site, and 0.046 ± 0.006 cm at the fresh water site (Figures 4.9 a & b for the marine and freshwater sites respectively). This is in agreement with the study by Warnken *et al*. [40] who showed that diffusive boundary layers can be as high as 0.15 cm in quiescent waters, and 0.023 cm in well stirred, turbulent solutions. The DBL is an important contributing factor to the diffusive layer thickness (Δg) in the DGT equations, and has been shown in this study to be present even in fast flowing waters. The concentrations of U calculated using the DGT equations were reduced by 50% in the marine site and 30% in the fresh water site without accounting for the effect of the DBL. The difference in DBL at the two sites could be attributed to the build up of pond weed at the freshwater site around the devices, which required clearing daily.

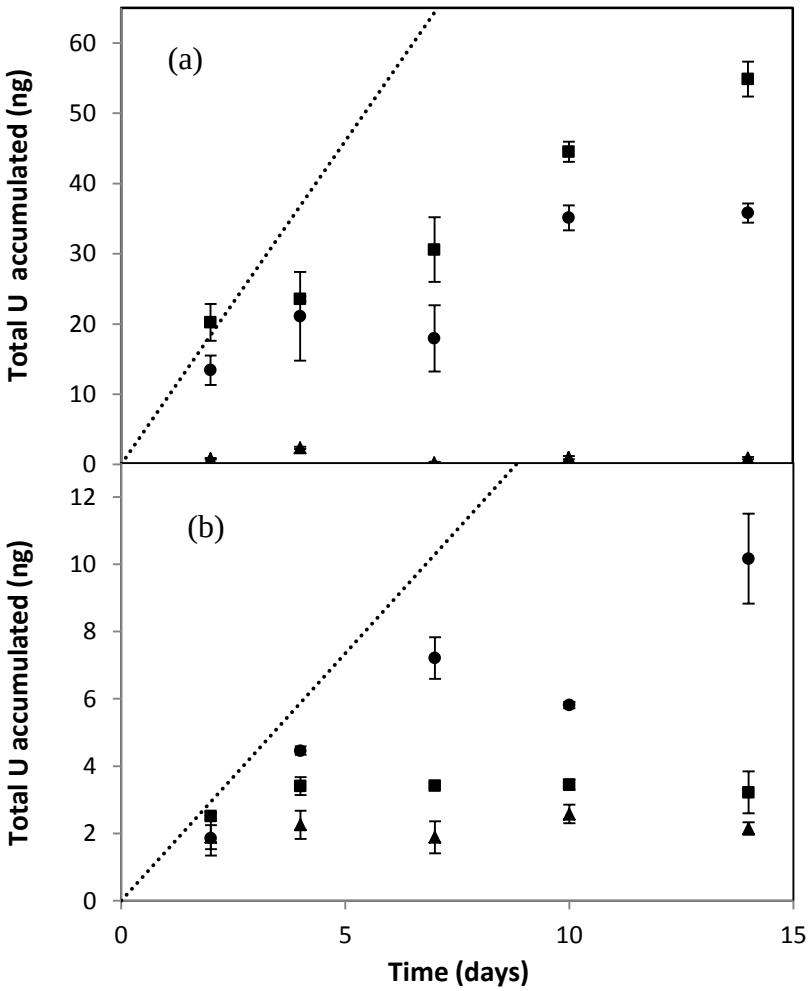

Figure 4.8: Mass accumulation with time in field trials, 14-day deployment for manganese dioxide (■), Metsorb (●) and Chelex-100 (▲): (a) marine deployment, average pH 8.2, average temperature 11°C, bulk solution concentration from spot sampling 3.0 µg L^{-1}, calculated diffusion coefficient 1.03 x 10^{-6} cm^2 s^{-1}; (b) fresh water deployment, average pH 7.9, average temperature 13°C, bulk solution concentration from spot sampling 0.4 µg L^{-1}, calculated diffusion coefficient 1.59 x 10^{-6} cm^2 s^{-1}. Dashed line represents model U uptake calculated from DGT equation (equation 4.2). Error bars are the standard error or the mean of triplicate measurements.

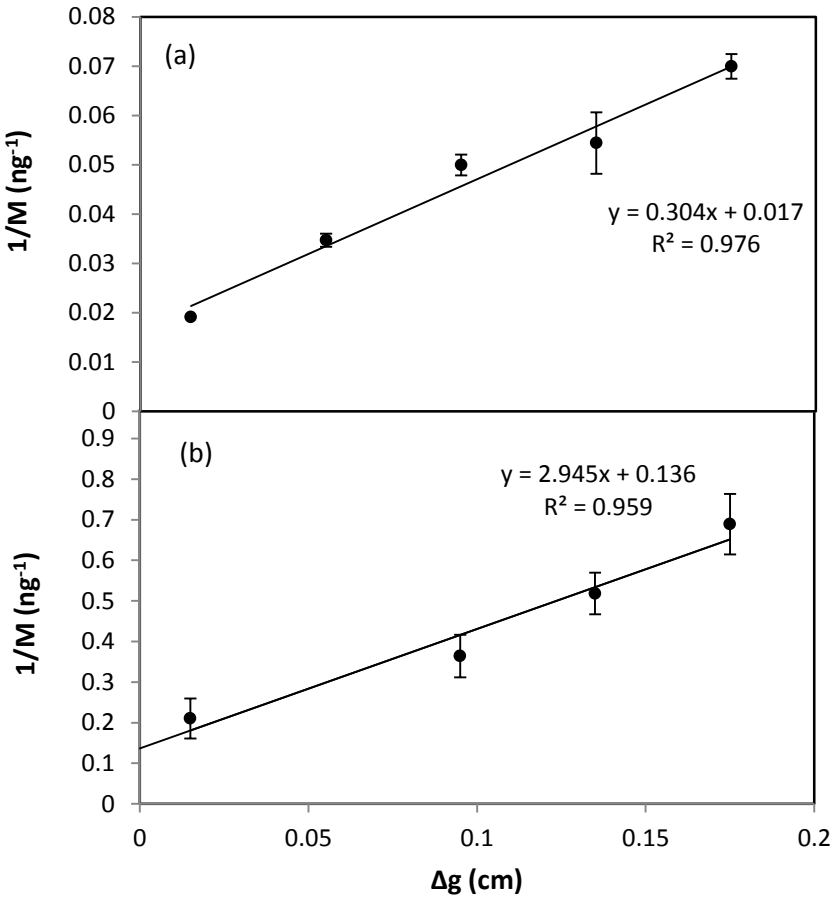

Figure 4.9 Plot of the reciprocal of mass (ng) accumulated with changing diffusive gel layer thickness to calculate the diffusive boundary layer for (a) the marine field site (DBL thickness 0.066 ± 0.013 cm) and (b) the fresh water field site (DBL thickness 0.046 ± 0.006 cm). Deployment time was 5 days for each site.

$^{235/238}$U isotopic ratios were also analysed for all field samples as shown in table 4.4. It was found that this ratio could be determined accurately after 2 days of deployment at both sites. The concentration of U in the River Lambourn averaged 0.4 µg L^{-1} throughout the deployment period, meaning U ratios were also detectable in the grab samples as no dilution was required prior to ICP-MS analysis. The marine site U concentration averaged 3.0 µg L^{-1} over the deployment period; however, with the 20 fold dilution required for direct analysis of the grab samples by ICP-MS, the concentration was reduced to 0.15 µg L^{-1}. This is at the limit of detection for the isotopic technique and meant that reproducible isotopic ratios were not possible. The seawater limit of detection could have been improved through the addition of a pre-concentration step such as that described by Zheng & Yamada [60], where an AG 1x8 anion exchange resin was used to pre-concentrate the U followed by a 0.1 M HCl elution. The Metsorb and the MnO_2 resins had better precision and accuracy for this technique than the Chelex-100. In this study, the ability to analyse the grab water samples provided a comparison for the DGT technique and showed that the U isotopic

signature was conserved during uptake by all three test resins. This has important implications for the application of DGT to long-term monitoring of radionuclides in aquatic systems and could be used as a tool for tracing pollution events and for measuring anthropogenic U additions to natural systems. The measurement of U isotopic signatures in and around nuclear installations is also a requirement of the U.K. Environmental Permitting Regulations 2010 [61]. Both field sites were found to have a natural $^{235/238}$U ratio of 0.00725.

Table 4.4 Results of $^{235/238}$U isotopic ratio analysis for each resin tested and the spot samples for the marine and freshwater field site. Natural $^{235/238}$U isotopic ratio is 0.00725.

Resin	**Marine**			**Fresh water**		
	Average isotopic ratio	RSD* (%)	Accuracy** (%)	Average isotopic ratio	RSD* (%)	Accuracy** (%)
Metsorb	0.00738 ± 0.0004	5.72	-1.79	0.00718 ± 0.0005	9.59	0.97
Chelex-100	0.00782 ± 0.0017	22.68	-7.86	0.00762 ± 0.0015	20.04	-5.10
MnO_2	0.00724 ± 0.0003	3.69	0.14	0.00752 ± 0.0006	7.57	-3.72
Grab	No data			0.00726 ± 0.0009	11.79	-0.14

* Standard deviation calculated as a % of the mean (precision).
** Calculated as (actual reading – measured/actual) x 100.

4.4 Conclusions and environmental monitoring applications

The application of DGT to the measurement of U in natural waters using Chelex-100, Metsorb and MnO_2 resins was investigated. It was found that in the laboratory all three resins performed well in low ionic strength solutions, but that only the MnO_2 resin was suitable for long term marine deployments. All three resins showed a good performance across an environmentally relevant range of ionic strengths, pHs and interfering and complexing agents. The complexing agent that was observed to have the most affect on U uptake by the resin gels was the HCO_3^- additions. Increasing the anionic strength of the solution inhibited uptake by the Chelex-100 and the MnO_2, whilst appearing to compete for binding sites on the Metsorb. The PO_4^{3-} additions only interfered with U uptake for very high PO_4^{3-} concentrations due to precipitation with insoluble species, anionic interferences (Chelex-100 and MnO_2) or direct competition for binding sites (Metsorb). Up to 250 mg L^{-1} Ca^{2+} additions, the Ca formed increasingly labile species with the U, enhancing the uptake. At 250 mg L^{-1} Ca^{2+} additions, the uptake of U by all three resins was reduced as a likely result of competition for binding site by the Ca^{2+}. The marine (average *salinity* = 30) deployment showed the U uptake by the Metsorb and MnO_2 DGTs to be linear and in agreement with the DGT equation for 4 days. Laboratory tests showed that Metsorb would be unable to predict U concentrations in sea water (*salinity* = 35) past 24 h, but the

deployment time was extended in the field potentially due to a lower salinity. The fresh water trials showed that the Metsorb DGT predicted the U concentration for 4 days and then 75% of total U up to 7 days. At the same fresh water deployment, the MnO_2 DGT predicted U concentrations for the first 2 days only. The Chelex-100 was found to be unsuitable for U measurements in the field as a result of oversaturation by competing ions as it was predicted to only accumulate cationic forms of U. A new application of DGT investigated in this study was the measurement of isotopic ratios of U down to concentrations of 0.1 µg L^{-1}. The isotopic ratio of U was conserved by all three resin gels. Another important factor investigated was the effect of the DBL. It was found that without the inclusion of the DBL, DGT calculations underestimated U concentrations by at least 50%. Further work is necessary to find a suitable actinide specific resin for inclusion into DGT devices in order to eliminate any effects by competing ions. In future research the use of a combined Metsorb/MnO_2 binding agent should be investigated for DGT measurements of U in a range of natural waters.

The technique presented in this chapter has applications in the environmental monitoring of U in aqueous systems. The World Health Organisation (WHO) drinking water limits for some selected actinides are presented in Chapter 2, to provide an initial benchmark for a regulatory environmental limit (as most aqueous discharge permits are unique to each nuclear establishment). The WHO drinking water limit for U is 30 ug L^{-1} or 0.4 Bq L^{-1}. By taking the LoD as 3 times the standard deviation of the blank plus the blank, the lowest detectable quantity of U on the resin can be calculated. By multiplying this by the elution volume (2 mL) and the dilution factor required for ICP-MS analysis (x 10), and then dividing by the elution factor (presented in section 4.3.1 as 0.84 for MnO_2, 0.83 for the Metsorb and 0.8 for the Chelex-100) (as detailed in equation 4.7), the limit of detection of U using the methodology described in this chapter can be calculated.

$$\frac{Resin\ blank\ x\ Elution\ volume\ x\ ICP{-}MS\ Dilution\ factor}{Elution\ factor} \qquad \text{Equation 4.7}$$

Taking the resin blanks (3 x standard deviation plus the blank) to be 0.06, 0.09 and 0.07 ng for MnO_2, Metsorb and Chelex-100 resins respectively with equation 4.7; this gives limits of detection of 1.4, 2.1 and 1.8 ng L^{-1} (or ~ 0.03 Bq L^{-1}) for MnO_2, Metsorb and Chelex-100 resins respectively. This is considerably less than the WHO drinking water limit for U of 30 µg L^{-1}, therefore making this a useful tool for

environmental monitoring. This resin is unlikely to be capacity limited in a freshwater environmental setting, as shown in Figures 4.6 and 4.8b, but due to capacity limitations in the marine environment (Figures 4.7 and 4.8a) all three resins have a limited usefulness in this environmental setting.

4.5 References

[1] J. Zhao, I.I. Fasfous, J.D. Murimboh, T. Yapici, P. Chakraborty, S. Boca, C.L. Chakrabarti, Kinetic study of uranium speciation in model solutions and in natural waters using Competitive Ligand Exchange Method, Talanta, 77 (2009) 1015-1020.

[2] T. Mathews, K. Beaugelin-Seiller, J. Garnier-Laplace, R. Gilbin, C. Adam, C. Della-Vedova, A Probabilistic Assessment of the Chemical and Radiological Risks of Chronic Exposure to Uranium in Freshwater Ecosystems, Environmental Science & Technology, 43 (2009) 6684-6690.

[3] G.R. Choppin, Actinide speciation in aquatic systems, Marine Chemistry, 99 (2006) 83-92.

[4] S. Cotton, The lanthanides and actinides, Macmillan Education Ltd, 1991.

[5] J. Lehto, X. Hou, Chemistry and analysis of radionuclides: laboratory techniques and methodology, Wiley-VCH, Weinheim, 2010.

[6] I.W. Croudace, P.E. Warwick, R.C. Greenwood, A novel approach for the rapid decomposition of Actinide(TM) resin and its application to measurement of uranium and plutonium in natural waters, Analytica Chimica Acta, 577 (2006) 111-118.

[7] B.S. Institution, Water quality - sampling, in: Guidance on passive sampling in surface waters, British Standards Publication, London, 2011, pp. 23.

[8] P.W. Swarzenski, M. Baskaran, Uranium distribution in the coastal waters and pore waters of Tampa Bay, Florida, Marine Chemistry, 104 (2007) 43-57.

[9] F. Riccobono, G. Perra, A. Pisani, G. Protano, Trace element distribution and 235U/238U ratios in Euphrates waters and in soils and tree barks of Dhi Qar province (southern Iraq), Science of the Total Environment, 409 (2011) 3829-3838.

[10] Y. Moliner-Martinez, P. Campins-Falco, P.J. Worsfold, M.J. Keith-Roach, The impact of a disused mine on uranium transport in the River Fal, South West England, Journal of Environmental Monitoring, 6 (2004) 907-913.

[11] G.R. Choppin, B.E. Stout, Actinide behavior in natural waters, Science of the Total Environment, 83 (1989) 203-216.

[12] E. Strady, G. Blanc, J. Schäfer, A. Coynel, A. Dabrin, Dissolved uranium, vanadium and molybdenum behaviours during contrasting freshwater discharges in the Gironde Estuary (SW France), Estuarine, Coastal & Shelf Science, 83 (2009) 550-560.

[13] L.L. Vintro, P.I. Mitchell, A. Omarova, M. Burkitbayev, H.J. Napoles, N.D. Priest, Americium, plutonium and uranium contamination and speciation in well waters, streams and atomic lakes in the Sarzhal region of the Semipalatinsk Nuclear Test Site, Kazakhstan, Journal of Environmental Radioactivity, 100 (2009) 308-314.

[14] P.H. Santschi, C. Bajot, M. Mantovani, D. Orciuolot, R.E. Cranston, J. Bruno, Uranium in pore waters from North Atlantic (GME and Southern Nares Abyssal Plain) sediments, Nature, 331 (1988) 155-157.
[15] A. Strezov, I. Yordanova, M. Pimpl, T. Stoilova, Natural radionuclide and plutonium content in Black Sea bottom sediments, Health Physics, 70 (1996) 70-80.
[16] M. Jurado Vargas, F. Vera Tomé, A. Martin Sánchez, M.T. Crespo Vázquez, J.L. Gascón Murillo, Distribution of uranium and thorium in sediments and plants from a granitic fluvial area, Applied Radiation & Isotopes, 48 (1997) 1137-1143.
[17] P. Zoriy, P. Ostapczuk, H. Dederichs, J. Hobig, R. Lennartz, M. Zoriy, Biomonitoring of environmental pollution by thorium and uranium in selected regions of the Republic of Kazakhstan, Journal of Environmental Radioactivity, 101 (2010) 414-420.
[18] J. Burger, M. Gochfeld, D.S. Kosson, C.W. Powers, S. Jewett, B. Friedlander, H. Chenelot, C.D. Volz, C. Jeitner, Radionuclides in marine macroalgae from Amchitka and Kiska Islands in the Aleutians: establishing a baseline for future biomonitoring, Journal of Environmental Radioactivity, 91 (2006) 27-40.
[19] D.D. Russell, W.B. Knowlton, Field portable electrochemical sensor for uranium and other actinides, in: U.P. Office (Ed.) Patent Application Publication, Boise State University, United States of America, 2006.
[20] N.W. Hayes, C.J. Tremlett, P.J. Melfi, J.D. Sessler, A.M. Shaw, Fibre optic system for detection of uranyl ions in the solution phase - art. no. 673917, in: G.W. Kamerman, O.K. Steinvall, K.L. Lewis, K.A. Krapels, J.C. Carrano, A. Zukauskas (Eds.) Electro-optical remote sensing, detection, and photonic technologies and their applications, International Society for Optical Engineering, Bellingham, 2007, pp. 73917-73917.
[21] I.J. Allan, J. Knutsson, N. Guigues, G.A. Mills, A.M. Fouillac, R. Greenwood, Evaluation of the Chemcatcher and DGT passive samplers for monitoring metals with highly fluctuating water concentrations, Journal of Environmental Monitoring, 9 (2007) 672-681.
[22] R.J.K. Dunn, P.R. Teasdale, J. Warnken, J.M. Arthur, Evaluation of the *in situ*, time-integrated DGT technique by monitoring changes in heavy metal concentrations in estuarine waters, Environmental Pollution, 148 (2007) 213-220.
[23] W. Davison, Fones G., Harper, M., Teasdale, P. And Zhang, H, Dialysis, DET and DGT: *In situ* diffusional techniques for studying water, sediments and soils., in: J.A.H. Buffle, G. (Ed.) *In situ* monitoring of aquatic systems: chemical analysis and speciation, John Wiley & Sons Ltd, 2000, pp. 74.

[24] W.J. Li, J.J. Zhao, C.S. Li, S. Kiser, R.J. Cornett, Speciation measurements of uranium in alkaline waters using diffusive gradients in thin films technique, Analytica Chimica Acta, 575 (2006) 274-280.
[25] W.J. Li, C.S. Li, J.J. Zhao, R.J. Cornett, Diffusive gradients in thin films technique for uranium measurements in river water, Analytica Chimica Acta, 592 (2007) 106-113.
[26] H. Vandenhove, K. Antunes, J. Wannijn, L. Duquene, M.V. Hees, Method of diffusive gradients in thin films (DGT) compared with other soil testing methods to predict uranium phytoavailability, Science of the Total Environment, 373 (2007) 542-555.
[27] J. Mihalik, P. Henner, S. Frelon, V. Camilleri, L. Fevrier, Citrate assisted phytoextraction of uranium by sunflowers: Study of fluxes in soils and plants and resulting intra-planta distribution of Fe and U, Environmental & Experimental Botany, 77 (2012) 249-258.
[28] C.M. Hutchins, J.G. Panther, P.R. Teasdale, F. Wang, R.R. Stewart, W.W. Bennett, H. Zhao, Evaluation of a titanium dioxide-based DGT technique for measuring inorganic uranium species in fresh and marine waters, Talanta, 97 (2012) 550-556.
[29] M. Gregusova, B. Docekal, New resin gel for uranium determination by diffusive gradient in thin films technique, Analytica Chimica Acta, 684 (2011) 142-146.
[30] J.L. Burnett, I. Croudace, P.E. Warwick, Pre-concentration of naturally occurring radionuclides and the determination of ^{212}Pb from fresh waters, Journal of Environmental Radioactivity, 102 (2011) 4.
[31] G. Koulouris, B. Slowikowski, R. Pilvio, T. Bostrom, M. Bickel, Pre-concentration of actinoids from waters: a comparison of various sorbents, Applied Radiation & Isotopes, 53 (2000) 279-287.
[32] C.E. Farnsworth, J.G. Hering, Hydrous manganese oxide doped gel probe sampler for measuring *in situ* reductive dissolution rates. 1. Laboratory development, Environmental Science & Technology, 44 (2009) 34-40.
[33] Y. Gao, W. Baeyens, S. De Galan, A. Poffijn, M. Leermakers, Mobility of radium and trace metals in sediments of the Winterbeek: Application of sequential extraction and DGT techniques, Environmental Pollution, 158 (2010) 2439-2445.
[34] M. Leermakers, Y. Gao, J. Navez, A. Poffijn, K. Croes, W. Baeyens, Radium analysis by sector field ICP-MS in combination with the diffusive gradients in thin films (DGT) technique, Journal of Analytical Atomic Spectrometry, 24 (2009) 1115-1117.

[35] E.P. Horwitz, R. Chiarizia, M.L. Dietz, DIPEX: A new extraction chromatographic material for the separation and preconcentration of actinides from aqueous solution, Reactive & Functional Polymers, 33 (1997) 25-36.

[36] H. Zhang, W. Davison, Direct in situ measurements of labile inorganic and organically bound metal species in synthetic solutions and natural waters using diffusive gradients in thin films, Analytical Chemistry, 72 (2000) 4447-4457.

[37] W.W. Bennett, P.R. Teasdale, J.G. Panther, D.T. Welsh, D.F. Jolley, New Diffusive Gradients in a thin film technique for measuring inorganic arsenic and selenium(IV) using a titanium dioxide based adsorbent, Analytical Chemistry, 82 (2010) 7401-7407.

[38] H. Zhang, W. Davison, Diffusional characteristics of hydrogels used in DGT and DET techniques, Analytica Chimica Acta, 398 (1999) 329-340.

[39] Tables of Physical & Chemical Constants in: 2.2.3 Viscosities, Kaye & Laby Online, 2005.

[40] K.W. Warnken, H. Zhang, W. Davison, Accuracy of the diffusive gradients in thin-films technique: diffusive boundary layer and effective sampling area considerations, Analytical Chemistry, 78 (2006) 3780-3787.

[41] S. Kerisit, C. Liu, Molecular simulation of the diffusion of uranyl carbonate species in aqueous solution, Geochimica Et Cosmochimica Acta, 74 (2010) 4937-4952.

[42] D.R. Kester, I.W. Duedall, D.N. Connors, R.M. Pytkowicz, Preparation of artificial seawater, American Society of Limnology & Oceanography, 12 (1967) 176-179.

[43] A.J. Robson, C. Neal, A summary of regional water quality for Eastern UK rivers, Science of the Total Environment, 194-195 (1997) 15-37.

[44] H.P. Jarvie, C. Neal, M.D. Jürgens, E.J. Sutton, M. Neal, H.D. Wickham, L.K. Hill, S.A. Harman, J.J.L. Davies, A. Warwick, C. Barrett, J. Griffiths, A. Binley, N. Swannack, N. McIntyre, Within-river nutrient processing in Chalk streams: The Pang and Lambourn, UK, Journal of Hydrology, 330 (2006) 101-125.

[45] C. Neal, H.P. Jarvie, A.J. Wade, M. Neal, R. Wyatt, H. Wickham, L. Hill, N. Hewitt, The water quality of the LOCAR Pang and Lambourn catchments, Hydrology & Earth System Science, 8 (2004) 19.

[46] C. Neal, M. Neal, H. Wickham, M. Harrow, The water quality of a tributary of the Thames, the Pang, southern England, The Science of The Total Environment, 251-252 (2000) 459-475.

[47] H. Zhang, W. Davison, *In situ* speciation measurements. Using diffusive gradients in thin films (DGT) to determine inorganically and organically complexed metals, Pure & Applied Chemistry, 73 (2001) 9-15.

[48] J.W. Murray, The surface chemistry of hydrous manganese dioxide, Journal of Colloid Interface Science, 46 (1974) 16.

[49] W. Yao, F.J. Millero, Adsorption of phosphate on manganese dioxide in seawater, Environmental Science & Technology, 30 (1996) 536-541.

[50] X.L. Tan, X.K. Wang, C.L. Chen, A.H. Sun, Effect of soil humic and fulvic acids, pH and ionic strength on Th(IV) sorption to TiO_2 nanoparticles, Applied Radiation & Isotopes, 65 (2007) 375-381.

[51] M. Olsson, A.M. Jakobsson, Y. Albinsson, Sorption of Pu(VI) onto TiO_2, Journal of Colloid Interface Science, 266 (2003) 269-275.

[52] M. Konstantinou, L. Pashalidis, Competitive sorption of Cu(II), Eu(III) and U(VI) ions on TiO2 in aqueous solutions - A potentiometric study, Colloida & Surface A-Physicochemical and Engineering Aspects, 324 (2008) 217-221.

[53] Bio-rad, Chelex 100 and Chelex 200 chelating ion exchange resin instruction manual, in: BioRad Laboratories (Ed.), 2000.

[54] D. Gorman-Lewis, P.C. Burns, J.B. Fein, Review of uranyl mineral solubility measurements, Journal of Chemical Thermodynamics , 40 (2008) 18.

[55] W. Dong, S.C. Brooks, Determination of the formation constants of ternary complexes of uranyl and carbonate with alkaline earth metals (Mg^{2+}, Ca^{2+}, Sr^{2+}, and Ba^{2+}) using anion exchange method, Environmental Science & Technology, 40 (2006) 4689-4695.

[56] A. Sanding, J. Bruno, The solubility of $(UO_2)^3(PO_4)^2.4H_2O_{(s)}$ and the formation of U(VI) phosphate complexes: Their influence in uranium speciation in natural waters, Geochimica Cosmochima Acta, 56 (1992) 4135-4145.

[57] J.G. Panther, P.R. Teasdale, W.W. Bennett, D.T. Welsh, H.J. Zhao, Titanium dioxide-based DGT technique for *in situ* measurement of dissolved reactive phosphorus in fresh and marine waters, Environmental Science & Technology, 44 (2010) 9419-9424.

[58] G.R. Choppin, Actinide speciation in the environment, Journal of Radioanalytical & Nuclear Chemistry, 273 (2007) 695-703.

[59] M. Gregusova, B. Docekal, H. Docekalova, Characterization of resin gels for diffusive gradient in thin films technique, Chemicke Listy, 102 (2008) 213-217.

[60] J. Zheng, M. Yamada, Determination of U isotope ratios in sediments using ICP-QMS after sample cleanup with anion-exchange and extraction chromatography, Talanta, 68 (2006) 932-939.
[61] Environmental Permitting Regulations (England and Wales) 2010, in: 675, Department for Environment, Food and Agriculture, England and Wales, 2010, pp. 212.

Chapter 5: Evaluation of the DGT as a tool for monitoring the long-term quality of water - uranium as a case study

5.1 Introduction

Currently monitoring of water quality relies on the collection of low volume grab (spot or bottle) water samples, usually on monthly, or at most weekly, time intervals. This approach has a number of limitations, being both expensive and time consuming, the possibility for introducing contamination in sample handling or during storage [1], and the potential to miss fluctuations in contaminant concentrations. For analytes having low aqueous concentrations, such as radionuclides, often large volumes (5-20 L) of water need to be collected and pre-concentrated to ensure good instrumental limits of detection [2]. To overcome some of these drawbacks, continuous in field auto-samplers [3] (active samplers) that are programmed to collect samples at set time intervals or during particular flow or meteorological conditions [4] can be used. This approach is costly and can also be associated with errors in terms of sample stability for monitoring both metals and nutrients [5, 6].

The use of *in situ* pre-concentration techniques, such passive sampling devices, can overcome many of these errors associated with grab sampling [7]. Furthermore, passive samplers can be used to measure both equilibrium and time-weighted averaged (TWA) concentrations over the deployment period. The latter approach can be beneficial in investigations where concentrations of a pollutant fluctuate widely, for instance from increased surface water flow as a result of a storm event, or with large tidal fluctuations [7, 8]. Passive samplers have the advantage of being relatively low-cost, non-mechanical, require no power and little maintenance and can be deployed in a range of field sites. Designs of passive sampler are varied and have been developed to measure a wide range of organics and metals. Examples include the Gaiasafe [9], Chemcatcher® for both metals [10] and organics [11, 12], permeable liquid membrane devices [13, 14] and diffusive gradients in thin films (DGT). The latter is the most widely used technique for measuring TWA concentrations of a number of metals and inorganic substances in a variety of aquatic environments. DGT measures the labile, dissolved fraction of analytes *in situ* [15]. The device consists of three layers: (i) a binding agent containing a resin with functional groups selective to the target ions, being held in a thin layer of hydrogel (binding gel); (ii) a layer of hydrogel of known thickness, which serves as the diffusive layer; and (iii) a protective outer membrane

with a known pore size. A diffusive boundary layer (DBL) that forms on the exposed face of the device must also be accounted for and added to the diffusive layer. After deployment, metal ions accumulated in the resin layer are eluted (e.g. with nitric acid) and the resultant extract analysed by a sensitive instrumental technique e.g. inductively coupled plasma-mass spectrometry (ICP-MS).

DGTs have been used for monitoring metals in the aquatic environment in a number of single deployment, short-term studies (for instance 4 d [16], 14 d (Chapter 4) and 31 d [17]). DGTs have also been deployed in the same location during two seasons with longer-term deployment periods (ranging from 13 to 36 d) [18], to show inter-seasonal variations of pollutants in the Sava River, Croatia. They were used for one-month deployments over five consecutive months [5] in the Lake Llyn Trawsfynydd, UK. The concentration of metals in highly fluctuating, transitional environments, such as estuaries, have been monitored using DGT in short-term studies [7, 19, 20]. Dunn *et al*. (2003) [21] showed that in highly fluctuating environments that concentration of metals can change significantly over 24 h and that these variations would therefore be missed by the use of infrequent grab sampling. There is little published data for freshwater systems, however, on the effects of long-term environmental changes (for instance seasonal changes in biological activity and water chemistry and flow rate) on the operational effectiveness of DGT devices. If DGT is to be used by regulatory agencies and to be fit a for purpose monitoring tool, further long-term field testing is required in conjunction with recognised standards such as the ISO 5667 [1]. In an attempt to investigate this, DGTs were used to monitor the concentrations uranium (U) continuously over a six-month period at two freshwater sites (River Enborne and the River Lambourn, Berkshire, UK) and compared the results against those from weekly grab water sampling. As U has a complex aqueous chemistry it was selected to demonstrate that the DGT technique can accumulate a highly reactive analyte in a system with fluctuating water quality.

U is not a priority substance in the European Union's Water Framework Directive [22] due to the high concentrations that can occur naturally. Environmental monitoring of anthropogenic and naturally occurring radionuclides in natural waters is a requirement of the environmental permits issued by the various environment agencies in the UK, and by the Industrial Pollution and Radiochemical Inspectorate for all users and holders of radioactive materials, under the Environmental Permitting Regulations (England and Wales) 2010 and Radioactive Substances Act 1993 [23]. These permits require the nuclear industry to continually undertake risk assessments of their

discharges to ensure environmental impacts are as low as is reasonably practicable [24]. This includes considering the use of new monitoring technologies such as DGT. U has been measured by DGT in artificial and natural waters in eight reported studies [16, 25-30]. There are a number of candidate binding phases effective for U. The TiO_2-based resin, Metsorb used in this study showed a high capacity for U. Isotopic ratios ($^{235/238}U$) of U were also measured over the field trials to see if the technique could also be used as a tool to identify sources of radioactive pollution.

5.2 Field locations

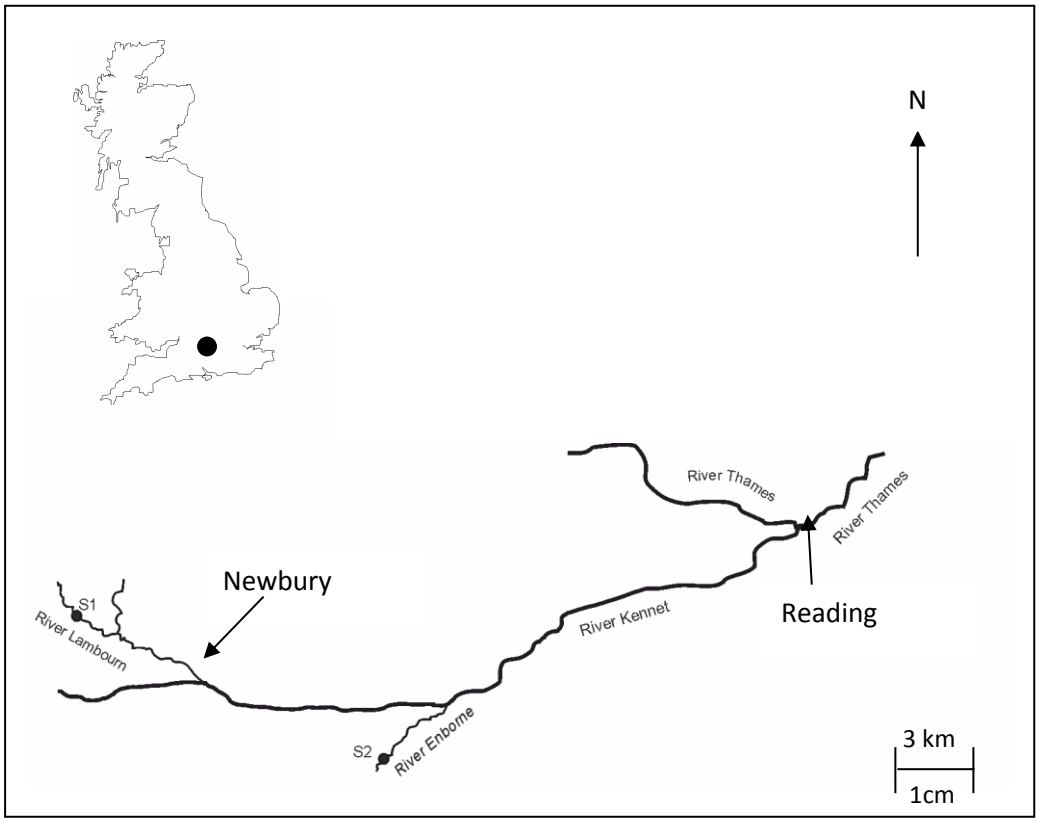

Figure 5.1. Location of field sites in the UK. Site 1 (S1) is located on the River Lambourn and site 2 (S2) on the River Enborne. Both rivers are tributaries of the River Kennet within the River Thames catchment.

Two freshwater field sites were used: site 1 (51.4469 N, -1.3838 W) was located on the River Lambourn at the village of Boxford, Berkshire, UK and site 2 (51.3792 N, -1.1855 W) on the River Enborne near Brimpton, Berkshire, UK. Both rivers are tributaries of the River Kennet. The River Lambourn has a Chalk catchment and is a fast flowing shallow channel with an average pH of 7.9-8 [31]. The mean flow and base flow indices were 1.71 m^3 s^{-1} and 0.97 respectively [32]. The River Enborne drains impermeable Tertiary sand, silt and clay deposits [33] and has a slow flowing deep channel with a pH ~7.8. The mean flow and base flow indices were 1.32 m^3 s^{-1} and 0.53. Schematics of the cross section of each river at the deployment site can be

seen in Figure 5.2 below, with approximate water heights based on average readings throughout the deployment period. To allow for safe access to the samplers, they were placed in the shallower zones of both rivers at a depth of approximately 0.5 m, out of the main flow channel.

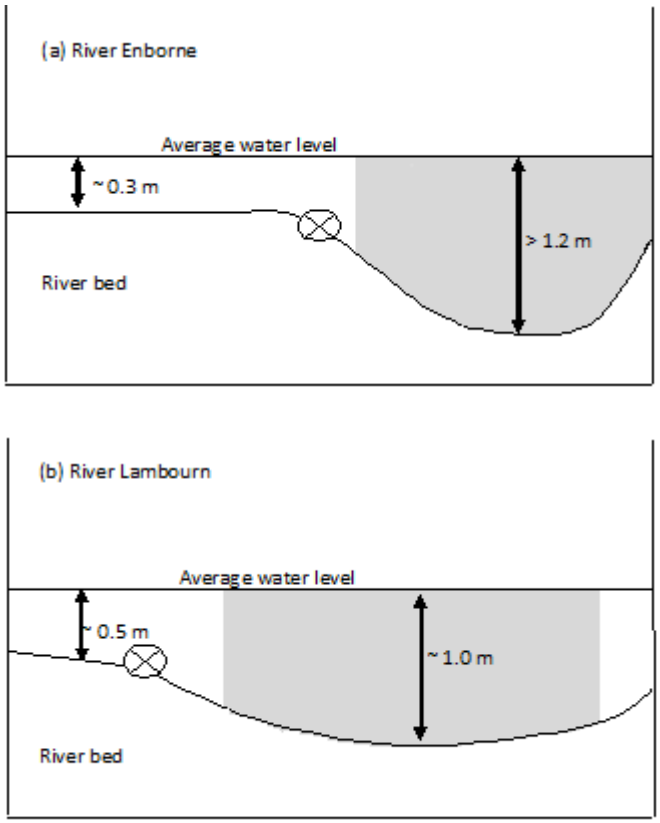

Figure 5.2 Diagram to demonstrate cross-section shapes of (a) the River Enborne and (b) the River Lambourn. Each diagram shows an approximate water height from the river bed at the shallow point (the entry point of the river for this study) on the left hand side of the diagrams, and the depth of main river channel. The main flow channel is depicted in grey, with the direction of flow away from the reader. The emplacement of the samplers is also marked on the diagrams using ⊗. The diagram is not to scale.

Mean monthly meteorological data was obtained from the Met Office Benson meteorological monitoring station (51.62 N, -1.097 W) (http://www.metoffice.gov.uk/public/weather/climate/benson) and from daily measurements taken by the Centre for Ecology and Hydrology (CEH), Wallingford, UK (51.6032 N, -1.1134 W) using a ground flush type rain gauge.

5.3 Design of field trial

A continuous monitoring programme was used to assess the performance of DGTs over part of three riverine seasons, from summer through to autumn and winter. During these periods it was expected that a wide variation in biological activity, flow regime and water chemistry would occur. DGTs were deployed between Perspex plates (15 x 7 cm, up to 8 devices per plate) (Figure 5.3) and attached to a rope and float and weighted to the river bed. The devices were deployed approximately 1.5 m from the river bank, out of the main flow channel to allow for access. Three DGT devices containing Metsorb™ resin gel were removed and replaced every week over a 21 week period from 24/08/2011 to 18/01/2012. Procedural blanks (in triplicate) were exposed to the field environment during deployment and retrieval of each set of samplers. Blanks were analysed in an identical manner to exposed field samplers.

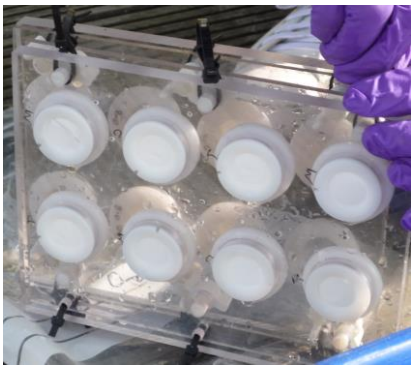

Figure 5.3. Photograph of DGTs held in place by a Perspex plate. The plate held up to eight devices. If more samplers were deployed then two Perspex plates were fixed back to back. The plate was deployed in the rivers a vertical position.

To assess the influence of the diffusive boundary layer (DBL) on the uptake of U, devices containing Metsorb™ were also deployed, with diffusive layer polyacrylamide (PAM) gel thicknesses (including 0.015 cm to account for the Supor membrane) of 0.015, 0.055, 0.095 and 0.135 cm, as per Warnken *et al.* [34]. The DBLs were measured on 12/10/2011, 07/12/2011, 05/01/2012 and 18/01/2012, corresponding to weeks 7, 15, 19 and 21 of the trial, so as to reflect two autumn and two winter seasonal measurements; with low and average rain fall in the autumn and winter respectively.

Triplicate grab samples of water from the two field sites were collected into acid washed LDPE bottles (1 L). An aliquot (20 mL) of water was filtered (0.2 µm pore size Supor filter) immediately into a polystyrene tube (30 mL) and acidified using 6 M HCl (40 µL). The acidified samples were stored in the dark at 4^{o}C until analysis. Water temperature, depth and flow rate were measured using a temperature YSI Castaway device (Yellow Springs, OH, USA), a rod and hydro-prop type flow meter (with a

detectable flow limit of ~5 cm s^{-1}) respectively. The pH was measured (1 L water sample in the LDPE bottle allowing no headspace for excess CO_2 to diffuse into the sample) in the laboratory using a Jenway 3410 Electrochemistry Analyser (Bibby Scientific Limited, , Staffordshire, UK). As part of the CEH Lambourn Observatory Project and the CEH Thames Initiative research platform, the Rivers Lambourn and Enborne were sampled weekly for major anions and cations (Table 5.1). Water quality analysis was undertaken at CEH laboratories (detail in Chapter 3, section 3.3). Discharge data for each site was obtained from the CEH National River Flow Archive, where measurements were taken at the crump weir located 51.3791 N, -1.1855 W, which is approximately 10 meters upstream of the River Enborne study site, and at the crump weir monitoring station (51. 24 42 N, 1.1932 W) River Lambourn at Shaw, Berkshire (approximate 13 km downstream of the Boxford deployment site).

5.4 Materials and methods

5.4.1 Materials and preparation of DGT

Chemicals were of analytical grade or better and supplied by Fisher Scientific Ltd. (Loughborough, UK), unless otherwise specified. Milli-Q (ultra-pure) water (> 18.2 MΩ cm, Millipore, Watford, UK) was used as the laboratory water. All U ICP-MS standards and were prepared in polystyrene (PS) containers from a 1000 mg L^{-1} in 2% HNO_3 (Spex Certiprep, Fisher Scientific Ltd.) stock solution. The ICP-MS internal standard was prepared from a 1000 mg L^{-1} in 2% HNO_3 (Spex Certiprep) bismuth stock solution. All plastic apparatus (including DGT housings) was soaked for 24 h in 10% HNO_3 and rinsed three times in Milli-Q water prior to use.

PAM diffusive gels (thickness 0.4, 0.8, 1.2 and 1.6 mm) were prepared according to Zhang and Davison [35]. The diffusive gels and filter membranes were stored in 0.01 M $NaNO_3$ prior to deployments to ensure ionic equilibrium between the diffusive gel and the deployment environment. The PAM binding gels were prepared with 1 g Metsorb™ HMRP powder (TiO_2 with an organic binder, < 50 µm; Graver Technologies, Glasgow, USA) according to the method described by Bennett *et al*. [36]. A disk of (0.2 µm pore size) Supor polyethylene sulfone (Pall Corporation, Portsmouth, UK) that was first acid washed in 1% HNO_3, tripled rinsed in Milli-Q water and stored in 0.01 M $NaNO_3$ was used as the outer membrane. DGT mouldings were obtained from DGT Research Ltd. (Lancaster, UK) and washed for 24 h in 10% HNO_3, and then rinsed three times in Milli-Q water prior to use. The devices were assembled according to Davison *et al*. [15] and stored at 4^{o}C in zip lock plastic bags, containing 1-2 mL of

0.01 M $NaNO_3$ in Milli-Q water (ionic strength matched to freshwater deployment site) to ensure the diffusion properties of the gels were not altered, and to prevent the gels drying out.

5.4.2 Measurement of total uranium

U was determined in all solutions by ICP-MS using an Agilent 7500ce series instrument (Agilent Technologies Inc., Japan). Total U was measured under normal plasma conditions in 'no gas mode', with the sample introduction system fitted with a micromist nebuliser. The instrument blank for U was 6 ng L^{-1} while the limit of detection (calculated by the Agilent Chemstation software) for U was 2 ng L^{-1}, with a measurement relative standard deviation better than 3%. Bismuth (*m/z* = 209; 25 µg L^{-1}) was used as an internal standard to compensate for any potential instrument drift. The certified fluvial reference material SLRS-5 (National Research Council Canada, Canada) was analysed directly for U and found to be within 1% of the stated values. The filtered and acidified grab water samples were analysed directly with no further dilution.

5.4.3 Measurement of uranium in DGT

After exposure, the Metsorb™ binding gels were removed from the DGT and eluted (48 h) with 1 M H_2O_2/ 1M HNO_3 (2 mL) solution (100 mL made by combining 90 mL 1.1 M HNO_3 and 10 mL H_2O_2). The elution of U from the Metsorb™ has been described in Chapter 4, where an elution factor of 0.83 was found. The eluent was then diluted 10 fold with Milli-Q water prior to instrumental analysis. The concentration of U (µg L^{-1}) measured by the ICP-MS in the eluent was multiplied by the dilution factor (×10) to give the actual U concentration (*Ce*). The absolute mass (*M,* ng) of the U in the binding gel was calculated using equation 5.1, where *M* is calculated taking into account the gel volume (*Vg*, cm^3), the eluent volume (*Ve*, mL), the measured concentration of uranium in the eluent (*Ce*, ng mL^{-1}) and the elution factor (*fe*) [35].

$$M = \frac{Ce(Vg+Ve)}{fe} \qquad \text{Equation 5.1}$$

M from equation 1 is then used to calculated the TWA concentrations (equation 5.2) where the concentration (C_{DGT}, ng mL^{-1}) was calculated using the mass of the analyte in the binding gel (*M*, ng), the thickness of the diffusive path length (diffusive gel and filter membrane) (Δg, cm), the diffusion coefficient of the analyte (*D*, cm^2 s^{-1})

(as determined for U at different pH's by Hutchins *et al*. [16]), deployment time (*t*, s) and the area of the sample exposure window (*A*, cm^2).

$$C_{DGT}=\frac{M\Delta g}{DtA} \qquad \text{Equation 5.2}$$

The diffusion coefficients from Hutchins *et al*. [16] were used and corrected for temperature using the Stoke's Einstein equation as per Zhang and Davison (2000) [35] (equation 5.3)

$$\frac{D_1\eta_1}{T_1}=\frac{D_2\eta_2}{T_2} \qquad \text{Equation 5.3}$$

The diffusion coefficients of uranyl carbonate ions in the diffusive gel and the water have been detailed in Chapter 3, section 3.1.1 and should be considered in calculating field DBLs and TWAs. The predominant uranyl species in both the field sites was ($Ca_2UO_2(CO_3)_3$), which at the average pH of the field sites had a similar diffusion coefficient in water (D_M^W) [37] as the diffusive gel (D_M^{gel}) (so$D_M^W : D_M^{gel}$= 1) and was therefore not accounted for here, meaning equation 5.2 could be used.

The diffusive boundary layer (δ) thickness was calculated using equation 5.5 after Warnken *et al.* [34]. A straight line plot of *1/M* versus *Δg* has a slope (*m*) of *1/($D_M^{gel}C_{DGT}At$)* and an intercept (*b*) of *δ/($D_M^W C_{DGT}At$)* as per equation 5.4 . The intercept (*b*) divided by the slope (*m*) of this plot gives the diffusive boundary layer thickness δ, as per equation 5.5. Diffusion coefficients calculated by Hutchins *et al.* [16] were used for the TWA calculations.

$$\frac{1}{M}=\frac{\Delta g}{DC_{DGT}At}+\frac{\delta}{DC_{DGT}At} \qquad \text{Equation 5.4}$$

$$\delta=\frac{b}{m} \qquad \text{Equation 5.5}$$

The thickness of the DBL was included in the C_{DGT} calculations for the field trials. The active sampling area (*A*) was 3.8 cm^2 instead of the 3.14 cm^2 used in the laboratory trials, as described by Warnken *et al.* [34] to account for lateral spread of the analyte across the surface of the DGT device.

Laboratory blanks were measured in triplicate and the average concentration per disk was determined for the Metsorb™ gel disks as 0.03 ± 0.02 ng and 0.3 ± 0.1 ng for ^{238}U and ^{235}U respectively.

5.4.4 Measurement of uranium isotopes

$^{235/238}U$ isotopic ratios were measured with an Agilent microflow (100 µL min^{-1}) PTFE self aspirating nebuliser, to eliminate any signal pulses caused by the peristaltic pump using a micro-mist concentric nebuliser. Isotopic ratios were determined with 3% RSD as low as 0.01 µg L^{-1} total uranium (0.725 x 10^{-4} µg L^{-1} ^{235}U). The certified reference material U005a (New Brunswick Laboratories, DoE, Washington, USA) was analysed and was found to be within 99.5% of the isotopic value (0.00509 $^{235/238}U$). The grab water samples were measured directly without any further dilution. For the isotopic signature of uranium found with DGT, the extraction eluate was diluted 10 fold prior to analysis.

5.4.5 Water chemistry

Grab water samples were taken at weekly intervals from the main flow of the river at each monitoring site. Sub-samples were immediately filtered (0.45 µm cellulose nitrate membrane, WCN grade: Whatman Ltd., Maidstone, UK) for subsequent analysis of dissolved determinands. Unfiltered sub-samples were taken for the determination of chlorophyll-a, total phosphorus and suspended particulate matter. Samples for chlorophyll-*a* were filtered and processed within 24 h. Details of the methodology can be found in Chapter 3 section 3.3. Table 5.1 details the water quality parameters measured. This data was provided by the Centre for Ecology and Hydrology as part of the Boxford Observatory Project and Thames Initiative.

Table 5.1. Water quality parameters measured as part of the CEH Boxford Observatory Project and Thames Initiative.

Anions	**Cations**	**Particulates and organics**
Soluble reactive phosphate (SRP)	Sodium (Na^+)	Chlorophyll *a* (Chl *a*)
Total dissolved phosphate (TDP)	Potassium (K^+)	Dissolved organic carbon (DOC)
Total phosphate (TP)	Calcium (Ca^+)	Suspended particulate material (SPM)
Ammonia (NH_4)	Magnesium (Mg^+)	
Dissolved reactive silicon (Si)	Boron (B^+)	
Total dissolved nitrate (TDN)	Iron (Fe^+)	
Nitrate (NO_3^-)	Manganese (Mn^{2+})	
Nitrite (NO_2^-)	Zinc (Zn^{2+})	
Sulphate (SO_4^{2-})	Copper (Cu^{2+})	
Fluoride (F^-)	Aluminium (Al^{3+})	
Chloride (Cl^-)		
Bromide (Br^-)		

5.4.6 Statistical analysis

The water quality results (including the weekly grab water sample measurements) were averaged over each week (mean of the reading at the beginning and at the end of each deployment week) and then subject to statistical analysis to identify any patterns between the two different techniques (grab sampling and DGT) used to measure the U concentration and fluctuating water quality. All statistical analysis was performed in IBM® SPSS® Statistics Version 20. The non-parametric one sample Shapiro-Wilk test was first used to test the data for normality (normality significance figure ≥ 0.05). If normality was established a Pearson's product-moment correlation was performed, if the data was not normally distributed then the non-parametric Spearman's ranking correlation coefficient was used ($P < 0.05$).

5.5 Results and discussion

5.5.1 DBL measurements

The DBL has been shown previously to be an important factor in the accuracy of the DGT technique in measuring TWA concentrations. Without the inclusion of the DBL in calculations, concentrations can be underestimated by up to 50%, as described in Chapter 4.

Several factors can affect the thickness and measurement accuracy of the DBL. These include fluctuations in water velocity [34], the deposition of particulate matter, bio-fouling by macro-fauna and the growth of bacterial mats [38] on the active sampling surface and the dissociation kinetics of organically bound metals at the solute interface of the sampler [39, 40]. Tables 5.2 and 5.3 show the thickness of the DBL measured in the River Enborne and River Lambourn respectively over the period of this study.

Table 5.2 Thickness of the diffusive boundary layer (DBL) measured at the River Enborne site.

Deployment week	Date	Thickness of DBL (cm)	R^2 of graph	DBL as a ratio of overall diffusive layer thickness (0.095 cm)
7	12/10/2011	0.141 ± 0.036	0.91	1.48
15	07/12/2011	0.086 ± 0.034	0.89	0.91
19	05/01/2012	0.047 ± 0.008	0.99	0.49
21	18/01/2012	0.037 ± 0.009	0.98	0.39

Table 5.3 Thickness of the diffusive boundary layer (DBL) measured at the River Lambourn site.

Deployment week	Date	Thickness of DBL (cm)	R^2 of graph	DBL as a ratio of overall diffusive layer thickness (0.095 cm)
7	12/10/2011	0.070 ± 0.022	0.93	0.74
15	07/12/2011	0.070 ± 0.032	0.86	0.74
19	05/01/2012	0.088 ± 0.009	0.99	0.93
21	18/01/2012	0.062 ± 0.018	0.99	0.65

The graphs showing the reciprocal of the accumulated mass against diffusive layer thickness (derived from equation 5.4) are shown in Figures 5.4 and 5.5 below for the Rivers Enborne and Lambourn respectively. The error associated with each DBL measurement is described in Chapter 3, and uses the standard deviation of the slope and the intercept. Tables 5.2 and 5.3 show that the thickness of the DBL represents a large component of the overall diffusive layer thickness. The ratio of the DBL to the gel diffusive layer varies in the River Lambourn throughout the deployment between 0.93 and 0.65, and decreases in the River Enborne from 1.48 to 0.39. This substantial addition to the diffusive layer provided by the DBL can therefore not be discounted from field measurements of U using DGT. The freshwater field deployments in Chapter 4 showed an under-estimation of dissolved U using the DGT devices by up to 50% when the DBL was not considered.

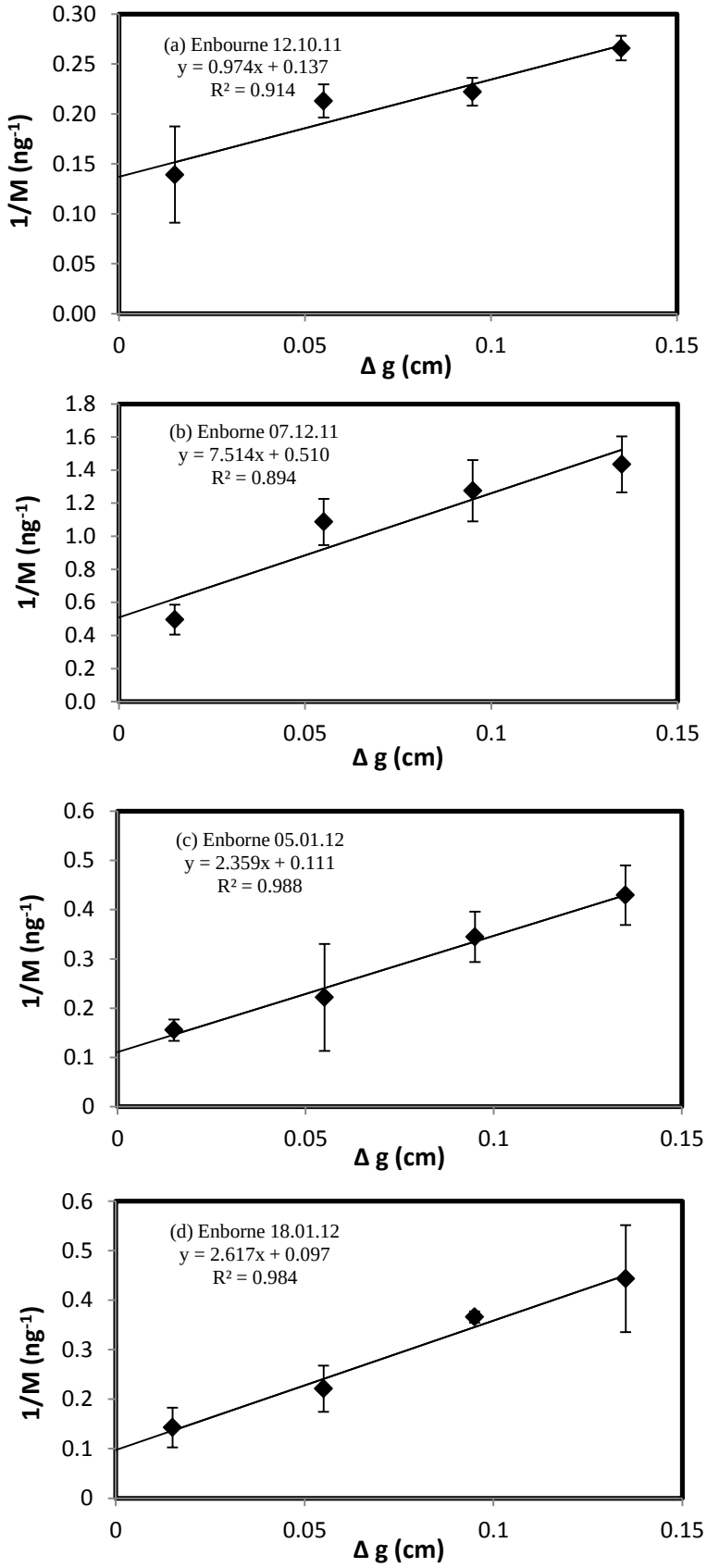

Figure 5.4 Reciprocal of the mass of U accumulated (in triplicate) plotted against the thickness of the diffusion layer used to calculate the thickness of the diffusive boundary layer (DBL) for the River Enbourne on the following dates a) 12.10.2011 b) 07.12.2011 c) 05.01.2012 d) 18.01.2012. Error bars represent the standard error of triplicate values of *1/M*.

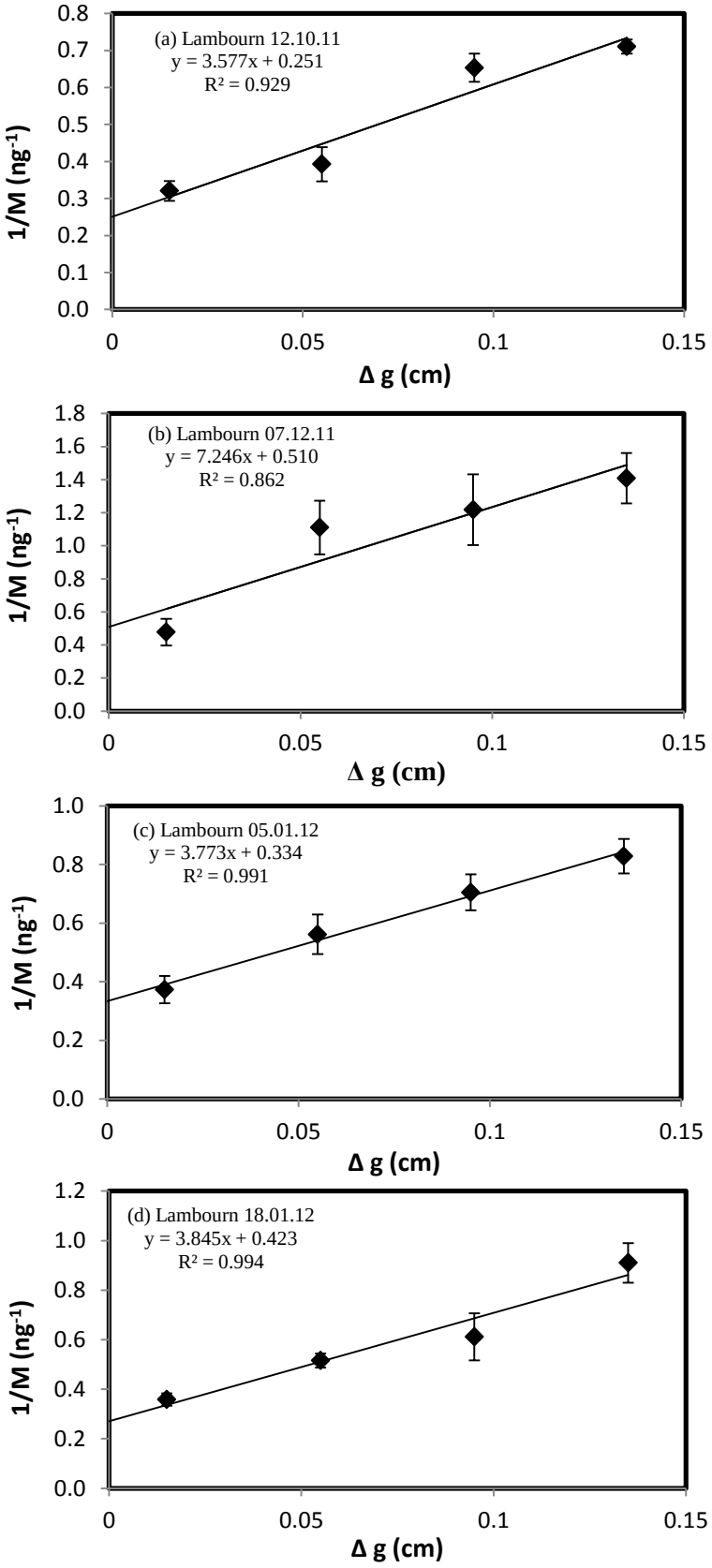

Figure 5.5 Reciprocal of the mass of U accumulated (in triplicate) plotted against the thickness of the diffusion layer used to calculate the thickness of the diffusive boundary layer (DBL) for the River Lambourn on the following dates a) 12.10.2011 b) 07.12.2011 c) 05.01.12 d) 18.01.2012. Error bars represent the standard error of triplicate values of *1/M*.

5.5.2 Effect of water flow rate on the thickness of the DBL

Water flow rate was measured at each deployment site to investigate if this may affect the thickness of the DBL. Flow rates were also back calculated from the discharge data provided by the National Rivers Flow Archive.

5.5.2.1 Flow rate data

No direct flow rate (m s^{-1}) data was available from the National Rivers Flow Archive for either of the deployment sites. This was calculated using Q = FA (where Q is discharge, m^3 s^{-1}, F is flow, m s^{-1} and A is cross-sectional area of the weir, m^2). Cross-section drawings of the weirs were provided by the Environment Agency. Discharge data (m^3 s^{-1}) has been used here to indicate each rivers response to precipitation events. An increase in rainfall may affect discharge through increased run off resulting in a higher volume of water passing through the sampling site, which in turn would increase the flow rate. Figure 5.6a shows that the River Enborne discharge is highly responsive to changing meteorological conditions, with short lag-times between peak rainfall and peak discharge [33]. Towards the winter months (December 2011 onwards) there is sustained precipitation which resulted in sustained higher flow conditions in the River Enborne. This can be attributed to the predominantly clay catchment area. The River Lambourn, which is a groundwater fed Chalk stream [31], maintained a relatively constant flow over the deployment period, with a slight increase in December 2011, as shown in Figure 5.6b. The permeable Chalk catchment of the River Lambourn attenuates any increase in surface run-off from increased precipitation that may affect discharge.

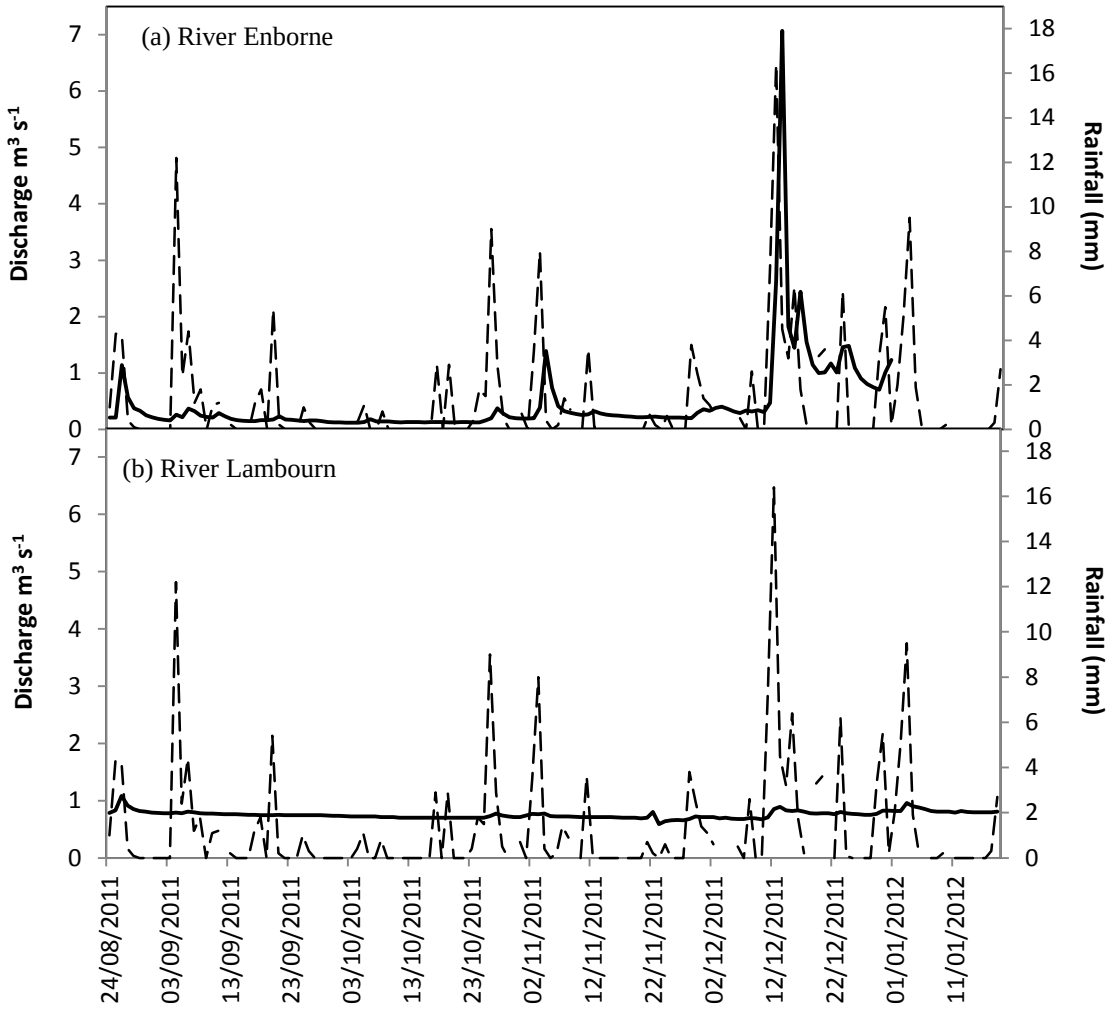

Figure 5.6 Regional rainfall data (dashed line) supplied by the CEH at the Wallingford Observatory (51.603166 N, -1.113393 W) using a groundflush type rain gauge, and river discharge data supplied by the Environment Agency's for England and Wales National River Flow Archive, for the (a) River Enborne and (b) the River Lambourn. The discharge data (solid line) for the River Lambourn is from the crump weir monitoring station (51^{o} 24 42.375 N, 1^{o} 19 32.092 W) located 13 km downstream of the sampling site. At the River Enborne, the Agency's flow monitoring station is at the deployment site (*Contains Environment Agency information © Environment Agency and database right).*

Figure 5.7 below shows the flow rate (m s^{-1}) calculated from the data shown in Figure 5.6. This provides an indication of the water velocity past the samplers during the deployment.

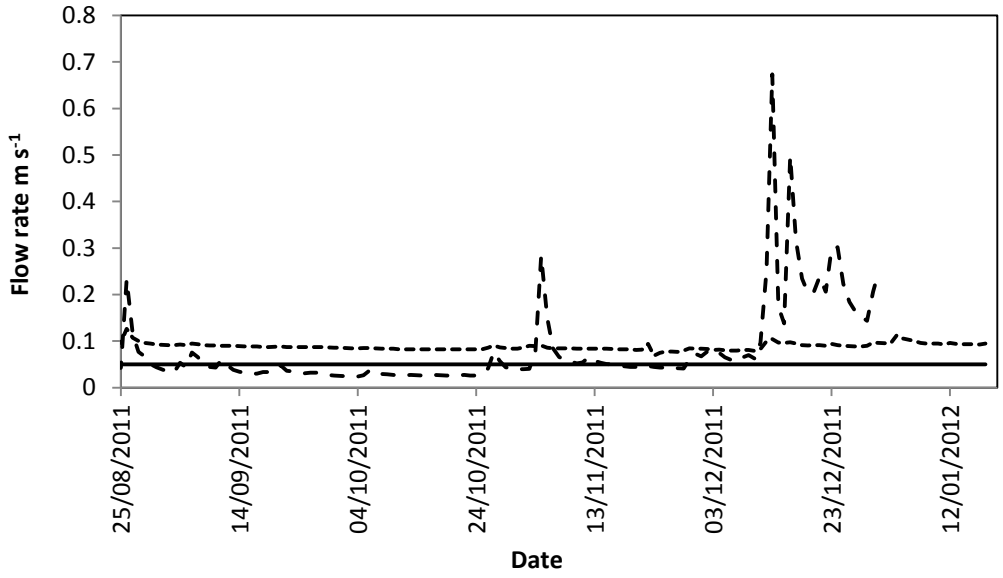

Figure 5.7 Flow rates (m s^{-1}) for the River Enborne (– –) and for the River Lambourn (·····) calculated from river discharge data supplied by the CEH National River Flow Archive. The crest widths for the River Enborne at Brimpton were 7.62 m (accounting for the width of both sluices and the concrete separator at the weir) and for the River Lambourn at Shaw, 10.67 m. The mean river height was used for each river to calculate the flow speed from the discharge (*Q*): $Q = m \times m\ s^{-1}$. The average height for the River Lambourn at Shaw was 0.8 m (data supplied by the Environment Agency for England and Wales) and for the River Enborne at Brimpton, 0.35 m, except from the 12–15/12/11, where a the bank-full level of 1.5 m was used due to exceptionally high flow. The solid line represents the minimum flow rate detectable by the flow meter used in this study. As the DGTs were situated out of the main flow channel in a low velocity pool to allow for ease of access, the flow measures recorded during the study were much less than those registered at the gauging station.

The lower discharge in the autumn months (September– November 2011) in the River Enborne, are directly related to the low rainfall experienced in the region. Table 5.4 shows that the rainfall experienced in the region was below average during this time. The impact of precipitation does not seem to affect flow rates in the Lambourn, which maintained a constant discharge.

Table 5.4. Regional rainfall data from the Benson Met Office Meteorological monitoring station (51.62 N, -1.097 W).

Year	Month	Rain (mm)	Seasonal Average rain (mm) (1971-2000)
2011	August	65.6	50.0
2011	September	31.8	51.3
2011	October	26.3	65.7
2011	November	28.4	65.0
2011	December	71.2	57.2
2012	January	34.6	53.9

The river height (m) and flow rate (m s^{-1}) were also measured at each deployment site (Table 5.5). There was little variation in flow conditions and river height at the River Lambourn site, which fits with the discharge and rainfall data in Figure 5.6. The River Enborne deployment site was generally very low flow, with a low water level, but with increasing discharge and precipitation (Figure 5.6) the river was inaccessible (14.12.11) or fast moving with a high discharge (21.12.11).

Table 5.5. Flow rates at the River Lambourn and River Enborne sites measured using a hydro-prop type flow meter. Each measurement was undertaken in triplicate, at 66% water column depth. The lowest flow detectable by the instrument was 5 cm s^{-1}. Where there is '< 5' the data is below the flow rate detectable by the meter used. Very heavy rain was experienced across the region on 11.12.11 to 17.12.11. This resulted in the River Enborne becoming too high to enter to take a reading on 14.12.11, with the 21.12.11 the only date that the flow meter registered a flow at the River Enborne where the samplers were deployed.

	Flow rate (cm s^{-1})		**Approximate depth (m)**	
Date	**River Lambourn**	**River Enborne**	**River Lambourn**	**River Enborne**
24/08/2011	10	< 5	0.4	0.5
05/10/2011	7	< 5	0.4	0.5
12/10/2011	8	< 5	0.5	0.4
19/10/2011	11	< 5	0.5	0.4
24/10/2011	8	< 5	0.5	0.3
02/11/2011	1	< 5	0.5	0.4
09/11/2011	7	< 5	0.5	0.4
16/11/2011	6	< 5	0.5	0.4
23/11/2011	7	< 5	0.5	0.6
30/11/2011	8	< 5	0.5	0.6
07/12/2011	7	< 5	0.6	0.7
14/12/2011	9	No data	0.6	1.5
21/12/2011	6	12	0.6	1.2
28/12/2011	8	< 5	0.6	1
05/01/2012	8	< 5	0.5	0.8
11/01/2012	7	< 5	0.5	0.8
18/01/2012	8	< 5	0.5	0.8

Figure 5.8 (a) and (b) illustrate the difference in the river conditions during high (Figure 5.8a) and low (Figure 5.8b) precipitation and discharge.

Figure 5.8a. Photo of high flow conditions (date 14.12.11) River Enborne. The circle shows the location of the float which is in this instance completely submerged. The conditions were judged too hazardous to retrieve the samplers on this sample date. Photo taken looking towards weir.

Figure 5.8b. Photo of very low flow conditions, River Enborne (12.10.11). Location chosen for ease of access. Photo taken looking away from weir.

5.5.2.2 Effect of flow rate on DBL

During the first 4 months of the deployment (August to late November 2011) the River Enbourn experienced below average precipitation (Table 5.4) in conjunction with lower flow rates (Table 5.5 and Figure 5.7) and discharge (Figure 5.6), and consequentially a larger DBL thickness of 0.141 ± 0.036 cm (Table 5.2) was measured. The flow rate in September and October 2011 was calculated to be ≤ 2 cm s^{-1} (Figure 5.7 and 5.5), with the river flow where the samplers were situated likely to be even lower, as this was outside the main flow channel. The sustained above average precipitation from the second week in December 2011 increased the discharge and reduced the thickness of the DBL to 0.086 ± 0.034 cm in December and 0.037 ± 0.009 cm in January 2012 (Table 5.2). December 2011 and January 2012 experienced average levels of precipitation, and higher fluvial flow rates, and hence a thinner DBL of averaging 0.042 cm over these two months. Figures 5.8 (a) and (b) show the differences in flow regime at the River Enborne over the deployment period with a potential difference in river height of up to 1.2 m. This demonstrates the need to fully

characterise the attributes of a field site prior to deployment, to ensure the devices remain submerged in a reasonably turbulent environment and are retrievable.

The very large DBL observed in October 2011 (Table 5.2), when the flow rate of the River Enborne was very low, is concurrent with that found under a laboratory setting by Warnken *et al*. [34] in quiescent conditions, where a large DBL of 0.15 ± 0.013 cm was observed (Table 5.6). Under laboratory conditions in previous studies, moderate flow rates up to 2 cm s^{-1} showed a reduction in the associated thickness of the DBL, with Warnken *et al*. [34] reporting a value of 0.044 ± 0.0014 cm, which is similar to the thickness of the DBL found in this study for the December 2011 and January 2012 deployments in the River Enborne.

Table 5.6. Examples of the thickness of the diffusive boundary layer (DBL) found in laboratory experiments in relation to flow or stir rate.

DBL and error (cm)	Flow rate or stir rate	Analyte(s)	Deployment time (h)	Ref.
0.023 ± 0.0032	High (≥ 100 rpm or > 2 cm s^{-1})	Cd	50	[34]
0.044 ± 0.0014	Moderate (60 rpm, < 2 cm s^{-1})	Cd	50	[34]
0.15 ± 0.013	None (0 rpm)	Cd	50	[34]
0.001 ± 0.0002 (average)	10 cm s^{-1}	Pb, Cd, Mn, Co, Cu plus the lanthanides	24, 48, 72	[41]

If the flow rate exceeds 2 cm s^{-1} (as for well stirred solutions) then it has been shown that the thickness of the DBL is not directly related to the flow rate of water [34, 42]. Warnken *et al*. [34] found for high flow rates, in a laboratory setting, the thickness of the DBL was 0.023 ± 0.0032 cm, which is in agreement to the DBL thicknesses (0.024 ± 0.002 cm) found by Scally *et al.* [43]. The flow rate in this study frequently exceeded 2 cm s^{-1} in the River Enborne, but the lowest measured DBL was 0.037 cm, which implies other factors than flow rate may also contribute to the DBL.

It is clear from the field measurements of the DBL at the River Enborne (Table 5.2) that the changing DBL was closely coupled to the flow rate (the $1/M$ v Δg plots used for each of the DBL measurements can be seen in Figure 5.4 a - d and the flow rate in Figure 5.7). As only 4 DBL measurements were taken over the deployment period, no statistical tests could be performed on the data. However, to obtain an indication of any effects a scatter plot of the DBL (cm) vs the flow rate (m^2s^{-1}) is shown in Figure 5.9, and includes data from both the Rivers Enborne and Lambourn. What can be seen from Figure 5.9 is that there is strong negative correlation between the flow rate and the thickness of the DBL i.e. the DBL decreases with increasing flow rate. It can also be

observed that the model that best fits the data is not a linear regression (with an R^2 value of 0.61), but a power regression (with an R^2 value of 0.85). This implies that as the DBL approaches the theoretical minimum of 0.023 cm found under laboratory conditions by Warnken *et al.* [34], the flow rate required to achieve this increases non-linearly. This may be because external factors to the flow rate maybe influencing the thickness of the DBL. If a linear model is applied to the data, as per Figure 5.9b, the flow rate required to attain a DBL thickness of 0.023 cm (shown as the point at which the solid linear regression line meets the dashed line representing the minimum measurement DBL) is > 20 cm s^{-1}, which is approximately 20 times higher than the findings by Warnken *et al.* [34]. Again, this indicates that other factors may be influencing the DBL other than flow rate.

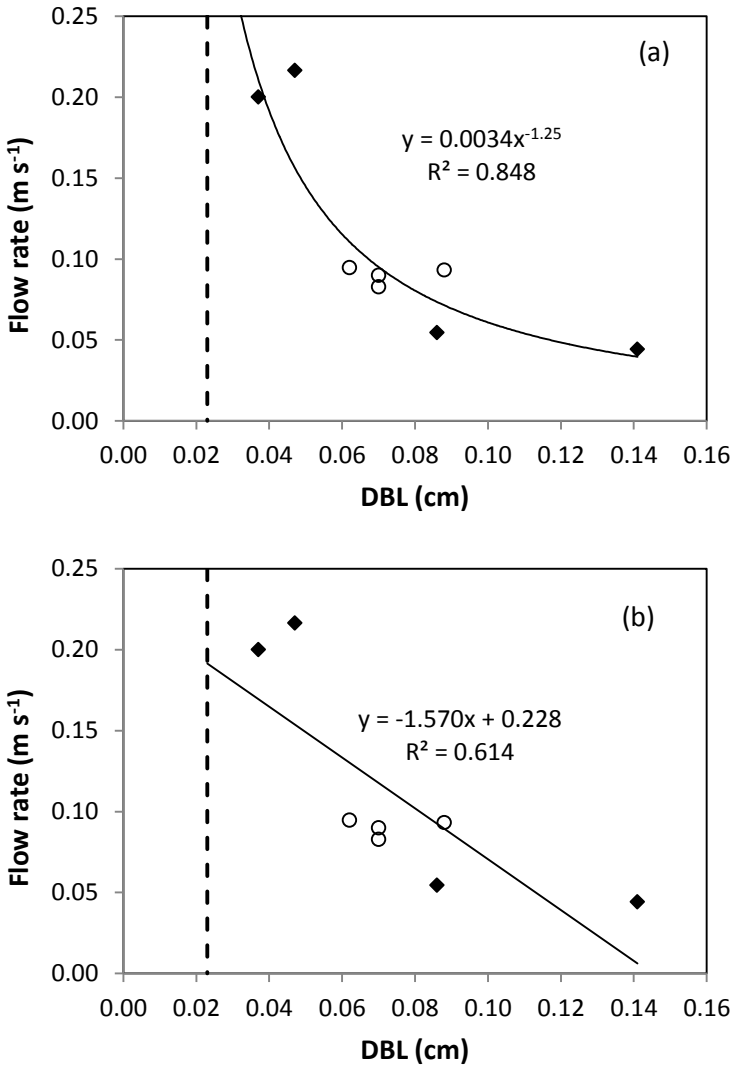

Figure 5.9 Graph showing the correlation with the flow rate (m s^{-1}) of the river and the size of the DBL (cm). The black diamonds represent data from the River Enborne and the open circles are data points from the River Lambourn. The black dashed line represents the theoretical minimum DBL from laboratory measurements as found by Warnken *et al*. [34]. Insert (a) shows the data with a linear regression (black line) and insert (b) shows the data with a power ($x^{-1.25}$) regression line fit.

The River Lambourn showed high variability in the thickness of the DBLs (Table 5.3 and Figures 5.5a-d) despite the discharge remaining at a steady state over the course of the deployment period (Figure 5.6). The flow rate for the River Lambourn over the deployment period averages 8 cm s^{-1} (Table 5.5 and Figure 5.6 and 5.7), which is higher for most of the deployment period than that in the River Enborne. The consistent and high (despite low precipitation) flow rates experienced by the River Lambourn is due to the Chalk catchment and the fact the river catchment is largely groundwater fed. The DBL found in October was 0.070 ± 0.022 cm, which is slightly higher than predicted in the laboratory (Table 5.6) for the flow rate. Over the course of the deployment period, the thickness of the DBL increased to 0.088 ± 0.009 cm in January 2012, which is twice that measured in the River Enborne and nearly four times that measured under laboratory conditions. The flow rate therefore does not give a good indication of the thickness of the DBL in the River Lambourn, which means external factors (such as biofouling) must be also taken into consideration.

DBL measurements in the field have been shown in other studies to differ significantly from those on the laboratory. Table 5.7 shows the thickness of DBLs found in the field, although there is a paucity of data. In a well stirred field environment, Warnken *et al*. [34] found the measured the thickness (0.026 ± 0.0017 cm) of the DBL closely matched their laboratory results. Thicker DBLs in the field have been reported, by Panther *et al*. [44] (0.080 ± 0.013 cm for PO_4) and Bennett *et al*. [36] (0.080 ± 0.013 cm for As and Se). Hutchins *et al*. [16] reported a DBL thickness of 0.003 ± 0.0006 cm when measuring concentrations of U in a freshwater system. Another consideration when comparing the thickness of DBLs found here to other field studies is the length of time the devices were deployed. DGTs are usually deployed for shorter periods (3–5 d) when examining properties of DBL. In this study, the deployment time was 7 d. A longer deployment is favourable when measuring low concentrations (ng L^{-1}) of a pollutant, as this allows more of the analyte to accumulate onto the resin, however, other factors e.g. biofouling may begin to dominate the uptake process.

Warnken *et al*. [34] suggested that when flow exceeds the 2 cm s^{-1} threshold, then the DBL thickness (present at 0.023 cm) could be discounted. Here a sampling area of 3.14 cm^2 can used (as opposed to 3.8 cm^2 which accounts for lateral diffusion at the DGT face) to offset the error when not accounting for the DBL, and when using a gel thickness of 0.8 mm. However, as is observed here and in other field studies (Table

5.7), there may be other factors influencing the thickness of the DBL than simply water flow rate.

Table 5.7 Examples of the thickness of DBL calculated in other field studies.

Analyte	Type of water	Location	Thickness of DBL (cm)	Flow rate	Deployment Time (d)	pH	Ref
U	Fresh	River Lambourn, UK	0.046 ± 0.006	Fast	5	7.8	Chapter 4
U	Marine	Southampaton Waters, UK	0.035 ± 0.019	Fast	5	8.2	Chapter 4
U	Fresh	Coomera River, Australia	0.003 ± 0.0006	Fast	4	7.5	[16]
Cd, Pb, Zn	Fresh	River Wyre, UK	0.026 ± 0.002	Fast	3	Not stated	[34]
As, Se	Fresh	Gold Coast, Australia	0.080 ± 0.013	Fast	4	7.5	[36]
As, Se	Marine	Gold Coast Broadwater, Australia	0.067 ± 0.007	Fast	4	7.9	[36]
PO_4	Fresh	Gold Coast, Australia	0.080 ± 0.013	Fast	4	7.5	[44]
PO_4	Marine	Gold Coast Broadwater, Australia	0.067 ± 0.007	Fast	4	7.9	[44]
Cd, Ni	Fresh	Lake Tantare, Canada	0.031 ± 0.02	Slow	13-14	5.3–5.6	[45]

5.5.3 Effects of water quality on the thickness of the DBL

5.5.3.1 Suspended particulate material and biofouling

Previous work has shown that biofouling and turbidity [34] can have an impact on the effectiveness of passive sampling devices. The River Enborne contained higher and fluctuating concentrations of suspended particulate material (SPM, mg L^{-1}) than the River Lambourn, but when plotted against the DBL thickness for both rivers (Figures 5.10 and 5.11 for the Rivers Enborne and Lambourn respectively), no trend was apparent. However, the importance of SPM should not immediately be dismissed, as any influence it has on the devices may be obscured by other factors with a greater influence (such as flow rate).

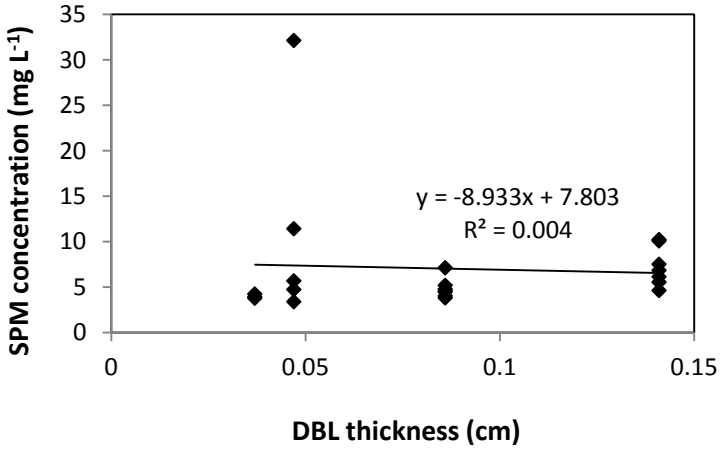

Figure 5.10 Suspended particulate material (SPM) (mg L^{-1}) concentration plotted against DBL thickness for the River Enborne. SPM data provided by the CEH as part of the Boxford Observatory Project and Thames Initiative.

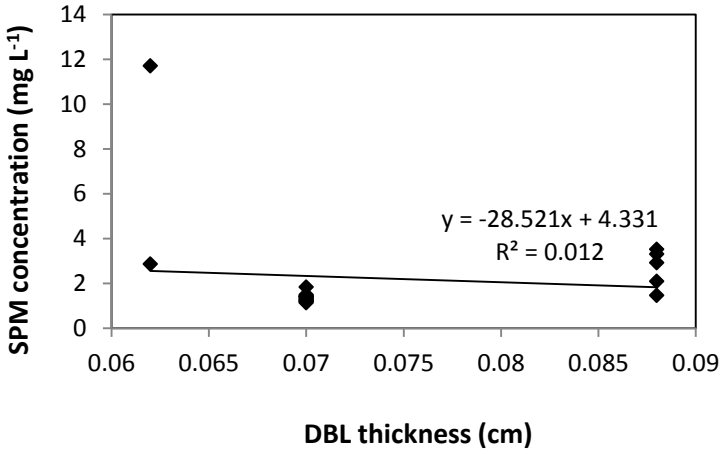

Figure 5.11 Suspended particulate material (SPM) (mg L^{-1}) concentration plotted against DBL thickness for the River Lambourn. SPM data provided by the CEH as part of the Boxford Observatory Project and Thames Initiative.

Particulates could potentially act to increase the thickness of the DBL by acting as an additional physical barrier to diffusion across the filter membrane or by supplying a source of dissociating U from particulate surfaces. At the diffusive interface (the surface of the filter membrane) where a concentration gradient will be present, there may be a resupply of U sorbed to the surface of the suspended particulates. Previous studies showed the presence of organic material in a river increases the sorption of U to particle surfaces [46]. This is supported by the fact that when the devices were retrieved, there was particulate matter collected on the active sampling surface (Figure 5.12). Supor® membranes are designed to inhibit microbial growth. However, if SPM accumulated on the surface of the membranes then this will provide sites for growth, with a microbial matt developing and potentially acting as a sink for the U [38]. This could account for variability in the measurements on the thickness of the DBL

depending on the depth of the microbial mat, but is an area for further work. The lower values of SPM found for the River Lambourn meant that this process may not be a contributing factor to the DBL at this site.

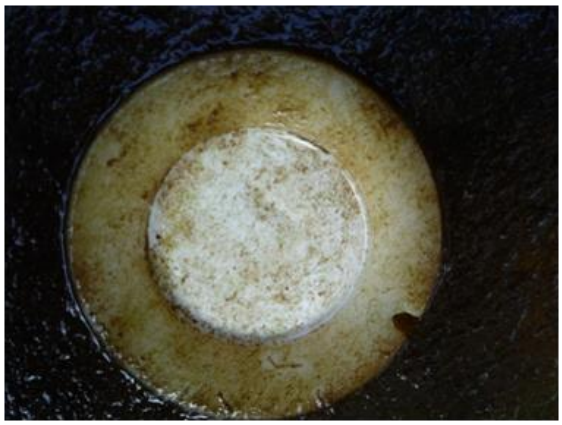

Figure 5.12. Typical image of DGT device after a 7 day deployment in the River Enborne.

DGTs deployed in the River Lambourn accumulated algae and macro-flora over the 7 day deployment. Previous work reported in Chapter 4 at this site, showed with daily removal of vegetation and for shorter deployment times (5 days) the thickness of the DBL was 0.046 ± 0.006 cm. However, rapid accumulated of macro-flora (Figures 5.13a - c) resulted in large measured DBLs with large associated errors (Table 5.3) over the deployment period. As there was little variation in flow rates at this site (Figures 5.6 and 5.7), due to its high base flow index (0.97); some of the variation occurring in the thickness of the DBL could be attributed to a biological source. Dragun *et al*. (2008) [18] also found limitations on the effectiveness of the DGT due to algal biofouling during long-term (13-36 d), single deployments during the spring. Ideally, DGTs should be deployed in a protective cage in areas prone to the build-up of algae and macro-flora, although this would not prevent the accumulation of periphyton on the surface of the devices. This is an area for further work as care should be taken not to reduce the water flow inside the cage.

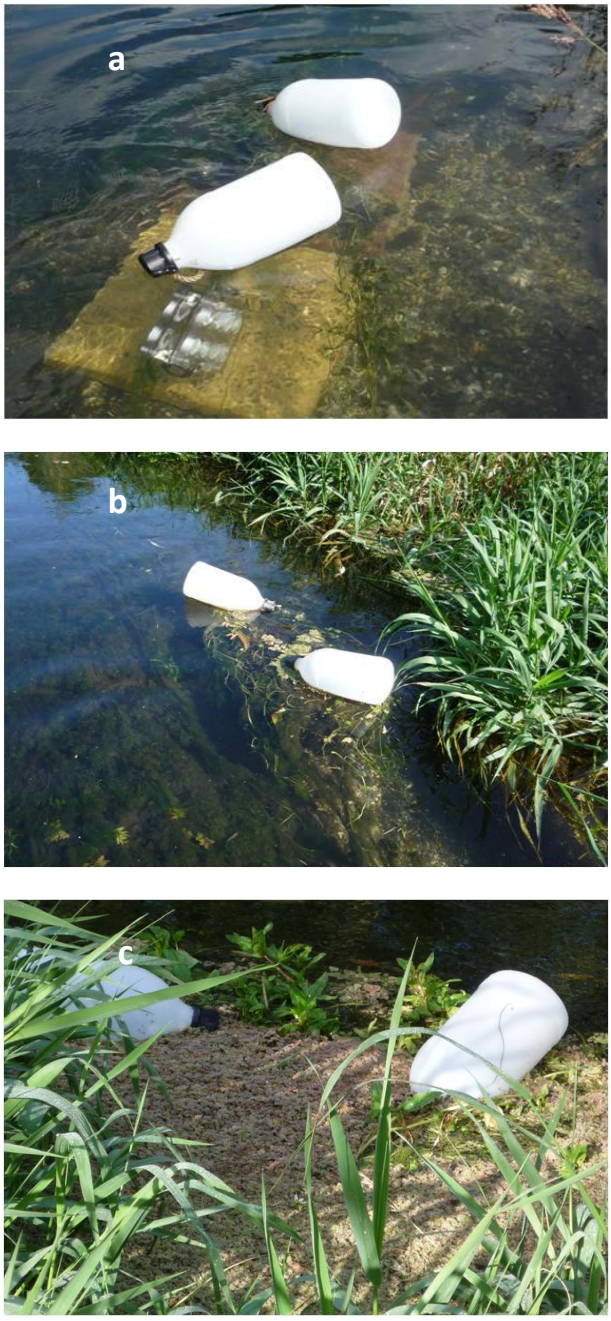

Figure 5.13a. Devices at the beginning of each weekly deployment after vegetation has been cleared, River Lambourn.

Figure 5.13b. Devices after 7- d deployment. Image shows algae accumulation, River Lambourn.

Figure 5.13c Devices after 7-d deployment. Image shows sub-surface macro-flora accumulation around the devices, River Lambourn.

Figures 5.14 and 5.15 show the chlorophyll a concentrations plotted against DBL thickness for the Rivers Enborne and Lambourn respectively. Despite the regular large accumulation of macro-flora around the devices as shown in Figure 5.13 for the River Lambourn, and the film of particulates that formed on a weekly basis on the

surface of the devices deployed in the River Enborne (that could also act as a bacterial matt), there was very little relationship between the DBL thickness and the biological activity (taken here as the chlorophyll a measurements) in either river. There is a slight observable trend in the River Enborne (Figure 5.14) that shows with increasing chlorophyll a concentrations, there is an increase in DBL thickness, although there is a large scatter to the data as shown by the R^2 value of 0.15. There was no observable trend in the River Lambourn (Figure 5.15). The effect of biological activity on the size of the DBL however cannot be ruled out and is an area for further research under more controlled conditions.

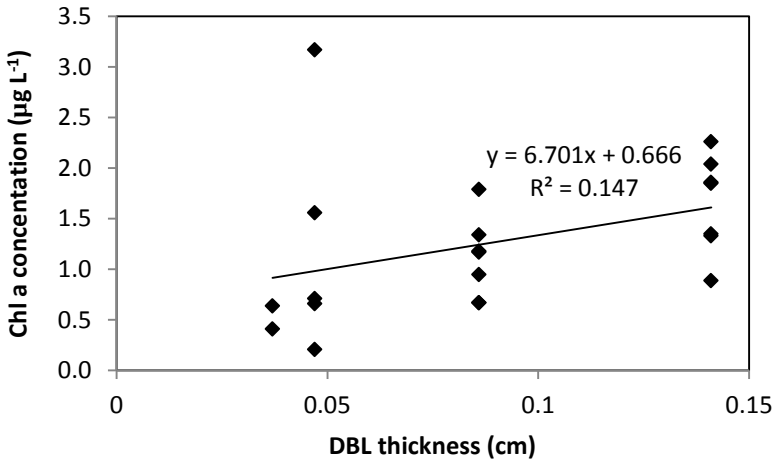

Figure 5.14 Chlorophyll a concentrations (µg L^{-1}) plotted against the DBL (cm) measured at the River Enborne over the deployment period. Data provided by the CEH as part of the Boxford Observatory Project and Thames Initiative.

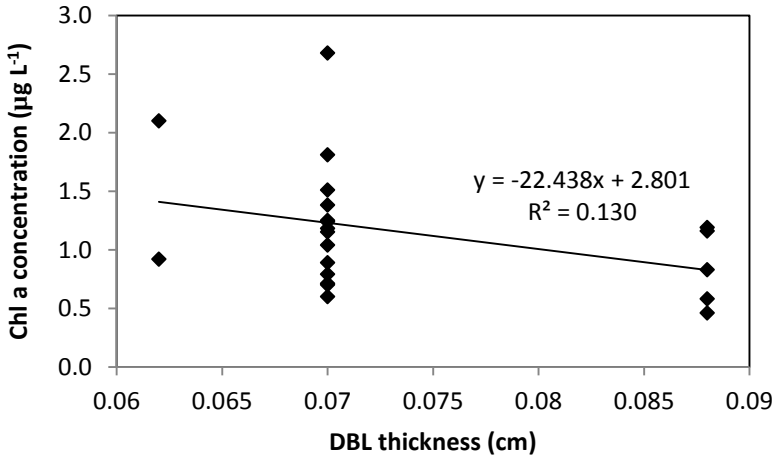

Figure 5.15 Chlorophyll a concentrations (µg L^{-1}) plotted against the DBL (cm) measured at the River Lambourn over the deployment period. Data provided by the CEH as part of the Boxford Observatory Project and Thames Initiative.

5.5.3.2 Dissolved organic carbon (DOC)

DBLs are both a physical layer where advective transport moves to diffusional transport processes, and/or an apparent layer of chemical dissociation of the analyte from a larger molecule such as dissolved organic matter [40, 47]. Levy *et al*. [47] showed that in the presence of organic ligands, metals demonstrated varying degrees of kinetic limitation dependent on dissociation rates, and therefore exhibited varying apparent diffusive boundary layer (ADBL) thicknesses. Scally *et al*. [48] also showed that in the presence of an organic ligand, copper and nickel exhibited kinetic limitations when measured by DGT, resulting in more mass being accumulated than predicted when thicker diffusive layer gels were used. This is due to the dissociating metal-ligand complex contributing to the flux of the metal ions accumulated by the resin layer. The possibility of the presence of a zone of chemical dissociation cannot be ignored in the case of U partly because of the large diffusive boundary layer measured *in situ* here as a result of more mass being accumulated in the DGT devices with thicker diffusive gel layers; and because of the high affinity of the actinides to organic material [49, 50].

This is particularly pertinent when 12 - 97% of the U species modelled (using Visual Minteq) were found as humic complexes (fulvic and humic acids) for the River Enborne, and up to 7% of the U bound to humates in the River Lambourn. The remainder of the species formed in both these rivers is dominated by $Ca_2UO_2(CO_3)_{3(aq)}$, $CaUO_2(CO_3)_3^{2-}$ and $UO_2(CO_3)_3^{4-}$. Warnken *et al*. [40] showed that the ADBL increased with metals that formed increasing strong complexes with dissolved organic matter. U at low uranium:humic acid (U:HA) ratios (such as for the Rivers Enborne and Lambourn with U:HA ratios of 4.17×10^{-5} and 1.81×10^{-4} respectively) has been shown to form very strong (bidentate) humic acid complexes that have slow dissociation kinetics ($k_d = 4.9 \times 10^{-5}$ s^{-1}) compared to higher U:HA ratios (i.e. > 0.01) ($k_d = 10^{-3}$ s^{-1}) [49]. In the presence of calcium carbonates, fewer bidentate species are formed, with more of the faster dissociating monodentate species predominating. The dissociation kinetics of U from organic material may have affected the thickness of the DBL for both rivers, particularly the River Enborne, although this would require further study in both field and laboratory settings to confirm. This potential zone of dissociation (ADBL) may account for the presence of an extended DBL (Table 5.2) in the River Enborne even during periods of high flow and discharge, where the thickness of the DBL was 0.046 cm, compared to 0.023 cm in a fast moving system under laboratory conditions (Table 5.6). However, no correlation was found between DOC and DBL in the River Enborne, as shown in Figure 5.16 (R^2 value of 0.008), potentially because there are

other stronger influencing factors such as flow rate, that make the impact of the DOC indistinguishable. Figure 5.17 shows that the River Lambourn DBL may be related to the DOC concentrations, as there is a positive trend (increasing DBL thickness with increasing DOC concentration), with an R^2 value of 0.64. The reason this trend may be evident for this deployment location, is that unlike the River Enborne, the flow rate is fairly constant throughout the deployment period (~0.09 m s^{-1}) and would therefore not mask the effects of other factors with less of an influence on DBL thickness, such as DOC, despite the DOC concentrations in the River Lambourn being 5 mg L^{-1} on average less than in the River Enborne (DOC concentrations are shown in Tables A5.2 and A5.5 for the Rivers Enborne and Lambourn respectively). This implies that the flow rate is a more important factor than dissociating U-organic complexes in defining the thickness of the DBL.

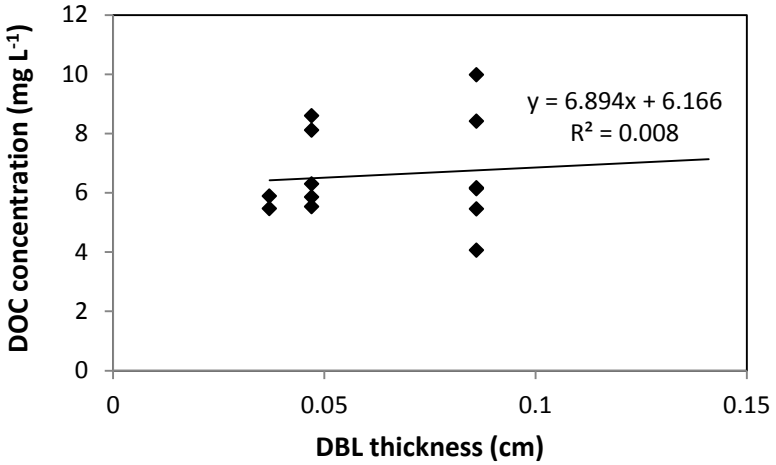

Figure 5.16. Dissolved organic carbon (DOC) (mg L^{-1}) plotted against the DBL (cm) measured at the River Enborne over the deployment period. Data provided by the CEH as part of the Boxford Observatory Project and Thames Initiative.

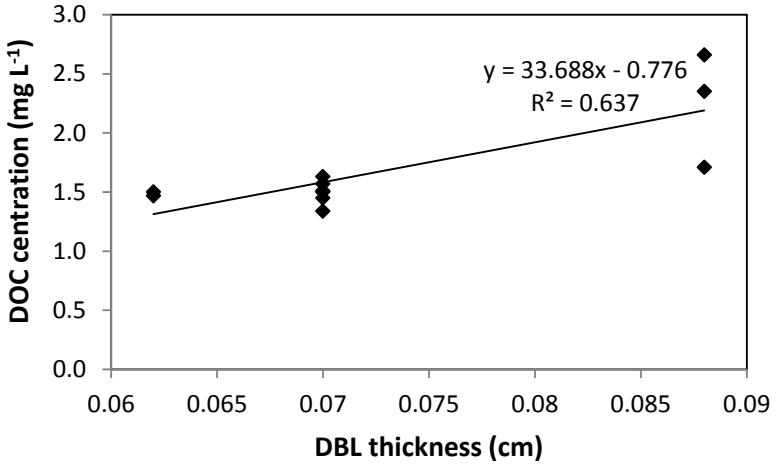

Figure 5.17. Dissolved organic carbon (DOC) (mg L^{-1}) plotted against the DBL (cm) measured at the River Lambourn over the deployment period. Data provided by the CEH as part of the Boxford Observatory Project and Thames Initiative.

5.5.3.3 Inorganic complexes

Another correlation was that of phosphate and the size of the DBL. Figures 5.18 and 5.19 show the phosphate concentrations plotted against the DBL thickness for the Rivers Enborne and Lambourn respectively. In the River Enborne a strong positive correlation was observed, with an R^2 value of 0.83, whilst no correlation was found for the thickness of the DBL with changing phosphate concentrations for the River Lambourn. The River Enborne in the sampling location is surrounding by agricultural land, whilst the sampling site at the River Lambourn is in a Site of Special Scientific Interest (SSSI). This means the River Enborn has fluctuating phosphate concentrations with runoff after precipitation events, similar to that found by Evan *et al*. [51]. The range of soluble reactive phosphate over the study period in the River Enborne is 133 µg L^{-1}, whilst in the River Lambourn it is only 43 µg L^{-1}. Phosphate is a strong U ligand, however it has been shown to be measurable using Metsorb-DGT devices [44]. Further work would be required to establish the cause of the relationship between phosphate and DBL thickness, although it is likely there are additional interactions between for instance the phosphate and the SPM. This may indicate the presence of phosphate metal oxyhydroxides interactions as per Evan *et al*. [51], both of which also strongly bind U and may therefore affect the DBL thickness. Phosphate can also form complexes with calcium and magnesium, both of which form ternary uranyl carbonate complexes. This means there could be the potential for more complex reactions occurring in the zone of dissociation on the surface of the DGT devices. Any

interactions and the effect on the DBL would require verification under controlled laboratory conditions.

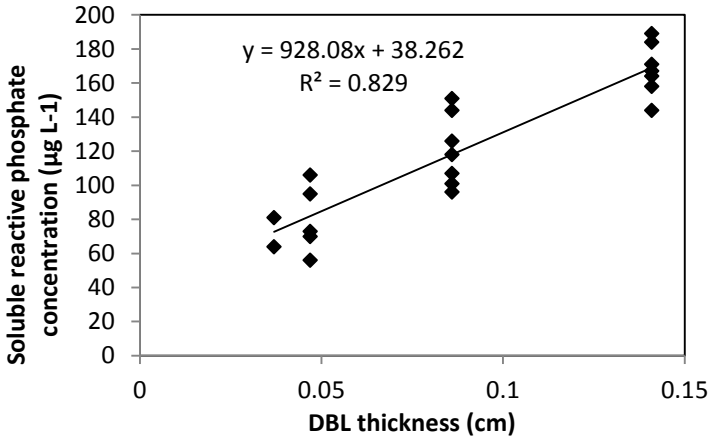

Figure 5.18 Phosphate (µg L^{-1}) plotted against the DBL (cm) measured at the River Enborne over the deployment period. Data provided by the CEH as part of the Boxford Observatory Project and Thames Initiative.

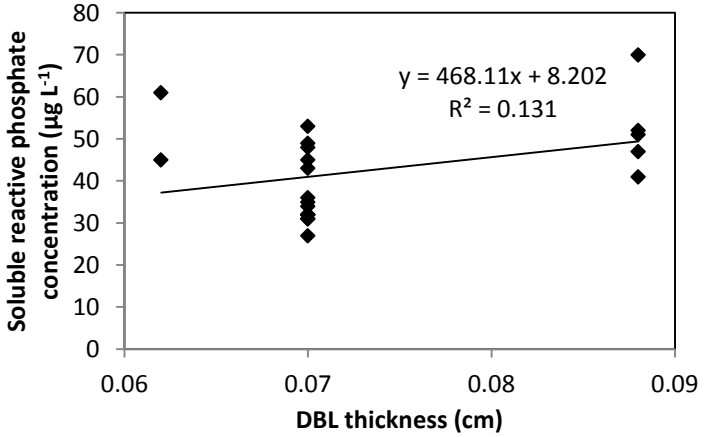

Figure 5.19 Phosphate (µg L^{-1}) plotted against the DBL (cm) measured at the River Lambourn over the deployment period. Data provided by the CEH as part of the Boxford Observatory Project and Thames Initiative.

Other U ligands that may have affected the size of the DBL could include the alkaline earth metals calcium and magnesium, both of which are known to form complexes with uranyl carbonate species [52]. The effect calcium and magnesium may have on the DBL is to hinder the diffusion of the U due to steric effects of the larger molecules formed. This could be further investigated under laboratory conditions to understand the role ternary uranium complexes. Figures 5.20 and 5.21 show the concentration of calcium over the deployment period plotted against the DBL thickness for the Rivers Enborne and Lambourn respectively. The River Enborne displays a weak

positive (increasing DBL thickness with increasing calcium concentrations) trend indicating that calcium may play a role in increasing the size of the DBL, but the River Lambourn shows no such correlation potentially because the calcium concentrations do not fluctuate to the same degree as in the River Enborne (the range of calcium concentrations in the River Enborne is ~30 mg L^{-1}, and in the River Lambourn it is ~7 mg L^{-1}).

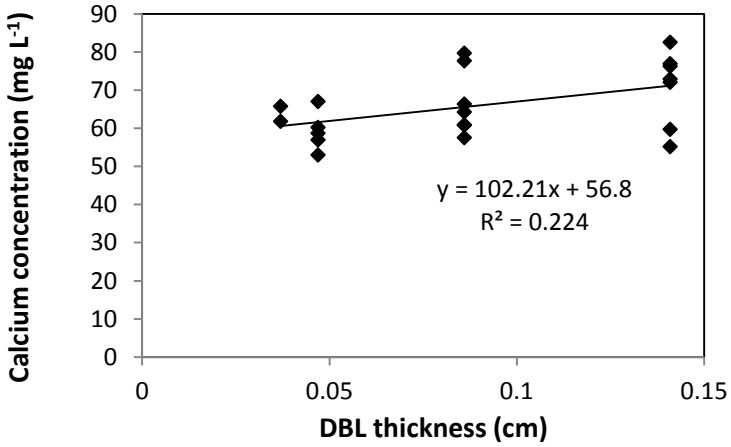

Figure 5.20. Calcium (mg L^{-1}) plotted against the DBL (cm) measured at the River Enborne over the deployment period. Data provided by the CEH as part of the Boxford Observatory Project and Thames Initiative.

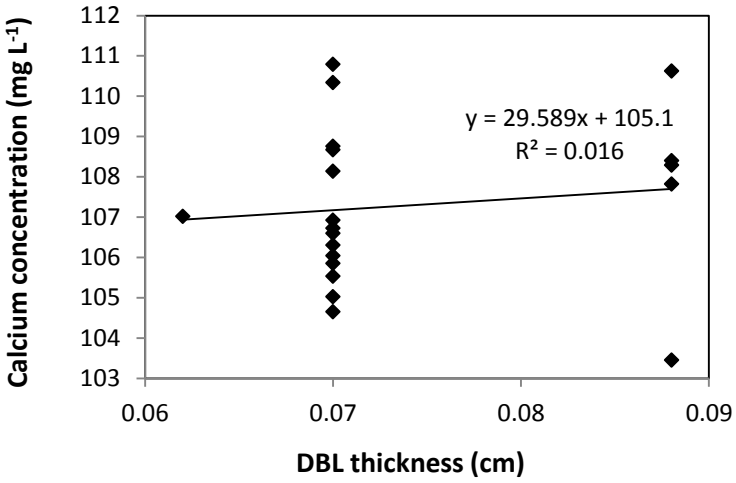

Figure 5.21. Calcium (mg L^{-1}) plotted against the DBL (cm) measured at the River Lambourn over the deployment period. Data provided by the CEH as part of the Boxford Observatory Project and Thames Initiative.

Figures 5.22 and 5.23 show the DBL thickness with dissolved magnesium concentration in the Rivers Enborne and Lambourn respectively. There is a trend of decreasing DBL thickness with increasing magnesium concentration in the River Enborn, with an R^2 value of 0.62. This could be because of interactions of the U with the magnesium, forming ternary carbonate complexes at the surface of the DGT device similar to calcium. No such trend was observed in the River Lambourn (Figure 5.23).

Any influence magnesium has on the DBL thickness would have to be investigated under controlled conditions.

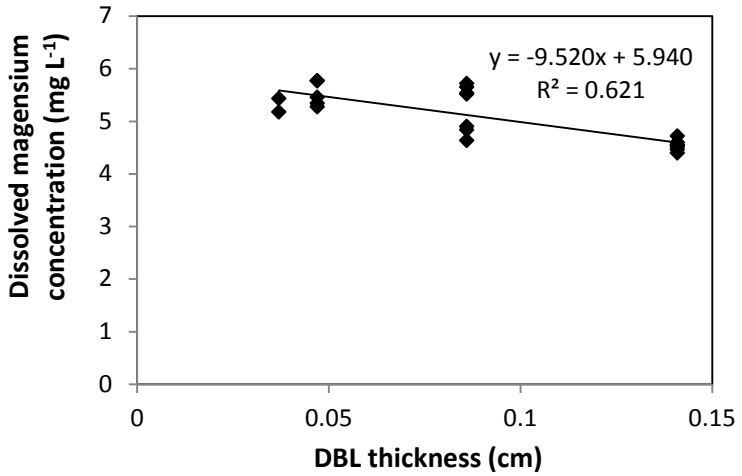

Figure 5.22. Magnesium (mg L^{-1}) plotted against the DBL (cm) measured at the River Enborne over the deployment period. Data provided by the CEH as part of the Boxford Observatory Project and Thames Initiative.

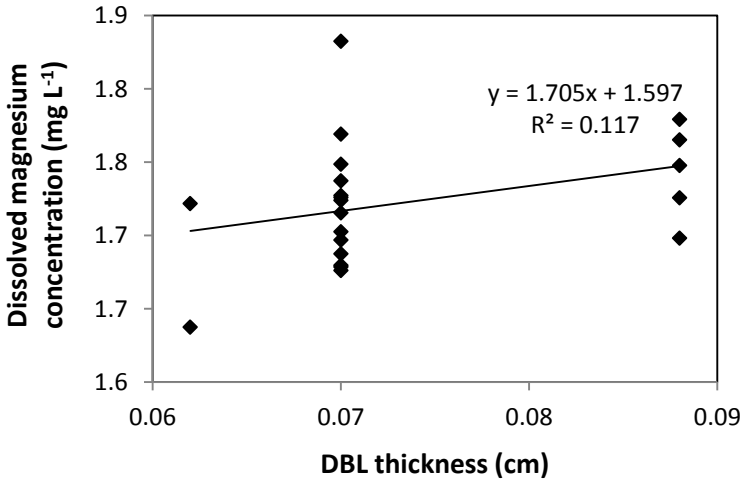

Figure 5.23. Magnesium (mg L^{-1}) plotted against the DBL (cm) measured at the River Labourn over the deployment period. Data provided by the CEH as part of the Boxford Observatory Project and Thames Initiative.

5.5.4 Calculation of TWA concentrations

The TWA concentrations of U were calculated using varying scenarios (Figures 5.24 and 5.25 for the Rivers Enborne and Lambourn repectively) (a) the average thickness of the DBL measured over the entire deployment period; (b) not accounting for a DBL; and (c) using the changing thicknesses of DBLs measured during the trial. The parameters e.g. water pH and temperature and diffusion coefficient used in these calculations are given in Table 5.8 below. The results tables for the TWA calculations

can be seen in Tables A5.7 and A5.8 (located in the appendix) for the Rivers Enborne and Lambourn respectively.

Table 5.8 Diffusion coefficients over the deployment period, using diffusion coefficient data from Hutchins *et al*. [16] and corrected using the Stokes Einstein equation (Equation 5.3).

Week	Date	River Lambourn			River Enborne		
		Temperature (^{o}C)	Diffusion coefficient (x 10^{-6} cm^{-2} s^{-1})	pH	Temperature (^{o}C)	Diffusion coefficient (x 10^{-6} cm^{-2} s^{-1})	pH
0	24/08/2011	15	1.99		15	2.08	
1	31/08/2011	14	1.87	7.95	14	1.92	7.62
2	07/09/2011	14	1.76	7.89	14	1.92	7.66
3	14/09/2011	14	1.87	7.98	14	1.92	7.67
4	23/09/2011	14	1.83	7.98	14	1.92	7.74
5	28/09/2011	15	1.96	7.86	14	2.09	7.69
6	05/10/2011	16	2.10	7.93	15	2.24	7.60
7	12/10/2011	11	1.37	7.92	16	1.43	7.63
8	19/10/2011	10	1.28	7.87	11	1.28	7.65
9	24/10/2011	12	1.57	7.78	10	1.61	7.71
10	02/11/2011	11	1.42	7.68	11	1.28	7.62
11	09/11/2011	10	1.22	7.76	11	1.35	7.47
12	16/11/2011	9	1.05	7.78	11	1.08	7.43
13	23/11/2011	7	0.78	7.77	9	1.02	7.48
14	30/11/2011	8	0.93	7.80	9	0.93	7.57
15	07/12/2011	8	0.90	7.74	8	0.61	7.64
16	14/12/2011	7	0.76	7.82	6	0.66	7.64
17	21/12/2011	9	1.01	7.81	6	0.73	7.54
18	28/12/2011	8	0.97	7.67	7	1.09	7.50
19	05/01/2012	9	1.01	7.70	9	0.89	7.52
20	11/01/2012	10	1.23	7.75	8	0.95	7.63
21	18/01/2012	10	1.23	7.76	8	0.95	7.72

Figures 5.24 and 5.25 show that the TWA concentrations generally lie mid-way between weekly spot data points. This was evident when there were rapid, short-lived, increases in the concentration of U during weeks 2 and 6 for the River Enborne (Figure 5.24), and weeks 2, 6 and 7 for the River Lambourn (Figure 5.25). During periods of relatively stability, the concentration of U measured in grab waters samples (weeks 20-22, River Lambourn and River Enbourn; and weeks 15-16, River Enborne) corresponded well with the TWA concentrations found with the DGT. This shows the effectiveness of the DGT in measuring accurately, fluctuating concentrations, despite the difficulties of predicting the thickness of the DBL. Murdock *et al*. [5] attempted to validate DGT as an *in situ* tool for measuring caesium. They found that over the 5-month study, both the concentrations of caesium measured by the DGT and in grab water samples were in close agreement, being within the 1 σ margin of error. No DBL

thickness was measured, and as there was close agreement between the two measurements, it was not an important parameter. The study was undertaken in a lake with little variation in flow and there was a constant input of caesium from the Magnox reactor sited located there. Longer deployment times mean more measurement errors can be introduced. This includes increased bio-fouling, susceptibility to changing flow rates, and saturation of the binding phase by other ions. Mengistu *et al*. [17] used DGT as a risk assessment tool, and undertook a single 31 d and a single 3 d deployment to measure seventeen metals (including U) in water polluted by mining tailings. They found 1-2 orders of magnitude reduction in the mass of metals accumulated in the DGT during the long-term deployments compared with the short-term deployments. It was found in Chapter 4 that there was decreased uptake of U by the DGT devices after 7 d, due to bio-fouling and saturation of the binding phase. For this reason, 7 d was chosen as the deployment period in this study.

DGT has been to measure other analytes in highly fluctuating environments, such as estuaries [19, 20, 53]. Montero *et al*. [19] deployed DGTs for 10 days in 13 estuaries draining into the Bay of Biscay and found a good correlation with previously measured concentrations of Cd, Cu, Ni and Zn using grab water samples. Dunn *et al*. [8] used the DGT to examine the effect of tidal cycles on aqueous concentrations of Cu, Ni, Pb and Zn, finding it to be an accurate and useful tool for short-term deployments (6h). Neither of these studies measured the presence of a DBL as it was assumed that in a very fast flow environment this would be negligible.

Figures 5.24 and 5.25 show how the TWA concentrations of U calculated over the deployment period vary with different DBL thicknesses; from no DBL accounted for, the average DBL calculated over the entire deployment period, and using the DBL calculated for different times in the trial. The importance of taking the DBL thickness into consideration is clearly demonstrated in Figures 5.24b and 5.25b, as the calculated TWA concentration for U is up to 60% less than in the River Enborne (particularly when the calculated DBL was higher) than measurements that account for the periodically measured DBL (Figure 5.24c and 5.25c) . For the River Lambourn there was an underestimation of the TWA concentration of U by up to 54% when no DBL is accounted for in the calculations, with the TWA calculations using the averaged DBL over the deployment time (Figure 5.25a) and the periodically measured DBL (Figure 5.25c) within ± 20%.

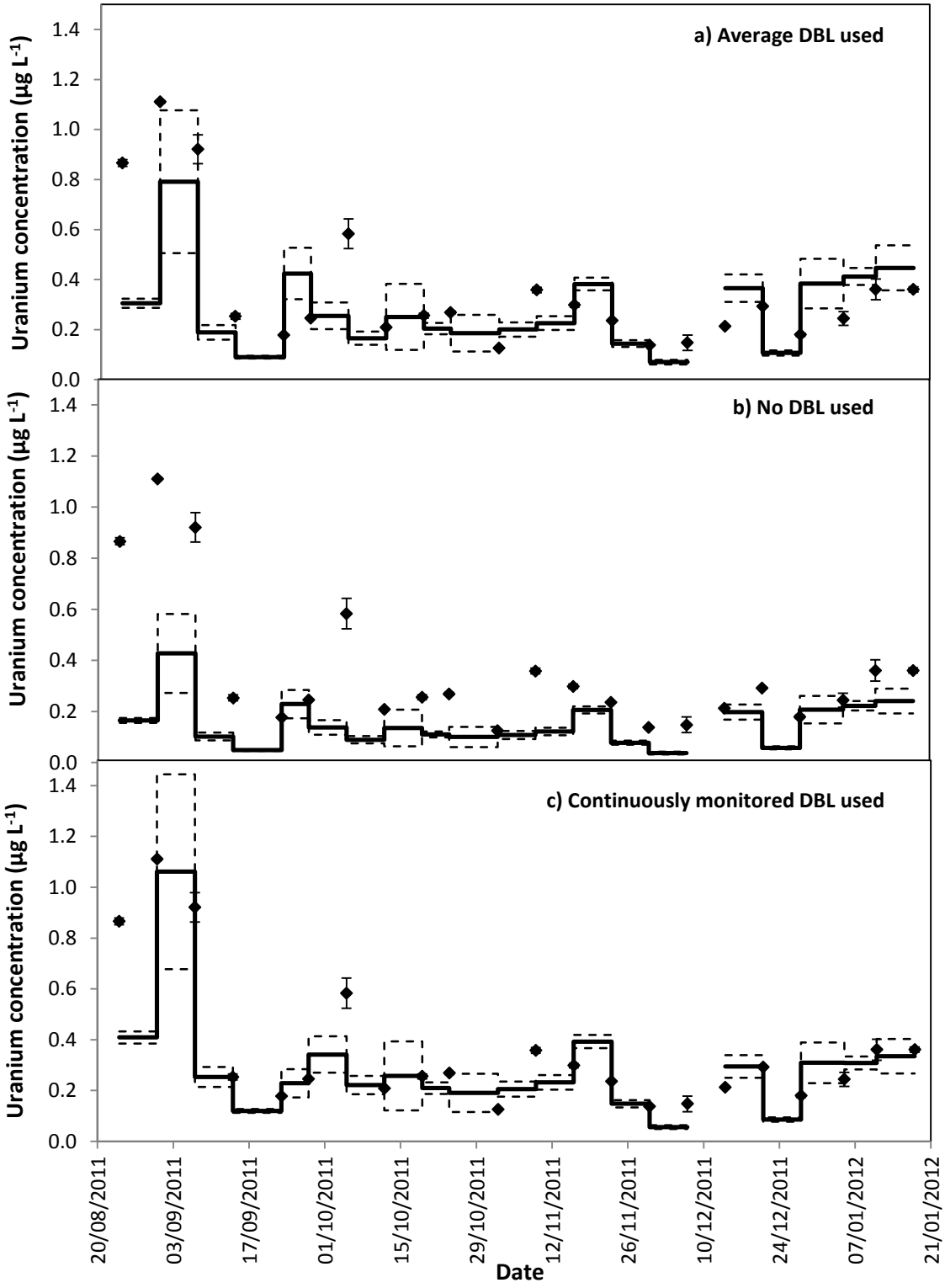

Figure 5.24. TWA concentrations measured by the DGT (-) and in grab water samples (♦) for uranium (µg L^{-1}) over a 22-week deployment from 24/08/2011 to 18/01/2012 for the River Enborne using different calculated DBL thicknesses. a) Average DBL thickness measured over the entire deployment, plus diffusive layer and filter membrane (0.078 + 0.095 = 0.173 cm). b) No DBL thickness accounted for, only the diffusive layer and filter membrane (0.095 cm). c) different DBL thicknesses calculated over the deployment: 24/8/2011–12/10/2011 (0.141 cm); 12/10/2011– 7/12/2011 (0.086 cm); 07/12/2011–05/01/2012 (0.047 cm); 05/01/2012–18/01/2012 (0.037 cm), plus diffusive layer and filter membrane (0.095 cm).

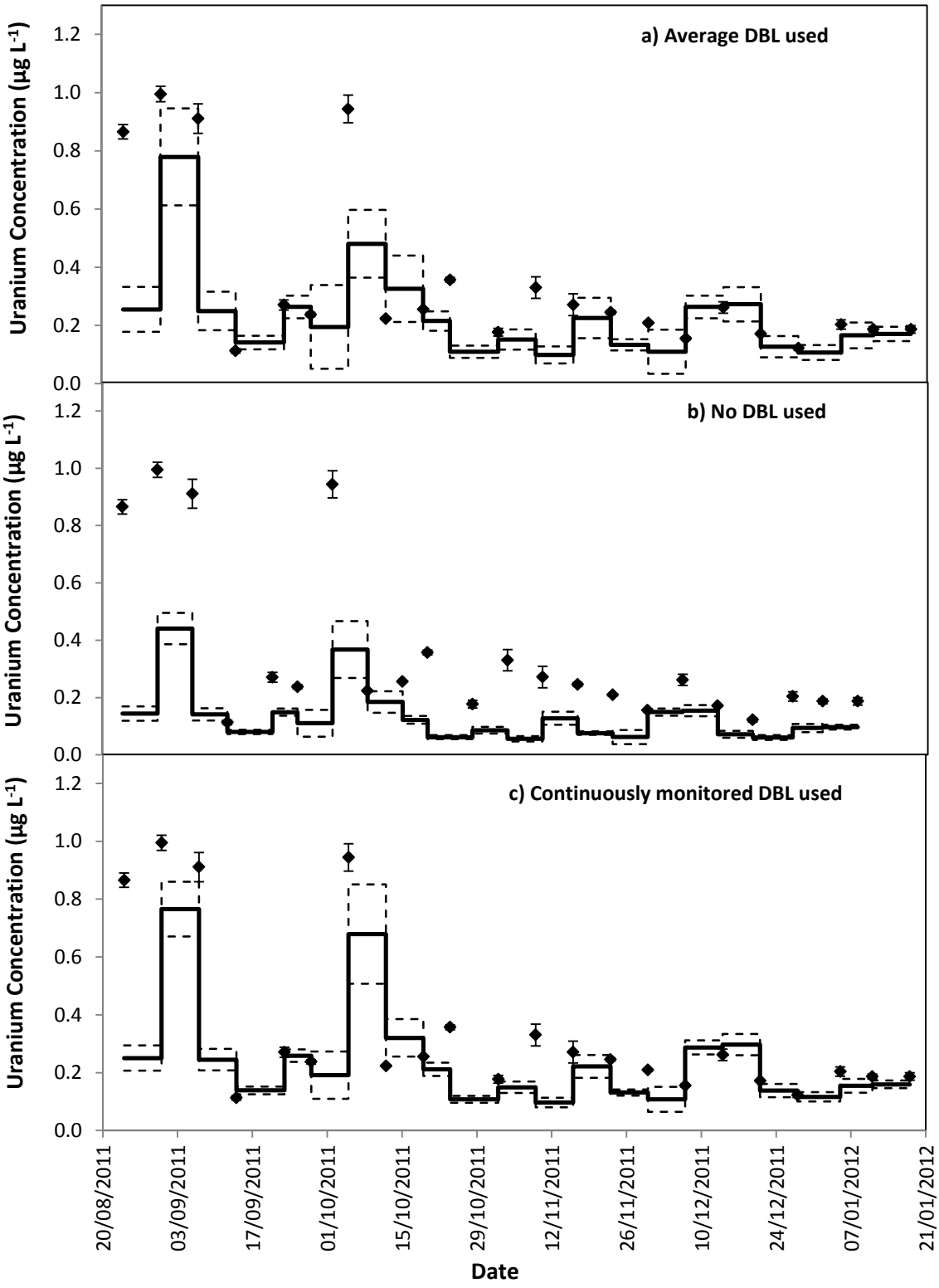

Figure 5.25. TWA concentrations measured by the DGT (-) and in grab water samples (♦) for uranium (µg L^{-1}) over a 22-week deployment from 24/08/2011 to 18/01/12 for the River Lambourn using different DBL calculations. a) Average DBL thickness measured over the entire deployment, plus diffusive layer and filter membrane (0.073 + 0.095 = 0.168 cm. b) No DBL thickness accounted for, only the diffusive layer and filter membrane (0.095 cm). c) different DBL thicknesses calculated over the deployment: 24/8/2011 – 12/10/2011 (0.070 cm); 12/10/2011 – 7/12/2011 (0.070 cm); 07/12/2011 – 05/01/2012 (0.088 cm); 05/01/2012 – 18/01/2012 (0.062 cm), plus diffusive layer and filter membrane (0.095 cm).

In this study there was a reduction in the TWA concentration of U by up to 60% when no DBL thickness was taken into consideration (Figures 5.24b and 5.25b). The closest agreement between the concentrations was observed in weeks 19 -21 for both deployment sites (Figures 5.24a and 5.25a) when the periodically measured DBL thicknesses over the deployment period were used. When the aqueous concentration of U was relatively stable, the TWA estimates (taking into account the measured DBL thickness) were 99-107% and 71–111% of those found with the grab water samples for the Rivers Enborne and Lambourn respectively. When using an averaged DBL thickness over the whole deployment period, this value rose to 124-136 % for the Enborne and lowered to 70–103% for the Lambourn. Using an averaged DBL thickness has less impact on the TWA concentrations in the River Lambourn than the River Enborne, most likely due to the fluctuating flow rates at the latter site. The lower flow periods, when the DBL is greater, will increase the averaged DBL thickness and will therefore result in an overestimation of the TWA estimates (Figure 5.24a, weeks 17–21, 14/12/2011– 8/01/2012).

To give an indication of the reliability of the DGT technique, the ratio of the TWA concentrations of U found with the device to the U concentrations found in weekly averaged grab water samples was made (Tables A5.7and A5.8, located in the Appendix). The closer to one this ratio is the more accurate the technique can be assumed to be, although there is the possibility that the concentrations have fluctuated throughout the week. Results are in agreement with previous work undertaken at these sites in Chapter 4, which showed that in alkaline streams after a 7 d deployment, approximately 80% of the dissolved U could be measured with accuracy. The River Enborne had an average accuracy of ~80% and the River Lambourn ~78%. The failure to achieve 100% accuracy can be attributed to factors such as biofouling, the U not being DGT labile, variations in concentration of U over the 7 d deployment, and an underestimation of the thickness of the DBL as this was not measured every week.

5.5.5 Water quality

The TWA concentrations of uranium found with the DGTs were compared to the weekly averaged water quality results to determine if any statistically significant relationships existed. Speciation distributions for U were made (Visual Minteq, version 3, beta (© 2010 KTH, Department of Land and Water Resources Engineering, Stockholm, Sweden) for each river for each week over the deployment (results in Table 5.8). U is highly soluble in aqueous environments, readily forming the uranyl ion (UO_2^{2+}) at pH < 4 to 5; at pH > 7 occurring as the stable uranyl carbonates $UO_2(CO_3)_2^{2-}$,

$UO_2(CO_3)_3^{4-}$ or its complexes; and under reducing conditions as U(IV) [54]. Aqueous chemistry and speciation is complex and is defined by the pH, Eh, ionic strength and the presence of organic and inorganic ligands [55]. U was used in this study due to its complex physico-chemistry and susceptibility to changes in water chemistry. In order to show the effectiveness of passive samplers in fluctuating environments, it was helpful to compare the DGT data against water quality data.

U has a high reactivity with complexing ligands (OH^- > CO_3^{2-} > HPO_4^{2-} > $H_2PO_4^-$ > F^- > SO_4^{2-} > Cl^-), surfactants or flocculating agents [55]. These could potentially influence the oxidation states of the radionuclide with changing aqueous concentrations potentially affecting uptake by the DGT. In the River Enborne, up to 97% of the dissolved U (depending on the ratio of U:DOC and calcium and alkalinity concentrations) was modelled to be complexed to DOC, with other U complexes including up to 60% $Ca_2UO_2(CO_3)^{2-}$ and up to 26% $Ca_2UO_2(CO_3)^3$ (Table 5.9). The River Lambourn due to the higher alkalinity and lower DOC concentrations had a lower quantity of humate bound U, with the majority of the U as $Ca_2UO_2(CO_3)^3$ (Table 5.10).

Table 5.9 Results of speciation modelling (% distribution) for the River Enborne, with CO_2 at atmospheric partial pressure, using Visual Minteq. The modelling data has been shown for all instances a DBL was measured, plus a deployment average. $FA2UO_{2(aq)}$ and $FAUO_2^{+}{}_{(aq)}$ represent mono- and bi-dentate uranium bonds to fulvic acid.

	Date				
Species	**12/10/2011**	**07/12/2011**	**05/01/2012**	**18/01/2012**	**Deployment Average**
UO_2OH^+	0.013	0.018		0.013	0.024
$UO_2(OH)_3^-$	0.023	0.045		0.035	0.039
$UO_2(OH)_{2\ (aq)}$	0.063	0.106	0.035	0.078	0.113
$Ca_2UO_2(CO_3)_{3\ (aq)}$	29.92	59.751	1.718	28.8	27.535
$CaUO_2(CO_3)_3^{2-}$	10.462	25.899	0.82	11.979	10.936
$UO_2CO_{3\ (aq)}$	0.176	0.295	0.081	0.159	0.287
$UO_2(CO_3)_2^{2-}$	0.407	0.924	0.076	0.336	0.512
$UO_2(CO_3)_3^{4-}$	0.203	0.599	0.031	0.54	0.299
$/FA2UO_{2(aq)}$	58.663	12.3	97.106	58.006	60.119
$/FAUO_2^{+}{}_{(aq)}$	0.068	0.061	0.114	0.052	0.132

Table 5.10 Results of speciation modelling (% distribution) for the River Lambourn, with CO_2 at atmospheric partial pressure, using Visual Minteq. The modelling data has been shown for all instances a DBL was measured, plus a deployment average. $FA2UO_{2(aq)}$ and $FAUO_2^{+}{}_{(aq)}$ represent mono- and bi-dentate uranium bonds to fulvic acid.

	Date				
Species	**12/10/2011**	**07/12/2011**	**05/01/2012**	**18/01/2012**	**Deployment Average**
UO_2OH^+				0.012	
$UO_2(OH)_3^-$	0.01	0.021		0.026	0.01
$UO_2(OH)_{2\,(aq)}$	0.015	0.048		0.064	0.019
$Ca_2UO_2(CO_3)_{3\,(aq)}$	79.043	73.819	79.099	75.098	79.462
$CaUO_2(CO_3)_3^{2-}$	18.92	17.899	19.182	18.349	19.415
$UO_2CO_{3\,(aq)}$	0.03	0.115	0.021	0.162	0.047
$UO_2(CO_3)_2^{2-}$	0.135	0.309	0.139	0.391	0.217
$UO_2(CO_3)_3^{4-}$	0.563	0.353	0.357	0.324	0.343
$/FA2UO_{2(aq)}$	1.282	7.418	1.186	5.563	0.481
$/FAUO_2^{+}{}_{(aq)}$					

The measured water quality data was averaged over each week of deployment (i.e. an average reading of day 1 and day 7 for the deployment week) (Tables A5.1 to A5.6 located in the appendix) and tested for a relationship against the DGT data (Table 5.11), in particular the $U:U_{DGT}$ ratio, which is a measure of the accuracy of the technique. It has been shown in Chapter 4 that calcium carbonate complexes do not inhibit the uptake of U using the Metsorb™ DGT except at extremely high Ca^{2+} concentrations (> 500 mg L^{-1}). However, U DOC complexes may affect the uptake by these devices as they are less labile [49]. At U:HA ratios below 0.1, as with the rivers in this study, it has been found that humic acids can suppress hydrolysis of U(VI) to promote formation of the U:HA complex with a larger portion of the U binding sites resulting in an increased in the non-labile fraction [49, 56]. In the River Enborne, there is a strong negative correlation the (S_P = -.475*) between the DOC concentration and $U:U_{DGT}$ ratio implying that with increased DOC in this system, there is a decline in the accuracy ($U:U_{DGT}$ ratio) of the DGT technique.

What can be seen in Table 5.11 is that in the River Lambourn there is a significant correlation between the $U:U_{DGT}$ ratio and soluble reactive phosphate (S_P = 0.628). This parameter was also shown to be correlated with the DBL thickness (section 5.5.4.3) in this study. This implies that the phosphate is potentially linked to the accuracy of this technique through interactions within the DBL. The DBL was hypothesised to be a zone of complex chemical interactions at the surface of the DGT device. Phosphate is a strong ligand for U ($UO_2PO_4^-$ has a logK of 13.23 at pH 7.8, which is comparable to the logK for $UO_2(CO_3)_2^{2-}$ of 16.61 at pH 7.8), and although no

complexes were modelled to form with uranium in the bulk solution, it does not rule out the possibility of interactions taking place within the DBL. In Chapter 4 phosphate was found not to affect U uptake by the Metsorb-DGT devices except at very high phosphate concentrations.

DOC and phosphate are key factors in this study affecting the accuracy of the DGT technique, but algae (chlorophyll a) concentrations should also be taken into account. Algae can take up U and has been trialled as a removal technique for this element in dilute mine waste waters [38]. However, U bound to algae has been shown to be susceptible to changing physical conditions (such as on the surface of the devices where a diffusion gradient exists) and desorb [57]. No relationship between the Chl *a* and the C_{DGT} for U was observed, however, further investigations are required into the effects of periphyton accumulation on DGT devices and the accuracy and precision of this technique. No relationships were found between the C_{DGT} U and water quality of the rivers, showing that the DGT technique for U operates independently from fluctuating water quality conditions.

Table 5.11. Results of Spearman's rank correlation coefficient for the River Enborne and River Lambourn using monitoring data that was averaged over each deployment week to make it comparable with TWA (DGT) concentrations fro uranium. Many of the distributions were found not to be normally distributed so the Spearman's (which is non-parametric test) was used in place of the Pearson's coefficient (a parametric test that requires normally distributed data). The 99% confidence limit (0.01) for a two tailed test was used, with a sample size of 21. The significance figure used was $r_s = 0.548$. If the test value was equal to or above this figure then the null hypothesis of no correlation was rejected (**correlation is significant at the 0.01 level (2-tailed); *correlation is significant at the 0.05 level (2-tailed)).

	River Enborne				River Lambourn			
	C_{DGT} (µg L^{-1})	**C_{DGT} error (µg L^{-1})**	**U grab (µg L^{-1})**	**U: C_{DGT} ratio**	**C_{DGT} (µg L^{-1})**	**C_{DGT} error (µg L^{-1})**	**U grab (µg L^{-1})**	**U: C_{DGT} ratio**
C_{DGT} (µg L^{-1})	1.000	.268	.745**	.489*	1.000	.399	.270	.501*
C_{DGT} error (µg L^{-1})	.268	1.000	.181	.299	.399	1.000	-.197	.370
U grab (µg L^{-1})	.745**	.181	1.000	.076	.270	-.197	1.000	-.613**
U:DGT ratio	.489*	.299	.076	1.000	.501*	.370	-.613**	1.000
pH	-.044	.142	.115	.045	.217	-.274	.573**	-.381
Alkalinity (µequiv L^{-1})	.186	.002	.517*	-.272	-.053	-.090	-.078	-.071
Chl *a* (µg L^{-1})	.206	.201	.347	-.158	.123	-.031	.445*	-.400
SPM (mg L^{-1})	.086	.325	.296	-.157	.068	.340	-.462*	.424
SRP (µg L^{-1})	.106	.265	.334	-.156	-.027	.205	-.608**	.628**
TDP (µg L^{-1})	.088	.182	.353	-.200	-.076	.213	-.523*	.434*
TP (µg L^{-1})	-.165	.247	-.116	.035	-.221	.233	-.669**	.455*
NH_4 (mg L^{-1})	-.268	-.055	-.335	.110	-.142	.010	-.497*	.312
Si (mg L^{-1})	.003	.311	-.126	.168	-.171	.204	-.514*	.396
DOC (mg L^{-1})	-.303	.062	-.167	-.475*	-.157	.085	-.477*	.389
TDN (mg L^{-1})	-.271	.244	-.300	-.126	-.257	-.112	-.106	-.022
F^- (mg L^{-1})	-.354	.333	-.411	.055	-.309	-.348	.029	-.379
Cl^- (mg L^{-1})	-.332	.035	-.270	-.089	-.163	.067	-.392	.238
NO_2^- (mg L^{-1})	-.360	.232	-.283	-.051	-.005	.297	-.369	.230
NO_3^- (mg L^{-1})	-.314	.225	-.313	-.241	-.151	.326	-.591**	.381
SO_4^{2-} (mg L^{-1})	-.215	.190	-.135	-.141	-.337	-.032	-.305	.161
Na^+ (mg L^{-1})	-.347	.196	-.232	-.077	.374	.281	-.338	.564**
K^+ (mg L^{-1})	-.111	.065	.034	.105	.021	.044	-.244	.398
Ca^{2+} (mg L^{-1})	-.391	-.078	-.550**	-.077	.046	.315	.201	-.202
Mg^{2+} (mg L^{-1})	.163	.200	.511*	-.172	.270	.312	.146	.086
B^+ (µg L^{-1})	.111	-.175	.144	-.191	.223	.319	-.088	.106
Fe^{2+} (µg L^{-1})	.172	.313	.496*	.012	.326	.030	.103	.077
Mn^{2+} (µg L^{-1})	-.102	.362	-.140	-.203	.243	.443*	-.372	.414
Zn^{2+} (µg L^{-1})	.166	.385	-.123	.135	.278	.179	.086	.128
Cu^+ (µg L^{-1})	.161	-.141	.185	-.055	-.221	.109	-.426	.305
Al^{3+} (µg L^{-1})	.092	-.118	-.005	-.115	-.063	.266	.022	-.053

5.5.6 Isotopic ratios of U

Table 5.12. $^{235/238}$U isotopic ratio analysis. Natural $^{235/238}$U isotopic ratio is 0.00725.

Sampling technique	River Enborne			River Lambourn		
	Average isotopic ratio	RSD* (%)	Accuracy ** (%)	Average isotopic ratio	RSD* (%)	Accuracy ** (%)
DGT	0.007302	2.8	-0.72	0.007314	2.9	-0.88
Grab	0.007181	1.8	0.96	0.007260	2.6	-0.15

* Standard deviation calculated as a % of the mean (precision).
** Calculated as (actual reading – measured/actual) x 100.

There are three naturally occurring isotopes of U: ^{238}U (99.276%), ^{235}U (0.718%) and ^{234}U (0.0056%), where the abundance is given by mass in brackets [49]. Significant quantities of U occur naturally in the environment, however, this element needs to be monitored due to its toxicity, mobility and radiological properties [58]. Isotopic composition can indicate if the U is of natural or anthropogenic origin as the 235:238 ratio is consistent in nature. As shown in Table 5.12 there is little difference between the isotopic composition of U measured in the grab water samples and the DGT. The accuracy of the DGT is within 1%, with a relative standard deviation of 2.85%, which is comparable to that found in Chapter 4 Table 4.4, where the accuracy and precision were 1 % and 10 % respectively. The better precision in this study could be as a result of the longer deployment times, thereby allowing greater quantities of U to accumulate onto the resin. Further refinement is required for the isotopic methodology to achieve better accuracy. At present, slight enrichments or depletions in the 235:238 ratio would not be detectable.

5.6 Implications for using DGT in environmental monitoring

The data presented here shows DGT can be used as a tool in long-term environmental monitoring programmes, even though seasonal variations in water flow and chemistry can have an impact on results. Water bodies with highly fluctuating flows require extensive DBL measurements. The thickness of the DBL is also affected by factors such as amount of SPM and biofouling. Ideally, the DBL needs to be measured for each deployment. For rivers with a high degree of biological activity, samplers should be mounted in a cage, and this particularly is advisable for longer-term deployments (> 4 d). In addition, recording other physical parameters such as water temperature and pH are essential in order to obtain a reliable value for the diffusion coefficient over the trial period. These factors aside, the DGT can provide valuable information on labile and bio-available concentrations of wide range pollutants over

long periods and give information that is complementary to that obtained with grab water sampling. At present, $^{235:238}U$ ratios that slightly enriched or depleted would not be detectable without further method development.

5.7 References

[1] British Standards Institution, Water quality - sampling, in: Guidance on passive sampling in surface waters, British Standards Publication, London, 2011, pp. 23.

[2] I.W. Croudace, P.E. Warwick, R.C. Greenwood, A novel approach for the rapid decomposition of Actinide^{TM} resin and its application to measurement of uranium and plutonium in natural waters, Analytica Chimica Acta, 577 (2006) 111-118.

[3] G. Wilson, N. McAllister-Hewlings, W.G. Beard, Environment Agency Requirement for the Operator Monitoring Programme for Radioactivity in the Environment around AWE Aldermaston and Burghfiled: Results for the Period October to December 2011, AWE Report, 2012, pp. 25.

[4] C.W. Anderson, S.A. Rounds, Use of continuous monitors and autosamplers to predict unmeasured water-quality constituents in tributaries of the Tualatin River, Oregon: U.S. Geological Survey Scientific Investigations Report, 2010, pp. 76.

[5] C. Murdock, M. Kelly, L.-Y. Chang, W. Davison, H. Zhang, DGT as an *in situ* tool for measuring radiocesium in natural waters, Environmental Science & Technology, 35 (2001) 4530-4535.

[6] W.A. House, M.S. Warwick, Intensive measurements of nutrient dynamics in the River Swale, Science of the Total Environment, 210 (1998) 111-137.

[7] I.J. Allan, J. Knutsson, N. Guigues, G.A. Mills, A.M. Fouillac, R. Greenwood, Evaluation of the Chemcatcher and DGT passive samplers for monitoring metals with highly fluctuating water concentrations, Journal of Environmental Monitoring, 9 (2007) 672-681.

[8] R.J.K. Dunn, P.R. Teasdale, J. Warnken, J.M. Arthur, Evaluation of the *in situ*, time-integrated DGT technique by monitoring changes in heavy metal concentrations in estuarine waters, Environmental Pollution, 148 (2007) 213-220.

[9] F. Haas, F. Pfeiffer, Water-Monitoring in an WWII explosive factory with Gaiasafe Passive Collectors, http://www.gaiasafe.de/popsclz.pdf.

[10] K. Runeberg, Chemcatcher: Performance of a passive sampling system for aquatic monitoring of metals, in: Department of Civil and Environmental Engineering, Chalmers University of Technology, Goteborg, 2005.

[11] R. Aguilar-Martinez, R. Greenwood, G.A. Mills, B. Vrana, M.A. Palacios-Corvillo, M.M. Gomez-Gomez, Assessment of Chemcatcher passive sampler for the monitoring of inorganic mercury and organotin compounds in water, International Journal of Environmental Analytical Chemistry, 88 (2008) 75-90.

[12] R. Greenwood, G.A. Mills, B. Vrana, I. Allan, R. Aguilar-Martinez, G. Morrison, Monitoring of priority pollutants in water using Chemcatcher passive sampling devices, in: R. Greenwood, G.A. Mills, B. Vrana (Eds.) Comprehensive Analytical Chemistry, Elsevier, 2007, pp. 486.

[13] V.I. Slaveykova, N. Parthasarathy, J. Buffle, K.J. Wilkinson, Permeation liquid membrane as a tool for monitoring bioavailable Pb in natural waters, Science of the Total Environment, 328 (2004) 55-68.

[14] B. Vrana, G.A. Mills, I.J. Allan, E. Dominiak, K. Svensson, J. Knutsson, G. Morrison, R. Greenwood, Passive sampling techniques for monitoring pollutants in water, Trac-Trends in Analytical Chemistry, 24 (2005) 845-868.

[15] W. Davison, Fones G., Harper, M., Teasdale, P. And Zhang, H, Dialysis, DET and DGT: *In situ* diffusional techniques for studying water, sediments and soils., in: J. Buffle, Horvai, G. (Ed.) *In situ* monitoring of aquatic systems: chemical analysis and speciation, John Wiley & Sons Ltd, 2000, pp. 74.

[16] C.M. Hutchins, J.G. Panther, P.R. Teasdale, F. Wang, R.R. Stewart, W.W. Bennett, H. Zhao, Evaluation of a titanium dioxide-based DGT technique for measuring inorganic uranium species in fresh and marine waters, Talanta, 97 (2012) 550-556.

[17] H. Mengistu, O. Roeyset, A. Tessema, T. Abiye, M. Demlie, Diffusive gradient in thin-films (DGT) as risk assessment and management tools in the Central Witwatersrand Goldfield, South Africa, Water SA, 38 (2012) 15-22.

[18] Z. Dragun, B. Raspor, V. Roje, The labile metal concentrations in Sava River water assessed by diffusive gradients in thin films, Chemical Speciation and Bioavailability, 20 (2008) 33-46.

[19] N. Montero, M.J. Belzunce-Segarra, J.L. Gonzalez, J. Larreta, J. Franco, Evaluation of diffusive gradients in thin-films (DGTs) as a monitoring tool for the assessment of the chemical status of transitional waters within the Water Framework Directive, Marine Pollution Bulletin, 64 (2012) 31-39.

[20] R.J.K. Dunn, P.R. Teasdale, J. Warnken, M.A. Jordan, J.M. Arthur, Evaluation of the in situ, time-integrated DGT technique by monitoring changes in heavy metal concentrations in estuarine waters, Environmental Pollution, 148 (2007) 213-220.

[21] R.J.K. Dunn, P.R. Teasdale, J. Warnken, R.R. Schleich, Evaluation of the diffusive gradient in a thin film technique for monitoring trace metal concentrations in estuarine waters, Environmental Science & Technology, 37 (2003) 2794-2800.

[22] C. European Parliament, Directive 2000/60/EC of the European Parliament and of the Council of 23 October 2000 establishing a framework for Community action in the field of water policy, 15.10.20.20 European Parliament, 2000.
[23] Environment Agency, Environmental Permitting Regulations 2010, DEFRA, The Stationary Office, London, 2010, pp. 186.
[24] Environment Agency, Radioactive Substances Regulation – Environmental Principles, in: Radioactive Substances Regulation, Environment Agency, Bristol, 2010.
[25] B. Docekal, M. Gregusova, Segmented sediment probe for diffusive gradient in thin films technique, Analyst, 137 (2012) 502-507.
[26] W.J. Li, J.J. Zhao, C.S. Li, S. Kiser, R.J. Cornett, Speciation measurements of uranium in alkaline waters using diffusive gradients in thin films technique, Analytica Chimica Acta, 575 (2006) 274-280.
[27] W.J. Li, C.S. Li, J.J. Zhao, R.J. Cornett, Diffusive gradients in thin films technique for uranium measurements in river water, Analytica Chimica Acta, 592 (2007) 106-113.
[28] H. Vandenhove, K. Antunes, J. Wannijn, L. Duquene, M.V. Hees, Method of diffusive gradients in thin films (DGT) compared with other soil testing methods to predict uranium phytoavailability, Science of the Total Environment, 373 (2007) 542-555.
[29] J. Mihalik, P. Henner, S. Frelon, V. Camilleri, L. Fevrier, Citrate assisted phytoextraction of uranium by sunflowers: Study of fluxes in soils and plants and resulting intra-planta distribution of Fe and U, Environmental and Experimental Botany, 77 (2012) 249-258.
[30] L. Duquène, H. Vandenhove, F. Tack, M. Van Hees, J. Wannijn, Diffusive gradient in thin films (DGT) compared with soil solution and labile uranium fraction for predicting uranium bioavailability to ryegrass, Journal of Environmental Radioactivity, 101 (2010) 140-147.
[31] H.P. Jarvie, C. Neal, M.D. Jürgens, E.J. Sutton, M. Neal, H.D. Wickham, L.K. Hill, S.A. Harman, J.J.L. Davies, A. Warwick, C. Barrett, J. Griffiths, A. Binley, N. Swannack, N. McIntyre, Within-river nutrient processing in Chalk streams: The Pang and Lambourn, UK, Journal of Hydrology, 330 (2006) 101-125.
[32] T.J. Marsh, M.L. Lees, Hydrometric Register and Statistics 1996-2000. Hydrological data UK series., in, Centre for Ecology and Hydrology / British Geological Survey, Wallingford, 2003, pp. 210.

[33] R.M.S. Smith, D.J. Evans, H.S. Wheater, Evaluation of two hybrid metric-conceptual models for simulating phosphorus transfer from agricultural land in the river enborne, a lowland UK catchment, Journal of Hydrology, 304 (2005) 366-380.
[34] K.W. Warnken, H. Zhang, W. Davison, Accuracy of the diffusive gradients in thin-films technique: Diffusive boundary layer and effective sampling area considerations, Analytical Chemistry, 78 (2006) 3780-3787.
[35] H. Zhang, W. Davison, Direct *in situ* measurements of labile inorganic and organically bound metal species in synthetic solutions and natural waters using diffusive gradients in thin films, Analytical Chemistry, 72 (2000) 4447-4457.
[36] W.W. Bennett, P.R. Teasdale, J.G. Panther, D.T. Welsh, D.F. Jolley, New diffusive gradients in a thin film technique for measuring inorganic arsenic and selenium(IV) using a titanium dioxide based adsorbent, Analytical Chemistry, 82 (2010) 7401-7407.
[37] S. Kerisit, C. Liu, Molecular simulation of the diffusion of uranyl carbonate species in aqueous solution, Geochimica Et Cosmochimica Acta, 74 (2010) 4937-4952.
[38] M. Kalin, W.N. Wheeler, G. Meinrath, The removal of uranium from mining waste water using algal/microbial biomass, Journal of Environmental Radioactivity, 78 (2004) 151-177.
[39] K.W. Warnken, W. Davison, H. Zhang, Interpretation of *in situ* speciation measurements of inorganic and organically complexed trace metals in freshwater by DGT, Environmental Science & Technology, 42 (2008) 6903-6909.
[40] K.W. Warnken, W. Davison, H. Zhang, J. Galceran, J. Puy, *In situ* measurements of metal complex exchange kinetics in freshwater, Environmental Science & Technology, 41 (2007) 3179-3185.
[41] Ø.A. Garmo, O. Røyset, E. Steinnes, T.P. Flaten, Performance study of diffusive gradients in thin films for 55 elements, Analytical Chemistry, 75 (2003) 3573-3580.
[42] Ø.A. Garmo, K.R. Naqvi, O. Røyset, E. Steinnes, Estimation of diffusive boundary layer thickness in studies involving diffusive gradients in thin films (DGT), Analytical and Bioanalytical Chemistry, 386 (2006) 2233-2237.
[43] S. Scally, W. Davison, H. Zhang, Diffusion coefficients of metals and metal complexes in hydrogels used in diffusive gradients in thin films, Analytica Chimica Acta, 558 (2006) 222-229.
[44] J.G. Panther, P.R. Teasdale, W.W. Bennett, D.T. Welsh, H.J. Zhao, Titanium dioxide-based DGT technique for *in situ* measurement of dissolved reactive phosphorus in fresh and marine waters, Environmental Science and Technology, 44 (2010) 9419-9424.

[45] M.C.Alfaro-De la Torre, P.Y. Beaulieu, A. Tessier, *In situ* measurement of trace metals in lakewater using the dialysis and DGT techniques, Analytica Chimica Acta, 418 (2000) 53-68.

[46] E.K. Lesher, B.D. Honeyman, J.F. Ranville, Detection and characterization of uranium-humic complexes during 1D transport studies, Geochimica Cosmochimic Acta, 109 (2013), 127-142.

[47] J.L. Levy, H. Zhang, W. Davison, J. Galceran, J. Puy, Kinetic signatures of metals in the presence of Suwannee River fulvic acid, Environmental Science & Technology, 46 (2012) 3335-3342.

[48] S. Scally, W. Davison, H. Zhang, *In situ* measurements of dissociation kinetics and labilities of metal complexes in solution using DGT, Environmental Science & Technology, 37 (2003) 1379-1384.

[49] J. Zhao, I.I. Fasfous, J.D. Murimboh, T. Yapici, P. Chakraborty, S. Boca, C.L. Chakrabarti, Kinetic study of uranium speciation in model solutions and in natural waters using Competitive Ligand Exchange Method, Talanta, 77 (2009) 1015-1020.

[50] J.J. Lenhart, S.E. Cabaniss, P. MacCarthy, B.D. Honeyman, Uranium(VI) complexation with citric, humic and fulvic acids, Radiochim Acta, 88 (2000) 345.

[51] D.J. Evans, P.J. Johnes, Physico-chemical controls on phosphorus cycling in two lowland streams. Part 1 – the water column, Science of the Total Environment, 329 (2004) 145-163.

[52] W. Dong, S.C. Brooks, Determination of the Formation Constants of Ternary Complexes of Uranyl and Carbonate with Alkaline Earth Metals (Mg2+, Ca2+, Sr2+, and Ba2+) Using Anion Exchange Method, Environmental Science and Technology, 40 (2006) 4689-4695.

[53] S. Meylan, N. Odzak, R. Behra, L. Sigg, Speciation of copper and zinc in natural freshwater: comparison of voltammetric measurements, diffusive gradients in thin films (DGT) and chemical equilibrium models, Analytica Chimica Acta, 510 (2004) 91-100.

[54] G.R. Choppin, Actinide speciation in aquatic systems, Marine Chemistry, 99 (2006) 83-92.

[55] S. Cotton, The lanthanides and actinides, Macmillan Education Ltd, 1991.

[56] S.J. Markich, Uranium speciation and bioavailability in aquatic systems: an overview, Science World Journal, 2 (2002) 707-729.

[57] C. Dienemann, G. Dudel, H. Dienemann, L. Stolz, Retention of radionuclides and arsenic by algae downstream of U mining tailings, Uranium Mining and Hydrogeology

III. BJ Merkel, B Planer-Friedrich and C Wolkersdorfer: Springer-Verlag Berlin Heidelberg New York, (2002) 605-614.
[58] T. Mathews, K. Beaugelin-Seiller, J. Garnier-Laplace, R. Gilbin, C. Adam, C. Della-Vedova, A probabilistic assessment of the chemical and radiological risks of chronic exposure to uranium in freshwater ecosystems, Environmental Science and Technology, 43 (2009) 6684-6690.

Appendix

Table A5.1. Concentrations of 0.45 µm filtered major cations in the River Enborne over the deployment period. The data has been averaged over each deployment week (average of data points taken closest to day 1 and day 7 of each week). Data provided by the CEH as part of the Boxford Observatory Project and Thames Initiative.

Week	Date	Na^+	K^+	Ca^{2+}	Mg^{2+}	B^+	Fe^{2+}	Mn^{2+}	Zn^{2+}	Cu^+	Al^{3+}
		mg L^{-1}	mg L^{-1}	mg L^{-1}	mg L^{-1}	µg L^{-1}	µg L^{-1}	µg L^{-1}	µg L^{-1}	µg L^{-1}	µg L^{-1}
		LOD = 0.01 mg L^{-1}				LOD = 0.5 µg L^{-1}					
1	31/08/2011	20.54	4.12	58.42	4.32	29.83	221.37	24.80	3.02	1.99	21.82
2	07/09/2011	20.97	4.19	63.64	4.47	29.68	212.92	27.80	2.90	2.11	19.96
3	14/09/2011	22.37	4.64	65.93	4.63	29.67	174.32	31.83	3.09	2.07	15.06
4	23/09/2011	23.03	4.71	68.02	4.63	29.67	133.10	30.85	3.51	1.78	10.24
5	28/09/2011	22.98	4.57	74.59	4.50	29.19	96.69	28.65	3.97	2.00	7.50
6	05/10/2011	24.09	4.66	77.74	4.53	29.36	68.39	32.04	4.53	2.63	8.19
7	12/10/2011	26.73	5.17	79.75	4.55	30.23	70.27	36.21	4.27	2.38	10.44
8	19/10/2011	26.95	5.39	77.32	4.57	30.24	82.13	32.63	3.55	2.17	10.99
9	24/10/2011	27.22	5.39	78.74	4.73	29.67	85.90	27.05	3.32	2.60	9.95
10	02/11/2011	24.74	5.35	70.33	4.86	29.32	100.10	25.21	3.13	2.19	8.18
11	09/11/2011	19.74	5.22	59.25	5.31	29.28	163.08	23.84	3.32	2.35	14.38
12	16/11/2011	20.00	5.19	59.20	5.62	29.43	208.57	24.65	4.68	3.85	21.85
13	23/11/2011	21.82	4.83	62.55	5.52	28.50	173.06	26.03	5.01	4.10	15.21
14	30/11/2011	22.08	4.64	65.33	5.58	26.74	131.00	22.91	3.76	2.83	9.09
15	07/12/2011	21.73	4.73	63.32	5.70	25.83	139.25	18.03	7.31	3.06	12.34
16	14/12/2011	22.68	4.68	59.48	5.76	24.95	159.93	14.24	11.36	4.65	17.25
17	21/12/2011	20.96	4.16	57.84	5.55	23.90	174.34	14.53	7.32	4.33	31.39
18	28/12/2011	16.47	3.72	55.01	5.39	24.06	219.40	17.99	3.19	2.43	69.39
19	05/01/2012	16.07	3.55	60.05	5.36	24.47	226.18	19.03	2.87	1.51	83.82
20	11/01/2012	15.78	3.32	64.44	5.22	24.42	165.69	17.40	2.68	1.73	47.88
21	18/01/2012	16.10	3.38	63.79	5.30	24.48	151.91	15.47	3.02	1.74	26.30

Table A5.2. Concentrations of major anions in the River Enborne over the deployment period. The data has been averaged over each deployment week (average of data points taken closest to day 1 and day 7 of each week). Data provided by the CEH as part of the Boxford Observatory Project and Thames Initiative. Greyed out boxes indicate no data available.

Week	Date	SRP	TDP	TP	NH_4	Si	DOC	TDN	F^-	Cl^-	NO_2^-	NO_3^-	$SO4^{2-}$
		µg L^{-1}	µg L^{-1}	µg L^{-1}	mg L^{-1}	mg L^{-1}	mg L^{-1}	mg L^{-1}	mg L^{-1}	mg L^{-1}	mg L^{-1}	mg L^{-1}	mg L^{-1}
1	31/08/2011	163.00	196.50	237.00	0.09	7.39		1.72	0.15	39.895	0.01	15.21	27.87
2	07/09/2011	157.50	199.50	249.00	0.07	7.48			0.08	20.662		7.86	13.66
3	14/09/2011	177.50	210.50	256.00	0.09	7.96			0.07	20.954		6.84	12.82
4	23/09/2011	186.50	208.50	251.00	0.06	8.23			0.14	42.863	0.01	17.40	25.91
5	28/09/2011	173.50	205.00	246.50	0.05	8.42			0.14	42.377	0.01	19.03	25.15
6	05/10/2011	161.00	197.50	249.50	0.05	8.66			0.14	43.891	0.09	17.52	24.61
7	12/10/2011	165.50	197.50	248.00	0.03	8.95			0.14	48.678	0.10	19.29	24.66
8	19/10/2011	159.00	193.00	227.50	0.04	8.95		2.79	0.11	49.187	0.02	19.92	24.50
9	24/10/2011	138.50	173.00	207.50	0.04	8.74	2.03	3.97	0.10	47.928	0.00	21.36	24.84
10	02/11/2011	135.00	164.50	194.50	0.05	8.23	4.75	2.86	0.12	42.923	0.26	17.22	24.53
11	09/11/2011	120.00	145.00	172.00	0.06	7.66	7.71	3.26	0.11	36.413	0.39	13.35	28.37
12	16/11/2011	107.00	127.00	157.50	0.06	7.92	9.19	3.30	0.11	38.092	0.18	14.57	30.03
13	23/11/2011	109.50	126.50	161.50	0.06	8.63	7.29	3.74	0.11	42.747	0.05	14.92	28.10
14	30/11/2011	104.00	123.50	151.50	0.06	8.87	6.15	2.02	0.11	44.019	0.18	16.79	27.86
15	07/12/2011	101.00	123.00	143.50	0.05	8.34	5.99		0.12	41.581	0.18	15.76	28.07
16	14/12/2011	100.50	118.50	147.50	0.07	7.61	5.68	2.02	0.19	44.037	0.01	15.71	29.23
17	21/12/2011	81.00	91.50	120.50	0.13	6.80	6.81	3.66	0.11	41.909	0.05	18.54	30.79
18	28/12/2011	64.50	75.00	140.50	0.12	6.06	8.35	1.64	0.12	33.300	0.04	17.91	30.09
19	05/01/2012	71.50	76.50	143.50	0.08	6.45	7.44		0.07	15.726	0.01	7.94	13.95
20	11/01/2012	67.00	70.00	94.50	0.10	7.13	5.88						
21	18/01/2012	72.50	79.00	107.50	0.09	7.33	5.67	1.09	0.06	17.114	0.07	8.47	14.83

Table A5.3 Concentration of particulates, pH and alkalinity in the River Enborne over the deployment period. The data has been averaged over each deployment week (average of data points taken closest to day 1 and day 7 of each week). Data provided by the CEH as part of the Boxford Observatory Project and Thames Initiative

Week	**Date**	**pH**	**Alkalinity**	**Suspended material**	
				Chl *a*	**SPM**
			µequiv L^{-1}	µg L^{-1}	mg L^{-1}
1	31/08/2011	7.62	2494.00	2.61	6.43
2	07/09/2011	7.66	2666.50	2.06	8.13
3	14/09/2011	7.67	2833.50	1.95	8.81
4	23/09/2011	7.74	2915.50	1.47	6.07
5	28/09/2011	7.69	3131.00	1.12	5.74
6	05/10/2011	7.60	3252.00	1.60	8.54
7	12/10/2011	7.63	3364.00	1.59	7.89
8	19/10/2011	7.65	3245.50	1.26	5.03
9	24/10/2011	7.71	3257.50	1.18	4.64
10	02/11/2011	7.62	2946.50	1.26	4.65
11	09/11/2011	7.47	2434.50	1.57	4.86
12	16/11/2011	7.43	2430.00	1.37	6.17
13	23/11/2011	7.48	2695.00	0.81	5.48
14	30/11/2011	7.57	2780.00	0.67	3.92
15	07/12/2011	7.64	2598.00	0.44	3.71
16	14/12/2011	7.64	2446.50	0.89	7.42
17	21/12/2011	7.54	2278.50	1.11	8.57
18	28/12/2011	7.50	2080.00	1.92	18.92
19	05/01/2012	7.52	2216.50	1.94	18.44
20	11/01/2012	7.63	2585.50	0.68	4.34
21	18/01/2012	7.72	2709.00	0.53	4.09

Table A5.4 Concentrations of 0.45 µm filtered cations in the River Lambourn over the deployment period. The data has been averaged over each deployment week (average of data points taken closest to day 1 and day 7 of each week). Data provided by the CEH as part of the Boxford Observatory Project and Thames Initiative.

Week	Date	Na^+	K^+	Ca^{2+}	Mg^{2+}	B^+	Fe^{2+}	Mn^{2+}	Zn^{2+}	Cu^+	Al^{3+}
		mg L^{-1}	mg L^{-1}	mg L^{-1}	mg L^{-1}	µg L^{-1}	µg L^{-1}	µg L^{-1}	µg L^{-1}	µg L^{-1}	µg L^{-1}
		LOD = 0.01 mg L^{-1}				LOD = 0.5 µg L^{-1}					
1	31/08/2011	9.56	1.69	108.91	1.77	14.96	4.10	1.07	6.48	0.30	<0.5
2	07/09/2011	9.45	1.74	108.15	1.75	14.77	4.25	0.77	5.66	<0.5	<0.5
3	14/09/2011	9.05	1.67	105.69	1.68	13.13	6.53	0.46	3.32	0.38	7.52
4	23/09/2011	9.27	1.77	105.43	1.68	13.48	6.60	0.48	2.17	<0.5	0.11
5	28/09/2011	9.30	1.80	105.87	1.68	13.41	3.93	0.49	2.66	1.63	-8.35
6	05/10/2011	9.34	1.67	107.43	1.71	13.31	3.74	0.41	2.34	1.98	1.94
7	12/10/2011	9.53	1.66	108.44	1.73	13.46	4.12	0.64	1.97	0.23	3.92
8	19/10/2011	9.39	1.77	107.39	1.71	13.13	4.75	0.82	2.83	0.03	0.21
9	24/10/2011	9.32	1.89	108.19	1.73	13.32	4.42	0.69	3.18	0.12	<0.5
10	02/11/2011	9.26	1.91	108.32	1.74	13.43	3.75	0.51	2.72	0.10	<0.5
11	09/11/2011	9.22	1.88	107.48	1.71	13.28	3.77	0.52	2.84	0.30	3.83
12	16/11/2011	9.33	1.88	106.66	1.72	13.11	3.18	0.52	3.17	0.64	0.86
13	23/11/2011	9.65	1.91	105.78	1.72	12.46	3.18	<0.5	2.92	0.53	<0.5
14	30/11/2011	9.95	1.94	106.76	1.74	12.20	4.08	<0.5	3.73	5.41	<0.5
15	07/12/2011	9.94	1.87	107.44	1.75	12.63	4.13	0.55	3.55	5.64	2.52
16	14/12/2011	12.63	2.34	105.86	1.76	13.78	4.64	0.84	4.13	4.37	2.40
17	21/12/2011	12.75	2.35	107.03	1.77	14.84	4.18	1.05	6.90	11.89	<0.5
18	28/12/2011	9.72	1.79	109.51	1.75	14.72	2.61	1.15	4.92	7.96	<0.5
19	05/01/2012	9.38	1.75	108.10	1.71	14.02	2.48	1.13	2.50	0.85	<0.5
20	11/01/2012	9.41	1.69	107.41	1.71	14.21	2.45	0.88	2.58	1.03	<0.5
21	18/01/2012	9.83	1.67	105.82	1.68	14.25	4.68	1.34	2.38	0.23	0.56

Table A5.5 Concentrations of major anions in the River Lambourn over the deployment period. The data has been averaged over each deployment week (average of data points taken closest to day 1 and day 7 of each week). Data provided by the CEH as part of the Boxford Observatory Project and Thames Initiative. Greyed out boxes indicate no data available.

Week	Date	SRP	TDP	TP	NH_4	Si	DOC	TDN	F^-	Cl^-	NO_2^-	NO_3^-	SO_4^{2-}
		µg L^{-1}	µg L-1	µg L-1	mg L-1	mg L^{-1}	mg L^{-1}	mg L^{-1}	mg L^{-1}	mg L^{-1}	mg L^{-1}	mg L^{-1}	mg L^{-1}
1	31/08/2011	26.0	39.0	41.0	0.06	7.66		4.07	0.13	18.02	0.06	33.89	12.35
2	07/09/2011	29.0	38.5	44.0	0.02	7.57			0.12	18.00	0.06	34.10	12.20
3	14/09/2011	31.5	37.0	46.5	0.08	7.50			0.12	17.47	0.06	33.39	12.16
4	23/09/2011	31.5	39.0	49.5	0.08	7.63			0.12	17.68	0.04	34.19	12.63
5	28/09/2011	33.0	38.0	53.5	0.03	7.81			0.19	43.85	0.01	17.93	16.58
6	05/10/2011	34.5	43.0	55.0	0.04	7.81			0.19	43.63	0.02	17.36	16.36
7	12/10/2011	35.0	45.5	51.5	0.03	7.89			0.06	8.94	0.02	17.07	6.26
8	19/10/2011	34.0	35.5	40.0	0.05	7.91							
9	24/10/2011	32.0	36.0	42.0	0.06	7.84	0.82	4.41	0.04	8.85	0.00	17.07	6.28
10	02/11/2011	37.5	46.5	50.0	0.04	7.88	1.49	8.69	0.09	17.58	0.02	34.22	12.46
11	09/11/2011	44.0	50.0	54.0	0.03	8.02	1.42	8.72	0.09	17.56	0.04	34.71	12.74
12	16/11/2011	49.0	55.0	61.0	0.03	8.08	1.48	8.80	0.10	17.37	0.04	34.23	13.02
13	23/11/2011	50.5	55.5	60.0	0.02	8.04	1.48	8.98	0.11	17.58	0.02	34.37	12.99
14	30/11/2011	48.5	51.0	57.0	0.04	8.00	1.54	9.15	0.12	18.10	0.00	35.49	13.34
15	07/12/2011	45.0	49.0	59.0	0.04	8.03	0.79	4.54	0.12	18.41	0.02	36.09	13.72
16	14/12/2011	55.5	66.0	73.0	0.13	7.95	1.18		0.11	22.73	0.16	37.12	14.63
17	21/12/2011	58.5	62.5	67.5	0.14	7.87	2.03	4.34	0.11	22.71	0.20	36.78	14.43
18	28/12/2011	49.0	50.0	80.5	0.08	8.02	2.19	8.57	0.11	18.39	0.12	34.95	13.00
19	05/01/2012	51.5	55.5	86.0	0.08	8.14	1.33	4.23	0.12	18.32	0.10	34.49	12.68
20	11/01/2012	48.5	70.0	80.0	0.05	8.10	0.75		0.12	18.33	0.08	35.61	12.79
21	18/01/2012	53.0	66.0	92.5	0.04	7.84	1.49		0.11	19.37	0.06	33.95	12.23

Table A5.6. Concentration of particulates, pH and alkalinity in the River Lambourn over the deployment period. The data has been averaged over each deployment week (average of data points taken closest to day 1 and day 7 of each week). Data provided by the CEH as part of the Boxford Observatory Project and Thames Initiative

Week	Date	pH	Alkalinity	Suspended material	
				Chl *a*	SPM
			µequiv L^{-1}	µg L^{-1}	mg L^{-1}
1	31/08/2011	7.95	4509	1.99	1.56
2	07/09/2011	7.89	4479	1.93	1.32
3	14/09/2011	7.98	4392	1.21	1.26
4	23/09/2011	7.98	4468	1.31	1.27
5	28/09/2011	7.86	4461	1.21	1.42
6	05/10/2011	7.93	4396	0.88	1.44
7	12/10/2011	7.92	4406	1.11	1.64
8	19/10/2011	7.87	4384	1.06	1.58
9	24/10/2011	7.78	4502	0.93	1.26
10	02/11/2011	7.68	4416	1.2	1.35
11	09/11/2011	7.76	4379	1.48	1.45
12	16/11/2011	7.78	4461	1.35	1.34
13	23/11/2011	7.77	4550	0.84	1.23
14	30/11/2011	7.80	4553	0.75	1.26
15	07/12/2011	7.74	4481	0.93	1.39
16	14/12/2011	7.82	4346	1.18	2.19
17	21/12/2011	7.81	4343	0.83	2.51
18	28/12/2011	7.67	4497	0.52	2.81
19	05/01/2012	7.70	4411	0.71	3.42
20	11/01/2012	7.75	4571	0.88	3.09
21	18/01/2012	7.76	4492	1.51	7.28

Table A5.7. Values (average of triplicate readings) for the TWA (DGT) concentrations of uranium and grab water sample concentrations of uranium, with error (standard error of triplicate measurements) for the River Enborne. DGT: weekly averaged ratio is also shown for comparison of the two measurements. The measurements shown were calculated using the changing DBL values over the deployment period.

Week number	**Date**	**Concentration of uranium, C_{DGT} (µg L^{-1})**		**Concentration of uranium in grab water samples (µg L^{-1})**		**Weekly averaged concentration of uranium in grab water samples (µg L^{-1})**	**Ratio of the averaged concentration of uranium in grab water samples: Concentration of uranium C_{DGT}**
		Average	±	Average	±		
0	24/08/2011	0.41	0.04	0.87	0.02	0.99	0.41
1	31/08/2011	1.06	0.00	1.11	0.01	1.02	1.04
2	07/09/2011	0.25	0.07	0.92	0.10	0.59	0.43
3	14/09/2011	0.12	0.01	0.25	0.02	0.22	0.56
4	23/09/2011	0.23	0.10	0.18	0.00	0.21	1.08
5	28/09/2011	0.34	0.03	0.25	0.00	0.41	0.83
6	05/10/2011	0.22	0.05	0.58	0.10	0.40	0.56
7	12/10/2011	0.26	0.05	0.21	0.00	0.23	1.13
8	19/10/2011	0.21	0.03	0.26	0.02	0.26	0.81
9	24/10/2011	0.12	0.01	0.27	0.01	0.20	0.60
10	02/11/2011	0.21	0.05	0.13	0.00	0.24	0.87
11	09/11/2011	0.24	0.05	0.36	0.02	0.33	0.72
12	16/11/2011	0.40	0.05	0.30	0.01	0.27	1.49
13	23/11/2011	0.15	0.03	0.24	0.00	0.19	0.81
14	30/11/2011	0.07	0.00	0.14	0.00	0.14	0.51
15	07/12/2011	No data		0.15	0.05	0.18	0.00
16	14/12/2011	0.30	0.08	0.21	0.00	0.25	1.17
17	21/12/2011	0.09	0.01	0.29	0.01	0.24	0.36
18	28/12/2011	0.23	0.02	0.18	0.01	0.21	1.08
19	05/01/2012	0.33	0.02	0.24	0.05	0.30	1.09
20	11/01/2012	0.36	0.02	0.36	0.07	0.36	0.99
21	18/01/2012	0.41	0.04	0.36	0.01	0.99	0.41

Table A5.8. Values (average of triplicate readings) for the TWA (DGT) concentrations of uranium and grab water sample concentrations of uranium, with error (standard error of triplicate measurements) for the River Lambourn. DGT: weekly averaged ratio is also shown for comparison of the two measurements. The measurements shown were calculated using the continuously measured DBL values over the deployment period.

Week number	**Date**	**Concentration of uranium, C_{DGT} (µg L^{-1})**		**Concentration of uranium in grab water samples (µg L^{-1})**		**Weekly averaged concentration of uranium in grab water samples (µg L^{-1})**	**Ratio of the averaged concentration of uranium in grab water samples: Concentration of uranium C_{DGT}**
		Average	±	Average	±		
0	24/08/2011			0.87	0.02		
1	31/08/2011	0.25	0.04	0.99	0.03	0.93	0.27
2	07/09/2011	0.77	0.09	0.91	0.05	0.95	0.80
3	14/09/2011	0.25	0.04	0.11	0.01	0.51	0.48
4	23/09/2011	0.14	0.01	0.27	0.02	0.19	0.72
5	28/09/2011	0.26	0.02	0.24	0.01	0.25	1.02
6	05/10/2011	0.19	0.08	0.94	0.05	0.59	0.32
7	12/10/2011	0.68	0.17	0.22	0.00	0.58	1.16
8	19/10/2011	0.32	0.06	0.26	0.00	0.24	1.34
9	24/10/2011	0.21	0.02	0.36	0.01	0.31	0.69
10	02/11/2011	0.11	0.01	0.18	0.01	0.27	0.40
11	09/11/2011	0.15	0.02	0.33	0.04	0.25	0.59
12	16/11/2011	0.10	0.02	0.27	0.04	0.30	0.32
13	23/11/2011	0.22	0.04	0.25	0.01	0.26	0.86
14	30/11/2011	0.13	0.01	0.21	0.00	0.23	0.58
15	07/12/2011	0.11	0.04	0.16	0.01	0.18	0.59
16	14/12/2011	0.29	0.02	0.26	0.02	0.21	1.38
17	21/12/2011	0.30	0.04	0.17	0.00	0.22	1.37
18	28/12/2011	0.14	0.02	0.12	0.01	0.15	0.94
19	05/01/2012	0.12	0.02	0.20	0.02	0.16	0.72
20	11/01/2012	0.16	0.02	0.19	0.01	0.20	0.79
21	18/01/2012	0.16	0.01	0.19	0.01	0.19	0.85

Chapter 6: Evaluation of DGT using a Diphonix® resin for monitoring dissolved uranium in natural waters

6.1 Introduction

Many pollutants enter the aquatic environment, but most are of anthropogenic origin. Monitoring these pollutants is necessary to maintain and protect water quality and this is mandated within environmental legislation e.g. the European Union's Water Framework Directive (WFD, 2000/60/EC). These activities include monitoring the discharge of radionuclides. Due to both their chemical and radiological properties, radionuclides are highly toxic [1]. Most of the substances enter the aquatic environment through discharges associated with the generation of nuclear power as well from contaminated waste products [2]. The monitoring of radionuclides in the aquatic environment usually relies on the collection of grab (bottle or spot) samples of water with subsequent analysis in the laboratory. This is can be time consuming and costly and often episodic fluctuations in the concentration of a pollutant can be missed. A number of alternative monitoring strategies have been proposed, including the use of passive sampling devices [3]. Several designs of passive sampler exist for different classes (e.g. non-polar and polar organics, organo-metallics and metals) of chemicals and these have been reviewed [3-5]. For monitoring inorganic substances, metals and radionuclides the diffusive gradients in thin films (DGT) sampler has been used extensively [6-9]. The device consists of a binding layer, which contains a specific resin with functional groups selective to the target ions; a layer of hydrogel of known thickness, which serves as the diffusive layer; and a protective outer membrane with a known pore size. DGT measures the labile, dissolved fraction of analytes [10] and pre-concentrates the analyte(s) *in situ* which reduces the risk of introducing contamination and chemical transformation of the sample [3].

Several workers have used DGT with different resin sorbents (copper ferrocyanide [11] and ammonium molybdophosphate [8] for ^{133}Cs, ^{134}Cs and ^{137}Cs; TEVA® resin for ^{99}Tc [12]; MnO_2 for Ra [13, 14]) to measure radionuclides in natural waters. For the measurement of total U, DGT sorbent phases include Chelex-100 [9, 15-17], Whatman DE 81 [15], Metsorb™ (TiO_2) [9, 18], Dowex resin [19].

To date an actinide specific resin has not been used in the DGT to monitor environmentally relevant actinides. The uptake of uranium (U) was assessed in this Chapter using a DGT containing a Diphonix® chelating ion exchange resin. This sorbent is available commercially from TrisKem (TrisKem International, Bruz, France) and has a strong affinity for tetra- and hexa-valent actinides [20]. The Diphonix resin is

comprised of a polymeric support containing geminally substituted diphosphonic acid groups and strongly hydrophilic sulfonic groups on a polymer backbone [21] (Figure 6.1 below). The presence of two functional groups means the resin is a dual-mechanism polymer and can be characterised as a chelating ion exchange resin [20]. The sulfonic acid cation exchange group allows for the rapid access of non-specific ions into the polymeric network, while the diphosphonic acid group is selective for a number of metal cations [21]. Diphosphonic acid is strongly acidic and chelates the U through either ionized or neutral diphosphonic acid ligands due to the coordination properties of the P=O groups [21]. The Diphonix® resin has been fully characterised by Chiariza *et al.* [22-30].

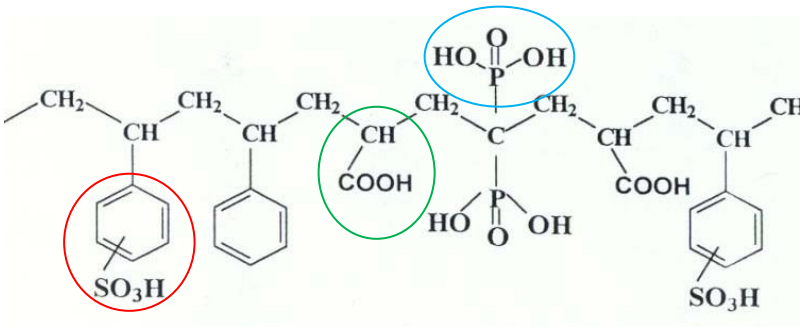

Figure 6.1 Stucture of Diphonix® resin showing the hydrophilic sulfonic functional groups (highlighted in red), the phosphonic acid groups (highlighted in blue) and carboxylic acid (highlighted in green) all of which are active in binding metal ions from solution (from TrisKem International Diphonix® fact sheet, http://www.triskem-international.com/iso_album/ft_resine_diphonix_en.pdf).

Diphonix® resin is a candidate resin for the measurement of U in natural waters in conjunction with DGT due to its high affinity for the actinides in weakly (< 0.1 M) acidic environments [21]. Figure 6.2 below shows the retention of the actinides americium, plutonium, uranium, thorium and neptunium with increasing acid concentrations. The retention is shown as a dry weight distribution ratio (D, mg L^{-1}), which is the ratio between the metal concentrations in the resin phase and in the solution in equilibrium with the resin, as shown in equation 6.1 below [25].

$$D = \left(\frac{A_o - A_f}{W}\right) / \left(\frac{A_f}{V}\right) \qquad \text{Equation 6.1}$$

where A_o and A_f are the aqueous phase activities (counts per minute) before and after equilibration, respectively; W is the dry weight if the resin (g) and V is the volume of the aqueous phase (mL).

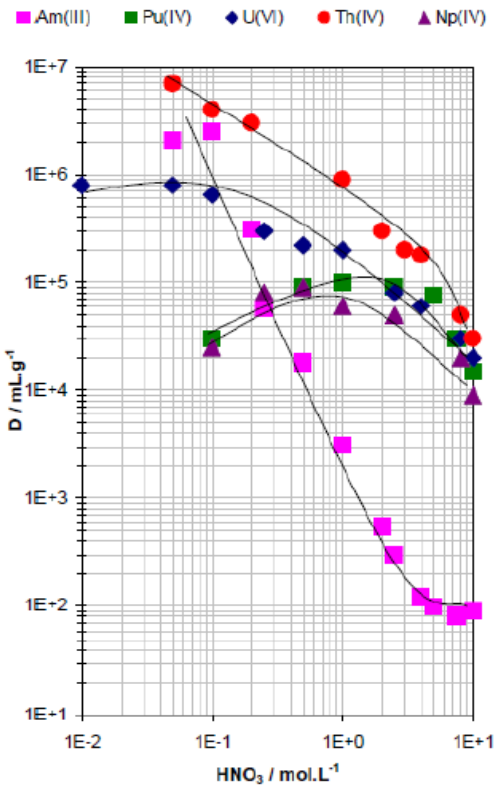

Figure 6.2 Acid dependency of retention of the actinides americium (Am), plutonium (Pu), uranium (U), thorium (Th) and neptunium (Np) on the Diphonix® resin, where D is the dry weight distribution ratio of the metal concentrations in the resin phase and the in the solution in equilibrium with the resin. From Chiarizia *et al.* [21].

In weakly acidic environments (HNO_3 < 0.1 M), it can be seen from Figure 6.2 that the distribution ratio for U is approximately 1 x 10^6 mL g^{-1}. Americium and thorium have higher distribution ratios of approximately 2 x 10^6 and 7 x 10^6 mL g^{-1} respectively. Plutonium and neptunium distribution ratios are lower at approximately 2 x 10^4 mL g^{-1}. These high distribution ratios across a range of actinides demonstrate the potential to extend the use of the Diphonix® resin to measure other actinides.

However, the complexation power of the Diphonix resin also extends to other metal cations, such as calcium (Ca^{2+}) aluminium (Al^{3+}) and iron (Fe^{2+}), the uptake of which may inhibit U uptake if they occur in higher concentrations than U [21]. The retention of some commonly occurring cations in natural waters can be seen in Figure 6.3 below.

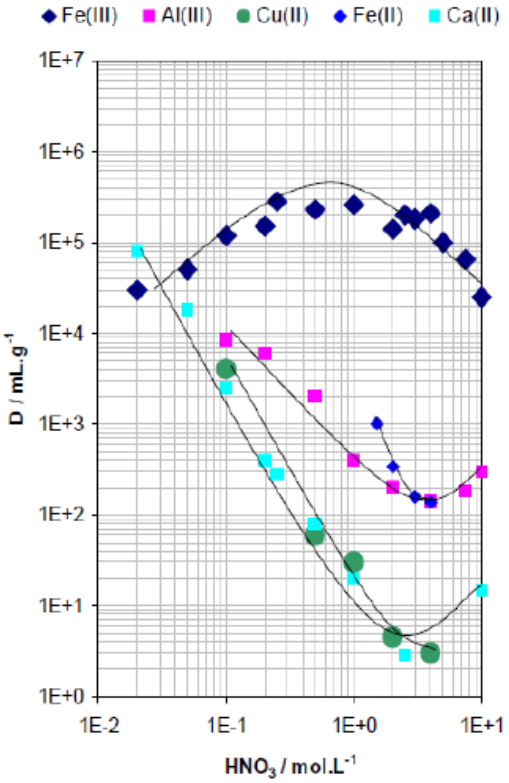

Figure 6.3 Acid dependency of retention of the commonly occurring cations iron (Fe^{2+} and Fe^{3+}), aluminium (Al^{3+}), copper (Cu^{2+}) and calcium (Ca^{2+}) on the Diphonix® resin, where D is the dry weight distribution ratio of the metal concentrations in the resin phase and the in the solution in equilibrium with the resin. From Chiarizia *et al.* [21].

Diphonix® resin has been used in previous studies to remove U from groundwater. Phillips *et al.* [31] showed that U could be successfully removed using Diphonix® from solutions with a pH > 5, and was also shown to be less sensitive to interferences by carbonates and nitrates, sulphates, iron, calcium and sodium than the Chelex-100 resin (investigated in Chapter 4).

As a consequence of the potential of other ions in solution to interfere with the uptake of U, the performance of the resin in the presence of complexing agents was evaluated [32]. As Diphonix® has a high affinity for common environmental interferences such as Ca^{2+} [21, 31], the uptake of uranium-calcium complexes and the competition of Ca^{2+} with UO_2^{2+} uptake was assessed. Carbonate interferences were assessed as the resin is a cation-exchanger and the uranium-carbonate complexes are neutral to anionic ($UO_2(CO_3)_2^{2-}$, $UO_2(CO_3)_3^{4}$) and so may not accumulate on the resin. The measurement of the accumulation of U over time in both artificial sea-water and low-ionic strength water was undertaken. In this study DGT sampler containing the Diphonix® resin were deployed in two aquatic environments, calcium carbonate-rich river water and in a marine harbour, and retrieved periodically over 10-days.

6.2 **Experimental**

Chemicals were of analytical grade or better and supplied by Fisher Scientific Ltd. (Loughborough, UK), unless otherwise specified. Milli-Q (ultra-pure) water (> 18.2 MΩ cm, Millipore, Watford, UK) was used as the laboratory water. All U ICP-MS standards and experimental working solutions were prepared in low density polyethylene (LDPE) or polystyrene (PS) containers with polypropylene lids (PP) from a 1000 mg L^{-1} in 2% HNO_3 (Spex Certiprep, Fisher Scientific Ltd.) U stock solution unless otherwise stated. The ICP-MS internal standard was prepared from a 1000 mg L^{-1} in 2% HNO_3 (Spex Certiprep) bismuth stock solution. These solutions were adjusted to a given pH by addition of either 1 M HNO_3 or 1 M NaOH, and to a given ionic strength by addition of $NaNO_3$, with the pH monitored throughout experiments. Solutions were equilibrated with atmospheric CO_2 for 24 h before use unless otherwise specified. All readings were undertaken in triplicate with containers open to the atmosphere to ensure continuing equilibration with the atmospheric pCO_2 (i.e. to ensure a constant inorganic carbon concentration throughout the experiments). All plastic apparatus was soaked for 24 h in 10% HNO_3 and rinsed three times in Milli-Q water prior to use.

6.2.1 Preparation of DGT devices

Polyacrylamide (PAM) diffusive gels (thickness 0.4, 0.8, 1.2 and 1.6 mm) were prepared according to Zhang and Davison [33] and described in Chapter 3, Section 3.1.1.. The gels contained 15% v/v acrylamide solution (Acros Organics, ThermoFisher, Loughborough, UK) and 0.3% v/v of patented agarose cross-linker (DGT Research Ltd., Lancaster, UK). *N,N,N',N'*-tetramethylenediamine (TEMED, Acros Organics) was used as the catalyst and a freshly prepared solution of 10% ammonium persulfate (Acros Organics) was used as the initiator for polymerisation. The diffusive gels were stored in either 0.01 M $NaNO_3$ or 0.4 M NaCl prior to either fresh water or sea water deployments, respectively.

The 0.4 mm thick PAM binding gels were prepared with Diphonix® resin supplied by TrisKem International (Bruz, France) in 10 mL gel solution prior to polymerisation, according to [33]. The Diphonix® resin is supplied with a high moisture content and therefore requires drying prior to fixation in the acrylamide.

DGT device mouldings were obtained from DGT Research Ltd. and washed for 24 h in 10% HNO_3, and then rinsed three times in Milli-Q water prior to use. The devices were assembled according to [10] and stored at 4°C in zip lock plastic bags,

containing 1-2 mL of water (matrix matched to deployment site) to ensure the diffusion properties of the gels were not altered, and to prevent the gels drying out. A disk of (0.2 µm pore size) Supor polyethylene sulfone (Pall Corporation, Portsmouth, UK) was used as the outer membrane.

6.2.2 Analysis of DGT devices

After exposure, the Diphonix® binding gel was removed from the DGT devices and eluted (48 h) with 1 M H_2O_2/1 M NaOH (2 mL) solution (100 mL made by combining 90 mL 1.1 M NaOH and 10 mL H_2O_2). After the marine deployments, the binding gels were first washed (5 mL) in Milli-Q water for 1 h to remove excess salts [34]. The eluents were then diluted 20 fold with Milli-Q water prior to instrumental analysis due to interference from the total dissolved solids, which are required to be < 2%. U was determined in all solutions by ICP-MS using an Agilent 7500ce series instrument (Agilent Technologies Inc., Japan). Total U was measured under normal plasma conditions in 'no gas mode', with the sample introduction system fitted with a micromist nebuliser. The instrument blank for U was 1 ng L^{-1} while the limit of detection (calculated by the Agilent Chemstation software) for U was 1 ng L^{-1}, with a measurement relative standard deviation better than 7%. Laboratory blanks were undertaken in triplicate for each experiment and the average concentration per disk was determined for the Diphonix® gel disks as 0.79 ± 0.08 ng and 0.5 ± 0.18 ng for ^{238}U and ^{235}U respectively. Bismuth (*m/z* = 209; 25 µg L^{-1}) was used as an internal standard to compensate for any potential instrument drift. The certified reference materials SLRS-5 and NASS-4 (National Research Council Canada, Canada) were analysed directly for SLRS-5 and after a 20-fold dilution for NASS-4 and were found to be within 1% of the stated values.

$^{235/238}U$ isotopic ratios were measured using an Agilent microflow (100 µL min^{-1}) PTFE self aspirating nebuliser, to eliminate any signal pulses caused by the peristaltic pump using the micromist concentric nebuliser. Isotopic ratios were determined with 3% standard deviation as low as 0.1 µg L^{-1} total U (0.000725 µg L^{-1} ^{235}U). The certified reference material U005a (New Brunswick Laboratories, DoE, Washington, USA) was analysed and was found to be within 99.5% of the isotopic value (0.00509 $^{235/238}U$).

6.2.3 Calculation of time-weighted average concentrations of uranium

The concentration of U measured by the ICP-MS in µg L^{-1} from the eluent was multiplied by the dilution factor (× 10) to give the U concentration (*Ce*). The absolute mass (*M*) of the U in the resin gel was then calculated using equation 6.2, where *M* is

calculated taking into account the gel volume (*Vg*, cm^3), the eluent volume (*Ve*, mL), the measured concentration of U in the eluent (*Ce*, ng mL^{-1}) and the elution factor (*fe*) [33].

$$M = \frac{Ce(Vg+Ve)}{fe} \qquad \text{Equation 6.2}$$

M from equation 6.2 is then used to calculated the TWA concentrations (equation 6.3) where the concentration (C_{DGT}, ng mL^{-1}) was calculated using the mass of the analyte in the binding gel (*M*, ng), the thickness of the diffusive path length (diffusive gel and filter membrane) (*Δg*, cm), the diffusion coefficient of the analyte (*D*, cm^2 s^{-1}) (as determined at different pHs for U by [9]), deployment time (*t*, s) and the area of the sample exposure window (*A*, cm^2).

$$C_{DGT} = \frac{M\Delta g}{DtA} \qquad \text{Equation 6.3}$$

The diffusion coefficients (*D*) were corrected for temperature (*T*, ^oC) using the Stokes-Einstein equation (equation 6.4) [35] and the viscosity of water (*η*, mPa s) [36]. Diffusion coefficients used for sea water were 10% lower than fresh water [10], due to increased viscosity of higher ionic strength solutions.

$$\frac{D_1\eta_1}{T_1} = \frac{D_2\eta_2}{T_2} \qquad \text{Equation 6.4}$$

The diffusion coefficients of uranyl carbonate ions in the diffusive gel and the water have been detailed in Chapter 3, section 3.1.1 and should be considered when calculating field DBLs and TWAs.

The diffusive boundary layer (δ) thickness was calculated using equation 6.5 after Warnken *et al.* [37] . A straight line plot of *1/M* vs *Δg* has a slope (*m*) of $1/(DC_{DGT}At)$ and an intercept (*b*) of $\delta/(DC_{DGT}At)$. The intercept (*b*) divided by the slope (*m*) of this plot gives the diffusive boundary layer thickness *δ*, also accounting for the discrepancies in diffusion coefficients of uranyl in the gel and water as described in Chapter 3, section 3.1.1, and as per equation 6.6.

$$\frac{1}{M} = \frac{\Delta g}{DC_{DGT}At} + \frac{\delta}{DC_{DGT}At} \qquad \text{Equation 6.5}$$

$$\delta = \frac{b}{m}\left(\frac{D_M^W}{D_M^{gel}}\right) \qquad \text{Equation 6.6}$$

The thickness of the DBL was included in the C_{DGT} calculations for the field trials using equation 6.7. The effective sampling area (A_e) was 3.8 cm^2 instead of the 3.14 cm^2 used in the laboratory trials, as described by Warnken *et al.* [37].

Equation 6.7 was used where the DBL had to be accounted for in the calculations as described in Chapter 3, section 3.1.1. The predominant uranyl species in the freshwater site ($Ca_2UO_2(CO_3)_3$) had a similar diffusion coefficient in water [38] as the diffusive gel (so$D_M^W : D_M^{gel} = 1$) and was therefore not accounted for here, meaning equation 6.3 could be used for the C_{DGT} calculations. The predominant uranyl species in seawater is $UO_2(CO_3)_2^{2-}$ which has a higher diffusion coefficient in water ($D_M^W : D_M^{gel} = 1.18$) [38] and was therefore accounted for in the C_{DGT} calculations using equation 6.7.

$$C_{DGT} = \frac{M(D_M^W \Delta g + D_M^{gel} \delta)}{t D_M^W D_M^{gel} A_e} \qquad \text{Equation 6.7}$$

6.2.4 Performance of Diphonix® resin

6.2.4.1 Uptake and elution efficiencies of U

The uptake efficiencies of the resin gel for U were determined using a batch method. Disks (0.19 cm^3) of the resin gel were placed in Fisher brand polystyrene (PS) vials (30 mL) and a solution (10 mL, 0.01 M $NaNO_3$ at pH 7 ± 0.2) containing 100 µg L^{-1} of U(VI) added for the uptake and elution efficiencies. The vials were shaken (48 h) on a rotating table (IKA® KS 130 Basil, Sigma-Aldrich Ltd., Gillingham, UK) at a set speed of 240 revolutions min^{-1}. Aliquots (1 mL) were taken and acidified (using 20 µL, 6 M HCl) before and after resin gel exposure to determine the mass balance and percentage uptake of U (as described in Chapter 3, Section 3.1.1). To determine the elution efficiencies (the quantity of U eluted from the resin as a ratio of the U taken up by the resin, as described in Chapter 3, Section 3.1.1), the resin gels were removed from the solutions and placed into new PS vials containing a trial eluent (shown in Table 6.1). The tubes were then agitated (48 h) on the rotating table and the resin gel removed. The eluents trialled using the method detailed above are shown in Table 6.1 below. Control experiments containing 10 mL of 100 µg L^{-1} of U, 0.01 M $NaNO_3$ at pH 7 ± 0.2 with no resin gels showed no sorption of U to the vessel.

Table 6.1 Eluents trialled to extract U complexed onto the Diphonix® resin. Eluent strength and volumes are also listed. The elution trials used 30 mL polystyrene tubes which were shaken with the resin gel (48 h) on a rotating table (IKA® KS 130 Basil, Sigma-Aldrich Ltd., Gillingham, UK) at a set speed of 240 revolutions min^{-1}.

Eluent	**Volume (mL)**
1M NaOH + 1M H_2O_2*	2
0.5 M NaOH + 1M H_2O_2**	2
0.2 M Na_4EDTA	10
0.2 M citric acid	1
8M HNO_3	2
1M HNO3 + 1M H_2O_2***	2

*100 mL made by combining 90 mL 1 M NaOH and 10 mL H_2O_2
**100 mL made by combining 90 mL 0.5 M NaOH and 10 mL H_2O_2
***100 mL made by combining 90 mL 1.1 M HNO3 and 10 mL H2O2

Two further elution trials were undertaken to achieve complete decomposition of the resin matrix in order to extract the U. The resin-gels were prepared and exposed to U as described above for the solution based eluents.

The first was microwave digestion (as per the study by [39] where concentrated nitric acid was used with microwave digestion) where reverse aqua regia (which is a 3:1 mixture of nitric acid (3 parts) and hydrochloric acid (1 part)) subject to microwaves at a frequency of 2.45 GHz and a temperature of 220^oC for a period of 35 minutes, was used to decompose the resin in order to extract the U.

The second digestion technique is a lithium metaborate fusion described by Croudace *et al*. [40]. Here the resin gels were heated in a 9 mL graphite crucible (SCP Science, Courtaboeuf, France) with 2 g lithium metaborate flux at 1100^oC for 15 minutes. The clear flux was then poured directly into 5 mL 8M HNO_3 and vigorously stirred until dissolved. The dissolved flux was then diluted 20 times (due to high lithium salt content) prior to analysis using ICP-MS.

6.2.4.2 Effect of pH and ionic strength on uptake of uranium

A batch method was used as per section 6.2.4.1. A 0.19 cm^3 disk of each resin gel was placed in a PS vial (30 mL) and exposed to solutions (20 mL) containing 100 µg L^{-1} of U (VI) in 0.01 M $NaNO_3$ at pH 4, 5, 6, 7, 8 and 9 (to test the effect of pH) or 100 µg L^{-1} of U (VI) in 0.01, 0.05, 0.1, 0.4, 0.7 and 1 M $NaNO_3$ at pH 7 (to test the effect of ionic strength). The vials were shaken (48 h) on a rotating table. One mL aliquots of the solution were taken and acidified (using 20 µL 6 M HCl) before and after resin gel exposure to determine the mass balance and percentage uptake of the U. Solutions were made up in the PS vials in triplicate for each pH value tested here with no addition of resin gels, to assess the sorption of U to the PS vials.

6.2.4.3 Effect of interferences and ligands on uptake of uranium

Effect of the presence of calcium (Ca^{2+}) and bicarbonate (HCO_3^-), as a potential interferences to U uptake by the Diphonix-DGT were tested. Table 6.2 details the concentrations used, which exceed typical environmental concentrations to ensure any effect from an episodic event (e.g. heavy rain, or flooding) can be seen. The high HCO_3^- concentrations are double those seen in some fluvial systems [41] but similar to that found in sea water, with Ca^{2+} five times that found in the field riverine (River Lambourn) test site and approximately that found in sea water. An acid washed PP container (3 L) containing a 0.01 M $NaNO_3$, 100 µg L^{-1} U solution (3 L) plus either Ca^{2+} or HCO_3^- was equilibrated for 24 h at pH 7.0 ± 0.4 for the Ca^{2+}, additions, and pH 7.8 ± 0.2 for the HCO_3^- additions. DGT devices were then deployed (24 h) in triplicate, then removed and eluted as per section 6.2.4.1. Two aliquots (1 mL) of the solution were taken daily from the exposure tank. One was filtered though a 0.2 µm filter and acidified (20 µL, 6 M HCl), the other was acidified (20 µL, 6 M HCl) to measure the concentration of U. Equation 6.4 was used to calculate the C_{DGT}, and this was compared to U concentrations in the grab water samples.

Table 6.2 Salt and concentration of ligands tested in this study.

Ligand (salt used)	**Salt concentrations tested in this study**		
Ca^{2+} ($CaCl_2.2H_2O$)	500 mg L^{-1}	250 mg L^{-1}	100 mg L^{-1}
HCO_3^- ($NaHCO_3$)	500 mg L^{-1}	250 mg L^{-1}	100 mg L^{-1}

6.2.4.4 Mass accumulation of uranium over time

To measure the uptake of U over time, DGT devices were exposed (5 days) in square polypropylene tanks (5 L) to 0.01 M $NaNO_3$ (low ionic strength water) plus 0.983 mM $NaHCO_3^-$ to buffer the solution to pH 7.7 (a similar pH to the freshwater field test site) or an artificial sea water solution (prepared following [42]) containing 100 µg L^{-1} U. Devices were removed in triplicate at the time intervals of 4, 8, 24, 48, 72, 96 and 120 h, and the resin gels eluted as per section 6.2.2. Two aliquots (1 mL) of the solution were taken daily from the exposure tank. One was filtered though a 0.2 µm filter and acidified (20 µL, 6 M HCl), the other was acidified (20 µL, 6 M HCl) with no filtration to ensure no precipitates were formed in the solution that may affect DGT uptake.

6.2.4.5 Field deployments

Two field sites (fresh water and marine) were used. The fresh water site (51.446933 N, -1.3838275 W) was located on the River Lambourn near Boxford, Berkshire, UK. The river has a Chalk fed aquifer catchment and an average pH of 7.8-8 [43]. DGT devices were deployed between Perspex plates (15 x 7 cm, 8 devices per plate) and attached to a rope and float and weighted to the river bed. The marine site was located adjacent to the National Oceanography Centre, Southampton, UK (50.891313 N, -1.3938260 W). This is a well mixed estuary with a salinity of 29 to 33 (dependent upon tidal fluctuations and fresh water inputs). The deployment site is located by an enclosed pontoon, and is therefore a low flow site with only the tidal fluctuations agitating the water. Devices were deployed as above 1 m below the water surface. Ropes were used to attach the exposure plate to the dock pontoon.

Three DGT devices containing the Diphonex® resin gel were removed on days 1, 2, 3, 5, 7 and 10 of the trial. To assess the influence of the diffusive boundary layer, DGTs containing the resin gel were deployed for 3 days with diffusive layer PAM gel thicknesses (including 0.015 cm to account for the Supor filter membrane) of 0.015, 0.055, 0.095 and 0.135 cm as per Warnken *et al.* [37]. Diffusion coefficients from Hutchins *et al.* [9] were used to calculate the time weighted average (TWA) concentrations of U over the different deployments. Grab samples of water (20 mL) collected each time a DGT device was retrieved, and were filtered (0.2 µm pore size Supor filter membranes) and acidified *in situ* with 6 M HCl (40 µL). Water temperature and pH were recorded each time a device was removed so that diffusion coefficients could be corrected for variations in environmental conditions. Triplicate procedural DGT blanks were exposed to the field environment during deployment and retrieval of the samplers. Blanks were eluted and analysed with the samples as above.

6.3 **Results and discussion**

6.3.1 Uptake and elution efficiencies and the effect of pH and ionic strength

Uptake and elution efficiencies were measured by exposing the Diphonix® gels to a known mass of U and then eluting the bound element. Uptake was 100% for U by Diphonix®, which has a very high affinity for the tetra- and hexavalent actinides even in acidic environments with reported distribution ratios (D) of ~ 20 000 for 10 M HNO_3, 500 for 4 M HF and 700 for 4 M H_2SO_4 [21]. This made extraction of U difficult to achieve using conventional acidic extractants. Elution techniques presented by other workers were trialled, such as a lithium metaborate fusion described by Croudace *et al*.

[40]. This technique has successfully extracted U and plutonium from an Actinide™ resin with a higher partition coefficient for the actinides than Diphonix®. However, due to the very small quantity of resin used in each resin gel layer, the recoveries here were very low (< 1%). Microwave digestion of the resins in reverse aqua regia was also trialled but the PAM gels evolved large volumes of gas on decomposition for this technique to be taken forward safely. Various eluents and techniques were trialled, the results of which are presented Table 6.3 below including an ethylenediaminetetraacetic acid (EDTA) eluent described by Maxwell *et al.* [44] for the extraction of beryllium from Diphonx®, citric acid (on the recommendation of Triskem), nitric acid (a commonly used eluent for DGT) and sodium hydroxide (successfully used to extract U from a titanium dioxide based resin [9]).

Table 6.3 Elution efficiency of the eluents trialled to extract U complexed onto the Diphonix® resin. Eluent strength and volumes are also listed. The elution trials used 30 mL polystyrene tubes which were shaken with the resin gel (48 h) on a rotating table (IKA® KS 130 Basil, Sigma-Aldrich Ltd., Gillingham, UK) at a set speed of 240 revolutions min^{-1}. The standard deviation is based on triplicate experiments.

Eluent	**Volume (mL)**	**Elution Efficiency (%)**	**Standard deviation**
1M NaOH + 1M H_2O_2	2	90	4.4
0.5 M NaOH + 1M H_2O_2	2	77	19.4
0.2 M Na_4EDTA	10	2.5	5.6
0.2 M citric acid	1	0.1	0.05
8M HNO_3	2	1.78	0.4
1M HNO3 + 1M H_2O_2	2	0.05	0.005

The eluent 1M NaOH / 1M H_2O_2 (2mL volume) was taken forward to elute the U from the Diphonix® resin-gels, as the recovery was the highest (at 90%). The major drawback to this eluent is the necessity for dilution to ensure that the total dissolved salt (TDS) content is < 2% for the ICP-MS analysis, to avoid signal suppression by the Na^+ ions. Another reason is to ensure that there is no corrosion to the glass introduction system and torch in the ICP-MS. The 20 fold dilution necessary for the NaOH could be avoided through the addition of a clean-up step to eliminate the sodium ions and convert to a mildly acidic solution, such as that described by Zheng & Yamada [45], where an AG 1x8 anion exchange resin was used to pre-concentrate the U followed by a 0.1 M HCl elution (which could then be directly analyed using ICP-MS). Sample clean-up is an area for further research.

There are a number of reasons the NaOH may have eluted the U from Diphonix®. Firstly, the NaOH could have been effective because at pH 14 the affinity of

U for the –OH groups in the resin and the formation constant of $UO_2(OH)_4^{-2}$ is higher than phosphorus containing ligands (such as the phosphonic acid functional groups in the Diphonix® resin). Similar elution efficiencies (95.2 ± 0.4%) for U using 1 M NaOH/1 M H_2O_2 with a TiO_2-based resin were found by [9]. Chiarizia *et al.* [25] describe the removal of chromium from Diphonix® using 0.33 M H_2O_2 in 1 M NaOH, which alters the oxidation state due to the sodium peroxide formed by the H_2O_2 NaOH mixture being strongly oxidizing. It can be seen from Figure 6.4 that the 0.33 M H_2O_2 in 1 M NaOH solution rapid removes the chromium from the Diphonix® at room temperature. It is possible that the stripping mechanism for U is similar to that displayed here for chromium.

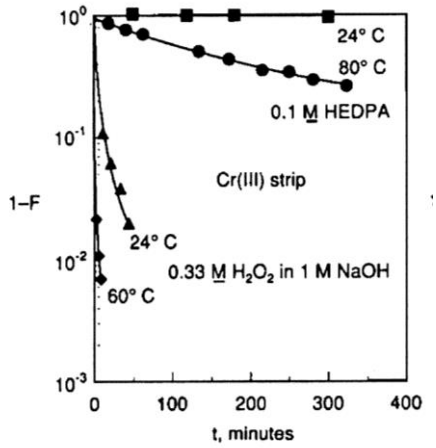

Figure 6.4 Kinetics of metal stripping from Diphonix® resin, where 1-F is the fractional attainment of equilibrium ($\ln(1\text{-}F) = -(k_f + k_r)t = -kt$ where k (s^{-1}) is the rate constant; k_f and k_r are the forward and reverse constants between the free metal and resin phase metal, and t is time (s)) From Chiarizia *et al.* [25].

Another reason the 1 M NaOH/ 1 M H_2O_2 solution may work so effectively at stripping the U from the Diphonix® resin, is that Diphonix® has 4 protonation constants (the pK_a for each proton that can be accepted per phosphonic acid group in the resin) which are $pK_1 = 1.5$; $pK_2 = 2.5$, $pK_3 = 7.2$ and $pK_4 = 10.5$ [24]. This means that the pK_1 and pK_2 protons are weakly bound and are easily dissociated (as the lower the pK_a the greater the magnitude of dissociation) and pK_3 and pK_4 protons are strongly bound and would require the addition of a strongly alkaline agent to entirely deprotonate the resin. As the Diphonix® is in the H^+ form, the U is coordinated to the P=O group as UO_2^{2+}. In this form the U acts as a hard Lewis acid and requires a strong alkali solution (such as sodium hydroxide) to fully dissociate from the resin.

NaOH solutions are not normally used in the radiochemical extraction and separation of actinides due to the precipitates formed by the tri- and tetra-valent actinides. Alternative elution schemes for use with Diphonix® resin include a

diphosphonic acid or HEDPA (1-hydroxyethylidene-1,1-diphosphonic acid) based eluent with oxidation using Fenton's reagent, followed by radiochemical separation using TRU (TRansUranium) resin (available from TrisKem) [46]. This scheme extracts very tightly bound actinides and separates them thus avoiding isobaric or spectral interferences during the analysis phase. This technique cannot be used without further purification steps with ICP-MS as phosphoric acid is highly corrosive to the nickel sampling and skimmer cones and the lens stack.

There was consistent uptake (100%) of U across all pH and ionic strengths tested (Figures 6.5 and 6.6) and was in agreement with previous studies showing phosphoric acid ligands take up U over a wide pH range [22].

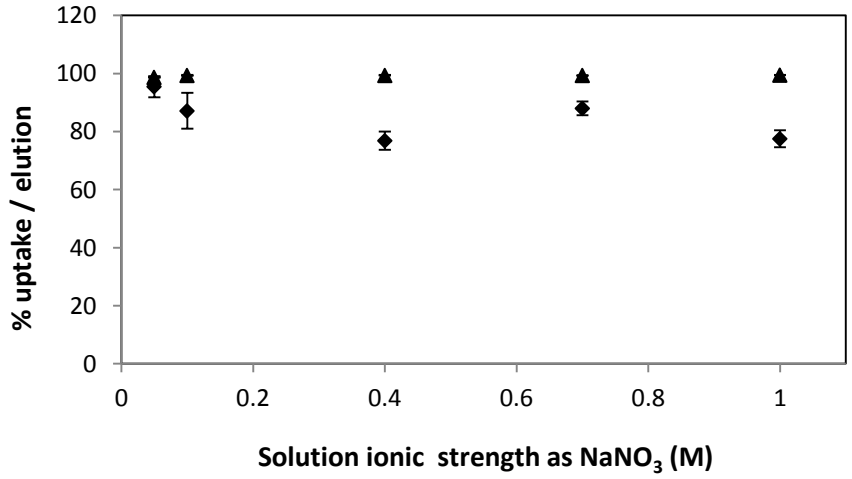

Figure 6.5. Uptake and elution efficiency of Diphonix® resin gel for U across a range of ionic strengths. Where ▲ are the uptake efficiencies and ◆ are the elution efficiencies for U. Uptake conditions were pH 7, 20 mL, 100 µg L^{-1} U. Error bars are the standard error of triplicate measurements.

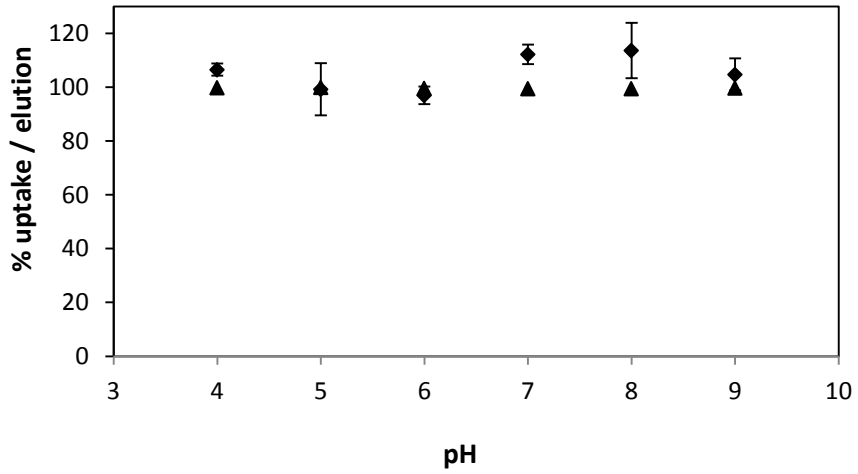

Figure 6.6. Uptake and elution efficiency of Diphonix® resin gel for U across a range pHs. Where ▲ are the uptake efficiencies and ◆ are the elution efficiencies for U. Uptake conditions were 0.01 M $NaNO_3$, 20 mL of 100 µg L^{-1} uranium. Error bars are the standard error of triplicate measurements.

6.3.2 Effect of interferences and ligands on uptake of uranium

Speciation distributions for each ligand tested were calculated using Visual Minteq, version 3, beta (© 2010 KTH, Department of Land and Water Resources Engineering, Stockholm, Sweden). This was undertaken in order to support the experimental work outlined in section 6.2.4.3. The DGT concentration of the solution over the deployment period in each tank was calculated using equation 6.3, and compared as a ratio to the concentration measured directly by grab samples. A ratio of 1:1 shows that the technique is working correctly and is unaffected by the ligand. All inorganic U complexes formed were initially assumed to be fully labile in this study.

Ca^{2+} ions formed complexes with UO_2^{2+} in the presence of atmospheric carbon dioxide at pH > 6.5. Calcium forms soluble $CaUO_2(CO_3)_3^{2-}$ and $Ca_2UO_2(CO_3)_3$ complexes [47, 48] (Figure 6.7b). Increasing the concentration of calcium in the exposure tanks did not affect the uptake of U by the Diphonix® resin (Figure 6.7a). The resin was either capable of dissociating and out-competing the anionic species or took up the U-Ca complexes directly.

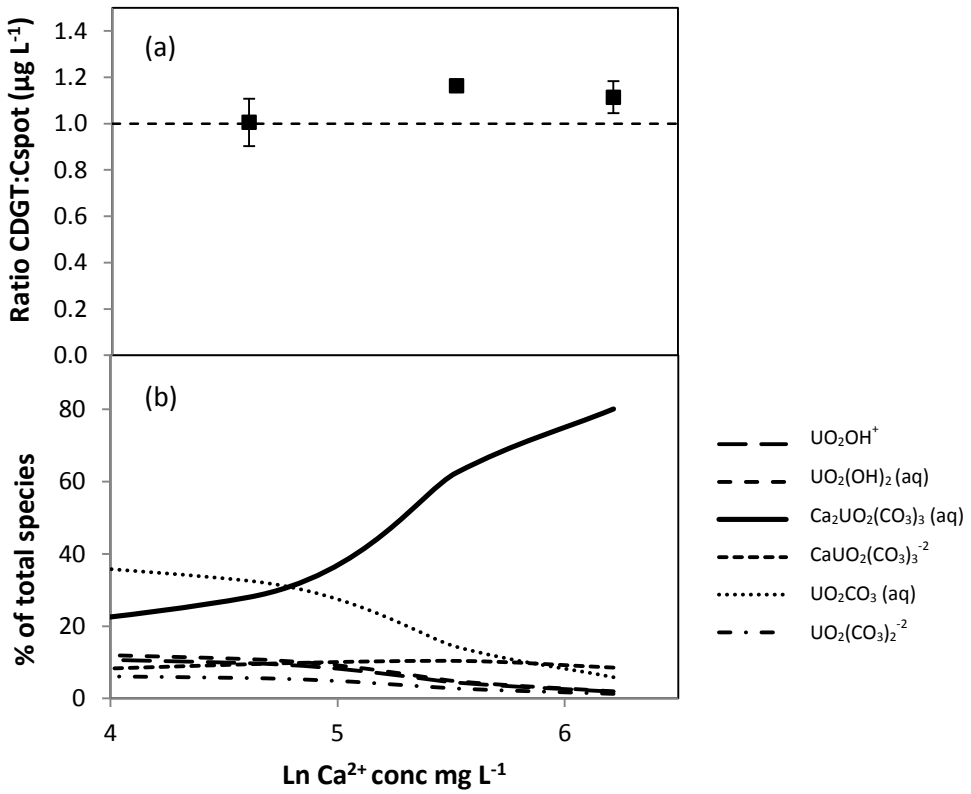

Figure 6.7 (a) Effect of Ca^{2+} on uptake of uU by the Diphonix® resin gel. Concentration of U in DGT (C_{DGT}) is shown as a ratio to the average concentration of the total U over the 24 h deployment period measured directly in the solution (C_{total}) across a range of Ca^{2+} concentrations from 100 mg L^{-1} to 500 mg L^{-1}; average pH 6.5 ± 0.2, average temperature 20°C, calculated diffusion coefficient 2.47 x 10^{-6} cm^2 s^{-1}. Dissolved and total U measurements were in close agreement, within error, with 100% of the U was predicted to be in solution using Visual Minteq (version 3 beta). Error bars are the standard error of triplicate readings (b) Prediction for U species calculated using Visual Minteq (version 3 beta) across Ca^{2+} concentrations from 100 mg L^{-1} to 500 mg L^{-1}, with a pH of 6.5, a U(VI) addition of 100µg L^{-1}, calculated ionic strength of 0.01 M, temperature of 20°C an atmospheric partial pressure of dissolved CO_2. Only the major uranyl species are shown.

Carbonate speciation with the uranyl ion accounts for 90–100% of U in the oceans [49]. The complexation of U with carbonate may affect uptake by the DGT devices used in this study. Other studies showed increasing the anionic strength of a solution, by adding HCO_3^-, can severely affect uptake [7]. Both Chelex-100 and Spheron-Oxin® resins showed a decrease in the uptake of U with increasing carbonate concentrations, probably as a result of the increasingly anionic species formed. There was no decrease in the uptake of U observed here (Figure 6.8a) as a result of carbonate complexation, due to the higher affinity of U for phosphonic acid. It is likely that uptake kinetics of U in the presence of strongly anionic ligands will be lower, but the di-phosphonic groups in the Diphonix® resin should dissociate the uranyl anion [22]. Even in the presence of high concentrations of anionic ligands, such as NO_3^-, Diphonix® was still capable of removing U from solution [31].

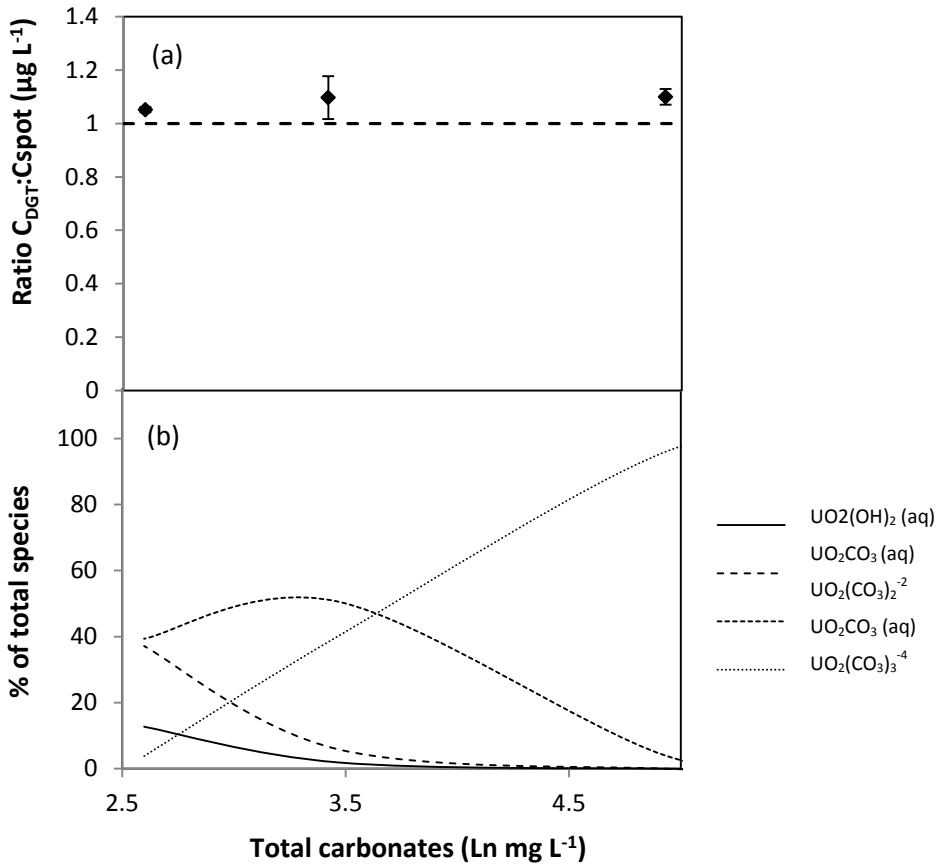

Figure 6.8 (a) Effect of CO_3^- on uptake of U by the Diphonix® resin gel. Concentration of U in DGT (C_{DGT}) is shown as a ratio to the average concentration of the total uranium over the 24 h deployment period measured directly in the solution (C_{total}) across a range of CO_3^- concentrations shown as total carbonate from 100 mg L^{-1} to 500 mg L^{-1}; average pH 7.8 ± 0.5, average temperature 21°C, calculated diffusion coefficient 3.45 x 10^{-6} cm^2 s^{-1}. Dissolved and total U measurements were in close agreement, within error, with 100% of the U predicted to be in solution using Visual Minteq (version 3 beta). Error bars are the standard error of triplicate readings (b) Prediction for U species calculated using Visual Minteq (version 3 beta) across CO_3^- concentrations from 100 mg L^{-1} to 500 mg L^{-1}, with a pH of 7.8, a U(VI) addition of 100µg L^{-1}, calculated ionic strength of 0.01 M, temperature of 21°C an atmospheric partial pressure of dissolved CO_2. Only the major uranyl species are shown.

6.3.3 Accumulation of uranium over time

6.3.3.1 Laboratory tank tests

In low ionic strength test solution the Diphonix® resin accumulated U as predicted equation 6.2 (Figure 6.9a). The predominant species present at pH 7.7 was $UO_2(CO_3)_2^{2-}$ with no precipitates formed. The device did not appear to be capacity limited under the experimental conditions. Using equation 6.3, the observed ratio of the DGT uptake of U/solution concentration of U was 1:1 for the entire deployment period. Deployments in artificial sea water (Figure 6.9b) showed DGTs have a linear uptake of U, but not as predicted by equation 6.3 after 4 h. This is similar to Chelex-100 in this medium [9]. Whilst Diphonix® has the capability to take up U from complex media in

the presence of high concentrations of CO_3^{2-}, uptake kinetics may be compromised by competition by commonly occurring cations such as Mg^{2+} and Ca^{2+}. Cumulatively these may act to reduce effectiveness of the DGT technique.

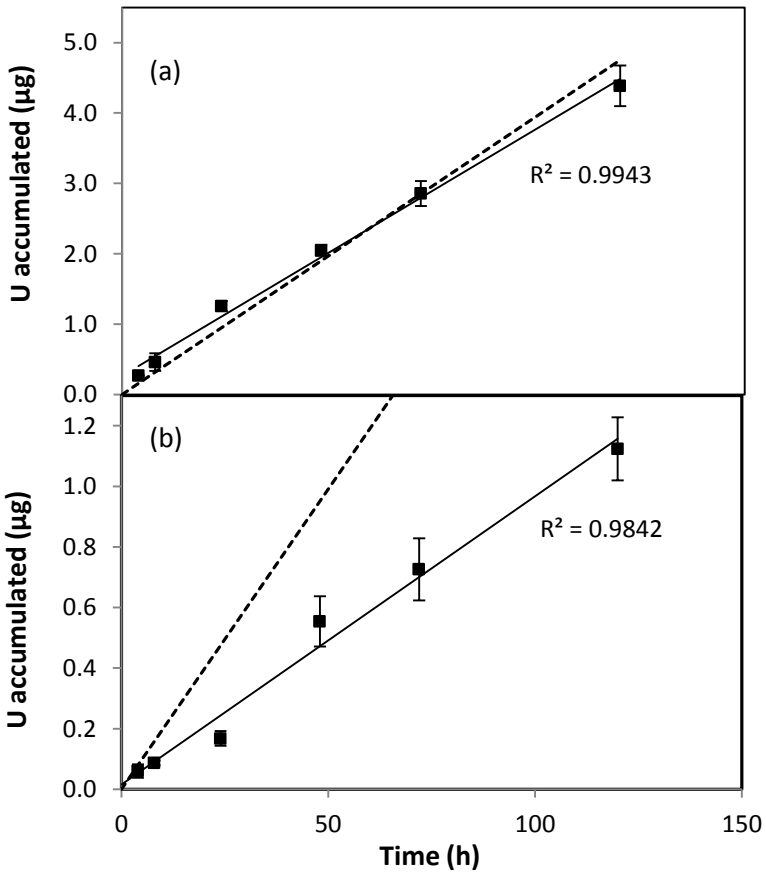

Figure 6.9(a). Mass of U accumulated with time for 120 h deployment in 0.01 M $NaNO_3$. Solution pH 7.7 ± 0.05, buffered using 0.983 mM HCO_3. Average concentration of U in the exposure tank was 106 µg L^{-1}, average temperature was 20°C and the calculated diffusion coefficient was 3.14 x 10^{-6} cm^2 s^{-1}; (b). Mass of U accumulated with time for 120 h deployment in artificial sea water. Solution pH 8.1 ± 0.05, average concentration of U the exposure tank was 104 µg L^{-1}, average temperature was 20°C and the calculated diffusion coefficient 3.35 x 10^{-6} cm^2 s^{-1}. Dashed lines represent model uptake of U as calculated from equation 2, using the average solution concentration of U; and the solid line represents the linear regression for the uptake of U during the linear uptake phase. Error bars are the standard error of triplicate measurements.

6.3.3.2 Field deployments

The average U concentration of the grab samples, which were taken each time a DGT sampler was retrieved, over the deployment period at the fresh water site was 0.2 µg L^{-1}. At this site 100% of the predicted (using equation 6.3) U was taken up for the first 7 days of the trial, after which the accumulation decreases to 70% of the predicted value by day 10 (Figure 6.10a). As U was not capacity limited under laboratory conditions in artificial freshwater and accumulated 4.4 µg U (Figure 6.9a), the field

limitation (reached at 4.3 ng U accumulated) is most likely as a result of biofouling of the diffusional surface area or the binding sites on the resin being filled.

The average U concentration at the marine site over the deployment period, as measured by grab samples each time a DGT sampler was retrieved, was 3.3 µg L^{-1}. This was similar to concentrations found at other marine sites. The predominant U species in the marine environment are $UO_2(CO_3)_2^{2-}$ and $UO_2(CO_3)_3^{4-}$, with self diffusion coefficients of 5.52 x 10^{-6} cm^2 s^{-1} at 25°C (as described in section Chapter 3 section 3.1.1.) This gives a $D_M^W : D_M^{gel}$ ratio of 1.18 which was considered when calculating the DBL (equation 6.5) and the C_{DGT} (equation 6.7 was used as opposed to equation 6.3 to account for the differences in the diffusion coefficients between the diffusive gel and the DBL). The DGT accumulated (within error range) U linearly for 3 days and was in agreement with equation 6.7, thereafter uptake departed from the predicted values. U in sea water exists predominantly as soluble uranyl carbonate anions, which were taken up under laboratory conditions, it can be reasoned that the high carbonate concentrations would not be responsible for the departure of the DGT values from the predicted values. This departure is potentially due to the complex matrix and the presence of other cations such as Mg^{2+} and Ca^{2+} competing for binding sites with the U. The deviation from the modelled uptake as per the C_{DGT} equation occurred under laboratory settings after 0.06 µg U had been accumulated. In the field, this departure from the modelled uptake occurred at 0.02 µg U accumulated. The discrepancy in the deployment time could be as a function of the U solution concentration (100 µg L^{-1} in the laboratory; 3.3 µg L^{-1} in the field) and the lower U accumulation in the field as a result of the complex matrix (only major ions were included in the laboratory trial solutions) resulting in ionic competition for binding sites on the resin.

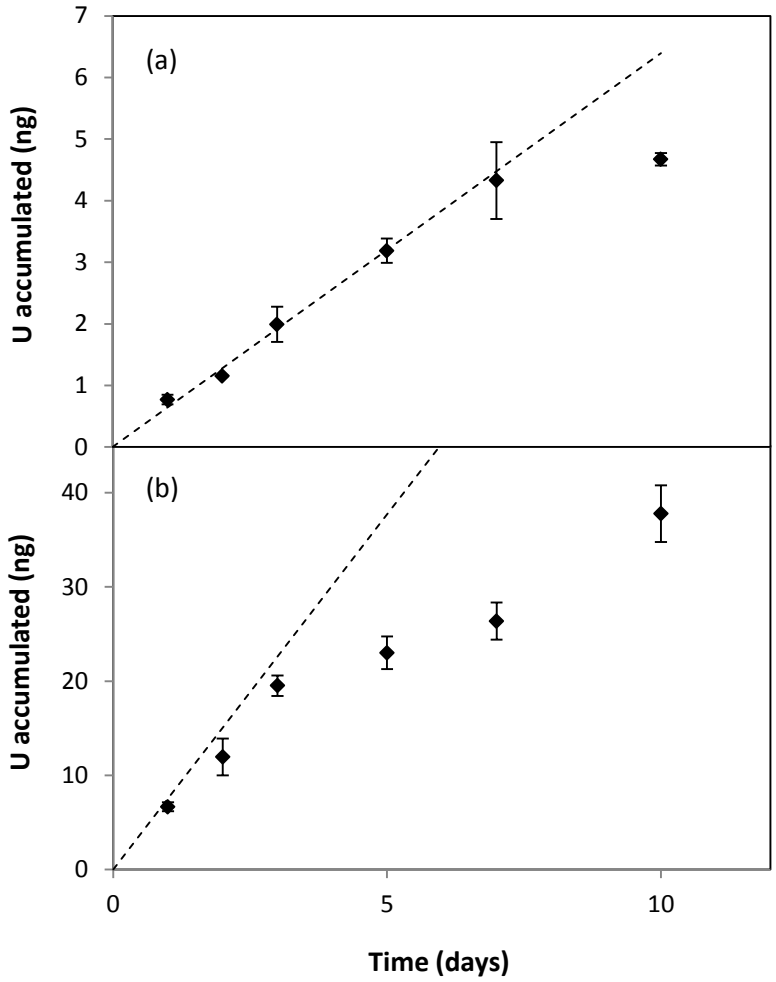

Figure 6.10: Mass of U accumulated with time for DGTs fitted with a Diphonix® resin in 10-day field trials (a). fresh water deployment, average water pH 7.9, average water temperature 12°C, average concentration of U in grab water samples 0.2 µg L^{-1}, calculated diffusion coefficient for uranium 1.59 x 10^{-6} cm^2 s^{-1}; thickness of DBL 0.062 ± 0.004 cm; (b) marine deployment, average water pH 8.2, average water temperature 13°C, average concentration of U in grab water samples 3.3 µg L^{-1}, calculated diffusion coefficient for U 1.43 x 10^{-6} cm^2 s^{-1}, thickness of DBL 0.091 ± 0.011 cm. Dashed lines represent model uptake of U as calculated from equation 2, using the average water concentration of U; and the solid line represents the linear regression for the uptake of U during the linear uptake phase. Error bars are the standard error of triplicate measurements.

At each site the average thickness of the DBL for the DGT was calculated according to equation 6.6, being 0.062 ± 0.004 cm at the fresh water site and 0.107 ± 0.013 cm at the marine site (Figures 6.11 and 6.12 respectively). This is in agreement (DBL = 0.046 ± 0.006 cm) with previous work at the fresh water site and but higher (DBL = 0.042 ± 0.019 cm) at the marine site. The concentrations of U calculated using equation 6.3 were reduced by up to 40% at the fresh water site and 50% at the marine site if the effect of the DBL was not accounted. The difference in DBL at the two sites could be attributed to differences in water turbulence. At the marine site the water flow

rate was low due to the enclosed nature of the dock the pontoon, only being agitated by tidal fluctuations.

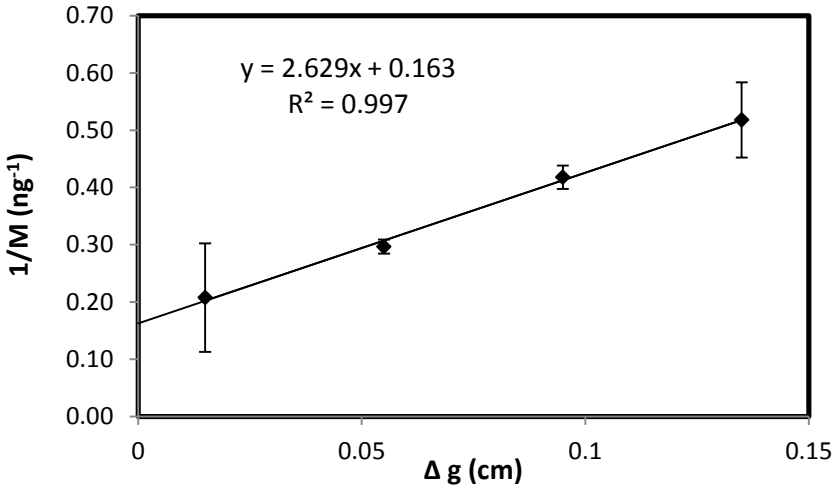

Figure 6.11. 1/Mass U accumulated by the Diphonix® resin with Δg to show the diffusive boundary layer (DBL) for the freshwater deployment. Devices were deployed for 3 days. Error bars are the standard error of triplicate measurements. DBL thickness calculated as 0.062 ± 0.004 cm using equation 6.5.

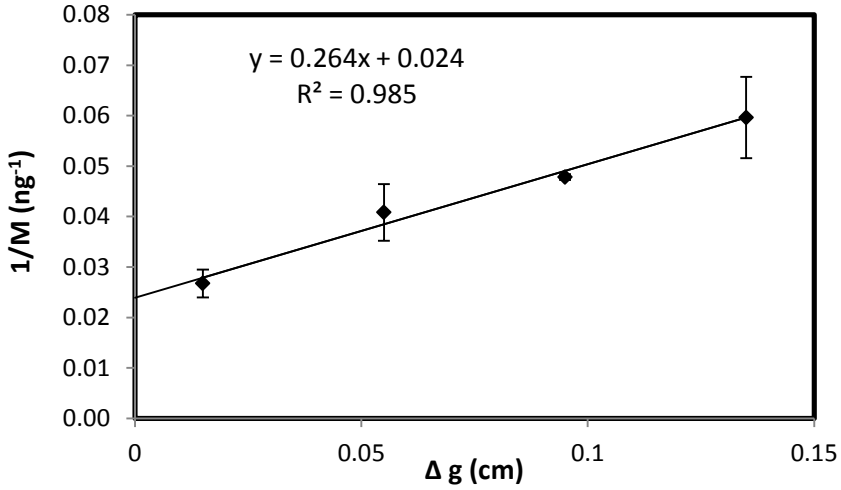

Figure 6.12. 1/Mass U accumulated by the Diphonix® resin with Δg to show the diffusive boundary layer (DBL) for the marine deployment. Devices were deployed for 3 days. Error bars are the standard error of triplicate measurements. DBL thickness calculated as 0.107 ± 0.013 cm using equation 6.5.

6.3.4 Isotopic ratios

Isotopic ratios ($^{235/238}$U) of U were measured for the DGT and grab samples and are detailed in Table 6.4. Both field sites in this study were found to have a natural $^{235/238}$U ratio of 0.00725. This ratio could be determined accurately after 1 day of deployment at the marine site and after 2 days at the fresh water site. The longer accumulation time needed at the fresh water site was a result of the lower concentrations

of U present. The average concentration of U in the River Lambourn was 0.2 µg L^{-1} and 3.3 µg L^{-1} at the marine site throughout the deployment period. The limiting factor in the measurement of isotopic ratios using ICP-MS is the low abundance of ^{235}U, which can be overcome through longer count times for this isotope. This means that the isotopic ratios were distinguishable in the grab samples at both deployment sites. The freshwater grab samples required no dilution and could be analysed directly with the ICP-MS; the seawater grab samples required a 20 fold dilution due to interferences of the high matrix. Diphonix® outperformed other resins used to measured isotopic ratios of U in these environments. The accuracy of the isotopic ratio measurements in this study were 0.25% and 1.2 % for marine and fresh water sites respectively. Values for the accuracy of these measurements for Chelex-100, Metsorb™ and MnO_2 resins ranged from 5-8 %, 1-2 % and 0.1-4.0 % respectively. These data support the use of the DGT in long-term environmental monitoring schemes for the actinides.

Table 6.4: Isotopic ratios ($^{235/238}U$) for Diphonix® resin and grab water samples found at the marine and fresh water sites. Natural isotopic ratio for $^{235/238}U$ is 0.00725.

	Marine Average isotopic ratio	RSD* (%)	Accuracy** (%)	**Fresh water** Average isotopic ratio	RSD* (%)	Accuracy** (%)
Diphonix® resin	0.00730	1.6	-1.38	0.00734	2.19	-1.2
Grab water sample	0.00735	2.55	-0.59	0.00723	1.51	0.25

*Standard deviation calculated as a % of the mean (precision).
**Calculated as (actual reading – measured/actual) x 100.

6.4 Conclusions and environmental monitoring applications

The performance of the Diphonix® resin used with DGT technique was assessed in the laboratory and under fresh water and marine field conditions. In the presence of competing ligands or cations (such as Ca^{2+} and CO_3^{2-} tested here), under laboratory conditions, the resin sorbed U in agreement with predictions. In seawater laboratory deployments, competing cations and anionic ligands a lower DGT uptake than the predicted uptake using the DGT equation was observed; probably as a result of competition for binding sites. Field trials showed that the accumulation of U was as predicted for up to 7 days in fresh water and only 3 days estuarine water, which are the maximum deployment times in the field for this technique. The thickness of the DBL in this study was larger than that previously measured at these field sites, probably as a result of varying flow conditions. The measurement of isotopic ratios of U was possible using the Diphonix® resin with a higher precision (1-2%) and accuracy (within 1.3%) than found in previous studies.

The technique presented in this chapter has applications in the environmental monitoring of U in aqueous systems. The World Health Organisation (WHO) drinking water limits for some selected actinides are presented in Chapter 2, and provide a benchmark for a regulatory environmental limit (as most aqueous discharge permits are unique to each nuclear establishment). The WHO drinking water limit for U is 30 ug L-1 or 0.4 Bq L^{-1}. The blank Diphonix® resin had a U measurement of 0.79 ± 0.08 ng; by taking the LoD as 3 times the standard deviation of the blank plus the blank, the lowest detectable quantity of U on the Diphonix® resin is 1.03 ng. Multiplying this by the elution volume (2 mL) and the dilution factor required for ICP-MS analysis (x 20), and then dividing by the elution factor (0.9) (as detailed in equation 6.8), gives a limit of detection of U on the Diphonix® resin using the methodology described in this chapter of 0.046 µg L^{-1}, or 0.5 x 10^{-4} Bq L^{-1}.

$$\frac{Diphonix\ blank\ x\ Elution\ volume\ x\ ICP{-}MS\ Dilution\ factor}{Elution\ factor}$$ Equation 6.8

This is considerably less than the WHO drinking water limits, therefore making this a useful tool for environmental monitoring. This resin is unlikely to be capacity limited in a freshwater environmental setting, as shown in Figures 6.9a and 6.10a, but due to capacity limitations in the marine environment (Figures 6.9b and 6.10b) the Diphonix® resin has limited usefulness in this environmental setting, despite the resin manufacturer (TrisKem International) quoting a cation (iron) resin loading capacity of > 10 g L^{-1} (wet resin).

Diphonix® has been shown to out-perform most other sorbents used with DGT for measuring U. Future research should be focused on extending the capabilities of the this method to examine other actinides. Diphonix® has been shown by previous workers to take up thorium, plutonium and americium [22]. The other actinides the LoD for this technique is lower than the WHO drinking water limits (and therefore potentially applicable to) are ^{232}Th, ^{235}U, ^{236}U, ^{244}Pu and ^{247}Cm. However, due to the potential for precipitates of thorium and americium being formed if eluting using an alkali solution (such as the NaOH used in this study), further work would be required to establish an elution technique that could also be used in conjunction with radiochemical separations. A clean up step, or further development of the HEDPA elution scheme may provide a method that is capable of measuring a wider range of actinides.

6.5 References

[1] T. Mathews, K. Beaugelin-Seiller, J. Garnier-Laplace, R. Gilbin, C. Adam, C. Della-Vedova, A Probabilistic Assessment of the Chemical and Radiological Risks of Chronic Exposure to Uranium in Freshwater Ecosystems, Environmental Science and Technology, 43 (2009) 6684-6690.

[2] B.E. Johnson, P.H. Santschi, R.S. Addleman, M. Douglas, J.D. Davidson, G.E. Fryxell, J.M. Schwantes, Collection of fission and activation product elements from fresh and ocean waters A comparison of traditional and novel sorbents, Applied Radiation and Isotopes, 69 (2011) 205-216.

[3] I.J. Allan, B. Vrana, R. Greenwood, G.A. Mills, J. Knutsson, A. Holmberg, N. Guigues, A.-M. Fouillac, S. Laschi, Strategic monitoring for the European Water Framework Directive, TrAC Trends in Analytical Chemistry, 25 (2006) 704-715.

[4] B. Vrana, G.A. Mills, I.J. Allan, E. Dominiak, K. Svensson, J. Knutsson, G. Morrison, R. Greenwood, Passive sampling techniques for monitoring pollutants in water, Trac-Trends in Analytical Chemistry, 24 (2005) 845-868.

[5] G.A. Mills, R. Greenwood, I.J. Allan, E. Lopuchin, J. Brummer, J. Knutsson, B. Vrana, Application of passive sampling techniques for monitoring the aquatic environment, in: J. Namiesnik, P. Szeter (Eds.) Analytical measurements in aquatic environments, CRC Press, 2009.

[6] N. Roig, M. Nadal, J. Sierra, A. Ginebreda, M. Schuhmacher, J.L. Domingo, Novel approach for assessing heavy metal pollution and ecotoxicological status of rivers by means of passive sampling methods, Environment International, 37 (2011) 671-677.

[7] M. Gregusova, B. Docekal, New resin gel for uranium determination by diffusive gradient in thin films technique, Analytica Chimica Acta, 684 (2011) 142-146.

[8] C. Murdock, M. Kelly, L.-Y. Chang, W. Davison, H. Zhang, DGT as an *in situ* tool for measuring radiocesium in natural waters, Environmental Science & Technology, 35 (2001) 4530-4535.

[9] C.M. Hutchins, J.G. Panther, P.R. Teasdale, F. Wang, R.R. Stewart, W.W. Bennett, H. Zhao, Evaluation of a titanium dioxide-based DGT technique for measuring inorganic uranium species in fresh and marine waters, Talanta, 97 (2012) 550-556.

[10] W. Davison, Fones G., Harper, M., Teasdale, P. And Zhang, H, Dialysis, DET and DGT: *In situ* diffusional techniques for studying water, sediments and soils., in: J.A.H. Buffle, G. (Ed.) *In situ* monitoring of aquatic systems: chemical analysis and speciation, John Wiley & Sons Ltd, 2000, pp. 74.

[11] W.J. Li, F.Y. Wang, W.H. Zhang, D. Evans, Measurement of stable and radioactive cesium in natural waters by the diffusive gradients in thin films technique with new selective binding phases, Analytical Chemistry, 81 (2009) 5889-5895.
[12] M.A. French, H. Zhang, J.M. Pates, S.E. Bryan, R.C. Wilson, Development and performance of the diffusive gradients in thin-films technique for the measurement of technetium-99 in seawater, Analytical Chemistry, 77 (2005) 4.
[13] M. Leermakers, Y. Gao, J. Navez, A. Poffijn, K. Croes, W. Baeyens, Radium analysis by sector field ICP-MS in combination with the diffusive gradients in thin films (DGT) technique, Journal of Analytical Atomic Spectrometry, 24 (2009) 1115-1117.
[14] Y. Gao, W. Baeyens, S. De Galan, A. Poffijn, M. Leermakers, Mobility of radium and trace metals in sediments of the Winterbeek: Application of sequential extraction and DGT techniques, Environmental Pollution, 158 (2010) 2439-2445.
[15] W.J. Li, J.J. Zhao, C.S. Li, S. Kiser, R.J. Cornett, Speciation measurements of uranium in alkaline waters using diffusive gradients in thin films technique, Analytica Chimica Acta, 575 (2006) 274-280.
[16] H. Vandenhove, K. Antunes, J. Wannijn, L. Duquene, M.V. Hees, Method of diffusive gradients in thin films (DGT) compared with other soil testing methods to predict uranium phytoavailability, Science of the Total Environment, 373 (2007) 542-555.
[17] L. Duquène, H. Vandenhove, F. Tack, M. Van Hees, J. Wannijn, Diffusive gradient in thin films (DGT) compared with soil solution and labile uranium fraction for predicting uranium bioavailability to ryegrass, Journal of Environmental Radioactivity, 101 (2010) 140-147.
[18] R. Dahlqvist, K. Andersson, J. Ingri, T. Larsson, B. Stolpe, D. Turner, Temporal variations of colloidal carrier phases and associated trace elements in a boreal river, Geochim. Cosmochim. Acta, 71 (2007) 5339-5354.
[19] W.J. Li, C.S. Li, J.J. Zhao, R.J. Cornett, Diffusive gradients in thin films technique for uranium measurements in river water, Analytica Chimica Acta, 592 (2007) 106-113.
[20] D. Kołodyńska, Diphonix Resin® in sorption of heavy metal ions in the presence of the biodegradable complexing agents of a new generation, Chemical Engineering Journal, 159 (2010) 27-36.
[21] R. Chiarizia, E.P. Horwitz, S.D. Alexandratos, M.J. Gula, Diphonix(R) resin: A review of its properties and applications, Separation Science and Technology, 32 (1997) 1-35.

[22] E.P. Horwitz, R. Chiarizia, H. Diamond, R.C. Gatrone, S.D. Alexandratos, A.Q. Trochimczuk, D.W. Crick, Uptake of metal ions by a new chelating ion-exchange resin. Part1: Acid dependencies of actinide ions, Solvent Extraction and Ion Exchange, 11 (1993) 943-966.

[23] R. Chiarizia, E.P. Horwitz, R.C. Gatrone, S.D. Alexandratos, A.Q. Trochimczuk, D.W. Crick, Uptake of metal ions by a new chelating ion-exchange resin. Part 2: Acid dependencies of transition and post-transition metal ions, Solvent Extraction and Ion Exchange, 11 (1993) 967-985.

[24] K.L. Nash, P.G. Rickert, J. Muntean, V., S.D. Alexandratos, Uptake of metal ions by a new chelating ion exchange resin. Part 3: Protonation constants via potentiometric titration and solid state 31P NMR spectroscopy., Solvent extraction and ion exchange, 12 (1994) 193-209.

[25] R. Chiarizia, E.P. Horwitz, S.D. Alexandratos, Uptake of metal ions by a new chelating ion exchange resin. Part 4: Kinetics, Solvent extraction and ion exchange, 12 (1994) 211-237.

[26] E.P. Horwitz, R. Chiarizia, S.D. Alexandratos, Uptake of metal ions by a new chelating ion-exchange resin. Part 5: The effect of solution matrix on actinides, Solvent Extraction and Ion Exchange, 12 (1994) 831-845.

[27] R. Chiarizia, E.P. Horwitz, Uptake of metal ions by a new chelating ion-exchange resin. Part 6: Calculations on the effect of complex anions on actinides, Solvent Extraction and Ion Exchange, 12 (1994) 847-871.

[28] R. Chiarizia, J.R. Ferraro, E.P. Horwitz, K.A. D'arcy, Uptake of metal ions by a new chelating ion-exchange resin. VII: Alkaline earth cations., Solvent Extraction and Ion Exchange, 13 (1995) 1063-1082.

[29] R. Chiarizia, K.A. D'arcy, E.P. Horwitz, S.D. Alexandratos, A.W. Trochimczuk, Uptake of metal ions by a new chelating ion exchange resin. Part 8: Simultaneous uptake of cationic and anionic species., Solvent Extraction and Ion Exchange, 14 (1996) 519-542.

[30] R. Chiarizia, E.P. Horwitz, K.A. D'arcy, S.D. Alexandratos, A.W. Trochimczuk, Uptake of metal ions by a new chelating ion exchange resin. Part 9: Silica grafter diphosphonic acid., Solvent extraction and ion exchange, 14 (1996) 1077-1100.

[31] D.H. Phillips, B. Gu, D.B. Watson, C.S. Parmele, Uranium removal from contaminated groundwater by synthetic resins, Water Research, 42 (2008) 260-268.

[32] E.P. Horwitz, R. Chiarizia, M.L. Dietz, DIPEX: A new extraction chromatographic material for the separation and preconcentration of actinides from aqueous solution, Reactive and Functional Polymers, 33 (1997) 25-36.

[33] H. Zhang, W. Davison, Direct in situ measurements of labile inorganic and organically bound metal species in synthetic solutions and natural waters using diffusive gradients in thin films, Analytical Chemistry, 72 (2000) 4447-4457.

[34] W.W. Bennett, P.R. Teasdale, J.G. Panther, D.T. Welsh, D.F. Jolley, New diffusive gradients in a thin film technique for measuring inorganic arsenic and selenium(IV) using a titanium dioxide based adsorbent, Analytical Chemistry, 82 (2010) 7401-7407.

[35] H. Zhang, W. Davison, Diffusional characteristics of hydrogels used in DGT and DET techniques, Analytica Chimica Acta, 398 (1999) 329-340.

[36] Tables of Physical & Chemical Constants in: 2.2.3 Viscosities, Kaye & Laby Online, 2005.

[37] K.W. Warnken, H. Zhang, W. Davison, Accuracy of the diffusive gradients in thin-films technique: diffusive boundary layer and effective sampling area considerations, Analytical Chemistry, 78 (2006) 3780-3787.

[38] S. Kerisit, C. Liu, Molecular simulation of the diffusion of uranyl carbonate species in aqueous solution, Geochimica Et Cosmochimica Acta, 74 (2010) 4937-4952.

[39] S.L. Maxwell III, S. Nichols, Actinide recovery method for large soil samples, Radioactivity and Radiochemistry, 11 (2000) 46-54.

[40] I.W. Croudace, P.E. Warwick, R.C. Greenwood, A novel approach for the rapid decomposition of Actinide$^{(TM)}$ resin and its application to measurement of uranium and plutonium in natural waters, Analytica Chimica Acta, 577 (2006) 111-118.

[41] A.J. Robson, C. Neal, A summary of regional water quality for Eastern UK rivers, Science of the Total Environment, 194-195 (1997) 15-37.

[42] D.R. Kester, I.W. Duedall, D.N. Connors, R.M. Pytkowicz, Preparation of artificial seawater, American Society of Limnology and Oceanography, 12 (1967) 176-179.

[43] H.P. Jarvie, C. Neal, M.D. Jürgens, E.J. Sutton, M. Neal, H.D. Wickham, L.K. Hill, S.A. Harman, J.J.L. Davies, A. Warwick, C. Barrett, J. Griffiths, A. Binley, N. Swannack, N. McIntyre, Within-river nutrient processing in Chalk streams: The Pang and Lambourn, UK, Journal of Hydrology, 330 (2006) 101-125.

[44] S.L. Maxwell Iii, M.A. Bernard, M.R. Nelson, L.D. Youmans, New method for removal of spectral interferences for beryllium assay using inductively coupled plasma atomic emission spectrometry, Talanta, 76 (2008) 432-440.

[45] J. Zheng, M. Yamada, Determination of U isotope ratios in sediments using ICP-QMS after sample cleanup with anion-exchange and extraction chromatography, Talanta, 68 (2006) 932-939.
[46] W.C. Burnett, D.R. Corbett, M. Schultz, E.P. Horwitz, R. Chiarizia, M. Dietz, A. Thakkar, M. Fern, Pre-concentration of actinide elements from soils and large volume water samples using extraction chromatography, Journal of Radioanalytical and Nuclear Chemistry, 226 (1997) 121-127.
[47] D. Gorman-Lewis, P.C. Burns, J.B. Fein, Review of uranyl mineral solubility measurements, Journal of Chemical Thermodynamics, 40 (2008) 18.
[48] W. Dong, S.C. Brooks, Determination of the formation constants of ternary complexes of uranyl and carbonate with alkaline earth metals (Mg^{2+}, Ca^{2+}, Sr^{2+}, and Ba^{2+}) using anion exchange method, Environmental Science and Technology, 40 (2006) 4689-4695.
[49] G.R. Choppin, Actinide speciation in the environment, Journal of Radioanalytical Nuclear Chemistry, 273 (2007) 695-703.

Chapter 7: The effect of field deployment strategies on the diffusive boundary layer of the DGT and the implications for TWA measurements

7.1 Introduction

Diffusive gradients in thin films (DGT) has been used extensively to measure metals [1-5] radionuclides [6, 7] and nutrients [8, 9] under laboratory and field conditions. However, few studies have considered the effects of a diffusive boundary layer (DBL) at the surface of the DGT devices. This extends the effective diffusion distance (Δg) of the analyte. In the initial development of the device this was thought to be negligible in the presence of any level of turbulence [4]. It has since been observed in the laboratory that even under high flow conditions, that a small, measurable DBL exists of approximately 0.2 mm [10]. Under field conditions, measured DBLs have shown large variation that may not be entirely attributable to physical process such as advection. Chapter 5 details the DBL measurements when DGTs were deployed between Perspex plates for 7 days over a 6 month period and ranged from 0.037 cm to 0.141 cm in high to low flow river conditions respectively. Examples of published DBLs measured in field are shown in Table 7.1, with the deployment method detailed, where described.

Table 7.1 Examples of published field or *in situ* DBL measurements, and the corresponding deployment technique used.

Deployment setting	Deployment method	Thickness of DBL (cm)	Flow rate	Deployment Time (d)	Ref
Fluvial	Not stated	0.003 ± 0.001	Fast	4	[11]
Fluvial	Not stated	0.026 ± 0.002	Fast	3	[10]
Fluvial	Not stated	0.080 ± 0.013	Fast	4	[12]
Estuarine	Not stated	0.067 ± 0.007	Fast	4	[12]
Fluvial	Not stated	0.080 ± 0.013	Fast	4	[8]
Estuarine	Not stated	0.067 ± 0.007	Fast	4	[8]
Lake	Nylon cord	0.031 ± 0.020	Slow	13-14	[13]
Lake	Plate	Not stated	Slow	5, 7, 14, 31	[14]

What is noticeable is the lack of reported deployment techniques. There have been studies undertaken to assess the thickness of the DBL and flow rate when a flume or controlled area is utilised and in low flow conditions [15]. There are many factors that can contribute to the thickness of the DBL in the field, including flow rate [10, 16], biofouling [17] and the presence of dissolved and colloidal organic material [18].

However, the deployment method has not been considered in any previous studies. The range of deployment methods (where detailed) in Table 7.1 also indicates that there is no standard deployment used by different workers. Another issue with field deployments and measurement of the DBL is that large variations exist between studies in the deployment time and the thickness of the DBL measured. Divis *et al*. [19] stated the DGT could be deployed between 1 h to several months; Gimpel *et al*. [16] successfully deployed DGT devices for 1 month, while in Chapter 4 it was found that after 1 week, biofouling and potential resin saturation prevented analyte accumulation in line with that predicted using the standard DGT equation. Whilst it is most likely that the flow rate and the degree of biofouling will be the greatest influences on the thickness of the DBL, deployment technique cannot be discounted because of the variations in geometry and size of the various deployment devices that may contribute to changes in flow around the devices, or biofouling accumulation.

This study examined the impact of varying deployment techniques and deployment time on the thickness of the DBL, and the implications this had for the measurement of TWA concentrations. Three deployment methods were chosen, representing the most widely used schemes: a protective cage with the samplers suspended inside, the samplers attached directly to a nylon line and the samplers held in place between two perspex plates with apertures that allow the samplers surface areas to be exposed to the water flow. The cage system is thought to protect the passive samplers from damage from flotsam and to prevent ensnarement by macro-flora. The fluid flow past the DGT samplers inside a cage system is theoretically unhindered as it passes through the gaps in the housing. A problem with this system is if the face of the cage facing upstream (i.e. the face that allows free flow through the cage) becomes obstructed and thereby hinders the flow through the cage thereby altering the flow regime. The simple line system allows unhindered flow around the DGT. It is also easy to use as devices can be attached directly to a nylon cord. However, there is the potential for entanglement of macro-flora and flotsam around the line. A plate system offers convenience as multiple devices can be deployed and the plate surface (which is also where the DGT diffusive face is located) can be directly parallel to the fluid flow to ensure maximum flow rate and minimum thickness of the DBL. However, shear stresses across the plate surface may increase the DBL proportionally from the distance of the surface (Figure 7.1).

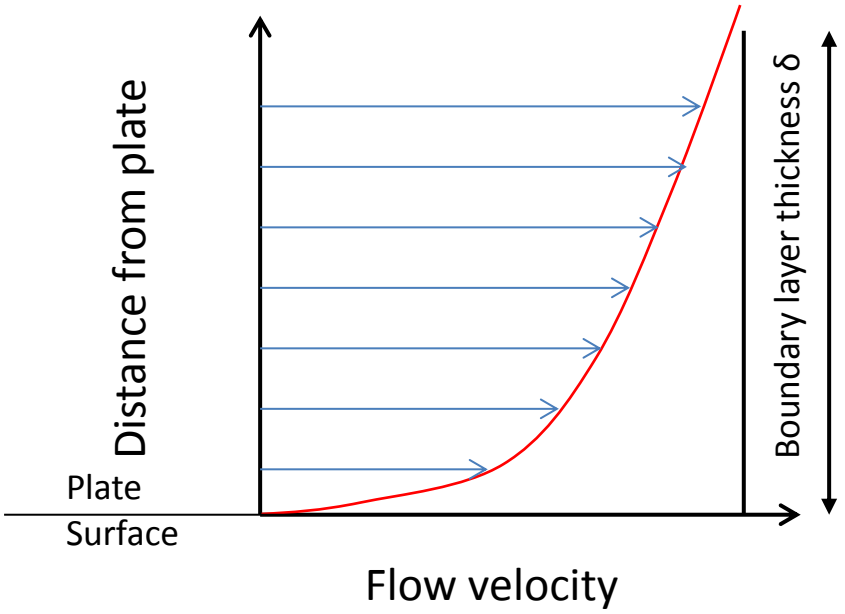

Figure 7.1 Effect of flow velocity near a planar surface. The further from the place surface, the higher the fluid velocity and the smaller the DBL.

7.2 Experimental

Chemicals were of analytical grade or better and supplied by Fisher Scientific Ltd. (Loughborough, UK) unless otherwise specified. Milli-Q (ultra-pure) water (> 18.2 MΩ cm, Millipore, Watford, U.K.) was used as the laboratory water. All uranium (U) ICP-MS standards and experimental working solutions were prepared in low density polyethylene (LDPE) or polystyrene (PS) containers with polypropylene lids (PP) from a 1000 mg L^{-1} in 2% HNO_3 (Spex Certiprep, Fisher Scientific Ltd.) U stock solution unless otherwise stated. The ICP-MS internal standard was prepared from a 1000 mg L^{-1} in 2% HNO_3 (Spex Certiprep) bismuth stock solution. All plastic apparatus was soaked for 24 h in 10% HNO_3 and rinsed three times in Milli-Q water prior to use.

7.2.1 Preparation of DGT devices

Polyacrylamide (PAM) diffusive gels (thickness 0.4, 0.8, 1.2 and 1.6 mm) were prepared according to Zhang and Davison [20], as described in Chapter 3. The gels contained 15% v/v acrylamide solution (Acros Organics, ThermoFisher, Loughborough, UK) and 0.3% v/v of patented agarose cross-linker (DGT Research Ltd., Lancaster, UK). N,N,N',N'-tetramethylenediamine (TEMED, Acros Organics) was used as the catalyst and a freshly prepared solution of 10% ammonium persulfate (Acros Organics) was used as the initiator for polymerisation. The diffusive gels were stored in 0.01 M $NaNO_3$. The 0.4 mm thick PAM binding gels were prepared with 1 g Metsorb^{TM} heavy metal removal powder (HMRP) powder (TiO_2 with an organic binder, < 50 µm; Graver

Technologies., Glasgow, USA) in 10 mL gel solution prior to polymerisation, according to the method described by Bennett *et al.* [12].

DGT device mouldings were obtained from DGT Research Ltd. and washed for 24 h in 10% HNO_3, and then rinsed three times in Milli-Q water prior to use. The devices were assembled according to Davison *et al.* [4] and stored at 4^{o}C in zip lock plastic bags, containing 1-2 mL of 0.01 M $NaNO_3$ to ensure the diffusion properties of the gels were not altered, and to prevent the gels drying out. A disk of (0.2 µm pore size) Supor polyethylene sulfone (Pall Corporation, Portsmouth, UK) was used as the outer membrane.

7.2.2 Analysis of DGT devices

After exposure, the Metsorb^{TM} binding gels were removed from DGT and eluted (48 h) with 1 M H_2O_2/1 M HNO_3 (2 mL) solution (100 mL made by combining 90 mL 1.1 M HNO_3 and 10 mL H_2O_2). U was determined in all solutions by ICP-MS using an Agilent 7500ce series instrument (Agilent Technologies Inc., Japan). Total U was measured under normal plasma conditions in 'no gas mode', with the sample introduction system fitted with a micromist nebuliser. The instrument blank for U was 6 ng L^{-1} while the limit of detection (calculated by the Agilent Chemstation software) for U was 2 ng L^{-1}, with a measurement standard deviation better than 3%. Laboratory blanks were undertaken in triplicate for each experiment and the average concentration per disk was determined as 0.03 ± 0.02 ng for ^{238}U. Bismuth (*m/z* = 209; 25 µg L^{-1}) was used as an internal standard to compensate for any potential instrument drift. The certified reference material SLRS-5 (National Research Council Canada, Canada) was analysed and found to be within 1% of the stated value.

7.2.3 Calculation of time-weighted average concentrations

The concentration of U measured by the ICP-MS in µg L^{-1} from the eluent was multiplied by the dilution factor (×10) to give the U concentration (*Ce*). The absolute mass (*M*) of the U in the resin gel was then calculated using equation 7.1, where *M* is calculated taking into account the gel volume (*Vg*, cm^3), the eluent volume (*Ve*, mL), the measured concentration of U in the eluent (*Ce*, ng mL^{-1}) and the elution factor (*fe*) [20].

$$M = \frac{Ce(Vg+Ve)}{fe} \qquad \text{Equation 7.1}$$

M from equation 7.1 was then used to calculate the thickness of the diffusive boundary layer (δ), also using equation 7.4 after Warnken *et al.*[10]. A straight line plot of *1/M* vs *Δg* has a slope (*m*) of $1/(DC_{DGT}At)$ and an intercept (*b*) of $\delta/(DC_{DGT}At)$, as per equation 7.2. The intercept (*b*) divided by the slope (*m*) of this plot gives the diffusive boundary layer thickness δ, as per equation 7.3.

$$\frac{1}{M} = \frac{\Delta g}{DC_{DGT}At} + \frac{\delta}{DC_{DGT}At} \qquad \text{Equation 7.2}$$

$$\delta = \frac{b}{m} \qquad \text{Equation 7.3}$$

The thickness of the DBL was included in the C_{DGT} calculations for the field trials. A difference in diffusion coefficients for uranyl between the δ and Δg terms did not need to be considered in this study as the predominant uryanl species is $Ca_2UO_2(CO_3)_3$ which has a similar diffusion coefficient in water at the average pH (pH7.9) of the field sites used in this study [23] as that calculated for U in the diffusive gel [11]. The sampling area (*A*) was 3.8 cm^2 instead of the 3.14 cm^2 used in the laboratory trials, as described by Warnken *et al.* [10]. The calculations for the standard deviation associated with the DBL measurements can be found in Chapter 3, section 3.1.4.

The slope (*m*) from the plot of equation 7.2 is then used to calculated the TWA concentrations (equation 7.4) where the concentration (C_{DGT}, ng mL^{-1}) was calculated using the slope (*m*) of equation 7.2, the thickness of the diffusive path length (diffusive gel and filter membrane) (Δg, cm), the diffusion coefficient of the analyte (*D*, cm^2 s^{-1}) (as determined at different pHs for U by Hutchins *et al.* [11]), deployment time (*t*, s) and the area of the sample exposure window (*A*, cm^2):

$$C_{DGT} = \frac{1}{mD_M^{gel}At} \qquad \text{Equation 7.4}$$

The diffusion coefficients (*D*) were corrected for temperature (*T*, °C) using the Stokes-Einstein equation (equation 7.5) [21] and the viscosity of water (η, mPa s) [22]:

$$\frac{D_1\eta_1}{T_1} = \frac{D_2\eta_2}{T_2} \qquad \text{Equation 7.5}$$

7.2.4 Field deployments

Two freshwater field sites were used: site 1 (51.4469 N, -1.3838 W) was located on the River Lambourn at the village of Boxford, Berkshire, UK and site 2 (51.3792 N, -1.1855 W) on the River Enborne near Brimpton, Berkshire, UK. Both

rivers are tributaries of the River Kennet. The River Lambourn has a Chalk catchment and is a fast flowing shallow channel with an average pH of 7.9-8 [24]. The mean flow and base flow indices were 1.71 m^3 s^{-1} and 0.97 respectively [25]. The River Enborne drains impermeable Tertiary sand, silt and clay deposits [26] and has a slow flowing deep channel with a pH ~7.8.

The DGT devices were deployed as per detailed in Table 7.2 in each river. Three DGT devices containing diffusive layer PAM gel thicknesses (including 0.015 cm to account for the Supor membrane) of 0.015, 0.055, 0.095 and 0.135 cm, as per Warnken *et al*. [10], were removed after 3 days and 7 days. Diffusion coefficients calculated by Hutchins *et al*. [11] were used to calculate the TWA concentrations. Spot samples of water (20 mL) were collected at the exposure sites and were filtered (0.2 µm pore size Supor filters) and acidified *in situ* with 6 M HCl (40 µL). Water temperature and pH were recorded each time a device was removed so that diffusion coefficients could be corrected for variations in environmental conditions.

Procedural DGT blanks (3 per resin) were prepared along with the deployed devices and exposed to the field environment during deployment and retrieval of the sample devices. The blanks were then eluted and analysed with the samples as above.

Table 7.2 Description of deployment methods.

	Deployment method
1	DGT held between Perspex plates (15 x 7 cm, 8 devices per plate) and attached to a rope and float and weighted to the river bed (Figure 7.2).
2	DGT devices attached directly to nylon cord (fishing line) which was attached to a float and weighted to the river bed (Figure 7.3).
3	DGT devices attached to the top of a protective plastic cage, with the DGT face pointing inwards to avoid sediment accumulation round the edge of the housing unit. The cage was attached to a rope and float, and weighted to the river bed (Figure 7.4).

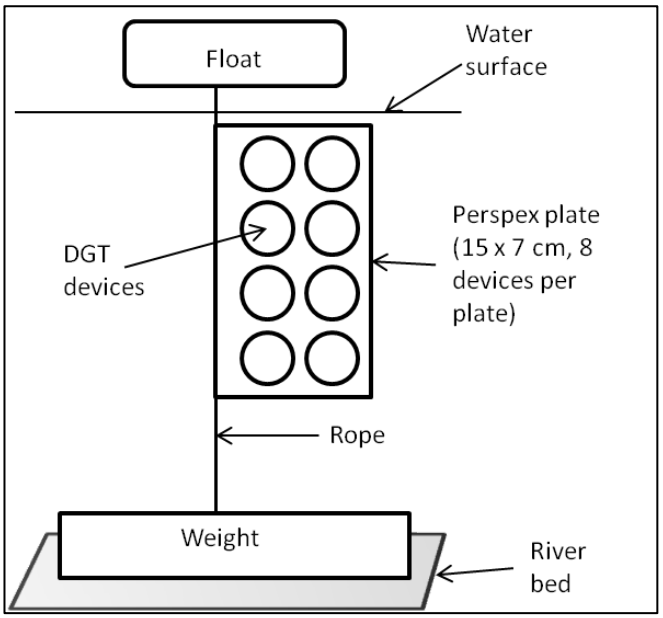

Figure 7.2 Deployment method 1: Perspex plates attached to rope anchored to river bed (not drawn to scale).

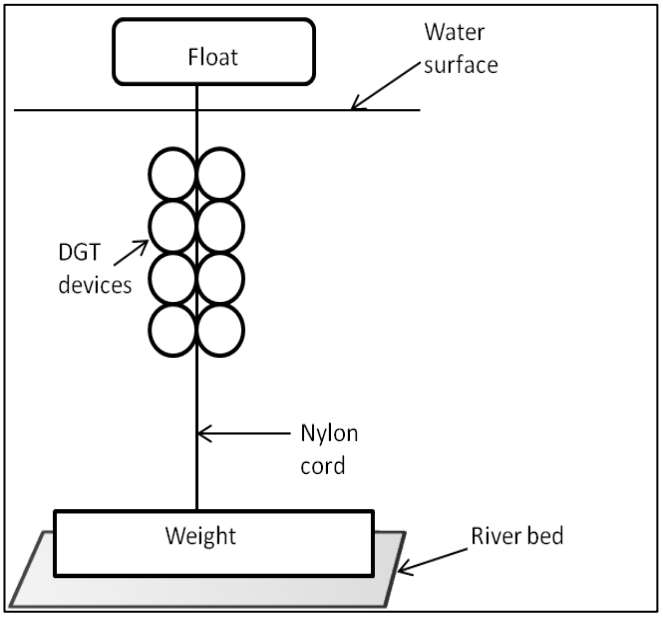

Figure 7.3 Deployment method 2: DGT devices attached directly to fishing line anchored to river bed (not drawn to scale).

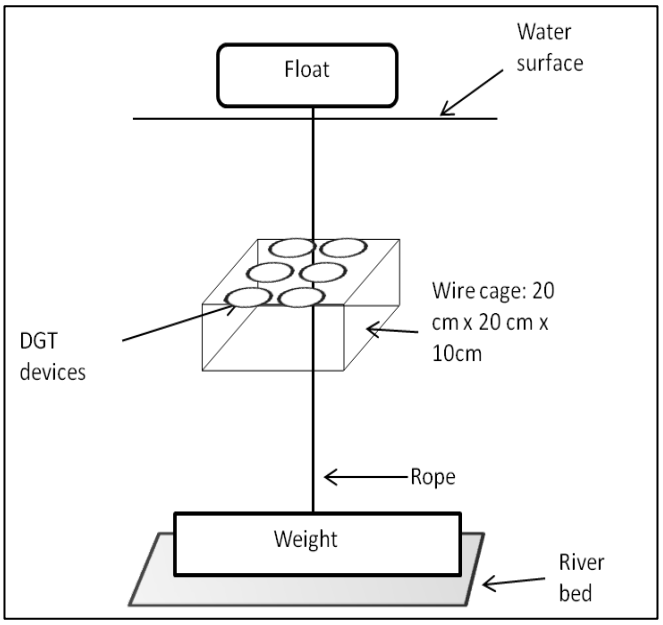

Figure 7.4 Deployment method 3: DGT devices attached to the top of a plastic coated wire mesh cage with the DGT facing inwards (not drawn to scale).

7.2.5 Statistical analysis

All statistical analysis was performed in IBM® SPSS® Statistics Version 20. The non-parametric one sample Shapiro-Wilk test was first used to test the data for normality (normality significance figure ≥ 0.05). The Shapiro-Wilk test was used because the sample size was very low ($n < 50$). If normality was established a one way ANOVA was performed to identify if any differences that existed between deployment time, site and deployment method were significant. If significant differences were found, a paired *t*-test was performed to establish where the differences were located within the data set.

7.3 Results and Discussion

Deployment methods and environmental conditions are shown in Table 7.3. The corresponding graphs as per equation 7.2 can be seen in Figure 7.5 (River Enborne) and Figure 7.6 (River Lambourn). Both deployment sites (the River Enborne and the River Lambourn) experienced similar temperatures and pHs throughout the deployment. The flow rate for the River Lambourn is higher due to the shallow fast flowing channel, whilst the flow rate in the River Enborne was lower as it is deeper and slower moving. Another consideration for this study is that the deployment site for the River Enborne was out of the main flow channel to allow for safe access for the deployment and retrieval of the DGT devices.

Table 7.3 Deployment methods, deployment times, locations, flow rate, temperature and pH. Flow rates calculated from river discharge data supplied by the CEH National River Flow Archive.

Deployment number	*1/M* v *Δg* Figure	River	Method	Days	Average flow rate ($m\ s^{-1}$)	Average temperature (^oC)	Average pH	Calculated diffusion coefficient ($x\ 10^{-6}\ cm^2\ s^{-1}$)
1	7.5 a	Enborne	Cage	3	0.04	13.9	8.02	1.8
2	7.5 b	Enborne	Line	3	0.04	13.9	8.02	1.8
3	7.5 c	Enborne	Plate	3	0.04	13.9	8.02	1.8
4	7.5 d	Enborne	Cage	7	0.04	13.9	8.02	1.8
5	7.5 e	Enborne	Line	7	0.04	13.9	8.02	1.8
6	7.5 f	Enborne	Plate	7	0.04	13.9	8.02	1.8
7	7.6 a	Lambourn	Cage	3	0.08	12.1	7.94	1.46
8	7.6 b	Lambourn	Line	3	0.08	12.1	7.94	1.46
9	7.6 c	Lambourn	Plate	3	0.08	12.1	7.94	1.46
10	7.6 d	Lambourn	Cage	7	0.08	12.1	7.94	1.46
11	7.6 e	Lambourn	Line	7	0.08	12.1	7.94	1.46
12	7.6 f	Lambourn	Plate	7	0.08	12.1	7.94	1.46

Table 7.4 gives the figures of merit for each of the deployment methods. Average RSD values are ~ 20%, with the majority of the devices taking up between 70-80% of the U measured in grab water samples. This is in line with that found in Chapter 4 for DGT devices fitted with a Metsorb^{TM} resin, where the quantity of U accumulated began to deviate from expected accumulations (when modelled using the DGT equation, equation 7.4) between 4 and 7 days of deployment in the field.

Table 7.4 shows that the RSD of the measured TWA concentrations of U was similar at the two deployment sites (RSD average 17.8% and 21.5% for the Rivers Enborne and Lambourn respectively). This shows that precision of the DGT devices did not vary greatly from site to site, which is an important factor when comparing TWA concentrations between sites. The River Enborne had consistently accurate (C_{DGT}/grab samples) values between the 3 d and 7d deployment of 81.3% for both deployment periods. The River Lambourn had an average accuracy over 3 days of 86.0%, which fell to an average of 51.3% when the devices are deployed for 7 days. DGT devices only accumulated 38 ± 4% of the available U when deployed for 7 days in the River Lambourn using the line and cage deployment methods. This may be as a result of the accumulation of macro-flora reducing the flow or partially restricting the water access to the DGT devices. The smallest DBL (0.042 ± 0.014 cm) was also measured for the line deployment, suggesting that flow rate may not be responsible for the low recovery and high variation in the results. This could be as a result of accumulation of periphyton or bacterial growth on the surface of the devices, although this would require further work to establish fully. The cage deployment at the River Lambourn for the 7 day deployment had a DBL of 0.081 ± 0.16 cm indicating that a more stagnant environment existed than for the line deployment, which may be responsible for the device only

accumulating 38% of the available U. For the 7 day deployment at the River Lambourn, the plate deployment method accumulated 58% of the available U, which is a 20% improvement on the cage and the line system. Again, this is most likely due to flow dynamics around the devices on the plate. The plate will be aligned parallel to the river flow direction, meaning the surfaces of the DGT devices will be subjected to the highest possible flow. The DBL measured for the cage deployment (deployed for only 3 days) at the River Lambourn was the thickest found in this study at 0.116 ± 0.018 cm. As the recovery for U this particular deployment was 83 ± 10%, it can be assumed that there is no restriction of access, but that the flow rate had been reduced inside the cage. This could be as a result of macro-flora becoming entangled around the cage and therefore reducing the flow rate across the surface of the devices.

The plate deployment methods (deployment numbers 3, 6, 9 and 12 in Tables 7.3 and 7.4) had an accuracy across field sites of 61% at the River Enborne and 70.5% at the River Lambourn, and deployment time of 77.3% for the 3 day deployment and 54.2% for the 7 day deployment. The line deployment methods (deployment numbers 2, 5, 8 and 11 in Tables 7.3 and 7.4) had an average accuracy of 84.2% at the River Enborne and 60.1% at the River Lambourn sites, with an accuracy with deployment time of 77.3% at 3 days and 66.9% at 7 days. The cage deployment methods (deployment numbers 1, 4, 7 and 10 in Tables 7.3 and 7.4) had an average accuracy of 73.5% at the River Enborne and 66.6% at the River Lambourn sites, with a decrease in accuracy in line with the plate deployments, of 83.8% at 3 days and 56.25% at 7 days.

Table 7.4 Summary of the thickness of DBL and TWA concentration of U according to pattern of deployment (see Table 7.3). The table includes the precision and accuracy of the TWA measurements when accounting for the DBL.

Deployment number	Grab water sample (µ g L^{-1})	Thickness of DBL (cm)	TWA* concentration (µ g L^{-1})	Accuracy** (%)	RSD*** of TWA (%)
			River Enborne		
1	0.25	0.074 ± 0.013	0.18 ± 0.02	72 ± 8	8
2	0.25	0.074 ± 0.007	0.18 ± 0.01	72 ± 8	12
3	0.25	0.052 ± 0.020	0.18 ± 0.04	72 ± 16	17
4	0.28	0.074 ± 0.017	0.27 ± 0.04	96 ± 14	35
5	0.28	0.093 ± 0.033	0.21 ± 0.05	75 ± 18	15
6	0.28	0.062 ± 0.019	0.14 ± 0.02	50 ± 7	20
			River Lambourn		
7	0.23	0.116 ± 0.018	0.19 ± 0.02	82 ± 9	11
8	0.23	0.050 ± 0.012	0.22 ± 0.03	96 ± 13	14
9	0.23	0.074 ± 0.013	0.19 ± 0.02	82 ± 9	18
10	0.24	0.081 ± 0.016	0.11 ± 0.05	38 ± 4	51
11	0.24	0.042 ± 0.014	0.09 ± 0.01	38 ± 4	11
12	0.24	0.094 ± 0.015	0.17 ± 0.04	58 ± 8	24

*Caluclated using equation 7.4
** (C_{DGT}/Grab sample) x 100 = %
*** (Standard deviation of triplicate measurements/average reading) x 100 = %

The DBLs found (see Chapter 5) using a plate system to deploy the DGT devices showed a wide variation, from 0.037 to 0.141 cm in the River Enborne, and 0.062 to 0.088 cm in the River Lambourn. The most influential factor in the formation of the DBL at the River Enborne was flow rate. The River Lambourn showed no statistically significant pattern of DBL thickness with flow rate, although a trend was apparent between DBL size and the dissolved organic content of the river; however the size of the DBL could also have been attributable to the large accumulation of macro-flora or periphyton and bacterial growth on the surface of the devices. These large accumulations were only overcome when there was daily removal of the pond weed and algae. This was achieved for the deployments detailed in Chapter 6, where the DBL for the River Lambourn was 0.062 ± 0.004 cm, and in Chapter 3 where the DBL was 0.046 ± 0.006 cm. The trend highlighted in Chapter 5 between the thickness of the DBL and the dissolved organic carbon (DOC) could also partially explain the increased accuracy with the higher DBL in the River Lambourn; the DBL could be acting a zone of dissociation of the U from DOC and a DBL incorporating this dissociation increases the accuracy of the DGT devices. However, this would require further work to quantify.

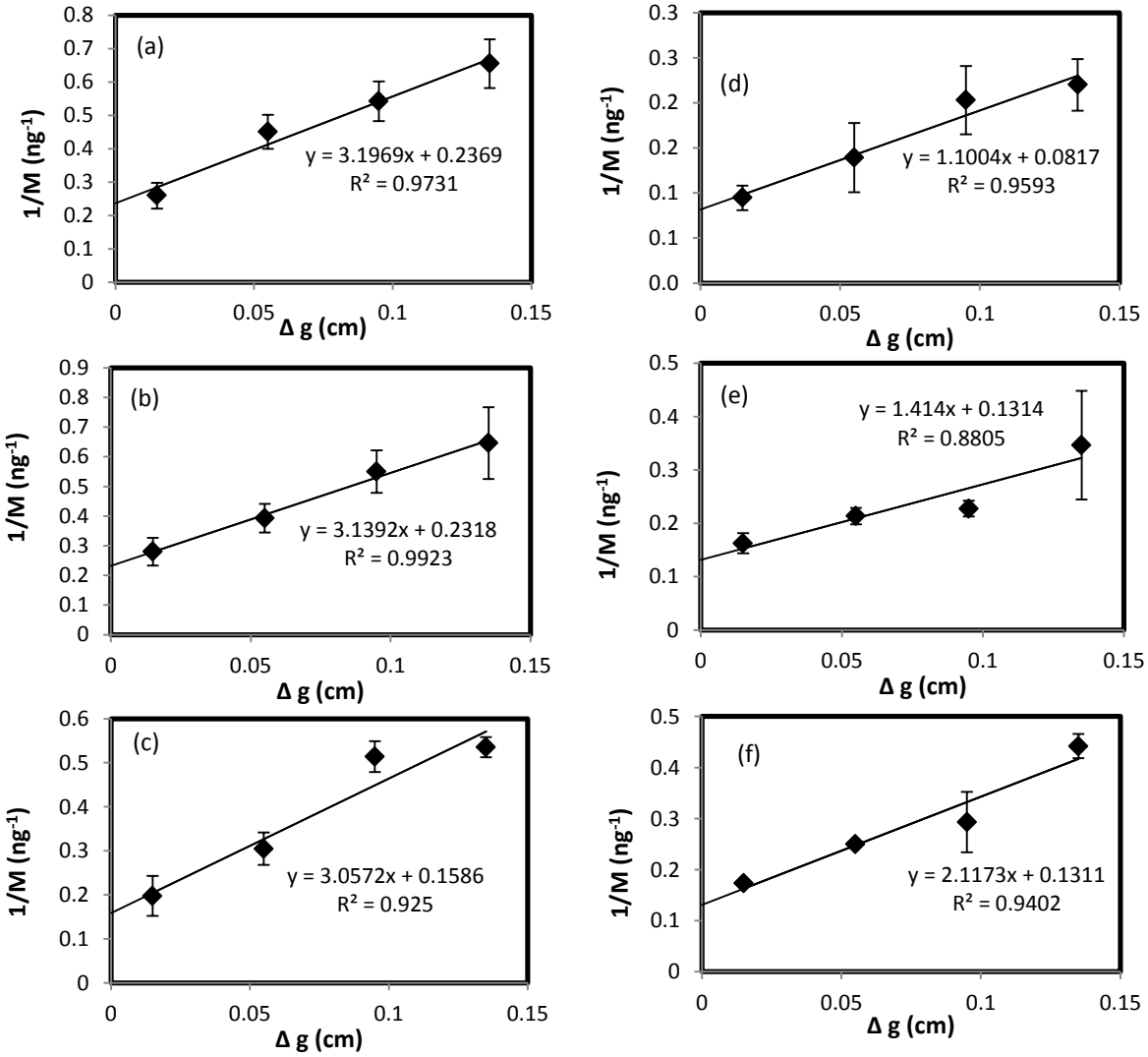

Figure 7.5 Straight line plot of *1/M* vs *Δg* has a slope (*m*) of $1/(DC_{DGT}At)$ and an intercept (*b*) of $\delta/(DC_{DGT}At)$ as per equations 7.4 and 7.5 for the River Enborne, where (a) is 3 d cage; (b) is 3 d line; (c) is 3 d plate; (d) is 7 d cage; (e) is 7 d line; and (f) is 7 d plate; as per the deployments given in Table 7.3. Error bars represent the standard error of triplicate measurements.

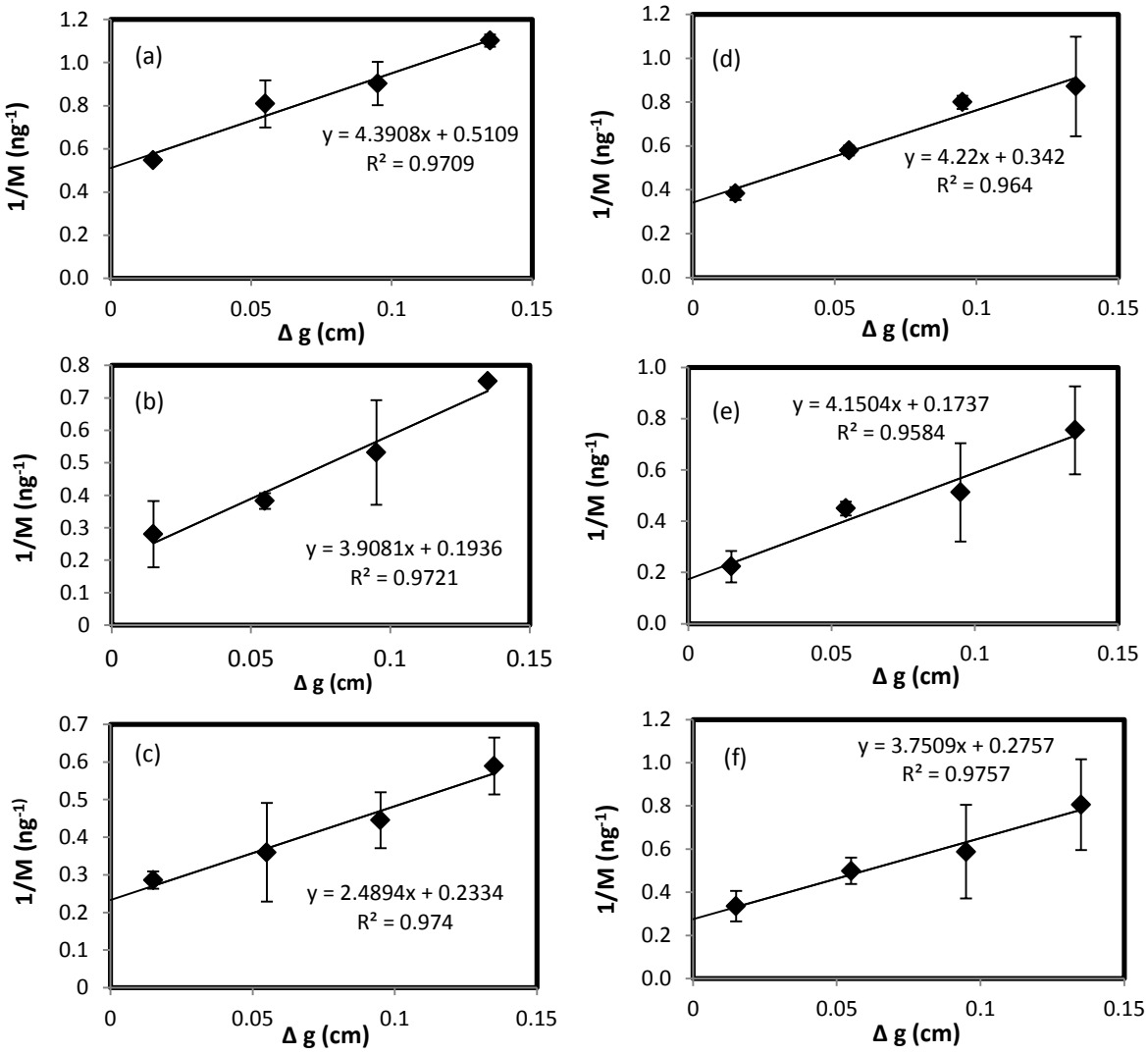

Figure 7.6 Straight line plot of *1/M* vs *Δg* has a slope (*m*) of $1/(DC_{DGT}At)$ and an intercept (*b*) of $\delta/(DC_{DGT}At)$ as per equations 7.4 and 7.5 for the River Lambourn, where (a) is 3 d cage; (b) is 3 d line; (c) is 3 d plate; (d) is 7 d cage; (e) is 7 d line; and (f) is 7 d plate; as per the deployments given in Table 7.3.

7.3.1 Statistical analyses

The Shapiro-Wilk normality test was applied to the DBL measurements from the following data groups to ensure that the parametric one-way ANOVA was appropriate:

It is important to test the normality of the data across these groups to ensure the assumption of the ANOVA that all data is normally distributed is not violated. Shapiro-Wilk has been taken as the test for normality as it is designed for smaller populations ($n < 50$). Where the significance level (P) > 0.05, the data is normally distributed.

All the data sets were found normally distributed, therefore the parametric one-way ANOVA could be used, which detects a variance in the means of populations. The

objective was to observe if the thickness of DBLs between groups (deployment site, deployment time and deployment method) were significantly different i.e. if DGT was to be deployed using 2 different deployment methods, would the DBL be significantly different as a result of the deployment technique? Two deployment sites were chosen to ensure any differences were not unique to one particular location with for instance large quantities of dissolved organic material or flora. The ANOVA test calculates an *F* ratio (ratio between the highest and lowest – or residual – variance) that is then compared to a reference *F* value, which is dependent upon the degrees of freedom (n-1) and the level of confidence (i.e. 95% or 99%). The null hypothesis (that the sample populations are not significantly different) is rejected when the *F* value > that the critical (or reference) *F* value, or if the *P* value is < 0.05 i.e. there is more than a 95% possibility of variance and the null hypothesis rejected. *P* values > 0.05 show that the results are not significant enough to reject the null hypothesis of no difference.

Table 7.5 One-way ANOVA results for DBL size with deployment method

SUMMARY						
Groups	*Count*	*Sum*	*Average*	*Variance*		
Line deployment	4	0.259	0.06475	0.00054		
Plate deployment	4	0.302	0.0755	0.000473		
Cage deployment	4	0.345	0.08625	0.000404		
ANOVA						
Source of Variation	*SS*	*df*	*MS*	*F*	*P-value*	*F crit*
Between Groups	0.000925	2	0.000462	0.978767	0.412462	4.256495
Within Groups	0.004251	9	0.000472			
Total	0.005175	11				

Where SS is the total sum of squares, the df is the degrees of feedom, and MS is the mean of squares calculated using the SS/df.

Table 7.6 One-way ANOVA results for DBL size with deployment time

SUMMARY						
Groups	*Count*	*Sum*	*Average*	*Variance*		
7 days	6	0.446	0.074333	0.000395		
3 days	6	0.46	0.076667	0.000636		
ANOVA						
Source of Variation	*SS*	*df*	*MS*	*F*	*P-value*	*F crit*
Between Groups	1.63E-05	1	1.63E-05	0.031662	0.862325	4.964603
Within Groups	0.005159	10	0.000516			
Total	0.005175	11				

Where SS is the total sum of squares, the df is the degrees of feedom, and MS is the mean of squares calculated using the SS/df.

Table 7.7 One-way ANOVA results for DBL size with deployment location

SUMMARY						
Groups	*Count*	*Sum*	*Average*	*Variance*		
River Enborne	6	0.429	0.0715	0.00019		
River Lambourn	6	0.477	0.0795	0.000806		
ANOVA						
Source of Variation	*SS*	*df*	*MS*	*F*	*P-value*	*F crit*
Between Groups	0.000192	1	0.000192	0.38531	0.548661	4.964603
Within Groups	0.004983	10	0.000498			
Total	0.005175	11				

Where SS is the total sum of squares, the df is the degrees of feedom, and MS is the mean of squares calculated using the SS/df.

It can be seen from Table 7.5 to 7.7 that there is no statistically significant variance in deployment method (Table 7.5), deployment time (Table 7.6) or deployment location (Table 7.7).

Table 7.8 to 7.12 test the accuracy, using a one-way ANOVA, of the TWA results from Table 7.4 against the deployment method (Table 7.8), deployment time (Table 7.9), for 3 day deployments (Table 7.10) and 7 day deployments (7.11) and deployment location (Table 7.12). It can be seen that the only significant effect on the deployment accuracy can be seen in Table 7.10 when examining the effect of a 3 day deployment at two deployment sites. Here the *F* value is 11.8 with a *P* value is 0.03, which demonstrates, with > 95% confidence that between the two deployment locations used here over a 3 day deployment period, there is a significant difference in accuracy between the two field locations. No other relationships can be inferred based on the statistical tests presented here as it is likely that more than one variable influences the accuracy of the devices.

Table 7.8 One-way ANOVA results for TWA accuracy with deployment method

SUMMARY						
Groups	*Count*	*Sum*	*Average*	*Variance*		
Line deployment	4	281	70.25	576.25		
Plate deployment	4	263	65.75	214.9167		
Cage deployment	4	289	72.25	617.5833		
ANOVA						
Source of Variation	*SS*	*df*	*MS*	*F*	*P-value*	*F crit*
Between Groups	88.66667	2	44.33333	0.09441	0.910799	4.256495
Within Groups	4226.25	9	469.5833			
Total	4314.917	11				

Table 7.9 One-way ANOVA results for TWA accuracy with deployment time

SUMMARY						
Groups	*Count*	*Sum*	*Average*	*Variance*		
3 days	6	476.8696	79.47826	89.79357		
7 days	6	354.7619	59.12698	532.5491		
ANOVA						
Source of Variation	*SS*	*df*	*MS*	*F*	*P-value*	*F crit*
Between Groups	1242.523	1	1242.523	3.993052	0.073601	4.964603
Within Groups	3111.714	10	311.1714			
Total	4354.237	11				

Table 7.10 One-way ANOVA results for TWA accuracy at 3 day deployment between deployment sites.

SUMMARY						
Groups	*Count*	*Sum*	*Average*	*Variance*		
River Enborne	3	216	72	0		
River Lambourn	3	260.8696	86.95652	56.71078		
ANOVA						
Source of Variation	*SS*	*df*	*MS*	*F*	*P-value*	*F crit*
Between Groups	335.5463	1	335.5463	11.8336	0.026294	7.708647
Within Groups	113.4216	4	28.35539			
Total	448.9679	5				

Table 7.11 One-way ANOVA results for TWA accuracy at 7 day deployment between deployment sites.

SUMMARY						
Groups	*Count*	*Sum*	*Average*	*Variance*		
River Enborne	3	221.4286	73.80952	539.966		
River Lambourn	3	133.3333	44.44444	144.6759		
ANOVA						
Source of Variation	*SS*	*df*	*MS*	*F*	*P-value*	*F crit*
Between Groups	1293.462	1	1293.462	3.778506	0.12383	7.708647
Within Groups	1369.284	4	342.321			
Total	2662.746	5				

Table 7.12 One-way ANOVA results for TWA accuracy with deployment location

SUMMARY						
Groups	*Count*	*Sum*	*Average*	*Variance*		
River Enborne	6	437.4286	72.90476	216.9687		
River Lambourn	6	394.2029	65.70048	622.7377		
ANOVA						
Source of Variation	*SS*	*df*	*MS*	*F*	*P-value*	*F crit*
Between Groups	155.7049	1	155.7049	0.370856	0.556119	4.964603
Within Groups	4198.532	10	419.8532			
Total	4354.237	11				

7.3.2 Deployment time and method

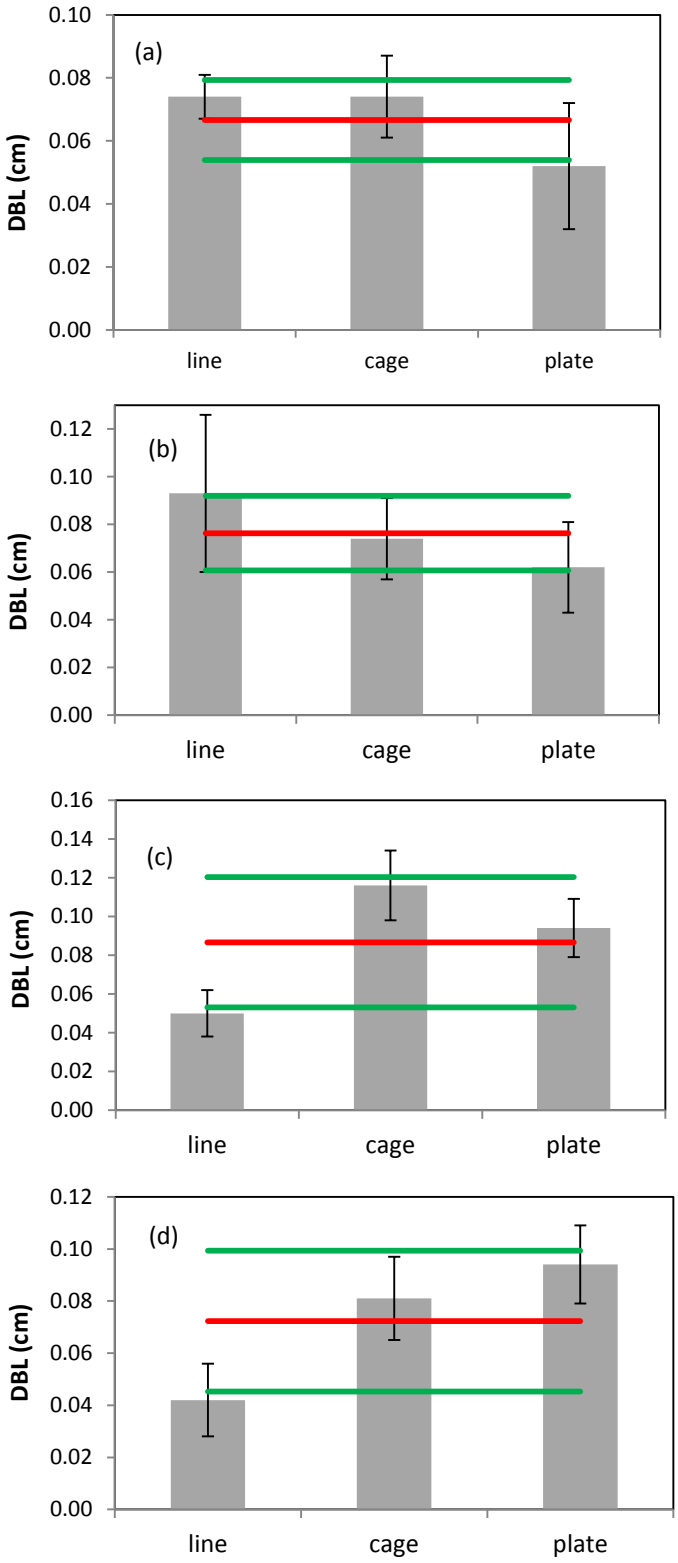

Figure 7.7 Comparison of the thickness of DBLs for each deployment site, grouped by deployment time where a) is the River Enborne 3 d deployment b) is the River Enborne 7 d deployment c) is the River Lambourn 3 d deployment and d) is the River Lambourn 7 d deployment. The error bars represent the standard deviation of the thickness of the DBL (as described in Chapter 3, section 3.1.4), the red lines are the average thickness of the DBL per graph and the green lines are one s.d. of the average thickness of the DBL for the deployment time in each river.

Figure 7.7 shows the variation in DBLs for each deployment method per river per deployment time. Using equation 7.5 and Figures 7.5 and 7.6 (which show equation 7.4) to calculate the DBL, the average of the calculated DBLs for each graph in Figure 7.7 were (a) 0.067 ± 0.012 cm, (b) 0.076 ± 0.015 cm, (c) 0.086 ± 0.034 cm and (d) 0.072 ± 0.027 cm. All the deployment methods, within error (± 1 standard deviation of the mean) lie in these ranges and so there appears to be little difference in the size of the DBL with deployment time. The one-way ANOVA performed on the data (Tables 7.6) to assess if the variance in means between the two deployment times tested here (3 d and 7 d) are significant shows no significant difference in DBL size when the DGT devices are deployed for either 3 d or 7 d. Deployment time was important to assess because for metals present in the environment at low concentrations, a better precision and accuracy can be obtained the more metal is accumulated onto the resin in the DGT devices. However, the longer the devices are deployed in the field the larger the error associated with biofilm formation. This could also include growth of bacterial mats and/or periphyton. No assumptions can be made on the impact of time on the DBL, as the only significant variation between time and the DBL thickness (Table 7.6) or TWA accuracy (Tables 7.9-7.11) is that there is a difference between the accuracy of the results at two deployment sites over 3 days (Table 7.10).

The line deployments performed better in the River Lambourn than the River Enborne because the latter has a higher flow regime. It appears that the accumulation of macro-flora that affected other deployment methods are not as important for the line deployments and the exposure to a faster flowing body of water is more effective for this method in achieving lower DBLs. The line deployments by Torre *et al*. [13] also had a lower DBL thicknesses (0.031 cm) than other reported deployment methods (detailed in Table 7.1). Murdock *et al*. [14] found that deploying the DGT devices on a line in a lake setting did not affect the accumulation of caesium. In this case the DBL was not measured but was assumed not to influence the DGT performance as the concentration of caesium found using the DGT devices was in close agreement with that measured in grab water samples. The data presented in Table 7.5 does not show any significant variation in DBL size between deployment methods.

The cage and the plate deployment DBLs were higher than the line deployments, for the River Lambourn with average measured DBLs of 0.099, 0.046 and 0.094 cm for the cage, line and plate deployments respectively. This difference in DBL for each of these deployments at this site is most likely as a result of the influence the larger geometries of the cage and plate system. This, particularly in the case of the River

Lambourn which has been shown in previous studies to be affected by large accumulations of macro-flora (Chapters 4 and 5), could encourage entanglement of vegetation around the devices and so obstruct the flow of water around the DGT devices. The average DBLs in the River Enborne of 0.074, 0.084 and 0.057 cm for the cage, line and plate deployment methods respectively demonstrates that the plate deployment on average, gives a smaller DBL. The River Enborne is less affected by vegetation accumulations in the short term (< 7d as shown in chapter 5), and the DBL has been previously shown to be governed by flow velocity at this site (chapter 5). Deploying the DGT samplers between two perspex plates allows for the sampling area of the devices to be aligned parallel to the direction of flow. This would allow for the highest fluid velocity over the DGT sampling areas. No significant differences were found however and the discussion here focuses on trends in the data.

The British Standard, BS EN ISO 5667-23:2011 [27] recommends that passive samplers are deployed in a manner to protect against damage that could be potentially caused by fast flowing waters or storm events. This is usually interpreted as deploying the samplers inside a protective cage, as per the EPA guidance on monitoring organic contaminants [28]. There is no clear advantage to deploying the devices using one particular method as found in this study. Deployment methods will in part depend upon the nature of the deployment site, length of deployment and the potential for changes in water flow. For instance, at a lake [13] the potential for sampler damage due to storm events would be lower than a fluvial setting. This makes the use of a line deployment suitable in this application. In the case of the long-term study (Chapter 5) where it is highly likely at some point the devices will be deployed during higher flow or storm activity, then a protective cage might be more appropriate. The plate technique presents a convenient method of ensuring all DGT devices are exposed to high fluid velocity as they are able to be aligned parallel to the predominant water flow direction.

7.4 Conclusions

This study tested the supposition that the deployment method and deployment time influenced the thickness of the DBL and hence the accuracy of the DGT devices. Three deployment methods were trialled, based on published studies or recommendations in Standards. The thickness of DBLs showed no statistical variation between the deployment sites, deployment times and deployment techniques. The accuracy (amount accumulated by DGT as a percentage of the dissolved U measured in grab water samples) did not vary greatly over the study, except for two instances when

the accuracy reduced to 47% and 36% for the line and cage systems respectively in the River Lambourn. This was attributed to biofouling by macro-flora, as the devices were shown to be working effectively as the plate deployments showed an accuracy of 71%. It is unlikely that any one factor affects the thickness of the DBL and that the deployment technique to be used should be determined on a case by case basis. The deployment time chosen would depend on the objectives of the study i.e. monitoring water quality as part of a regulatory scheme but would be unlikely to exceed 7 days (the point in this trial where accuracy decreased in the River Lambourn). What this study demonstrated is that the thickness of the DBL should be measured each time a device is deployed in the field as natural systems are complex with several factors always working together to influence the effectiveness of passive sampling technique.

7.5 References

[1] N. Roig, M. Nadal, J. Sierra, A. Ginebreda, M. Schuhmacher, J.L. Domingo, Novel approach for assessing heavy metal pollution and ecotoxicological status of rivers by means of passive sampling methods, Environment International, 37 (2011) 671-677.

[2] I.J. Allan, J. Knutsson, N. Guigues, G.A. Mills, A.M. Fouillac, R. Greenwood, Chemcatcher (R) and DGT passive sampling devices for regulatory monitoring of trace metals in surface water, Journal of Environmental Monitoring, 10 (2008) 821-829.

[3] R. Buzier, M.H. Tusseau-Vuillemin, J.M. Mouchel, Evaluation of DGT as a metal speciation tool in wastewater, Science of the Total Environment, 358 (2006) 277-285.

[4] W. Davison, G. Fones, M. Harper, P. Teasdale, and H. Zhang, Dialysis, DET and DGT: *In situ* diffusional techniques for studying water, sediments and soils., in: J. Buffle, Horvai, G. (Ed.) *In situ* monitoring of aquatic systems: chemical analysis and speciation, John Wiley & Sons Ltd, 2000, pp. 74.

[5] J. Gimpel, H. Zhang, W. Davison, A.C. Edwards, *In situ* trace metal speciation in lake surface waters using DGT, dialysis, and filtration, Environmental Science & Technology, 37 (2003) 138-146.

[6] M.A. French, H. Zhang, J.M. Pates, S.E. Bryan, R.C. Wilson, Development and performance of the diffusive gradients in thin-films technique for the measurement of technetium-99 in seawater, Analytical Chemistry, 77 (2005) 4.

[7] W.J. Li, F.Y. Wang, W.H. Zhang, D. Evans, Measurement of stable and radioactive cesium in natural waters by the diffusive gradients in thin films technique with new selective binding phases, Analytical Chemistry, 81 (2009) 5889-5895.

[8] J.G. Panther, P.R. Teasdale, W.W. Bennett, D.T. Welsh, H.J. Zhao, Titanium dioxide-based DGT technique for *in situ* measurement of dissolved reactive phosphorus in fresh and marine waters, Environmental Science & Technology, 44 (2010) 9419-9424.

[9] S. Mason, R. Hamon, H. Zhang, J. Anderson, Investigating chemical constraints to the measurement of phosphorus in soils using diffusive gradients in thin films (DGT) and resin methods, Talanta, 74 (2008) 779-787.

[10] K.W. Warnken, H. Zhang, W. Davison, Accuracy of the diffusive gradients in thin-films technique: Diffusive boundary layer and effective sampling area considerations, Analytical Chemistry, 78 (2006) 3780-3787.

[11] C.M. Hutchins, J.G. Panther, P.R. Teasdale, F. Wang, R.R. Stewart, W.W. Bennett, H. Zhao, Evaluation of a titanium dioxide-based DGT technique for measuring inorganic uranium species in fresh and marine waters, Talanta, 97 (2012) 550-556.

[12] W.W. Bennett, P.R. Teasdale, J.G. Panther, D.T. Welsh, D.F. Jolley, New diffusive gradients in a thin film technique for measuring inorganic arsenic and selenium(IV) using a titanium dioxide based adsorbent, Analytical Chemistry, 82 (2010) 7401-7407.
[13] M.C.A.-D.l. Torre, P.-Y. Beaulieu, A. Tessier, In situ measurement of trace metals in lakewater using the dialysis and DGT techniques, Analytica Chimica Acta, 418 (2000) 53-68.
[14] C. Murdock, M. Kelly, L.-Y. Chang, W. Davison, H. Zhang, DGT as an *in situ* tool for measuring radiocesium in natural waters, Environmental Science & Technology, 35 (2001) 4530-4535.
[15] E. Uher, M.-H. Tusseau-Vuillemin, C. Gourlay-France, DGT measurement in low flow conditions: diffusive boundary layer and lability considerations, Environmental Science: Processes & Impacts, (2013).
[16] J. Gimpel, H. Zhang, W. Hutchinson, W. Davison, Effect of solution composition, flow and deployment time on the measurement of trace metals by the diffusive gradient in thin films technique, Analytica Chimica Acta, 448 (2001) 93-103.
[17] Z. Dragun, B. Raspor, V. Roje, The labile metal concentrations in Sava River water assessed by diffusive gradients in thin films, Chemical Speciation and Bioavailability, 20 (2008) 33-46.
[18] J.L. Levy, H. Zhang, W. Davison, J. Galceran, J. Puy, Kinetic signatures of metals in the presence of Suwannee River fulvic acid, Environmental Science & Technology, 46 (2012) 3335-3342.
[19] P. Divis, H. Docekalova, V. Smetkova, Gel techniques for *in situ* measurement in natural waters, soils and sediments, Chem. Listy, 99 (2005) 640-646.
[20] H. Zhang, W. Davison, Direct *in situ* measurements of labile inorganic and organically bound metal species in synthetic solutions and natural waters using diffusive gradients in thin films, Analytical Chemistry, 72 (2000) 4447-4457.
[21] H. Zhang, W. Davison, Diffusional characteristics of hydrogels used in DGT and DET techniques, Analytica Chimica Acta, 398 (1999) 329-340.
[22] Tables of Physical & Chemical Constants in: 2.2.3 Viscosities, Kaye & Laby Online, 2005.
[23] S. Kerisit, C. Liu, Molecular simulation of the diffusion of uranyl carbonate species in aqueous solution, Geochimica Et Cosmochimica Acta, 74 (2010) 4937-4952.
[24] H.P. Jarvie, C. Neal, M.D. Jürgens, E.J. Sutton, M. Neal, H.D. Wickham, L.K. Hill, S.A. Harman, J.J.L. Davies, A. Warwick, C. Barrett, J. Griffiths, A. Binley, N.

Swannack, N. McIntyre, Within-river nutrient processing in Chalk streams: The Pang and Lambourn, UK, Journal of Hydrology, 330 (2006) 101-125.
[25] T.J. Marsh, M.L. Lees, Hydrometric Register and Statistics 1996-2000. Hydrological data UK series., in, Centre for Ecology and Hydrology / British Geological Survey, Wallingford, 2003, pp. 210.
[26] R.M.S. Smith, D.J. Evans, H.S. Wheater, Evaluation of two hybrid metric-conceptual models for simulating phosphorus transfer from agricultural land in the river enborne, a lowland UK catchment, Journal of Hydrology, 304 (2005) 366-380.
[27] B.S. Institution, Water quality - sampling, in: Guidance on passive sampling in surface waters, British Standards Publication, London, 2011, pp. 23.
[28] U.S.E.P. Agency, Guidelines for using passive samplers to monitor organic contaminants at superfund sediment sites, in: Sediments assessment and monitoring sheet # 3, US EPA, U.S., 2012, pp. 30.

Chapter 8: Binding kinetics of uranium with the DGT resin gel layer

8.1 Introduction

Diffusive gradients in thin films (DGT) has been used for the *in situ* measurements of trace metals [1] and nutrients [2] as part of environmental monitoring schemes [3]; to measure kinetic exchange between metals and organics [4] and to discriminate between organic and inorganically bound metals in aquatic systems [5]. Dissolved organic matter (DOM) is important in the transport, fate and bioavailability of trace metals [6] and it is therefore important to understand metal-organic interactions. As DGT is used as a tool to approximate the bioavailability of metals in aquatic environments it is essential to fully investigate the interactions between metal speciation and the device. In order for the DGT equation to hold, the theory relies on a number of assumptions including that there are no kinetic limitations to the uptake of the metal (discussed in Chapter 9); that saturation effects (i.e. the front portion of the resin layer has an excess of binding sites) are negligible [7]; that the resin layer acts as a perfect planar sink [8] and has a dissolved metal concentration of zero at the resin layer interface [9]. The latter assumption holds true if the system in which the DGT is deployed is fully labile. In the presence of organics where there are partially labile complexes present, there may be some diffusion of the metal-ligand complex into the resin layer because they may not fully dissociate at the resin layer surface. This can provide information on the lability of the metal complexes formed and can provide variability in the calculation of dissociation kinetics of the metal ligand complexes when examining the apparent diffusive boundary layer (ADBL), thereby making it important to determine (described in Chapter 9). It has been indicated in previous chapters (see Chapter 5) that the presence of dissolved organic ligands in natural waters may affect the rate of uptake of the metals by DGT through complexation and subsequent slow dissociation kinetics [10]. The effect of organic complexation may be manifest by extending the diffusive boundary layer (DBL) beyond the thickness that should exist for the degree of advection present during the deployment [11].

Previous studies have used DGT to assess lability of trace metals and subsequently the bioavailability. Work undertaken by Mongin *et al*. [9] analysed the lability of trace metals as a measure of their penetration parameter into the resin phase. They suggested that without considering the penetration depth of a metal ion complex into the resin layer, DGT often underestimated the concentration of metal ions in solution. By considering the penetration parameter, partially labile complexes that were

unable to dissociate in the diffusive gel layer are included in the calculations, thereby rendering some inert species more labile than previously assumed. This acts to increase the degree of lability and therefore the flux of metal to the DGT device.

Penetration effects have been shown previously for other metal ligand complexes for instance cadmium-nitrilotriacetic acid (Cd-NTA) [9], nickel-nitrilotriacetic acid (Ni-NTA) [12], nickel-fulvic acid (Ni-FA) [12], and for free metals (Mn, Co, Ni, Cu, Cd and Pb) [7] by employing DGT devices with multiple resin layers. It was found that for free metals the penetration was generally negligible [7], but for the complexed metal, particularly for those complexes with a very low dissociation rate (i.e. Ni-NTA) the metal complex diffused through the front resin layer, fully dissociating in the back layer [12]. It is not unreasonable to assume that the metal-ligand complex will continue diffusing through the resin layer if it is partially labile, as the binding agent is held within the same hydrogel used in the diffusion membrane [9, 13].

If the penetration parameter is considered, then the DGT is exposed to a greater proportion of the metal in solution due to increased lability of any partially labile metal-organic complexes, thereby increasing the lability of the overall system [14].

Uranium (U) complexes with both organic and inorganic ligands (anions and cations). Humic substances (HS) comprise of fulvic acid (FA), humic acid (HA) and humin which represent 40-99% of the DOC in natural waters and are important complexing agents for U in this environment [10]. FA reduces the activity of U thereby reducing its bioavailability. Binding of U with HA is stronger than with FA and is more dependent on pH [10, 15]. As HA is increasingly soluble with increasing pH, this study centres on U binding with HA in alkaline waters with a pH similar to the field sites used in this thesis. It is important to assess the potential for partially labile U complexes to the overall flux to the DGT because HS are generally thought to decrease the bioavailability of metals. This is particularly so for U as the activity of the ion decreases in the presence of HA, however, if these complexes can contribute to the flux of metals to sensors such as DGT (which are used to mimic uptake by biota [16]) then it could indicate that these complexes are more bioavailable than previously assumed.

In this series of experiments, resin capacity (or availability) was not deemed a determining factor in the accumulation of U because of the results reported in Chapter 4. This showed, with mass accumulation over time experiments, that there was no limitation over 5 days in the laboratory or between 4 – 7 days in the field. This set of experiments was only conducted under laboratory conditions for 24 h, and in the field

for 3 days. The structure and operation of the DGT has been previously discussed in Chapter 3.

8.2 Model description

The following model was described by Levy *et al.* [7]; the model derivations can be found therein. Metal-ligand (in this instance the resin is the ligand) undergoes a first-order or *pseudo*-first-order dissociation [10], where in the instance of the metal resin binding, $k_{a,R}$ and $k_{d,R}$ are the association (or formation) and dissociation rate constants respectively for the metal (*M*) binding to the resin (*R*) [7, 14]:

$$M + R \underset{k_{d,R}}{\overset{k_{a,R}}{\rightleftharpoons}} MR \qquad \text{Equation 8.1}$$

R, which represents the binding sites on the resin is assumed to be immobile and homogeneously distributed within the resin disk [14]. The DGT theory relies on the complexant concentration exceeding the metal solution concentration, and so equation 8.1 is assumed to be rapid and the net reaction far to the right and irreversible. The resin (in this instance Metsorb^{TM}) is also assumed to out compete other ligands (*Li*) in solution:

$$ML_i + Metsorb^{TM} \rightarrow MMetsorb^{TM} + L_i \qquad \text{Equation 8.2}$$

It is assumed that the metal-organic complex does not form ternary complexes with the resin, and that it has to fully dissociate in order to bind [9]. In steady state conditions, the diffusion of the free metal into the resin can be described using equation 8.3 below which accounts for the diffusion coefficient of the metal in the resin gel layer ($D_{M,R}$) (cm^2 s^{-1}) (which in this model is taken as equal to that within the diffusive gel layer, as both are comprised of the same hydrogel with similar pore sizes), association and dissociation, as per equation 8.1, and C_M is the concentration of free metal (*M*), C_{MR} is the concentration (*C*) of metal (*M*) bound to the resin (*R*), (*x*) describes a spatial position in the area of the exposed plane in the resin gel and $\frac{\partial[m]}{\partial t}$ is the changing mass accumulated with time (*t*),

$$\frac{\partial[M]}{\partial t} = 0 = D_{M,R}\frac{\partial^2 C_M}{\partial x^2} - k_{a,R}C_M + k_{d,R}C_{MR} \qquad \text{Equation 8.3}$$

If an excess of binding sites is assumed (as per equation 8.2), then the concentration of resin sites (C_R) is be taken as constant then:

$$k_{d,R}C_{MR} \rightarrow k_{a,R}C_R C_M \qquad \text{Equation 8.4}$$

Where the dissociation (as per equation 8.2) is negligible and the metal binding to the resin sites is not in equilibrium with dissociation (i.e. equation 8.4 sits far to the right thereby indicating no resin saturation effect) equation 8.3 reduces to:

$$\frac{d^2C_M}{dx^2} = \frac{k\prime_{a,R}}{D_M}C_M = \frac{C_M}{{\lambda_M}^2} \qquad \text{Equation 8.5}$$

and where $k'_{a,R} = k_{a,R}C_R$, or the conditional effective association rate constant for the metal with the resin, a penetration parameter (λ_M) (μm) can be found which is related to the mean distance of diffusion necessary for all metal to be bound to the resin (the point at which C_M in the resin = 0) from:

$$\lambda_M = \sqrt{\frac{D_{M,R}}{k\prime_{a,R}}} \qquad \text{Equation 8.6}$$

Accounting for any boundary layer conditions at the resin-diffusive layer interface is important particularly when comparing the accumulation of metal in each of the resin layers. So by integrating the boundary layer conditions detailed in equation 8.3 $\left(\left(\frac{\partial C_M}{\partial x}\right)_{x=0} = 0\right)$ and incorporating the resin thickness (r) (mm) ($C_M(x = r) = C_M^r$), the concentration at the resin boundary layer (C_M^r) can be described using:

$$C_M(x) = C_M^r \frac{cosh\left(\frac{x}{\lambda_M}\right)}{cosh\left(\frac{r}{\lambda_M}\right)} \qquad \text{Equation 8.7}$$

Assuming that the resin phase acts as a constant sink for the metal, allowing a steady state to be reached and steady free metal concentrations in the resin then accumulation time, t (s), must be accounted for:

$$C_{MR}(x,t) = k'_{a,R}C_M(x)t = k'_{a,R}C_M^r \frac{cosh\left(\frac{x}{\lambda_M}\right)}{cosh\left(\frac{r}{\lambda_M}\right)}t \qquad \text{Equation 8.8}$$

λ_M is the parameter of interest for calculations of penetration depth of the metal into the resin, and this in turn can be used to evaluate the association kinetics between the metal and resin using equation 8.6. This is determined here experimentally by calculating the ratio of accumulated metal in each of the resin layers used in the experiments (2 or 3 layers).

If using 2 resin layers of equal thickness, the ratio of the number of moles (*M*) of metal accumulated in the front layer (n_f) $\left(\frac{r}{2} < x < r\right)$to the number of moles of metal accumulated in the back resin layer (n_b) $\left(0 < x < \frac{r}{2}\right)$ can be used to calculate λ_M:

$$n_f = tAk'_{a,r}\frac{C_M^r}{cosh\left(\frac{r}{\lambda_M}\right)}\lambda_M\left[sinh\left(\frac{r}{\lambda_M}\right) - sinh\left(\frac{r}{2\lambda_M}\right)\right] \quad \text{Equation 8.9}$$

$$n_b = tAk'_{a,r}\frac{C_M^r}{cosh\left(\frac{r}{\lambda_M}\right)}\lambda_M\left[sinh\left(\frac{r}{2\lambda_M}\right)\right] \quad \text{Equation 8.10}$$

the ratio of equation 8.9: equation 8.10 gives:

$$\frac{n_f}{n_b} = \frac{sinh(\frac{r}{\lambda_M})}{sinh(\frac{r}{2\lambda_M})} - 1 = 2cosh\left(\frac{r}{2\lambda_M}\right) - 1 \quad \text{Equation 8.11}$$

where *r* is the total thickness of the resin layer (front plus back layer) and *A* is the resin surface area (cm^2) or sampling window.

Calculating λ_M using the model for using three resin layers of equal thickness can be achieved by relating mass accumulated in each resin slice. The metal accumulated in the front layer (n_f) $\left(\frac{2r}{3} < x < r\right)$, middle layer ($n_m$) $\left(\frac{r}{3} < x < \frac{2r}{3}\right)$ and the back resin layer (n_b) $\left(0 < x < \frac{r}{3}\right)$ is given by:

$$n_f = tAk'_{a,r}\frac{C_M^r}{cosh\left(\frac{r}{\lambda_M}\right)}\lambda_M\left[sinh\left(\frac{r}{\lambda_M}\right) - sinh\left(\frac{2r}{3\lambda_M}\right)\right] \quad \text{Equation 8.12}$$

$$n_m = tAk'_{a,r}\frac{C_M^r}{cosh\left(\frac{r}{\lambda_M}\right)}\lambda_M\left[sinh\left(\frac{2r}{3\lambda_M}\right) - sinh\left(\frac{r}{3\lambda_M}\right)\right] \quad \text{Equation 8.13}$$

$$n_b = tAk'_{a,r} \frac{C_M^r}{cosh\left(\frac{r}{\lambda_M}\right)} \lambda_M \left[sinh\left(\frac{r}{3\lambda_M}\right)\right]$$ Equation 8.14

From equations 8.12 to 8.14 the ratio of moles of metal accumulated in each resin layer is given using the following:

$$\frac{n_m}{n_b} = \frac{sinh\left(\frac{2r}{3\lambda_M}\right) - sinh\left(\frac{r}{3\lambda_M}\right)}{sinh\left(\frac{r}{3\lambda_M}\right)}$$ Equation 8.15

$$\frac{n_f}{n_m} = \frac{sinh\left(\frac{r}{\lambda_M}\right) - sinh\left(\frac{2r}{3\lambda_M}\right)}{sinh\left(\frac{2r}{3\lambda_M}\right) - sinh\left(\frac{r}{3\lambda_M}\right)}$$ Equation 8.16

$$\frac{n_f}{n_b} = \frac{sinh\left(\frac{r}{\lambda_M}\right) - sinh\left(\frac{2r}{3\lambda_M}\right)}{sinh\left(\frac{r}{3\lambda_M}\right)}$$ Equation 8.17

$$\frac{n_f}{n_{Total}} = \frac{sinh\left(\frac{r}{\lambda_M}\right) - sinh\left(\frac{2r}{3\lambda_M}\right)}{sinh\left(\frac{r}{\lambda_M}\right)}$$ Equation 8.18

Using any of equations 8.15–8.18 will give the λ_M. This study compares each of the methods to ensure consistency within the data and establish errors in calculating λ_M.

The penetration depth of the metal ligand into the resin layer (λ_M) accounts for the slope of the hyperbolic tangent ($y = tanh(x)$) to the profile shown in the insert of Figure 8.1 below. In the figure (i), (ii) and (iii) represent the profiles of the metal penetration through the resin layer. Slope (iii) represents the tangent to the profile at the resin boundary layer (x = r):

$$\frac{dc_M(x=r)}{dx} = \frac{C_M^r}{\lambda_M} tanh\left(\frac{r}{\lambda_M}\right)$$ Equation 8.19

To find the penetration depth, the x intercept of the linear model (x = r) through the resin (Figure 8.2 c ii) can be used. Using the slope (the tangent of the slope of x = r) above (equation 8.19) the equation of the straight line (figure 8.2 c ii) can be calculated using:

$$C_M^{linear}(x) - C_M^r = \frac{C_M^r}{\lambda_M}(x - r)$$ Equation 8.20

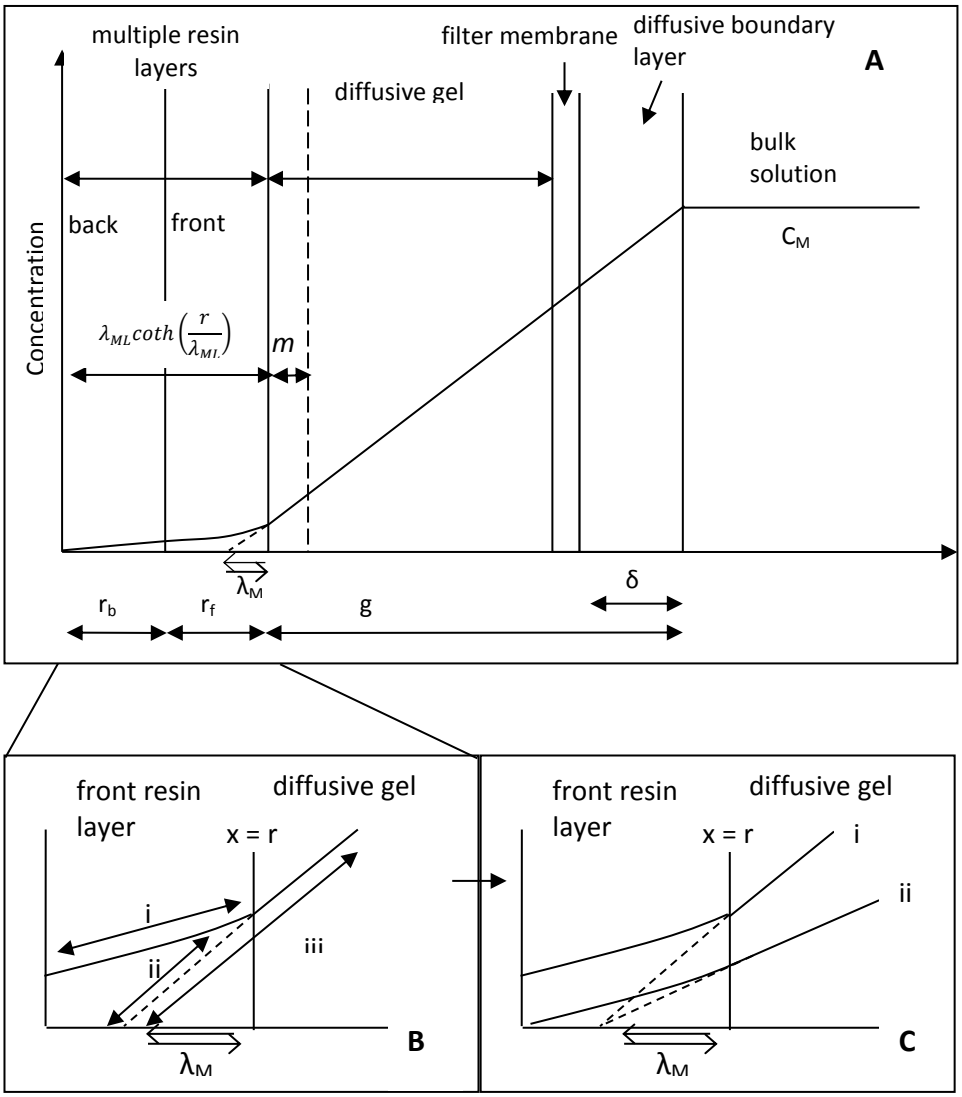

Figure 8.4 The concentration profile of metal ion *M* in a DGT device consisting of a resin with (**A**) defined front (*f*) and back (*b*) region (with a thickness (*r*) *rf* and *rb* respectively) and a diffusion layer (*g*) consisting of a diffusive gel, a filter membrane and the diffusive boundary layer (with thickness δ). The value λ_M is the mean distance that metal can penetrate into a resin layer and is defined as $\lambda_M coth\left(\frac{r}{\lambda_M}\right)$*;* shown more clearly in the insert (**B**): (i), (ii) and (iii) refer to the profiles used in the calculation of the penetration parameter and $x = r$ is the resin diffusive gel interface (described by equations 8.19 and 8.20) and in the second insert (**C**) (i) represents a small *g* and (ii) a large *g*. It demonstrates that the distance the metal travels through the resin layer is irrespective of the diffusive layer thickness with all the dashed lines converging at point $x = r - \lambda_M coth\left(\frac{r}{\lambda_M}\right)$. *m* (in insert **A**) is the thickness of the reaction layer ($m\ tanhh\ (\frac{g}{m})$) (adapted from Levy *et al*. [7] and Uribe *et al*. [13]).

If $C_M^{linear}(x)$ = 0 then the effective penetration depth can be given as:

$$x = r - \lambda_M \coth\left(\frac{r}{\lambda_M}\right) \qquad \text{Equation 8.21}$$

$\lambda_M coth\left(\frac{r}{\lambda_M}\right)$ is the minimum thickness of the resin layer at which the free metal concentration falls to zero, if a linear concentration profile is assumed. If this distance is greater than the resin layer thickness (> r), this indicates that the metal ions reach the bottom of the resin layer without fully binding to the resin sites (C_M > 0 at x = 0). When the metal resin association constants are fast or the resin layer is sufficiently thick $r \gg \lambda_M, coth\left(\frac{r}{\lambda_M}\right) \approx 1$ then λ_M is simply the distance of penetration of the metal ion before being fully bound to the resin sites.

The steady state concentration profile (as shown in Figure 8.1, insert **B**, line iii) is just a straight line from the resin boundary layer ($C_m(x = r) = C_M^r$) until ($C_m(x = r + g) = C_M^*$) and can be related to the number of moles of the metal ion arriving by diffusion and the consumption of metal by the resin. So the DGT equation (equation 8.24) can be used for the accumulated of moles with g being replaced with an 'effective' gel thickness that accounts for the penetration depth of the metal into the gel layer given by $g + \lambda_M coth\left(\frac{r}{\lambda_M}\right)$ (from Levy *et al.* [7]):

$$n(t) = A\frac{D_M(C_M^* - C_M^r)}{g}t = \frac{AD_M C_M^* t}{g}\frac{tanh\left(\frac{r}{\lambda_M}\right)}{\frac{\lambda_M}{g} + tanh\left(\frac{r}{\lambda_M}\right)} = \frac{AD_M C_M^* t}{g + \lambda_M coth\left(\frac{r}{\lambda_M}\right)} \qquad \text{Equation 8.22}$$

Equation 8.22 describes the use of the penetration parameter within the DGT equation, the effects of which on the DGT calculations are discussed later.

8.3 Experimental

Chemicals were of analytical grade or better and supplied by Fisher Scientific (Loughborough, UK), unless otherwise specified. Milli-Q (ultra-pure) water (> 18.2 MΩ cm, Millipore, Watford, UK) was used as the laboratory water. All U ICP-MS standards and experimental working solutions were prepared in low density polyethylene (LDPE) or polystyrene (PS) containers with polypropylene lids (PP) from a 1000 mg L^{-1} in 2% HNO_3 (Spex Certiprep, Fisher Scientific) U stock solution unless otherwise stated. The ICP-MS internal standard was prepared from a 1000 mg L^{-1} in 2% HNO_3 (Spex Certiprep) bismuth stock solution. These solutions were adjusted to a given pH by addition of either 1 M HNO_3 or 1 M NaOH, and to a given ionic strength by addition of $NaNO_3$, with the pH monitored throughout experiments. Solutions were equilibrated with atmospheric CO_2 for 24 h before use unless otherwise specified. All readings were undertaken in triplicate with containers open to the atmosphere to ensure continuing equilibration with the atmospheric pCO_2 (i.e. to ensure a constant inorganic carbon concentration throughout the experiments). All plastic apparatus was soaked for 24 h in 10% HNO_3 and rinsed three times in Milli-Q water prior to use.

8.3.1 Analysis of DGT devices

The Metsorb^{TM}-DGT devices were prepared as per Chapter 3, after Zhang and Davison [5], with either 1, 2 or 3 resin layers. After exposure, the Metsorb^{TM} and MnO_2 binding gels were removed from the DGT devices and eluted (48 h) with 1 M H_2O_2/1 M HNO_3 (2 mL) solution (100 mL made by combining 90 mL 1.1 M HNO_3 and 10 mL 35% H_2O_2). The eluents were then diluted 10 fold with Milli-Q water prior to instrumental analysis by ICP-MS using an Agilent 7500ce series instrument (Agilent Technologies Inc., Japan), as per Chapter 3.

8.3.2 Calculation of time-weighted average concentrations

The concentration of U measured by the ICP-MS in µg L^{-1} from the eluent was multiplied by the dilution factor (×10) to give the U concentration (*Ce*). The absolute mass (*M*) of the U in the resin gel was then calculated using equation 8.23, where *M* is calculated taking into account the gel volume (*Vg*, cm^3), the eluent volume (*Ve*, mL), the measured concentration of U in the eluent (*Ce*, ng mL^{-1}) and the elution factor (*fe*) [5], which was reported in Chapter 4 as 0.84 .

$$M = \frac{Ce(Vg+Ve)}{fe}$$ Equation 8.23

M from equation 8.23 is then used to calculated the TWA concentrations (equation 8.24) where the concentration (C_{DGT}, ng mL^{-1}) was calculated using the mass of the analyte in the binding gel (*M*, ng), the thickness of the diffusive path length (diffusive gel and filter membrane) (*Δg*, cm), the diffusion coefficient of the analyte (*D*, cm^2 s^{-1}) (as determined at different pHs for U by Hutchins *et al.* [17]), deployment time (*t*, s) and the area of the sample exposure window (*A*, cm^2).

$$C_{DGT}=\frac{M\Delta g}{DtA}$$ Equation 8.24

The diffusion coefficients (*D*) were corrected for temperature (*T*, ^oC) using the Stokes-Einstein equation (equation 8.25) [18] and the viscosity of water (*η*, mPa s) [19]:

$$\frac{D_1\eta_1}{T_1} = \frac{D_2\eta_2}{T_2}$$ Equation 8.25

The diffusive boundary layer (δ) thickness was calculated using equation 8.26 after Warnken *et al.* [20]. A straight line plot of *1/M* vs *Δg* has a slope (*m*) of $1/(DC_{DGT}At)$ and an intercept (*b*) of $\delta/(DC_{DGT}At)$. The intercept (*b*) divided by the slope (*m*) of this plot gives the diffusive boundary layer thickness δ, as per equation 8.27.

$$\frac{1}{M} = \frac{\Delta g}{DC_{DGT}At} + \frac{\delta}{DC_{DGT}At}$$ Equation 8.26

$$\delta = \frac{b}{m}\left(\frac{D_M^W}{D_M^{gel}}\right)$$ Equation 8.27

where D_M^W and D_M^{gel} represent the diffusion coefficients of U in water and in the diffusive gel respectively. The thickness of the DBL was included in the C_{DGT} calculations for the field trials. The sampling area (*A*) was 3.8 cm^2 instead of the 3.14 cm^2 used in the laboratory trials, as described by Warnken *et al.* [20] and discussed in Chapter 3.

8.3.3 Laboratory Deployments

Two acid washed PP containers (5 L) containing a 0.01 M $NaNO_3$, 100 µg L^{-1} U solution (3 L) plus 0.983 mM $NaHCO_3^-$ to buffer the solution to pH 7.8 (the pH of the field sites used in this project and to prevent sorption of U to the walls of the PP

containers), and one of the containers having a 1 mg L^{-1} HA as sodium salt (Sigma Aldrich, Fisher Scientific Ltd.), were equilibrated for at least 24 h. The HA was added in a ratio of 10:1 HA:U ratio because at that ratio the U begins to bind to the HA, and so some effect may be seen of the HA on the U penetration depth under laboratory conditions [10]. DGT devices containing each type of resin gel (either 1 resin layer, 2 resin layers or 3 resin layers) were deployed (24 h) in triplicate, removed and eluted as per section 2.2. One mL aliquots of the exposure tank solution were taken at the start and end of each experiment and acidified (using 20 µL 6 M HCl) to measure the concentration of U. Equation 8.24 was used to calculate the C_{DGT}, and this was compared to uranium concentrations in the grab samples.

8.3.4 Field deployments

Two freshwater field sites were used: site 1 (51.4469 N, -1.3838 W) was located on the River Lambourn at the village of Boxford, Berkshire, UK and site 2 (51.3792 N, -1.1855 W) on the River Enborne near Brimpton, Berkshire, UK. Both rivers are tributaries of the River Kennet. The River Lambourn has a Chalk catchment and is a fast flowing shallow channel with an average pH of 7.9-8 [21]. The mean flow and base flow indices were 1.71 m^3 s^{-1} and 0.97 respectively [22]. The River Enborne drains impermeable Tertiary sand, silt and clay deposits [23] and has a slow flowing deep channel with a pH ~7.8. DGT devices were deployed between perspex plates (15 x 7 cm, 8 devices per plate) and attached to a rope and float and weighted to the river bed.

Three DGT devices containing each resin gel combination (1 layer, 2 layers or 3 layers) were deployed for 3 days at each site. To assess the presence of the diffusive boundary layer, DGT devices containing the Metsorb™ gel were deployed for 3 days with diffusive layer PAM gel thicknesses (including 0.015 cm to account for the Supor membrane) of 0.015, 0.055, 0.095 and 0.135 cm, as per Warnken *et al.* [20]. Diffusion coefficients calculated by Hutchins *et al.* [17] were used for the TWA calculations. Spot samples of water (20 mL) were collected at the exposure sites and were filtered (0.2 µm pore size Supor filters) and acidified *in situ* with 6 M HCl (40 µL). Water temperature and pH were recorded each time a device was removed so that diffusion coefficients could be corrected for variations in environmental conditions.

Procedural DGT blanks (3 per resin) were prepared along with the deployed devices and exposed to the field environment during deployment and retrieval of the sample devices. The blanks were then eluted and analysed with the samples as above.

Water quality parameters were measured as part of the CEH Boxford Observatory Project and Thames Initiative by the Centre for Ecology and Hydrology. The details of the analysis are in Chapter 3. These parameters were used in the speciation modelling for the field deployments. All speciation distributions were calculated using Visual Minteq, version 3, beta (© 2010 KTH, Department of Land and Water Resources Engineering, Stockholm, Sweden) and was performed for both laboratory and field deployments. As the laboratory deployments had a known quantity of HA added, the Nica Donan model was used to model the U. As the HS has not been characterised in the River Lambourn and the River Enborne, the Stockholm Humic Acid (SHM) model was used for speciation modelling of the field sites as it does not discriminate between HA and FA. It provides information on weak (monodentate) and strong (bidentate) binding sites.

8.4 Results and discussion

8.4.1 Laboratory deployments

The mass of U accumulated in each resin layer was converted to moles in order to calculate the penetration depth and the rate association constants of the metal:resin ligand. Table 8.1 shows the moles of U accumulated in each resin layer, plus the total U accumulated by each DGT device (sum of U accumulated in each layer per device). The U accumulated in each resin layer is also shown as a percentage of the total U accumulated per device. It can be seen that, as expected, the front resin layer sorbs the majority of the U, with 88% sorbed by the front layer in the presence of HA, and 85% sorbed by the front layer with no ligand present.

Table 8.1 Mean (± standard error) of triplicate measurements of U accumulation in 0.4 mm Metsorb^{TM} resin gel layers: front (f), middle (m), back (b) or total (T) (nM per resin layer) when exposed to a 3 L solution of 100 µg L^{-1} U, I = 0.01 M $NaNO_3$, 0.983 mM HCO_3^- buffer, pH 7.8.

Resin layer number	**Experiment**		**HA:U (10:1)**	**U (no ligand)**
	Measured U in exposure tank (nM)			
	0.2 µm filtered		0.242	0.330
	not-filtered		0.409	0.316
1	*1 resin layer only*		2.319 ± 0.126	2.750 ± 0.205
	2 resin layers			
2	2 x 0.4 mm	T	2.518 ± 0.068	2.180 ± 0.103
3	2 x 0.4 mm	f	2.217 ± 0.070	1.860 ± 0.012
4	2 x 0.4 mm	b	0.301 ± 0.126	0.319 ± 0.109
	3 resin layers			
5	3 x 0.4 mm	T	2.535 ± 0.105	2.880 ± 0.064
6	3 x 0.4 mm	f	1.987 ± 0.004	2.700 ± 0.054
7	3 x 0.4 mm	m	0.462 ± 0.104	0.144 ± 0.043
8	3 x 0.4 mm	b	0.086 ± 0.033	0.036 ± 0.012
	% of total metal accumulated in the front or back layer			
	2 x 0.4 mm	f	88.06	85.36
	2 x 0.4 mm	b	11.94	14.64
	3 x 0.4 mm	f	78.39	93.75
	3 x 0.4 mm	m	18.23	5.01
	3 x 0.4 mm	b	3.38	1.24

At the pH of the experiment with no HA, the U species will comprise 43% $UO_2(CO_3)_2^{2-}$ and 45% $UO_2(CO_3)_3^{4-}$, with the remaining U as hydrolysed species. With the addition of HA at a ratio to U of 10:1, so 1 mg L^{-1} Ha and 100 µg L^{-1} U, the percentage of U as $UO_2(CO_3)_2^{2-}$ reduces to 0.029 % and $UO_2(CO_3)_3^{4-}$ reduces to 0.03 % with 61.195 % of the U bound to the phenolic groups HA2-$UO_{2(aq)}$, and 0.308 % bound to the carboxylic groups as HA1-$UO_{2(aq)}$. A full list of species distribution is shown in Table 8.2.

Table 8.2 Visual Minteq output results for the U speciation modelling for each experiment (with and without HA addition). HA1- and HA2- represent the % of U predicted to organically bond with the carboxylic and phenolic groups in the HA respectively.

Experiment	% distribution	Species
HA:U 10:1	1.447	HA2-$UO_2(6)_{(aq)}$
	0.27	UO_2OH^+
	1.083	$UO_2(OH)_3^-$
	1.945	$UO_2(OH)_{2\ (aq)}$
	5.815	$UO_2CO_{3\ (aq)}$
	36.688	$UO_2(CO_3)_2^{2-}$
	38.162	$UO_2(CO_3)_3^{4-}$
	14.587	HA1-$UO_2(6)_{(aq)}$
U only	0.324	UO_2OH^+
	1.299	$UO_2(OH)_3^-$
	2.335	$UO_2(OH)_2$ (aq)
	6.982	$UO_2CO_{3\ (aq)}$
	43.889	$UO_2(CO_3)_2^{2-}$
	45.167	$UO_2(CO_3)_3^{4-}$

The complexation proportions (Table 8.2) represent the most probable HA-U complexation scenarios, but because all humic substances are highly heterogeneous [10] it can be very difficult to precisely model complexation. HA has been used in these experiments as the first approximation of U-organic complexes because U binds very strongly to HA across a wider pH range than other organics such as fulvic acid (FA) and tannic acid (TA) [24].

The U bound to each resin layer in nM is shown in Figure 8.1. What can be seen in both Table 8.1 and Figure 8.2 is that when three resin layers are deployed, very little of the U is accumulated in the back layers (numbers 4 and 8, Figure 8.1) with equal accumulation occurring (within error) with and without HA present in the test solution. This supports the findings by Zhao *et al*. [10] that in the presence of carbonates, U binds to the more labile groups in the HA. Table 8.2 shows that only 1.447 % of the U is bound to the phenolic groups in the HA. This study used a carbonate buffer of 0.983 mM to act as pH buffer and to prevent the U from sorbing to exposure tank walls, while Zhao *et al*. [10] used 4 mM in order to buffer their solution to pH 10. The pH was chosen for this study as 7.8 because this best reflects average pH of both the field deployment sites. Further work would be necessary to test the penetration depth in a wider range of pH values and in the presence of other buffers.

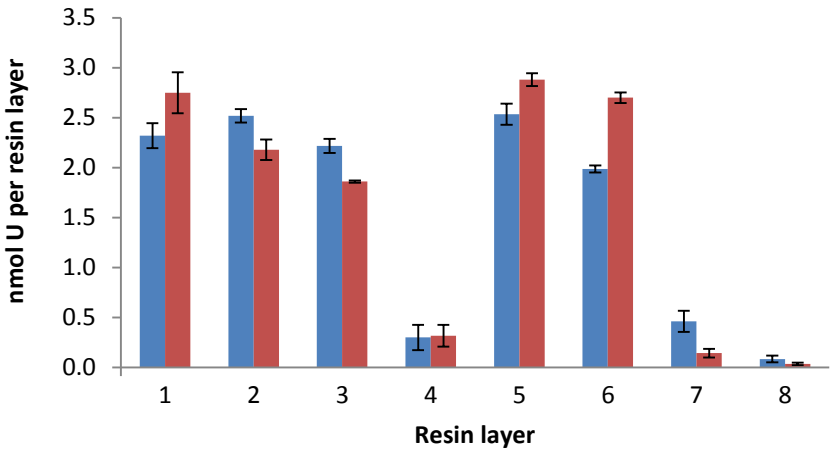

Figure 8.2. U accumulated (nM) in each resin layer for the U:HA experiment (blue), U only (red). Where the x-axis number corresponds to a resin layer described in Table 8.1. Error bars are the standard error of the mean of triplicate readings.

Compared with other metals such as Ni, U binds less strongly to HA [10], with much of the U bound as a weak electrostatic attraction in this case. One measure of the strength of the U-HA complex is through examining the rate association constants ($k'_{a,R}$ in s^{-1}), calculated by isolating $k'_{a,R}$ from equation 8.5 as shown in Table 8.3. $k'_{a,R}$ were calculated to be 6.31 to 8.03 x 10^{-3} s^{-1} using either 2 or 3 layers of resin gel respectively when no HA is present, and 5.03 to 3.82 x 10^{-3} s^{-1} using either 2 or 3 layers of resin gel respectively with a HA:U ratio of 10:1. These results show a slight decrease in the rate of association of the metal in the presence of HA. This might be a consequence of the U dissociation from the phenolic groups on the HA, as the carboxylic groups are thought to be fully labile. The rate association constants found by Levy *et al*. [7] at pH 7 are appreciable higher for the metals tested (Mn, Co, Ni, Cu, Cd and Pb) and fall in the range (when 2 resin layers are used to predict $k'_{a,R}$) 4.9 x 10^{-2} to 1.1 x 10^{-1} s^{-1}. Their experiments were conducted at ~ 23^{o}C, whilst here the average temperature was ~ 18^{o}C. However a 5^{o}C temperature discrepancy should not cause a rate constant to change by one to two orders of magnitude. It is more likely that the metals trialled by Levy *et al*. [7] have a higher affinity for the microchelex resin trialled than the U does for the Metsorb^{TM} in this study.

Table 8.3. Estimation of the rate of association ($k'_{a,R}$ in s^{-1}) of U with the Metsorb™ resin at pH 7.8 for multiple layer (MLR) DGT devices. $k'_{a,R} = D_{MR}/\lambda_M^2$ where $D_{MR} = D_M$ ($cm^2\ s^{-1}$) and λ_M^2 is expressed in cm. Diffusion coefficients in the gel were calculated for the average temperature of each experiment: UO_2^{2+} only, 18°C, diffusion coefficient 2.97 x 10^{-6} cm s^{-1} ; HA:U, 17°C, diffusion coefficient 2.52 x 10^{-6} cm s^{-1}.

MRL device	UO_2^{2+} (no ligand)	HA:U 10:1
2 x 400 µm (r = 800 µm)	6.31 x 10^{-3}	5.03 x 10^{-3}
3 x 400 µm (r = 1200 µm)	8.03 x 10^{-3}	3.82 x 10^{-3}

The penetration depth was calculated using two resin layers (equation 8.11) and 3 resin layers (equations 8.15-8.18). The results can be seen in Table 8.4 below. What is noticeable is that the penetration depth is similar (within error) when the U is complexed with carbonate or HA of 217 ± 27 µm and 224 ± 68 µm respectively for the experiment utilising two resin layers. Levy *et al.* [7] undertook their study at pH values 4, 5 and 7. At pH 7.8, the U is forms highly labile complexes with the carbonate used both as the buffer and dissolved from atmospheric CO_2. The study by Levy *et al.* [7] only examined penetration depth of free metal ions, with no organic complex accounted for. The results in this study also showed that increasing the number of resin layers under a laboratory setting does not increase the penetration depth of the U.

Table 8.4. Estimation of the penetration depth and λ_M (µm) of U^+ within the Metsorb™ resin at pH 7.8 for multiple layer (MLR) DGT devices in the presence of no ligand, and with a 1 mg L^{-1} addition of humic acid to give a humic acid:uranium ration of 10:1. r is the total thickness of the resin layers. Errorr are the standard error of the mean of triplicate readings.

MRL device	UO_2^{2+} (no ligand)	HA:U 10:1
2 x 400 µm (r = 800 µm)	217 ± 15	224 ± 39
3 x 400 µm (r = 1200 µm)	192 ± 42	256 ± 9

To determine if there is any relationship between penetration depth and the association rate constant the two were plotted against each other (Figure 8.3). The U data was taken from this study and the other metals taken from Levy *et al.* [7]. A negative trend was found with an R^2 value of 0.67 and a relationship of decreasing penetration depth with an increasing association rate coefficient (Analysis of Variance (ANOVA) P = 0.03*; if $P < 0.05$ then the null hypothesis of no relationship can be rejected*) with a negative gradient of -1213x. If U were removed from this graph then the relationship is firmer (ANOVA P = 0.02) but with a lower gradient of -338x. It stands to reason that the lower the residence time of the metal in the resin layer (i.e. the

faster it is removed from solution and bound in the resin or the higher the association rate constants) the less distance it can penetrate into the resin layer.

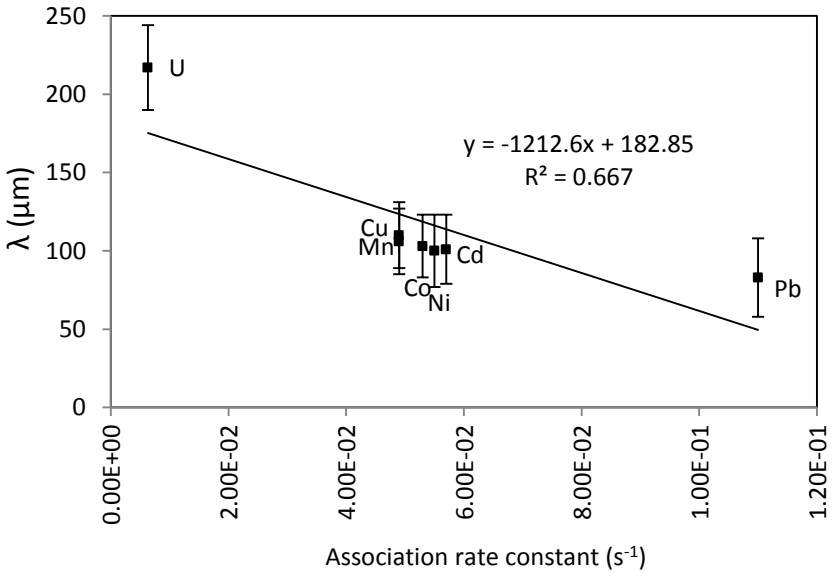

Figure 8.3 Scatter plot of the penetration distance against the association rate constant for uranium (from this study, no ligand, pH 7.8 at 18^{o}C) and for Mn, Co, Ni, Cu, Cd and Pb all from Levy *et al.* [7] (pH7, 22 ^{o}C no ligand present).

This study examined different methods in estimating the penetration depth of the U into the resin layer by deploying devices with different numbers of the resin layers and calculating the ratio of U at each resin layer with the hyperbolic function of the penetration curve of the U through the resin layer. Figures 8.4 and 8.5 examine the results gained by employing devices of differing number of resin layers with and without the HA ligand addition. Large errors occurred when the U is not complexed to the HA, but a slightly and consistently higher penetration depth when HA is present (although as previously stated this actually lies within errors and so this difference is not significant). The decrease in variation observed with the addition of the HA could be as a result of the HA reducing the rate of reaction of the U with the resin binding sites as discussed previously and shown in Table 8.2. This may result in a more even distribution of the U throughout the resin layers, despite any heterogeneity introduced during the resin gel manufacture. Using 2 resin layers rather than 3 produces more consistent results, potentially as a result of poor technique when constructing the devices with 3 resin layers. Another reason for the discrepancies between the two techniques could be as a result of heterogeneity in the distribution of resin within the resin gel. The Metsorb^{TM} acts as a catalyst for polymerisation, and therefore increases the polymerisation rate when casting the resin gels. This may not allow sufficient time for the resin beds to settle fully on one side of the gel, as observed with Chelex-100.

The more resin layers that are used, the more apparent the affect of this heterogeneity becomes.

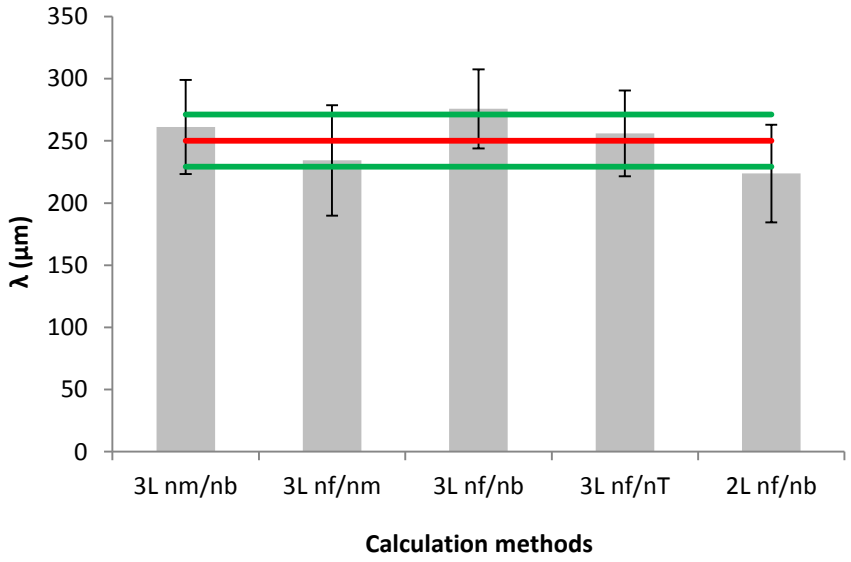

Figure 8.4. Comparison of penetration depth (λ in µm) of U with the addition of HA using described calculation methods using 3 reins gel layers and 2 resin gel layers (nM of U accumulated in nm middle layer; nb back layer; nf front layer; nT total of layers). 3L nm/nb uses equation 9.15; 3L nf/nm uses equation 9.16; 3L nf/nb uses equation 9.17; 3L nf/nT uses equation 9.18; and 2L nf/nb uses equation 9.11. The red line represents the mean penetration depth and the green lines 1 S.D. Error bars are the standard error of the mean of triplicate readings.

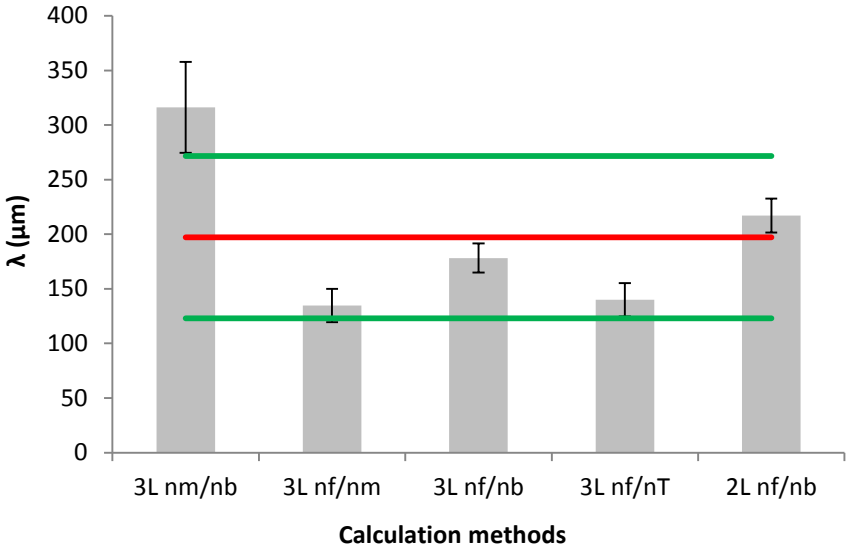

Figure 8.5 Comparison of penetration depth (λ in µm) of U with no addition of HA using described calculation methods using 3 reins gel layers and 2 resin gel layers (nM of U accumulated in nm middle layer; nb back layer; nf front layer; nT total of layers). 3L nm/nb uses equation 9.15; 3L nf/nm uses equation 9.16; 3L nf/nb uses equation 9.17; 3L nf/nT uses equation 9.18; and 2L nf/nb uses equation 9.11. The red line represents the mean penetration depth and the green lines 1 S.D. Error bars are the standard error of the mean of triplicate readings.

For more tightly bound metal-ligand complexes such as the Cd-NTA complex assessed by Uribe et al. [13], it has been found that increasing the resin layer thickness increased the lability; and the metal-ligand complex was able to dissociate to a point where the concentration of dissolved metal in the resin layer was 0. Mongin et al. [9] found that lower than predicted DGT uptake of Cu and Ni in a fluvial deployment could have been as a consequence of the partially labile complexes they form with HS. If the resin layer thickness had been increased in this instance it may have allowed complete dissociation of both these metal complexes and rendered the system fully labile. In the case of U, it is unlikely that increasing the resin layer thickness beyond the standard 400 µm would alter the lability under laboratory conditions as the measured penetration depths lie below this value.

8.4.2 Field deployments

Devices containing each combination of resin layers (1, 2 or 3 layers) were deployed in triplicate for 3 days in both the River Lambourn and the River Enborne. Devices containing various diffusive layer thicknesses (0.015, 0.055, 0.095 and 0.135 cm) were also deployed in order to assess the DBL. Field blanks were treated identically to the field samples, but were not deployed in the river. Field blanks average 0.59 ng U per disk. The River Enborne was at low flow (mainly due to the location of the samplers in the river out of the main channel to allow for safe access), with a pH of 8 and average temperature of 13^{o}C. The River Lambourn was a high flow river (~ 8 cm s^{-1} over the deployment) with a pH of 8.1 and average temperature of 11^{o}C. The bulk solution concentrations filtered through 0.22 µm were 0.33 µg L^{-1} and 0.22 µg L^{-1} for the River Enborne and River Lambourn respectively. The plots of 1/*M* to estimate the thickness of the DBL can be seen in Figures 8.6 and 8.7. The DBL for the low flow River Enborne was 0.075 cm +/- 0.011 cm and for the faster flowing River Lambourn was 0.043 +/- 0.025 cm.

C_{DGT} TWA calculations using equations 8.23 and 8.24 gave values for the River Enborne of 0.38 ± 0.001 µg L^{-1} and for the River Lambourn of 0.25 ± 0.03 µg L^{-1}; both are in close agreement with the grab samples values. From these values it is clear that no further corrections due to penetration distance are needed because 100% of the dissolved U in this deployment was DGT labile. However, DOC values were low during this deployment, particularly for the River Enborne so it is still important to assess the application of the calculations for the penetration parameter in a field setting.

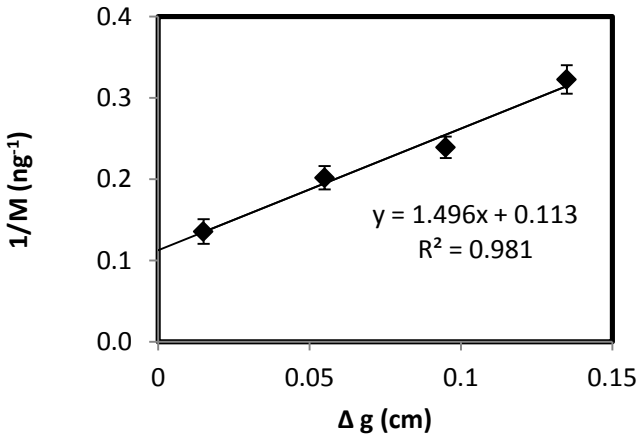

Figure 8.6 1/*M* U accumulated for each diffusive layer thickness as per equation 8.26 in order to estimate the thickness of the DBL (equation 8.27) for the River Enborne. From this plot, the DBL was found to be 0.075 cm +/-0.011 cm. Error bars are the standard error of the mean of triplicate readings.

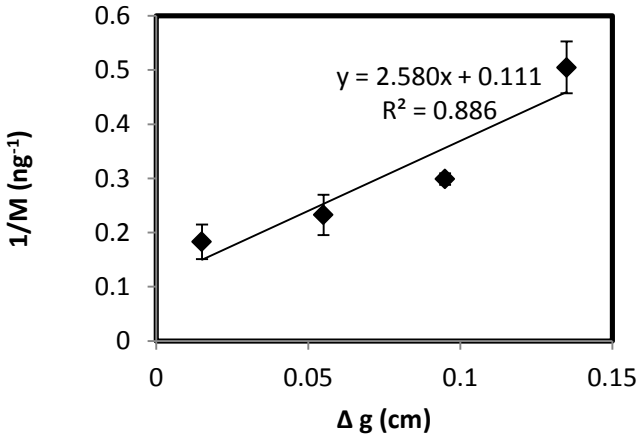

Figure 8.7 1/*M* U accumulated for each diffusive layer thickness as per equation 8.26 in order to estimate the thickness of the DBL (equation 8.27) for the River Lambourn. From this plot, the DBL was found to be 0.043 cm +/-0.025 cm. Error bars are the standard error of the mean of triplicate readings.

Table 8.5 shows the results of the speciation modelling using Visual Minteq and based on the water quality parameters provided by the CEH. The River Enborne demonstrated slightly higher complexation of U with DOC than the River Lambourn, but there is only 0.372 % and 0.161% of the U complexed with the stronger bidentate sites ($FA2UO_2$) for the Rivers Enborne and Lambourn respectively during this deployment period Previous deployments detailed in Chapter 5 have shown higher quantities of U to be bound to HA, particularly in the River Enborne. The SHM used here to calculate the U-organic complexes does not discriminate between HA and FA.

Table 8.5 U speciation distribution as a % of total U for deployment site at pH 8. Modelled using Visual Minteq with SHM DOC parameters. $FA2UO_2^+$ are the weak monodentate bonds and $FA2UO_2$ are the strong bidentate groups in the humic acid. Some of the parameters used in the speciation calculations are given at the bottom of the table for each deployment site.

	Species distribution as % total uranium	
Uranyl species	**River Enborne**	**River Lambourn**
$Ca_2UO_2(CO_3)_{3\,(aq)}$	72.44	72.6
$CaUO_2(CO_3)_3^{2-}$	26.433	26.487
$UO_2(CO_3)_2^{-2}$	0.128	0.128
$UO_2(CO_3)_3^{-4}$	0.609	0.61
$FA2UO_2^+(6)_{(aq)}$	0	0
$FA2UO_2(6)_{(aq)}$	0.372	0.161
DOC (mg L^{-1})	3.61	2.18
Ca^{2+} (mg L^{-1})	88.9	102.9
Alkalinity (µ equiv. L^{-1})	3918	4369

During this deployment the speciation was very similar between the two rivers. The River Lambourn due to its continuous aquifer feed and chalk catchment does not have the same flow and variability from precipitation run-off as the River Enborne. This results in the DOC concentrations being more stable. DOC measurements undertaken as routine in the CEH monitoring of both these sites shows that the DOC range for the River Lambourn since January 2012 is only 0.86 to 4.13 mg L^{-1}, with one peak to 8.03 mg L^{-1}. The River Enborne DOC concentrations typically fluctuate between 3.1 and 15.64 mg L^{-1}, with the DOC concentrations frequently exceeding 10 mg L^{-1}.

An understanding of *in situ* speciation and methods of applying these is important, particularly for those metal that readily bind to organic and inorganic complexes [4]. This is because of the heterogeneity of HS in natural systems, which lead to a wide range of mixtures of binding sites and respective association + dissociation rates together with stability constants. Due to the complexity of natural systems, an average of these readings may be necessary from multiple deployments over a longer time frame. Li *et al*. [24] showed experimentally that U binding to organics in mixed organic solutions is different from a single idealised laboratory solution. It was shown that the stability constants for the U-HA complex reduced in the presence of another competitive ligand such as EDTA. This may change again in the presence of inorganic ligands, such as those present in natural systems.

Table 8.6 Mean (± 1 standard error) of triplicate measurements of U accumulation in 0.4 mm Metsorb™ resin gel layers: front (f), middle (m), back (b) or total (T) (nM per resin layer) when deployed in the River Enborne and the River Lambourn.

Experiment		River Enborne	River Lambourn
Measured U in exposure tank (pM)			
0.2 µm filtered		1.4	0.91
non-filtered		1.5	0.86
1 resin layer only		25.25 ± 0.61	9.31 ± 0.51
2 resin layers			
2 x 0.4 mm	f	37.34 ± 3.38	18.59 ± 4.71
2 x 0.4 mm	b	19.91 ± 6.30	10.95 ± 4.76
2 x 0.4 mm	T	57.26 ± 3.06	29.54 ± 3.09
3 resin layers			
3 x 0.4 mm	f	19.22 ± 1.85	1.678 ± 0.84
3 x 0.4 mm	m	9.46 ± 0.14	2.478 ± 0.52
3 x 0.4 mm	b	9.62 ± 1.97	4.887 ± 1.71
3 x 0.4 mm	T	38.30 ± 2.80	9.043 ± 2.53
% of total metal accumulated in the front or back layer			
2 x 0.4 mm	f	65.22	62.94
2 x 0.4 mm	b	34.78	37.06
3 x 0.4 mm	f	50.18	18.56
3 x 0.4 mm	m	24.70	27.40
3 x 0.4 mm	b	25.11	54.04

Table 8.6 shows the pM and the % of the U accumulated by each resin layer of the multiple layer devices. Immediately noticeable from this table is that the quantity of U accumulated by the back layers in the 3 resin layer devices is more than that accumulated by the front layers when deployed in the River Lambourn. This makes equations 8.15 to 8.18 unsolvable through iteration and gives an effective penetration distance as infinite and could therefore be interpreted as an inert system. As the ratio of the quantity of U accumulated in the front layer to the back layer approaches 1 (which in this case it is 0.8) the penetration distance increases to infinity, meaning that there is not enough resin thickness for the metal concentration to fall to zero [7]. This could be as a result of very tightly bound U complexes, but is most likely assembly error, as the devices in the River Enborne did not display similar U distributions, but had a similar quantity of organically complexed U. Another possibility is that the front resin layer in the River Lambourn deployment became saturated with other ions in the bulk solution, hence violating the assumption that there is an excess of resin binding sites. Previous work though has shown in this river that the Metsorb™ resin does not become depleted in binding sites after 3 days (see Chapters 4 and 5).

Table 8.7. Estimation of the penetration depth and λ_M (μm) of U within the Metsorb^{TM} resin for multiple layer (MLR) DGT devices deployed at both field sites. nda - there is no data available (nda), which in this case is as a result of the equations being unsolvable. The depth for the 3 layer device for the River Enborne excludes the nm/nb calculation (equation 8.15) as it is anomalously high at > 1000 μm. The error represents the standard error of the mean of triplicate measurements.

MRL device	River Enborne	River Lambourn
2 x 400 μm (r = 800 μm)	364 ± 86	321 ± 171
3 x 400 μm (r = 1200 μm)	571 ± 25	nda

The penetration depth shown in Table 8.7 for the 3 layer device excludes 1 calculation set (nm/nb, equation 8.15) as the solution here gives a very high value of 1000 μm. This high figure distorts the average value and the associated errors. The calculations can be seen graphically with (Figure 8.8) and without (Figure 8.9) this reading. The data is presented with and without this anomalously high reading in order to more clearly identify variation between the calculation methods in the remaining data set. Figure 8.9 shows that all the calculation methods predict similar penetration depths within error.

The calculated penetration depths can be found for the MRL devices with 2 resin layers for both deployment sites, and for 3 layers for just the River Enborne. These figures are higher than those found under ideal laboratory conditions. If the 2 resin layer DGT is taken separately, the laboratory readings (even when complexed with HA) were only 223 μm, where in the field they are 364 μm and 321 μm for the Rivers Enborne and Lambourn respectively. When 3 resin layers were used for the field deployments, the River Enborne had a penetration value of 519 μm, and the River Lambourn reading was not discernible as previously discussed. Under laboratory conditions, when complexed with HA, this value is only 250 μm. The HA:U ratio under laboratory conditions was 10:1, and in the field it was nearly 10,000:1 for both deployment sites, which might indicate very strong binding to the HS, particularly at high pH. However, due to the high pH and alkalinity, most of the organically bound U was modelled to be bound to the weaker sites (Table 8.5). So even though U binding to HS increases with increasing pH, the influence of the carbonate system means that predominantly weaker DOC sites are filled [10]. Another possibility for the differences in penetration depth between the laboratory and field experiments is that the front resin layers become saturated by other ions present at higher concentrations, such as Ca or Mg. This may also account for the differences when using the 2 or 3 layers methodology to calculate

the penetration depth. As the front resin layers become increasingly saturated, the U diffuses through the gel layers where more binding sites are available. This could create a diffusion gradient through to the rear gel layers, which is not reflective of the dissociation of the U from HS.

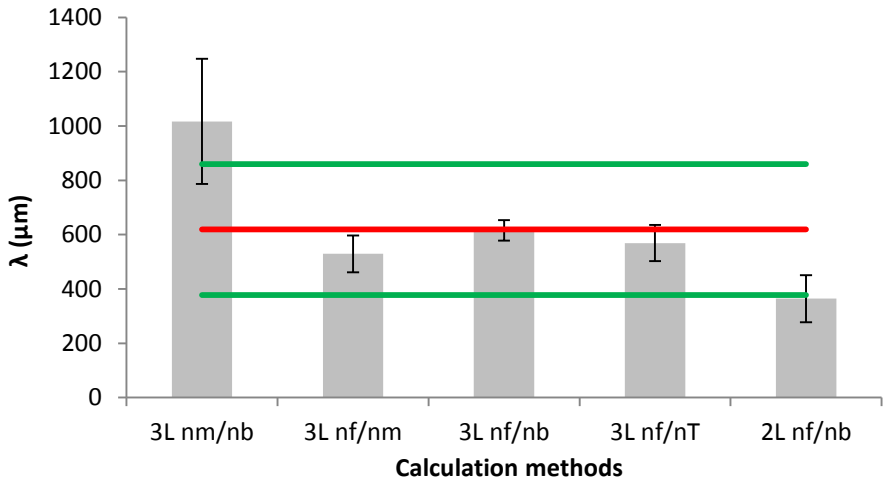

Figure 8.8 Comparison of U penetration depth (λ in μm) for the River Enborne using described calculation methods using 3 reins gel layers and 2 resin gel layers (nM of U accumulated in nm middle layer; nb back layer; nf front layer; nT total of layers). 3L nm/nb uses equation 8.15; 3L nf/nm uses equation 8.16; 3L nf/nb uses equation 8.17; 3L nf/nT uses equation 8.18; and 2L nf/nb uses equation 8.11. The red line represents the mean penetration depth and the green lines 1 S.D. Error bars are the standard error of the mean of triplicate measurements.

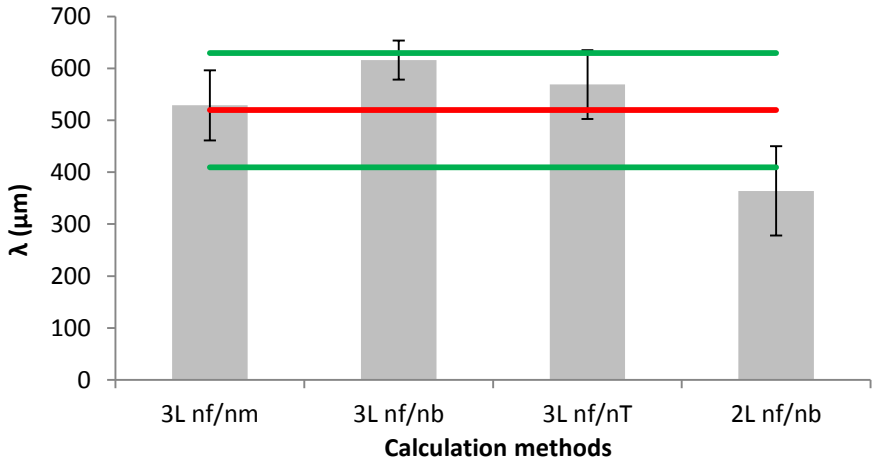

Figure 8.9 Comparison of U penetration depth (λ in μm) for the River Enborne using described calculation methods using 3 reins gel layers and 2 resin gel layers (nM of U accumulated in nm middle layer; nb back layer; nf front layer; nT total of layers). 3L nm/nb is omitted; 3L nf/nm uses equation 8.16; 3L nf/nb uses equation 8.17; 3L nf/nT uses equation 8.18; and 2L nf/nb uses equation 8.11. The red line represents the mean penetration depth and the green lines 1 S.D. Error bars are the standard error of the mean of triplicate measurements.

The association rate constants shown in Table 8.8 are a lot lower than those found under laboratory conditions even in the presence of HA (5.03×10^{-3} s^{-1} for 2 resin layers and 3.82×10^{-3} s^{-1} for 3 resin layers). This lower rate could be as a result of the

DGT devices being deployed in a more complex system and other competing ions consuming resin binding sites faster than the U, even if the U is dissociating quickly. Competition with other ions that are taken up by Metsorb™ has previously been thought to interfere with the DGT uptake of U. However, for the short (3 d) deployment time here, this is unlikely. What is significantly different between the laboratory deployment and the field deployment is the Ca concentrations in the field resulting in over 70% of the dissolved U bound as $Ca_2UO_2(CO_3)_{3(aq)}$ (Table 8.5). The effect of Ca-U species has not yet been tested under laboratory conditions. It could be that the U species, due to their large size, suffer steric effects in the diffusive and resin gel. Most likely is that the interfering ions are binding to the front layer leading to the violation of the assumption of an excess binding sites (equation 8.2) which forces the U species to diffuse further into the resin gel layer. This could be tested by the addition of more resin to the gel during the production stage of the DGT devices to examine if this is a contributing factor to low association rates, and corresponding high penetration depths.

Table 8.8. Estimation of the rate of association ($k'_{a,R}$ in s^{-1}) of U with the Metsorb™ resin at pH 7.8 for multiple layer (MLR) DGT devices. $k'_{a,R} = D_{MR}/\lambda_M^2$ where $D_{MR} = D_M$ ($cm^2\ s^{-1}$) and λ_M^2 is expressed in cm. Diffusion coefficients in the gel were calculated for the average diffusion coefficient; the River Enborne was 1.97 x 10-6 $cm^2\ s^{-1}$, and the River Lambourn 1.27 x 10^{-6} $cm^2\ s^{-1}$.

MRL device	River Enborne	River Lambourn
2 x 400 µm (r = 800 µm)	1.20 x 10^{-3}	1.23 x 10^{-3}
3 x 400 µm (r = 1200 µm)	4.20 x 10^{-4}	nda

8.4.3 Penetration distance limits

The blank DGT probes were assembled as per the experimental parameters, but not exposed to a solution. The average resin blank was 0.55 ng or 2.3 pM. The minimum detectable penetration depth is important to describe as this provides a level of resolution for the technique. This is determined using the ratio between the metal concentration accumulated in the front layer of the DGT device and the blank resin gel, under each of the experimental conditions. Levy *et al*. [7] described a penetration distance of 100 µm that could not be accurately resolved. When r (total resin layer distance) = 800 µm, the penetration limit was calculated to be 59 µm, which is similar to the mid-range achieved by Levy *et al*. [7] of 40-90 µm. The precision (RSD) of the technique when r = 800 µm is 22% (similar to the 20% found by Levy *et al*. [7]) and when r = 1200 µm (3 resin layers used), this increased to 25%.

The resin capacity did not have to be considered in this work because previous work in Chapter 4 has shown that the Metsorb^{TM} resin was not capacity limited under these experimental conditions (100 µg L^{-1} U for 24 h). pH was not an important variable compared with the study by Levy *et al*. [7] because TiO_2 is amphoteric and has been previously shown to be unaffected by changing pH as a U sorbent . The mean penetration distance found by Levy *et al*. [7] increased with decreasing pH due to increasing protonation of the Chelex resin, resulting in fewer binding sites available for the metals.

8.4.4 Implications for DGT calculations

To understand the effect that the penetration distance may have on the DGT calculations, the concentration of the U accumulated at the resin layer boundary compared with the U concentration in the bulk solution needs to be quantified. The following equations (which are used to derive equation 8.22) were only applied to the laboratory data. This was due to the field data showing high variability and with, potentially, extraneous factors affecting the penetration depth that have not been fully explored in a laboratory setting, such as the impact of mixed organic and inorganic ligands.

The concentration of U at the resin surface (C_M^r) can be related to the total amount of U accumulated by all resin layers using (from Levy *et al*. [7]);

$$n = A\frac{D_M(C^* - C_M^r)}{g}t = A\frac{D_M C^*}{g + \lambda_M \coth\left(\frac{r}{\lambda_M}\right)}t \qquad \text{Equation 8.28}$$

with C_M^r is isolated from equation 8.28 by:

$$C_M^r = \frac{\frac{\lambda_M}{g}}{\frac{\lambda_M}{g} + tanh\left(\frac{r}{\lambda_M}\right)} C_M^* = \frac{C_M^*}{1 + \frac{g}{\lambda_M} tanh\left(\frac{r}{\lambda_M}\right)} \qquad \text{Equation 8.29}$$

when r >> λ_M, $\coth\left(\frac{r}{\lambda_M}\right) \rightarrow 1$, then equation 8.28 becomes:

$$n(T) \approx \frac{AD_M C_M^* t}{g + \lambda_M} \qquad \text{Equation 8.30}$$

which shows the effective gel thickness increasing by the penetration distance of U into the resin gel layer.

If $r << \lambda_M$ then:

$$n(T) \approx \frac{AD_M C_M^* t}{g+\left(\frac{\lambda_M^2}{r}\right)}$$ Equation 8.31

which means that a factor (larger than 1 x $\left(\frac{r}{\lambda_M}\right)$) of the penetration distance (λ_M) which is already larger than r is added to g. In this set of experiments, $r > \lambda_M$, so equation 8.31 need not be considered. If the λ_M << g and r > λ_M, which can be found using

$$\frac{g}{\lambda_M} tanh\left(\frac{r}{\lambda_M}\right) \gg 1$$ Equation 8.32

then C_M^r = 0 and the standard equation applies because the resin gel acts as a planar sink:

$$n(T) = \frac{AD_M C_M^* t}{g}$$ Equation 8.33

In Table 8.9 $coth\left(\frac{r}{\lambda_M}\right)$ for both experimental conditions was ~1, and that $\frac{g}{\lambda_M} tanh\left(\frac{r}{\lambda_M}\right) \gg 1$ for both experimental conditions. This implies that the standard DGT equation should hold under these settings. However, because $C_M^r : C_M^*$ = 0.14 and 0.17 for the U only and U-HA experimental condition respectively, the effect of the penetration parameter should be further explored and trialled against real data. Levy *et al*. [7] found that for tightly organically bound metals, such as Ni, the $C_M^r : C_M^*$=0.16, and up to 0.63 for Mn, so the values obtained for U of 0.14 and 0.17 are not highly significant. The fact that the penetration parameter (based on 2 resin layers) is 217 µm and 224 µm for U only and U-HA cannot be ignored. The Metsorb™ resin particles are < 50 µm, but cannot be assumed to be uniformly distributed because the TiO_2 acts as a polymeriser inducing very fast polymerisation of the polyacrylamide gel it is held in for the DGT devices. Unlike the Chelex-100 resin gel manufacturing process, where the resin beads are given time to settle on one face of the resin layer, the Metsorb™ may have a less planar distribution due to faster setting times. This may then induce penetration of the U into the resin layer due to reduced uptake at the resin layer boundary. The net effect is to result in a higher $C_M^r : C_M^*$ value, contradicting the solutions to equations 8.28 and 8.32. If $C_M^r : C_M^*$ was extremely low, such as found by Levy *et al*. [7] for Mn, Co, Ni, Cu, Cd and Pb at pH 5 and 7, it can be assumed that the U ion is consumed by the resin layer in a very small binding zone and the DGT can be assumed to be acting as a perfect sink.

Table 8.9 Calculated parameters to determine the magnitude of the effect of the penetration parameter on the DGT measurements, and whether the standard DGT equation applies.

	U only	**HA:U 10:1**
C_M^r (using equation 9.29)	5.06 x 10^{-8} M	4.15 x 10^{-8} M
C_M^* (in M, using analysed bulk solution concentrations)	3.3 x 10^{-7} M	7.09 x 10^{-7} M
$C_M^r : C_M^*$	0.14	0.17
$\coth\left(\frac{r}{\lambda_M}\right)$ (isolated from equation 9.28)	1	1.003
$\frac{g}{\lambda_M} tanh\left(\frac{r}{\lambda_M}\right)$ (equation 9.32)	6.1	4.8

Taking equation 8.30 and increasing the diffusive thickness by the penetration parameter, the C_{DGT} calculation effectively increases by a factor of $(g + \lambda_M)/g$, which here is 1.18 for UO_2^{2+} only, and 1.21 when HA is added to the system, the results of which can be seen in Table 8.10.

Table 8.10. C_{DGT} calculations accounting for the affect of resin penetration. A key to the table is given below. The C_{DGT} concentrations were given for the 2 resin layer scenarios, and for the standard 1 resin layer DGT set up.

Diffusion coefficient (x 10^{-6} cm^2 s^{-1})	**U solution concentration (µg L^{-1})**	**U total accumulated on resins (ng)**	**C_{DGT} (µg L^{-1})**	**C_{DGT} plus correction factor**	**Correction factor $(g + \lambda_M)/g$**
2.97	79 ± 2.4	693.2 ± 24.6	79.2 ± 2.8	93.5 ± 2.8	1.18
2.97	79 ± 2.4	595.4 ± 2.8	68 ± 0.3	80.2 ± 0.3	1.18
2.97	79 ± 2.4	657.7 ± 84.3	74.8 ± 5.6	88.3 ± 5.6	1.18
2.52	97±1.6	599.3 ± 16.1	108.4 ± 2.9	131.1 ± 3.5	1.21
2.52	97 ± 1.6	527.7 ± 16.6	95.4 ± 3.0	115.5 ± 3.6	1.21
2.52	97 ± 1.6	551.9 ± 29.9	99.8 ± 5.4	120.8 ± 6.8	1.21

Key for Table 8.10

1a Total of resin layers when 2 resin layers used, uranium only
1b Top resin layer only used, when 2 resin layers deployed, uranium only
1c 1 resin layer only used, uranium only
2a Total of resin layer when 2 resin layer used, HA:U 10:1 complex
2b Top resin layer only used, when 2 resin layers deployed, HA:U 10:1 complex
2c 1 resin layer only used, HA:U 10:1 complex

When the inorganic deployment solution of UO_2^{2+} is considered (mo HA present), the correction factor makes very little difference to the C_{DGT} concentrations; which with and without the correction factor are similar to the grab sample values within error. When HA is added to the system the correction factor, due to increased penetration distance, increases to 1.21. It gives C_{DGT} readings that are 120-130% larger than the grab sample values.

The results in Table 8.10 assume that the diffusion coefficient in the resin gel is the same as the diffusive layer gel, but it is possible that this is not the case due to tortuosity effects. This may be particularly relevant for U and U-HA considering

possible steric effects. In turn this will reduce the estimation of the resin penetration factor, and therefore the size of the C_{DGT} correction factors because the rate of binding decreases in the resin layer with an increased diffusion of the metal through it, and a decreased residence time of the metal ion in this layer. The factor of decrease would be equal to[7]:

$$\frac{g+\left(\frac{D_{M,gel}}{k\prime_{a,R}}\right)\left(\frac{1}{\lambda_M}\right)}{g} \qquad \text{Equation 8.34}$$

Using equation 8.34 above, the simple U experiment decreases by a factor of 1.18 due to tortuosity, which is equal to the correction factor resulting from the U penetration into the resin layer. In the U-HA system, the tortuosity effects only decrease the concentrations by a factor of 1.19, indicating that there is still a correction factor to be considered when HA is present. The results are displayed in Table 8.11. The presented, when taking into account the various correction factors, are similar to the grab samples, within error.

Table 8.11 C_{DGT} calculations accounting for the affect of resin penetration and the tortuosity. A key to the table is given below. The C_{DGT} concentrations were given for the 2 resin layer scenarios, and for the standard 1 resin layer DGT set up.

U solution concentration (µg L^{-1})	**CDGT (µg L^{-1})**	**Penetration correction factor $(g + \lambda_M)/g$**	**Tortuosity reduction factor**	**CDGT plus correction factors**
79 ± 2.4	79.2 ± 2.8	1.18	1.18	79.2 ± 3.2
79 ± 2.4	68 ± 0.3	1.18	1.18	68 ± 0.4
79 ± 2.4	74.8 ± 5.6	1.18	1.18	74.8 ± 6.4
97 ± 1.6	108.4 ± 2.9	1.21	1.19	111.1 ± 3.0
97 ± 1.6	95.4 ± 3.0	1.21	1.19	97.9 ± 3.1
97 ± 1.6	99.8 ± 5.4	1.21	1.19	102.3 ± 5.8

Key for table 8.11

1a Total of resin layers when 2 resin layers used, U only
1b Top resin layer only used, when 2 resin layers deployed, U only
1c 1 resin layer only used, U only
2a Total of resin layer when 2 resin layer used, HA-U 10:1 complex
2b Top resin layer only used, when 2 resin layers deployed, HA-U 10:1 complex
2c 1 resin layer only used, HA-U 10:1 complex

What must be noted in these calculations is that there was no correction in the diffusion coefficients for the HA. At higher HA:U ratios, as explored in the next chapter, the hindrance of diffusion by the HA of the U is considered in the lability calculations. However at a HA:U ratio of 10:1 over 24 h, this system was found to be fully labile using the U diffusion coefficients. The difference in diffusion coefficients

should be taken into account in experiments where the HA:U ratio is increased and the weak electrostatic bonds are replaced by the stronger organic bonds.

There are some limitations and areas for further research within this model and identified by Levy *et al.* [7]: the variable diffusion coefficients, as previously discussed; and the fact that this assumes a 1:1 binding ratio with the metal and the resin sites. There may be other combinations not being considered that would affect the association rate constants such as MR_2, $M(HR)_2$ [7] (where MR is the metal-resin bond); *quasi* steady state is assumed as per equation 8.1, despite the fact that the metal to resin ratio will be changing as resin binding sites are consumed. Another large factor, which could account for many of the results presented here is that there may not be an even distribution of resin throughout the binding layer; with a uniform layer at the binding layer interface absent or a highly heterogeneous in binding site concentrations, which could also affect the concentration of resin binding sites in each resin slice. The filling up of binding sites by competing ions is not considered, and would have to be explored as discussed in the field data presented here.

Further research into the penetration distance of U includes using a different resin, such as Diphonix® or Chelex-100, which both have longer polymerisation times, making the distribution of the resin beads easier to manipulate. This could be important as the data presented here indicates that heterogeneity in the manufacturing process of the Metsorb™ resin gels could have a large impact on the U uptake, particularly in the field.

8.5 Conclusions

Data presented here shows that U is labile in a system where the U is complexed to carbonate and weakly bound to HA. The penetration of U into the resin gel layer has been shown to be larger than other metals such as Cu, Ni, Pb, Mn, Co and Cd, due to lower association kinetics, attributable to the lower affinity of the U to the resin used here (TiO_2 based resin compared with Chelex-100 in other studies). Field trials have shown that the penetration parameter is greatly increased when compared to a laboratory setting by 100-200 μm. There are different explanations for this including some violations of the model assumptions such as an excess of resin binding sites. This could be violated because of the competition from other cations and anions in the field, however, this would require further investigation under laboratory conditions at various concentrations and mixtures of interferences. Accounting for the factor increase of the diffusive layer that is as a result of the increased penetration into the resin layer, and the

factor decrease due to tortuosity effects, which are very important for a large cation such as U, the effect on the prediction of C_{DGT} U is minimal. It was observed that with HA additions, the tortuosity parameter became less than the correction factor resulting from penetration into the resin layer. It is clear that further work is required to fully assess the penetration parameter under higher HA:U conditions, using a variety of resins and in the presence of interfering ions (such as Ca, which forms ternary complexes with U) over a range of pH values (due to changing speciation of U with pH). It is unlikely that DGT devices with multiple resin layers would need to be deployed to assess U concentrations in natural waters due to the lability of the metal and its organic complexes (particularly in alkaline settings). It has been demonstrated in this chapter that 1 resin layer is sufficient to obtain a time weighted average in this particular environmental setting (high pH calcium-carbonate dominated systems).

8.6 References

[1] C. Murdock, M. Kelly, L.-Y. Chang, W. Davison, H. Zhang, DGT as an *in situ* tool for measuring radiocesium in natural waters, Environmental Science & Technology, 35 (2001) 4530-4535.

[2] J.G. Panther, P.R. Teasdale, W.W. Bennett, D.T. Welsh, H.J. Zhao, Titanium dioxide-based DGT technique for *in situ* measurement of dissolved reactive phosphorus in fresh and marine waters, Environmental Science & Technology, 44 (2010) 9419-9424.

[3] H. Mengistu, O. Roeyset, A. Tessema, T. Abiye, M. Demlie, Diffusive gradient in thin-films (DGT) as risk assessment and management tools in the Central Witwatersrand Goldfield, South Africa, Water South Africa, 38 (2012) 15-22.

[4] K.W. Warnken, W. Davison, H. Zhang, J. Galceran, J. Puy, *In situ* measurements of metal complex exchange kinetics in freshwater, Environmental Science & Technology, 41 (2007) 3179-3185.

[5] H. Zhang, W. Davison, Direct *in situ* measurements of labile inorganic and organically bound metal species in synthetic solutions and natural waters using diffusive gradients in thin films, Analytical Chemistry, 72 (2000) 4447-4457.

[6] I.I. Fasfous, T. Yapici, J. Murimboh, N.M. Hassan, C.L. Chakrabarti, M.H. Back, D.R.S. Lean, D.C. Grégoire, Kinetics of trace metal competition in the freshwater environment: some fundamental characteristics, Environmental Science & Technology, 38 (2004) 4979-4986.

[7] J.L. Levy, H. Zhang, W. Davison, J. Puy, J. Galceran, Assessment of trace metal binding kinetics in the resin phase of diffusive gradients in thin films, Analytica Chimica Acta, 717 (2012) 143-150.

[8] J. Levy, H. Zhang, W. Davison, J. Puy, J. Galceran, Does the Chelex resin in DGT devices really act as a perfect planar sink for metals? Kinetic limitations of DGT measurements, Geochimica Et Cosmochimica Acta, 74 (2010) A586-A586.

[9] S. Mongin, R. Uribe, J. Puy, J. Cecilia, J. Galceran, H. Zhang, W. Davison, Key Role of the Resin Layer Thickness in the Lability of Complexes Measured by DGT, Environmental Science & Technology, 45 (2011) 4869-4875.

[10] J. Zhao, I.I. Fasfous, J.D. Murimboh, T. Yapici, P. Chakraborty, S. Boca, C.L. Chakrabarti, Kinetic study of uranium speciation in model solutions and in natural waters using Competitive Ligand Exchange Method, Talanta, 77 (2009) 1015-1020.

[11] J.L. Levy, H. Zhang, W. Davison, J. Galceran, J. Puy, Kinetic signatures of metals in the presence of Suwannee River Fulvic Acid, Environmental Science & Technology, 46 (2012) 3335-3342.
[12] M.R. Shafaei Arvajeh, N. Lehto, Ø.A. Garmo, H. Zhang, Kinetic studies of Ni organic complexes using diffusive gradients in thin films (DGT) with double binding layers and a dynamic numerical model, Environmental Science & Technology, 47 (2012) 463-470.
[13] R. Uribe, S. Mongin, J. Puy, J. Cecilia, J. Galceran, H. Zhang, W. Davison, Contribution of partially labile complexes to the DGT metal flux, Environmental Science & Technology, 45 (2011) 5317-5322.
[14] J. Puy, R. Uribe, S. Mongin, J. Galceran, J. Cecilia, J. Levy, H. Zhang, W. Davison, Lability criteria in diffusive gradients in thin films, Journal of Physical Chemistry A, 116 (2012) 6564-6573.
[15] J.J. Lenhart, S.E. Cabaniss, P. MacCarthy, B.D. Honeyman, Uranium(VI) complexation with citric, humic and fulvic acids, Radiochimica Acta, 88 (2000) 345.
[16] L. Duquène, H. Vandenhove, F. Tack, M. Van Hees, J. Wannijn, Diffusive gradient in thin films (DGT) compared with soil solution and labile uranium fraction for predicting uranium bioavailability to ryegrass, Journal of Environmental Radioactivity, 101 (2010) 140-147.
[17] C.M. Hutchins, J.G. Panther, P.R. Teasdale, F. Wang, R.R. Stewart, W.W. Bennett, H. Zhao, Evaluation of a titanium dioxide-based DGT technique for measuring inorganic uranium species in fresh and marine waters, Talanta, 97 (2012) 550-556.
[18] H. Zhang, W. Davison, Diffusional characteristics of hydrogels used in DGT and DET techniques, Analytica Chimica Acta, 398 (1999) 329-340.
[19] Tables of Physical & Chemical Constants in: 2.2.3 Viscosities, Kaye & Laby Online, 2005.
[20] K.W. Warnken, H. Zhang, W. Davison, Accuracy of the diffusive gradients in thin-films technique: diffusive boundary layer and effective sampling area considerations, Analytical Chemistry, 78 (2006) 3780-3787.
[21] H.P. Jarvie, C. Neal, M.D. Jürgens, E.J. Sutton, M. Neal, H.D. Wickham, L.K. Hill, S.A. Harman, J.J.L. Davies, A. Warwick, C. Barrett, J. Griffiths, A. Binley, N. Swannack, N. McIntyre, Within-river nutrient processing in Chalk streams: The Pang and Lambourn, UK, Journal of Hydrology, 330 (2006) 101-125.

[22] T.J. Marsh, M.L. Lees, Hydrometric Register and Statistics 1996-2000. Hydrological data UK series., in, Centre for Ecology and Hydrology / British Geological Survey, Wallingford, 2003, pp. 210.
[23] R.M.S. Smith, D.J. Evans, H.S. Wheater, Evaluation of two hybrid metric-conceptual models for simulating phosphorus transfer from agricultural land in the river enborne, a lowland UK catchment, Journal of Hydrology, 304 (2005) 366-380.
[24] W.C. Li, D.M. Victor, C.L. Chakrabarti, Effect of pH and uranium concentration on interaction of uranium(VI) and uranium(IV) with organic ligands in aqueous solutions, Analytical Chemistry, 52 (1980) 520-523.

Chapter 9: Kinetic signature and lability of uranium in the presence of humic acid

9.1 Introduction

Biological activity of a metal is related to the concentration of the free metal ion, and the bioavailability of organically complexed metals [1]. In dyanamic systems such as rivers, where the inputs of dissolved organic carbon (DOC) may fluctuate with rainfall, runoff and surrounding land use, prediction of the metal bioavailability can be difficult to determine. Measurement of bioavailability can be achieved through numerical modelling, using such programmes as WHAM [2], Visual Minteq [3] or PHREEQC [4]. Other methods of determining the bioavailability of the organically complexed metals include assessing dissociation rates in that particular system. This provides an indication of the lability of the metal and therefore how readily it will take part in biological reactions. Lability is used to measure the contribution of various components of a dissolved metal to the flux to biological systems. The degree of lability (ζ) has been described by Mongin *et al.* [5] as:

$$\xi = \frac{J - J_{free}}{J_{labile} - J_{free}} \qquad \text{Equation 9.1}$$

where J denotes the actual metal flux, J_{free} is the free metal flux if there was no contribution from the complexed or inert component, and J_{labile} is the metal flux expected if the complexed metal was fully labile. This examines the ratio of the free metal to the labile metal, or the contribution of the metal-complex to the flux compared to a fully labile system. Uribe *et al*. [6] also described the term lability in the terms of uptake of a metal ion by an organism (or sensor) being limited by either the diffusion of the metal ion-complex or by the dissociation kinetics. A fully labile system is where the contribution of the metal-organic complex to the flux is negligible because the dissociation kinetics are very fast. An inert system is where the dissociation kinetics of the metal-organic complex are so slow that they cannot contribute to the flux of metal to the sensor or organism. Lability is influenced by a number of factors including the kinetics of the metal-ligand association and dissociation, the size of the sensor (or organism), the mixture of ligands in a system and the rate and processes that sorb or consume the target analyte [7].

Examples of previous work to define lability have used competitive ligand exchange models (CLEM) to estimate the dissociation rates of uranium (U), based on

the principle that U dissociation is related to the rate of uptake of U by a ligand (such as Chelex-100 resin [1, 8] or humic substances [9]). Passive sampling techniques such as diffusive gradients in thin films (DGT) take up only the bio-available or labile fractions of metals in aquatic systems [10], which includes the metal ions dissociating from dissolved organics that may not be sorbed by the receiving phase or resin. The contribution of fast and slow dissociating organically bound metals provides further information about the potential toxicity of a metal, with more recent studies using DGT to estimate association, dissociation and stability constants of organo-metal complexes [11, 12].

Interactions between U and DOC have been shown so far in this thesis to be critical in determining speciation of U in natural fluvial systems. Marine systems are governed by carbonate chemistry and U complexes formed reflect this [13]. However, due to the dynamic nature of fluvial water quality (as shown in Chapter 5), the complexes U form may fluctuate and therefore change the interaction of U with the DGT devices. These changes can affect the lability of U, associated diffusion coefficients, and hence affect the uptake of U by DGT. This provides important information as to the bioavailability of U. In a system where dissociation kinetics of the complex are fast and occur prior to the metal ligand diffusing through to the resin layer, the system is thought to be *fully labile*. In a system where the U-ligand does not fully dissociate along the diffusion path through the DGT diffusive layer, it is thought to be *partially labile* [11, 12, 14] or kinetically limited.

The underpinning principle of DGT is based upon a steady state flux of the metal ion through the diffusive layer, with a zero concentration at the resin interface (assuming the metal binds quickly and irreversibly to the resin and that the binding sites are evenly distributed in the resin gel layer and in excess) [14]. By varying the thickness of the diffusive layer, the time taken for a metal ligand to dissociate can be altered i.e. the longer the diffusional pathway, the greater amount of the metal ligand can dissociate, effectively increasing the lability of the complex [12, 15]. Varying the length of the diffusional pathway has been used previously to estimate the thickness of DBL, which has been considered as a purely physical phenomenon, based entirely on flow rate and advective processes. However, the possibility of a layer of dissociation of the metal-ligand should be considered in addition to the physical DBL. This is particularly evident when previous field data is examined. Warnken *et al*. [11] established the physical thickness of the DBL as ~ 0.23 mm when the flow rate is > 0.2 cm s^{-1}. DBL

values reported in this thesis from field measurements (Table 9.1) are far in excess of this value, even in high flow conditions.

Table 9.1 Summary table of measured field DBLs in this study so far in the fluvial settings, the River Lambourn and the River Enborne.

River	Deployment time (d)	DBL (cm)	Flow rate ($m\ s^{-1}$)	Chapter
Lambourn	5	0.046 ± 0.006	0.09	4
	7	0.070 ± 0.022	0.09	5
	7	0.070 ± 0.032	0.08	5
	7	0.088 ± 0.009	0.09	5
	7	0.062 ± 0.018	0.09	5
	3	0.074 ± 0.013	0.09	7
	7	0.094 ± 0.015	0.08	7
Enborne	7	0.141 ± 0.036	0.03	5
	7	0.086 ± 0.034	0.04	5
	7	0.047 ± 0.008	0.22	5
	7	0.037 ± 0.009	0.20	5
	3	0.052 ± 0.020	0.05	7
	7	0.062 ± 0.019	0.05	7

The data in Table 9.1 indicates that the thickness of the DBL is consistently higher than the predicted laboratory-based estimates [16, 17]. Speciation modelling (see Chapter 5) of the water quality data of these field sites, showed that up to 90% of the U in the River Enborne is complexed with organic material, whilst in the River Lambourn only up to 7% of the U is organically complexed, with the majority of the U complexed as carbonate species in this system. Theoretically, the DBL should be the same, between the River Lambourn and the River Enborne with the one exception being the very low flow measurement in the River Enborne (the first DBL reading in Table 9.1 for the River Enborne). What this implies is that other processes are affecting the size of the DBL. This chapter explores the possibility of a zone of dissociation existing in addition to the physical DBL, which has been termed an apparent diffusive boundary layer (ADBL) [11, 12, 14].

Chapter 8 presented data on association rates of U and Metsorb^{TM} resin and the penetration of uranyl ions (UO_2^{2+}) and U complexed with humic acid (HA) into the resin gel layer, as an indication of the lability of U. What was found in Chapter 8 was that the penetration depth of U into the resin layer was high, but the cause of this was uncertain. As the systems used in Chapter 8 were fully labile, one theory explaining the high penetration factor was heterogeneity in the resin gel introduced during the resin layer fabrication process. Here, lability is directly measured using a kinetic signature or term g_{kin}^{P} that is derived from the discrepancy of the ADBL and DBL values, accounting

for the dissociation rate constants of the metal-ligand [12]. The kinetic term can then be used to calculate the log *K* (the complexation stability constant) and to quantify how labile the complex is [12].

Both Levy *et al*. [12] and Warnken *et al*. [11] have undertaken studies to examine metal complex kinetics *in situ* by calculating the ADBL. A thicker ADBL was found in the field than under laboratory conditions, which was determined to be as a function of the strength of the metal-ligand complex and dissociation kinetics. This Chapter will determine the stability constants and kinetic signature for U in a simple laboratory solution with HA additions. Two pH values were used: 7.8 (to reflect the pH of the field sites used in this study) and pH 5 to estimate the lability of U complexes and to determine if the supply of dissociating organically bound U to DGT devices was kinetically limited.

9.2 Materials and Methods

Chemicals were of analytical grade or better and supplied by Fisher Scientific (Loughborough, U.K.), unless otherwise specified. Milli-Q (ultra-pure) water (> 18.2 MΩ cm, Millipore, Watford, U.K.) was used as the laboratory water. All uranium ICP-MS standards and experimental working solutions were prepared in low density polyethylene (LDPE) or polystyrene (PS) containers with polypropylene lids (PP) from a 1000 mg L^{-1} in 2% HNO_3 (Spex Certiprep, Fisher Scientific) U stock solution unless otherwise stated. The ICP-MS internal standard was prepared from a 1000 mg L^{-1} in 2% HNO_3 (Spex Certiprep) bismuth stock solution. The experimental solutions were adjusted to a given pH by addition of either 1 M HNO_3 or 1 M NaOH, and to a given ionic strength by addition of $NaNO_3$, with the pH and temperature monitored throughout experiments. Solutions were equilibrated with atmospheric CO_2 for 24 h before use unless otherwise specified. All HA solutions were prepared using HA as sodium salt (Sigma Aldrich, Fisher Scientific Ltd), from a stock solution of 1000 mg L^{-1} HA in 0.1 M NaOH. All readings were undertaken in triplicate with containers open to the atmosphere to ensure continuing equilibration with the atmospheric pCO_2 (i.e. to ensure a constant inorganic carbon concentration throughout the experiments). All plastic apparatus was soaked for 24 h in 10% HNO_3 and rinsed three times in Milli-Q water prior to use.

9.2.1 Analysis of DGT devices

The Metsorb-DGT devices were prepared as per Chapter 3, after Zhang and Davison [10], with diffusive layer thicknesses of 0.015 cm (filter only), 0.055 cm, 0.95 cm and 0.135 cm. After exposure, the Metsorb binding gels were removed from the DGT devices and eluted (48 h) with 1 M H_2O_2/1 M HNO_3 (2 mL) solution (100 mL made by combining 90 mL 1.1 M HNO_3 and 10 mL 35% H_2O_2). The eluents were then diluted 10 fold with Milli-Q water prior to instrumental analysis by ICP-MS using an Agilent 7500ce series instrument (Agilent Technologies Inc., Japan), as per Chapter 3.

9.2.2 Model description and calculations

To determine the quantity of U accumulated by each of the resin disks, the concentration of U measured by the ICP-MS in µg L^{-1} from the eluent was multiplied by the dilution factor (×10) to give the U concentration (*Ce*). The absolute mass (*M*) in ng of the U in the resin gel was then calculated using equation 9.2, where *M* is calculated taking into account the gel volume (*Vg*, cm^3), the eluent volume (*Ve*, mL), the measured concentration of U in the eluent (*Ce*, ng mL^{-1}) and the elution factor (*fe*) [10], which was found to be 0.84 in Chapter 4.

$$M = \frac{Ce(Vg+Ve)}{fe} \qquad \text{Equation 9.2}$$

The diffusive boundary layer (δ) thickness was calculated using equations 9.3 and 9.4 after Warnken *et al.* [16] . A straight line plot of *1/M* vs *Δg* has a slope (*m*) of $1/(DC_{DGT}At)$ and an intercept (*b*) of $\delta/(DC_{DGT}At)$:

$$\frac{1}{M} = \frac{\Delta g}{DC_{DGT}At} + \frac{\delta}{DC_{DGT}At} \qquad \text{Equation 9.3}$$

The intercept (*b*) divided by the slope (*m*) of this plot gives the diffusive boundary layer thickness δ:

$$\delta = \frac{b}{m}\left(\frac{D_M^W}{D_M^{gel}}\right) \qquad \text{Equation 9.4}$$

and from the 1/*M* plots as per equation 9.3, the C_{DGT} can be found using equation 9.5

$$C_{DGT} = \frac{1}{bD_M^{gel}At} \qquad \text{Equation 9.5}$$

where D_M^{gel} is the diffusion coefficient of the metal in the gel and D_M^W the diffusion coefficient in water (from Kerisit and Liu [18] as described in Chapter 3). Diffusion coefficients in the gel were as determined at different pHs for U by Hutchins *et al.* [19] and were corrected for temperature (T, ^{o}C) using the Stokes-Einstein equation (equation 9.6) [20] and the viscosity of water (η, mPa s) [21]:

$$\frac{D_1\eta_1}{T_1} = \frac{D_2\eta_2}{T_2} \qquad \text{Equation 9.6}$$

To calculate the impact that metal complexation has on the uptake of U by DGT, the following model was developed by Levy *et al.* [12] to link the variances in diffusion characteristics between free and complexed metals, the stability of the metal ligand complex and the diffusive boundary layer. Metal ligand association is described as:

$$M + L \underset{k_d}{\overset{k_a}{\rightleftharpoons}} ML \qquad \text{Equation 9.7}$$

The ligand is assumed to be in excess and equal to the bulk concentration (c_L), with c_M and c_{ML} the concentrations of the metal and metal complex respectively. The stability or equilibrium constant of the metal-ligand complex:

$$K = \frac{c_{ML}}{c_M c_L} = \frac{k_a}{k_d} \qquad \text{Equation 9.8}$$

A 1:1 HA:U binding ratio is assumed despite the heterogeneity of the HA molecule. This complex stoichiometry of 1:1 is defined as a metal ion bound to an unknown number of functional groups within 1 HA molecule [22]. This allows for simplicity and for 1 stability constant (equation 9.8) to be used. The results consider the kinetic limitations of the total and tightly complexed binding sites in a humic molecule to avoid over-simplification of the system.

The flux of metal to the DGT device considers the ratio of diffusion coefficients in the gel ($\varepsilon^{gel} = D_{ML}^{gel}/D_M^{gel}$) and water ($\varepsilon^{w} = D_{ML}^{w}/D_M^{w}$) to account for diffusion both within the gel and the water forming the DBL, and the global stability constant $K' = K_{CL}^{*} = (c_{ML}^{*})/(c_M^{*})$ of the metal ligand complex (with * indicating bulk solution concentrations) and assuming quasi-steady state (from Puy *et al.* [14], and Warnken *et al.* [11] but with the penetration factors added in by Levy *et al.* [23, 24] and discussed in Chapter 8):

$$\frac{1}{M} = \left[\frac{\delta}{M_M D_M^W (1+\varepsilon^W K') c_M^* At} + \frac{g_{kin}^P}{M_M D_M^{gel} (1+\varepsilon^{gel} K') c_M^* At} + \frac{g}{M_M D_M^{gel} (1+\varepsilon^{gel} K') c_M^* At}\right]$$ Equation 9.9

g_{kin}^P is g_{kin} described by Warnken *et al*. [11] but includes the penetration of the metal ligand into the resin layer (λ_{ML}):

$$g_{kin}^P \equiv \frac{\varepsilon^{gel} K' m tanh\frac{g}{m}}{1+\varepsilon^{gel} K' m tanh\frac{g}{m}\left(\frac{1}{\varepsilon^{gel} K'}+1\right)\frac{1}{\lambda_{ML}} tanh\frac{r}{\lambda_{ML}}}$$ Equation 9.10

where *r* is the resin thickness and μ is the reaction layer thickness (explained in Chapter 8):

$$\mu = \sqrt{\frac{D_M}{k_a'}}$$ Equation 9.11

m is the disequilibrium parameter. This arises when the resupply of the metal is not in equilibrium with the dissociating metal complexes and metal consumption by the resin [6]. This disequilibrium zone can extend into the resin layer [6, 12, 14]:

$$m = \mu\sqrt{\frac{\varepsilon^{gel} K'}{1+\varepsilon^{gel} K'}}$$ Equation 9.12

λ_{ML} is can be calculated from *m* and μ by [12, 14]:

$$\lambda_{ML} = \sqrt{\frac{D_{ML}}{k_d}} = \sqrt{\varepsilon^{gel} K' \mu} = m\sqrt{1+\varepsilon^{gel} K'}$$ Equation 9.13

The ADBL can be measured by plotting 1/*M* for multiple devices with a range of diffusion layer thicknesses and can also be used to identify the kinetic dissociation distance g_{kin}^P (cm):

$$ADBL = \frac{i}{s} = \frac{D_M^{gel}(1+\varepsilon^{gel} K')}{D_M^W (1+\varepsilon^W K')}\delta + g_{kin}^P = P\delta + g_{kin}^P$$ Equation 9.14

where *P* can be isolated from equation 9.14:

$$P = \frac{D_M^{gel}(1+\varepsilon^{gel} K')}{D_M^W (1+\varepsilon^W K')}$$ Equation 9.15

The factor $P = \frac{D_M^{gel}(1+\varepsilon^{gel} K')}{D_M^W (1+\varepsilon^W K')}$ can vary between D_M^{gel}/D_M^W, which is 0.81 and 0.58 for the pH 7.8 and pH 5 experiments respectively, and $D_M^{gel}\varepsilon^{gel}/D_M^W\varepsilon^W$ when $C_M << C_{ML}$, which is 0.14 and 0.10 for the pH 7.8 and pH 5 experiments respectively [11]. As HA is the ligand, this has a D_{ML}^{gel} of 7% that of uncomplexed metal ions (D_M^{gel}) [25] (in the study by Levy *et al*.[12], fulvic acid has been used as the binding ligand, which due to its smaller size has a D_M^{gel} of 20% of uncomplexed metal). This very low diffusion coefficient value for HA is as a result of steric effects. D_{ML}^W is 0.4 D_M^W [11, 26] based on the self diffusion coefficient of uranium at 18°C being 4.61 x 10^{-6} cm^2 s^{-1} [18]

and an average of HA diffusion coefficients of various HA types measured in water [26].

Using experimental data on ADBL, μ can be calculated using equation 9.16, P can be can be calculated using equation 9.15 and δ using an iterative process on equation 9.14; m and λ_{ML} can then be calculated using equations 9.12 and 9.13 above:

$$g_{kin}^{P} = \frac{\varepsilon K\prime\mu}{1+\sqrt{\varepsilon K\prime}tanh\frac{r}{\sqrt{\varepsilon K\prime\mu}}} \qquad \text{Equation 9.16}$$

The lability degree (ξ) was also calculated using equation 9.17 [6]:

$$\xi = 1 - \frac{1+\varepsilon K\prime}{\varepsilon K' + \frac{g}{m}coth\left(\frac{g}{m}\right) + \frac{g}{\lambda_{ML}}(1+\varepsilon K')tanh\left(\frac{r}{\lambda_{ML}}\right)} \qquad \text{Equation 9.17}$$

where ξ= 1 the metal ligand system is fully labile.

Full derivation of the equations detailed above can be found in Levy *et al*. [12].

9.2.3 Effect of flow rate on the diffusive boundary layer (DBL)

A physical DBL was established under a variety of flow conditions (high medium and low) with no organic ligand in a laboratory setting in order to confirm that U has a similar thickness of DBL under high flow conditions as previously established by Warnken *et al*. [16] for other metals.

To investigate the effect of flow rate on the DBL thickness, three acid washed PP containers (5 L) containing a 0.01 M $NaNO_3$, 100 µg L^{-1} U solution (3 L) and 0.983 mM $NaHCO_3^-$ to buffer the solution to pH 7.8 (the pH of the field sites used in this study and to prevent sorption of U to the walls of the PP containers), were equilibrated for at least 24 h. The stir rates of the 3 tanks were set to 0 rpm, 200 rpm and 400 rpm in order to mimic low, moderate and high flow conditions respectively. DGT devices containing different diffusive gel layer thickness previously described (0.015 cm, 0.055 cm, 0.095 cm and 0.135 cm) were then deployed (24 h) in triplicate, then removed and eluted as per Section 9.2.1. One mL aliquots of the exposure tank solution were taken at the start and end of each experiment and acidified (using 20 µL 6 M HCl) to measure the concentration of U. Equation 9.5 was used to calculate the C_{DGT}, and this was compared to U concentrations in the grab samples.

9.2.4 Effect of humic acid on the diffusive boundary layer (DBL)

To investigate the effect of humic acid on the DBL thickness, three acid washed PP containers (5 L) containing a 0.01 M $NaNO_3$, 100 µg L^{-1} U solution (3 L) and 0.983 mM $NaHCO_3^-$ to buffer the solution to pH 7.8 (the pH of the field sites used in this

study and to prevent sorption of U to the walls of the PP containers), were equilibrated for at least 24 h. The stir rates of the 3 experimental tanks were set at a stir rate of 400 rpm (in order to replicate high flow conditions so that flow rate would not contribute to any change in the DBL) with three different HA concentrations to reflect three HA:U ratios. The HA concentrations were 100 mg L^{-1} (HA:U 1000:1), 10 mg L^{-1} (HA:U 100:1) and 1 mg L^{-1} (HA:U 10:1). DGT devices containing different diffusive gel layer thickness previously described (0.015 cm, 0.055 cm, 0.095 cm and 0.135 cm) were then deployed (24 h) in triplicate, then removed and eluted as per Section 9.2.1. One mL aliquots of the exposure tank solution were taken at the start and end of each experiment and acidified (using 20 µL 6 M HCl) to measure the concentration of U. Equation 9.5 was used to calculate the C_{DGT}, and this was compared to U concentrations in the grab samples.

9.2.5 Investigating the presence of the apparent diffusive boundary layer (ADBL)

To investigate the presence of an ADBL, four acid washed PP containers (5 L) containing a 0.01 M $NaNO_3$, 100 µg L^{-1} U solution (4 L) plus 0.983 mM L^{-1} $NaHCO_3^-$ to buffer the solution to pH 7.8 (the pH of the field sites used in this study and to prevent sorption of U to the walls of the PP containers) in two of the containers, with two containers having no buffer and adjusted to pH 5, were equilibrated for at least 24 h. One of each of the experimental containers with pH 7.8 and pH 5 had an HA addition of 10:1 and the other container 100:1 (so 1 mg L^{-1} HA in 1 tank at pH 7.8 and pH 5, and 10 mg L^{-1} HA in 1 tank at pH 7.8 and pH 5). The stir rates of the tanks were set to 400 rpm. DGT devices containing different diffusive layer thickness previously described (0.015 cm, 0.055 cm, 0.095 cm and 0.135 cm) were then deployed for 8 d (to ensure adequate U accumulation for accurate determination of ADBL, as described by Levy *et al.* [12]) in triplicate, then removed and eluted as per Section 9.2.1. One mL aliquots of the exposure tank solution were taken each day during the experiment and acidified (using 20 µL 6 M HCl) to measure the concentration of uranium. Equation 9.5 was used to calculate the C_{DGT}, and this was compared to U concentrations in the grab samples.

A blank exposure tank containing a 0.01 M $NaNO_3$, 100 µg L^{-1} U solution (3 L) pH 5 was prepared and a blank (no HA) experiment run for 24. The results for the blank (no HA) pH 7.8 condition described in section 9.2.3 were used as the blank for the ADBL pH 7.8 experiments.

9.3 Results

9.3.1 Effect of flow rate on the diffusive boundary layer (DBL)

Initial experiments were performed to assess the size of the physical DBL (δ) for U and confirm that the effect of stir rate under laboratory conditions were similar to other metals tested in previous work [16, 17]. For each experiment the DGT devices with variable diffusive layer thickness (0.015, 0.055, 0.095 and 0.135 cm) were deployed for 24 hours in an exposure tanks with 100 μg L^{-1} U at pH 7.8 with 3 different stir rates. The mass accumulated was plotted, as per equation 9.3, and the DBLs calculated according to equation 9.4 and shown in Table 9.2 below.

Table 9.2 Measured DBL thickness (cm) at three stir rates to reflect low, medium and high flow rate conditions, where I = 0.01M, pH 7.8, 17°C, deployment time is 24 h and the U addition is 100 μg L^{-1}.

Flow	Stir rate (rpm)	DBL (cm)	1/M v Δg plot R^2
High	400	0.025 ± 0.002	0.99
Medium	200	0.032 ± 0.011	0.98
Low	0	0.062 ± 0.004	0.99

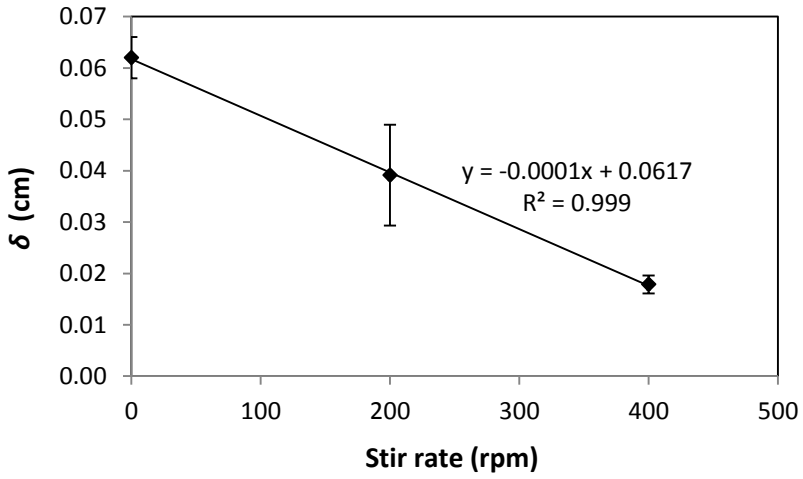

Figure 9.1 DBL thickness (δ) (cm) with changing stir rate, where I = 0.01M, pH 7.8, 17°C, deployment time is 24 h and the U addition is 100 μg L^{-1}. Error bars are the DBL uncertainties, as described in Chapter 3.

The physical DBL (seen in Table 9.2 and Figure 9.1) increases linearly (R^2 = 0.99) with decreased turbulence, thereby increasing the thickness of diffusive pathway of the analyte, and decreasing the influence of advective transfer of the analyte to the DGT device. The results of 0.025 ± 0.002 cm at 400 rpm (high stir rate) are consistent with those obtained in the study by Warnken *et al.* [16] , which found that even in highly turbulent waters (magnetic stirrer rpm = 1000) a very small diffusion layer exists on the surface of the DGT of ~ 0.023 cm. The DBL results for the stagnant conditions

(0 rpm) are not as large as those obtained by Warnken *et al*. [16] , which were up to 0.15 cm, and could be as a result of differing experimental conditions (tank size, deployment time). The DBL for U was 0.062 ± 0.004 cm when the stir rate was zero in this experiment.

9.3.2 Effect of humic acid on the diffusive boundary layer (DBL)

Experiments were then conducted to observe any changes in the size of the DBL with increasing HA:U ratios as an indication of the potential presence of an ADBL. Here, DGT devices with variable diffusive gel thickness (0.015, 0.055, 0.095 and 0.135 cm) were deployed for 24 hours in well stirred (stir rate, 400 rpm) exposure tanks with 100 µg L^{-1} U at pH 7.8 with HA additions of 1, 10 and 100 mg L^{-1}, which represent HA:U ratios of 10:1, 100:1 and 1000:1 respectively. The results are shown in Table 9.3 and Figure 9.2 below. The physical DBL under high stir conditions had been measured at 0.025 ± 0.002 cm (Table 9.2). The results shown in Table 9.3 indicate that the DBL increases with increasing HA:U ratio. There could be several explanations for this. Potentially the HA has precipitated out of solution and coated the surface of the DGT devices; thereby creating a physical barrier to diffusion and providing the illusion of an increased DBL. However, as the HA was first prepared in 0.1 M NaOH and then used in a slightly alkaline solution (pH 7.8), it is unlikely the HA will precipitate out as it is soluble in neutral to alkaline conditions [9]. An alternative explanation is that the U is binding with the HA to create a zone of complex dissociation and effectively extending the size of the DBL.

Table 9.3 Measured DBL thickness (cm) at three HA concentrations; where I = 0.01M, pH 7.8, 17°C, deployment time is 24 h and the U addition is 100 μg L^{-1}.

HA:U ratio	HA concentration (mg L^{-1})	DBL (cm)	1/M v Δg plot R^2
10:1	1	0.084 ± 0.020	0.93
100:1	10	0.077 ± 0.007	0.92
1000:1	100	0.152 ± 0.005	0.97

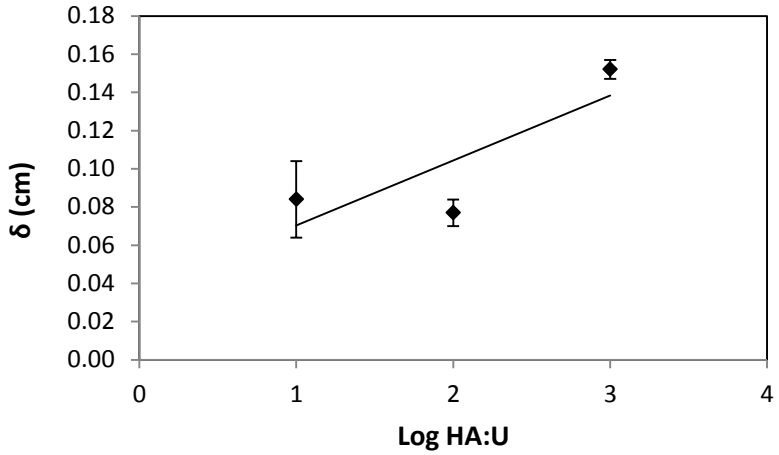

Figure 9.2 DBL thickness (δ) (cm) with changing HA:U ratio, where I = 0.01M, pH 7.8, 17°C, deployment time is 24 h and the U addition is 100 μg L^{-1}. Error bars are the DBL uncertainties, as described in Chapter 3, section 3.1.4. HA concentrations shown in log form because of the large range of concentrations tested.

From the initial DBL data shown in Table 9.3 and Figure 9.2, it can be seen that increasing the HA:U ratio has an effect on the DBL thickness. When the HA:U ratio is between 10 to 100, the affect on the DBL is unchanged (within error), however the DBL is still approximately four times larger than that in the experimental tank without HA. This implies a sharp increase in the thickness of the DBL as U binds to the HA, with another increase after the HA:U ratio exceeds 100. This may be as a result of the U binding to different functional groups within the HA. There are three common binding mechanisms between a metal cation and HA: weak electrostatic attraction, weak organic binding with the carboxylic groups, and strong organic binding to the phenolic groups [11]. Other functional groups exist in the HA structure such as amino, sulfhydryl and quinine groups but because of their low abundance, they are not considered to be as influential in cation binding [27]. As the minor phenolic sites bind U tighter than the carboxylic sites (which form the majority of the HA binding sites) it is suggested that these are occupied by the metal ion first, then as the metal loading increases, the carboxylic sites fill, decreasing in stability with increasing metal:ligand ratio [8, 9]. What this suggests is that the DBL increases incrementally as the U dissociates from the different functional groups. The binding of the U to the HA was modelled using Visual

Minteq, Nica-Donnan DOC parameters because the NICA (non ideal competitive adsorption) model can account for non-ideal binding to heterogeneous ligands [27] (such as humic substances) and provide specific bonding information for HA, rather than a generic humic molecule. The results of the speciation modelling can be seen in Table 9.4. Previous studies have found that U is bound to two distinctive binding sites on an HA molecule, with a difference in stability constants in the order of 10^2 [28], which are possibly the weakly acidic phenolic sites with a high affinity for U, and the lower affinity carboxylic sites. However, it should be noted that due to the heterogeneous and continuous nature of a HA molecule, it can be difficult to determine the exact contribution of the binding sites to the dissociation rate constants. Instead Zhao *et al*. [9] used a kinetic term to distinguish between two binding phases for the U-HA molecule: fast (labile) and slow (non-labile) components. As previously stated, the dissociation of U from HA is likely to be responsible for the increasing DBL thickness, or ADBL when chemical rather than physical processes dominate.

Table 9.4 U speciation distribution as a % of total U for each experimental solution containing HA and for the blank solution at pH 7.8. Modelled using Visual Minteq with NICA-Donan DOC parameters. HA1 are carboxylic groups and HA2 are the phenolic groups in the humic acid.

Species	**% U species distribution**			
	1 mg L^{-1} HA	10 mg L^{-1} HA	100 mgL^{-1} HA	No HA
UO_2OH^+	0.27	0.046	0	0.324
$UO_2(OH)_3^-$	1.083	0.187	0	1.299
$UO_2(OH)_{2\,(aq)}$	1.945	0.335	0	2.336
$UO_2CO_{3\,(aq)}$	5.815	1.001	0	6.982
$UO_2(CO_3)_2^{-2}$	36.688	6.315	0.031	43.889
$UO_2(CO_3)_3^{-4}$	38.162	6.563	0.032	45.167
HA1-$UO_2(6)_{(aq)}$	14.587	77.288	84.75	0
HA2-$UO_2(6)_{(aq)}$	1.447	8.265	15.179	0

When the HA:U ratio is 10:1 (when HA is 1mg L^{-1} here) it can be seen from Table 9.4 that the majority of the U is complex as carbonate species, with only 1.5% of the total dissolved U is bound to the phenolic groups and 14.6% to the carboxylic groups. The increase in U binding to phenolic groups with increasing HA concentration at pH 7.8 can be seen in Table 9.4. What is also noticeable is that U in the carbonate form is less than 0.1% of the total U species when the HA addition is 100 mg L^{-1}. This may act to reduce the lability of the U, hence increasing the DBL and the concurrent y-intercept on the 1/*M* plot.

The U species formed at pH 5 can be found in Table 9.5 below. There are few carbonate species present at this pH with no addition of HA, with predominantly uranyl

and hydrolysed uranyl species. In the presence of 1 mg L^{-1} HA, the uranyl forms phenolic bonds but to a lesser extent than at pH 7.8 where there is a higher concentration of carbonate species. However there are a greater % of carboxylic complexes formed at pH 5 than pH 7.8, in addition to some weak electrostatic attraction between the HA and the uranyl cation. Examination of the distribution of the uranyl cation at various pH's with HA shows that as the HA increases in alkaline waters, the U preferentially binds to the strong phenolic sites, and at pH 5, the U bonds with HA are weaker.

Table 9.5 U speciation distribution as a % of total U for each experimental solution containing HA and for the blank solution at pH 5. Modelled using Visual Minteq with NICA-Donan DOC parameters. HA1 are carboxylic groups and HA2 are the phenolic groups in the humic acid. +2D represents a weak electrostatic bond between the humic substance and the uranyl cation.

Species	**% U species distribution**		
	1 mg L^{-1} HA	**10 mg L^{-1} HA**	**No HA**
UO_2^{2+}	20.198	0.138	69.011
UO_2OH^+	8.287	0.057	28.31
$(UO_2)_2(OH)_2^{2+}$	0.034	0	0.35
$UO_2(OH)_{2\,(aq)}$	0.095	0	0.324
$UO_2CO_{3\,(aq)}$	0.283	0	0.968
$UO_2NO_3^+$	0.3	0	1.025
$(6)UO_2{+}2D_{(aq)}$	0.196	0.017	0
$HA1\text{-}UO_2(6)_{(aq)}$	69.914	98.377	0
$HA2\text{-}UO_2(6)_{(aq)}$	0.691	1.408	0

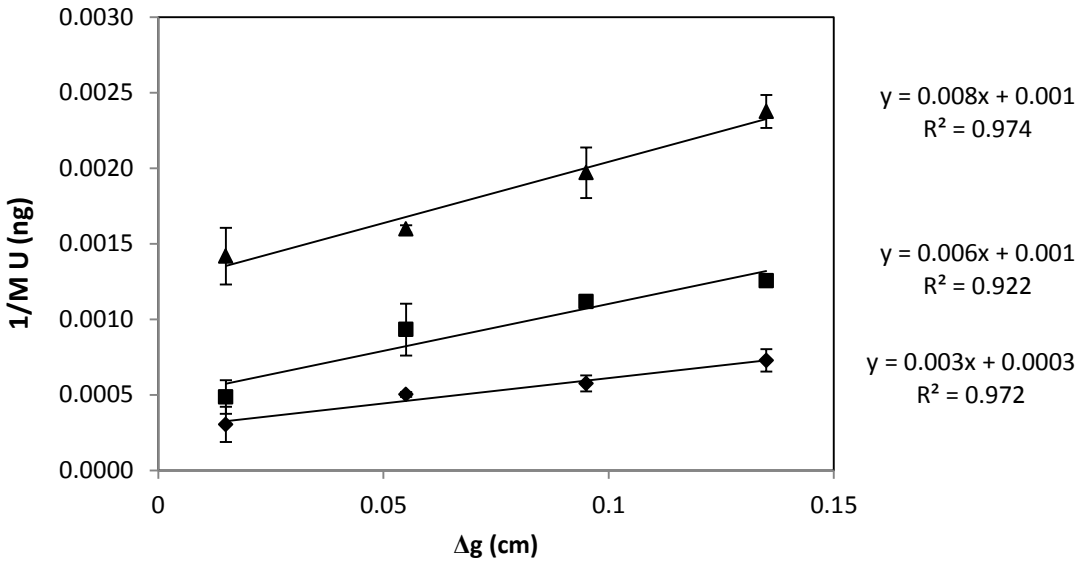

Figure 9.3 1/*M* against diffusive gel thickness plots (as per equation 9.3) for the DBL measurements with increasing HA additions. Diamonds represent a 1 mg L^{-1} HA addition (HA:U 10:1), 10 mg L^{-1} (HA:U 100:1) are shown by the squares and the triangles represent 100 mg L^{-1} HA addition (HA:U 1000:1). Error bars are the standard error of triplicate measurements.

When the 1/*M* plots are shown graphically (Figure 9.3) it can be seen that with each successive increase in HA addition, the 1/*M* plot shifts vertically (the y-intercept increases). This demonstrates the presence of an ADBL, as described in a study by Warnken *et al* [11], which demonstrated this vertical shift experimentally for the nine metals in the presence of DOC. When a system is fully labile, the 1/*M* plot has a lower y-intercept, as shown in Figure 9.4. Warnken *et al* [11] found that an increase in the ADBL was associated with an increase of the 1/*M* y-intercept.

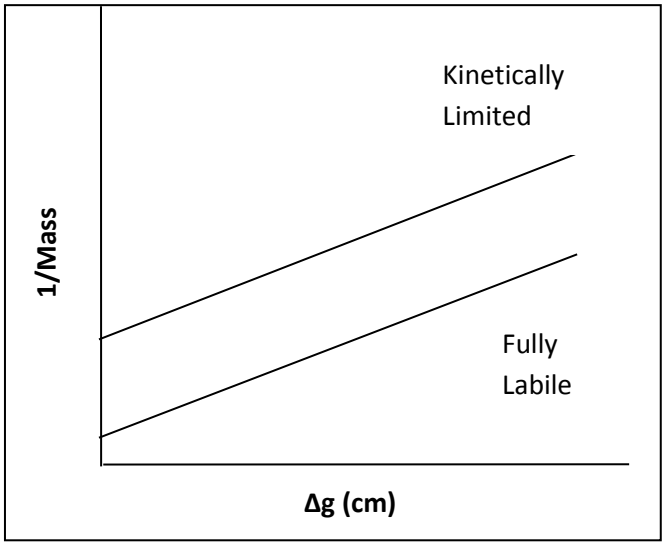

Figure 9.4 Illustration of the shift in the y-intercept the 1/M with Δ g (cm) for a fully labile and a kinetically limited system (after Warknen *et al.* [11]).

9.3.3 Investigating the presence of the apparent diffusive boundary layer (ADBL): kinetic limitations

The reciprocal of the mass accumulated by each DGT devices for each experiment was plotted against Δ*g* as per equation 9.3 and can be seen in Figures 9.5 and 9.6. U speciation in each of the experimental solutions was modelled using Visual Minteq, the results of which are presented in Tables 9.4 and 9.5. As previously discussed, kinetic limitation can be identified visually by examining the shift in the y-intercept for the 1/*M* Δ*g* plots (Figure 9.4). Figure 9.5 shows the 1/*M* plots for the pH 7.8 experiments for HA additions of 1 and 10 mg L^{-1}, and the blank (no HA additions) experiments. What can be seen is that increasing concentrations of HA increases the y-intercept and implies the potential for a kinetic effect of the U-HA complex on U uptake by DGT. Figure 9.6 shows the 1/M plot for the experiments at pH 5 for increasing HA additions. The y-intercept is not shifted from the blank as in pH 7.8. Table 9.6 below details all the figures of significance from the 1/M plots for all experiments undertaken. The ADBL is 0.025 cm larger in the pH 7.8 HA:U 100:1 experiment than its counterpart

at pH 5, with the HA:U 10:1 experiment having an ADBL 0.015 cm thicker at pH 7.8 than pH 5. The ADBL is thinner in these experiments than those presented in Section 9.3.1, where the ADBL at pH 7.8 is 0.084 ± 0.007 cm and 0.007 ± 0.02 cm for HA:U 10:1 and 100:1 respectively. This could be due to the differences in deployment time (24 h and 8d), which were also found by Mongin *et al.* [5] to affect the degree of lability of a metal complex.

Table 9.6 ADBL (cm) values from each experiment. The error of the DBL is the standard deviation of the slope and intercept errors, as described in Chapter 3, section 3.1.4.

Experimental Conditions	**y-intercept**	**Slope**	**R^2**	**ADBL (cm)**
pH 7.8 HA:U 100:1	0.00091 ± 0.00028	0.02677 ± 0.00325	0.97	0.034 ± 0.011
pH 7.8 HA:U 10:1	0.00032 ± 0.00007	0.01332 ± 0.00077	0.99	0.024 ± 0.005
pH 7.8 no HA	0.00046 ± 0.00006	0.01854 ± 0.00065	0.99	0.025 ± 0.003
pH 5 HA:U 100:1	0.00077 ± 0.00033	0.09093 ± 0.00869	0.98	0.008 ± 0.004
pH 5 HA:U 10:1	0.00044 ± 0.00034	0.04897 ± 0.00388	0.98	0.009 ± 0.007
pH 5 no HA	0.00269 ± 0.00109	0.12766 ± 0.01243	0.99	0.023 ± 0.009

Using the ADBL $1/M$ plots, the C_{DGT} concentration for each experimental setting can be calculated using equation 9.5 as detailed in Table 9.7 below. What can be seen is that the U is DGT labile until the HA:U ratio of 100:1, after which only ~50% of the dissolved U is accumulated by the DGT devices. Previous sorption studies (Chapter 4) and the experiments undertaken by Hutchins *et al*. [19] to find the diffusion coefficients of U, all observed significant sorption of U to the experimental tank without a buffer. The experiments undertaken at pH 5, were done so without a buffer, the effect of which can be seen by the very low average grab sample concentrations. However, this does not seem to have affected the results as the C_{DGT}:grab sample ratios are ~1.0 for all HA scenarios. This means that taking into account the variance in diffusion coefficients between the U and the U-HA, the system is fully DGT labile at pH 5. At pH 7.8, only 60% of the U was measured, meaning that the DGT was unable to accumulate 40% of the available U. This is potentially due to either a kinetic limitation, or it is only partially labile.

Table 9.7 C_{DGT} measurements using the 1/M plots for each experimental condition. Diffusion coefficients account for the ratio of the U bound to the HA.

Experimental Conditions	Slope (*b*)	Diffusion coefficient (x 10^{-6} cm^2 s^{-1})	Deployment time (s)	CDGT (µg L^{-1}) (1/*m*DtA)	Average 0.2 µm filtered grab sample concentration (µg L^{-1})	C_{DGT}:grab
pH 7.8 HA:U 100:1	0.0683	0.18	691200	38.2	64	0.6
pH 7.8 HA:U 10:1	0.0341	0.18	691200	76.6	71	1.1
pH 7.8 no HA	0.0185	2.52	86400	79.1	85	0.9
pH 5 HA:U 100:1	0.0909	0.19	691200	26.9	26	1.0
pH 5 HA:U 10:1	0.0490	0.19	691200	6.6	8	0.8
pH 5 no HA	0.1277	2.68	86400	11.3	9	1.3

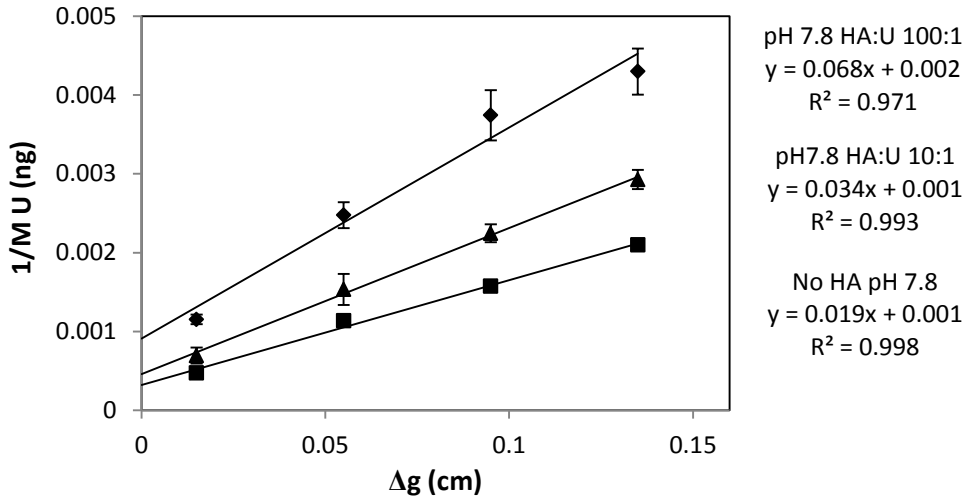

Figure 9.5 Plot of reciprocal of mass of U (ng) accumulated at pH7.8 at HA:U ratios of 100:1 (diamonds) and 10:1 (squares) and when no HA present (triangles). Error bars are the standard error of triplicate measurements. Where the error bars cannot be seen they are smaller than the data point.

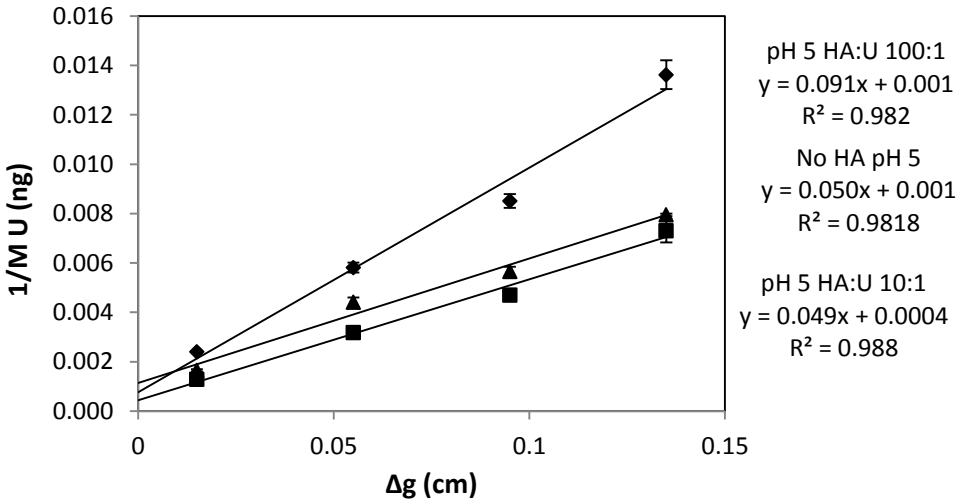

Figure 9.6 Plot of reciprocal of mass of U (ng) accumulated at pH 5 at HA:U ratios of 100:1 (diamonds) and 10:1 (squares) and when no HA present (triangles). Error bars are the standard error of triplicate measurements. Where the error bars cannot be seen they are smaller than the data point.

As g (diffusive gel layer thickness) increases, the mass of U accumulated by a DGT device decreases due to the longer diffusive pathway. As the graphs show the reciprocal of the mass accumulated, the lower the point on the y-axis, the higher the mass accumulated by the DGT devices. Figure 9.5 shows that the experiment at HA:U 100:1 accumulated the least U at pH 7.8. This is because the diffusion coefficient of metal-organic complexes is lower than that for free metal ions as a result of steric effects of the larger molecule. Fulvic acid (FA) has a diffusion coefficient of 20% of the free metals [25] whilst HA has a diffusion coefficient of only 7% of free metals in solution [26]. The diffusion of organically bound metals is similar for most metals, as it is the size of the organic molecule that dictates the diffusion coefficient rather than the metal ion. With an increase of g there is an increase in the time for the organically bound U to dissociate into the free metal ion and contribute to the flux of U to the resin layer. This means that the slope of the linear regression through $1/M$ v Δg will be lower with an increased contribution of dissociated U. From Table 9.6 above it can be seen that the slopes of the linear regression for the experiments at pH 7.8 increase with the increased HA concentrations. The experiments conducted at pH 5 do not show an increase in the y-intercept, with only the very high HA:U ratio of 100:1 showing any potential increase in dissociating U contribution to the DGT flux, although this does not appear to have impacted the thickness of the ADBL. The ADBLs found for these experiments are considerably lower than the ADBL found for the initial HA experiments described in Section 9.3.2. This could be as a result of the difference in deployment times, although the initial HA experiments used HA:U ratios of 1000,

rather than the maximum of 100 here. Further work would be required to establish if deployment time affect the kinetics of the U transfer to the DGT in the presence of organics.

As shown in Table 9.4 and 9.5, less U is bound to the HA (as modelled in Visual Minteq) at pH 7.8 than pH 5 because the carbonate system out-competes the HA ligand, at low HA:U ratios. Less U may be taken up at pH 5 that at pH 7.8 because of protonation of the HA binding sites competing with the UO_2^{2+} ion. This means that the U is also less strongly bound to the HA at pH 5 than at pH 7.8.

The full range of g_{kin}^{P} (cm) values using various fractions of the HA ligand can be seen in Table 9.8 below. Example calculation matrices can be seen in Tables A1 and A2 (located in the Appendix end of this Chapter).

Table 9.8 Results of the of the g_{kin}^{P} (cm) calculations for each experiment, with U = 100 µg L^{-1}(c*), and *I* = 0.01 M for the HA molecule as a whole and for the phenolic / high affinity sites only; λ_{ML} (mm) is the calculated penetration distance of the metal into the resin layer (as per equation 9.13); *P* is the factor defined by equation 9.14. Log*K'* is the stability constant as per c_{ML}*/c_M*; and ζ is the lability factor as per equation 9.17. Where the experimental calculations of g_{kin}^{P} < 0, then µ = 0, λ_{ML} = 0 and ζ = 1.00.

pH	HA:U	HA binding sites	c* (µg/l)	Fraction of M bound to HA	*P*	Log *K'*	g_{kin}^{P} (cm)	λ_{ML} (mm)	ζ
7.8	10:1	All	96.0	0.16	0.77	6.85	0.0047	0.0686	0.959
	10:1	Phenolic	96.0	0.02	0.81	6.15	0.0036	0.0604	0.923
	100:1	All	103.0	0.86	0.25	6.56	0.0278	0.1669	0.805
	100:1	Phenolic	103.0	0.05	0.58	5.71	0.0196	0.1400	0.731
5	10:1	All	73.6	0.74	0.35	6.51	0.0009	0.0315	0.992
	10:1	Phenolic	73.6	0.01	0.58	4.83	0	0	1
	100:1	All	98.2	0.98	0.10	5.62	0.0066	0.0814	0.949
	100:1	Phenolic	98.2	0.01	0.21	4.15	0.0042	0.0648	0.950

Levy *et al*. [12] found the increasing potential for kinetic limitation by organically complexed metals with decreasing pH, with a corresponding upward shift of the y-intercept, leading to large g_{kin}^{P}. When complexation is negligible, *P* approaches $D_{M\text{-}gel}/D_{M\text{-}w}$ (which has been calculated to be 0.81 and 0.58 for pH 7.8 and pH 5 respectively), which can be seen in the table above at pH 5 with a HA:U ratio of 10.1, when only the phenolic binding sites are accounting for in the calculations. When complexation dominates, *P* approaches $D_M^{gel}\varepsilon^{gel}/D_M^{w}\varepsilon^{w}$ (which has been calculated to be 0.14 and 0.10 for pH 7.8 and pH 5 respectively). Table 9.8 shows that the phenolic site only calculations all have high *P* with the exception of the pH 5 at HA:U 100:1. The g_{kin}^{P} (cm) in this study is negligible for the experiments performed at pH 5, with correspondingly high lability (ζ) factors near 1.00, demonstrating that at this pH, even

though 100% of the U is bound to HA (Table 9.5), it is a fully labile system and does not affect DGT measurements. This may be due to the protonation of the phenolic HA binding sites, leaving the U to loosely bind to carboxylic sites and form weak electrostatic attractions with the HA. What is observable in Table 9.8 is that the lability factors decrease with increasing pH, even at low HA:U concentrations, where more of the U is complexed as carbonates (as seen in Table 9.4). The fraction of the metal bound to the complex is important because this complex will affect the ratio of the diffusion coefficient as a result of the free metal or organically bound metal, which in turn affects the *P* value in the calculations. The g_{kin}^{P} (cm) is affected at pH 7.8 with increased loading of HA in a system. This increases the quantity of phenolic sites available to U for complexation, which in turn lowers the lability. The phenolic site binding at pH 7.8 HA:U 100:1 lowers the lability factor to 0.73 and has a corresponding g_{kin}^{P} of 0.020 cm and λ_{ML} of 0.140 mm. When all the HA is considered in the calculation with all binding sites, the lability increases to 0.81 (potentially due to more U able to dissociate from the carboxylic sites), but the penetration parameter (λ_{ML}) and the kinetic distance (g_{kin}^{P}) increase to 0.167 mm and 0.028 cm, most likely because there is more of the U bound to a greater number of binding sites. When $g_{kin}^{P} > \delta$, then dissociation of the metal-organic complex is not rapid enough to discount a kinetic limitation and the kinetic distance becomes larger than the physical DBL identified previously of 0.025 cm It is most likely that at this point (HA:U 100:1, pH7.8) lability would begin to present a limitation in DGT measurements in a fluvial system. What has been observed by Benedetti *et al*. [27] is that as the pH increases, the influence of the high affinity phenolic sites increases on binding of U. This increases the pH dependence of U binding to HA, with HA forming stronger complexes with U at higher pH [22, 29].

The penetration parameter (λ_{ML}) at pH 7.8 HA:U 10:1 was found to be 0.069 mm, which is lower to the findings of the previous chapter (Chapter 8) which found that the distance required for the U to fully dissociate in the resin layer was 0.223 ± 0.67 mm. The resolution of the calculations used in Chapter 8 could not resolve a distance below 0.1 mm, which the majority of the readings here fall beneath. This increases the uncertainty here associated with any of the results < 0.1 mm, which include all of those at pH 5.

The higher the metal:ligand ratio, the lower the potential for kinetic limitation in this study, which is similar to findings by Levy *et al*.[12]. The degree of lability is the ratio of the flux of free metal to the DGT with the dissociation of the complexed metal flux to the DGT. The closer the lability factor is to 1, the more labile a system is. The

penetration distance is the theoretical distance in the resin layer the complex requires to fully dissociate, and should increase as the lability factor decreases, due to increased residence time of the complexed metal in the gel layer. Mongin *et al*. [5] and Uribe *et al.* [6] have also examined the link between the lability of trace metals and the penetration distance into the resin layer, and found that as the resin thickness increased as did lability of the metal. This is because there was more time available for dissociation of the metal from the organic complex. For instance, when modelling the cadmium (Cd) nitrilotriacetic acid (NTA) complex lability, Uribe *et al.* [6] initially found a lability factor of 0.1 (an inert complex), but when the penetration parameter into the resin gel layer was introduced into the calculations, the lability increased to approximately 1, which is fully labile.

In comparison to the lability of other metals studied, U is highly labile at pH 5. The study by Levy *at al*. [12] demonstrated the lowest lability factors at pH 5 were 0.55, 0.75 and 0.78 for cobalt, copper and lead respectively, whilst at pH 7 the lability factor was > 0.8 for all metals tested with the exception of copper, which forms very strong organic complexes. The contrasting data obtained by Levy *at al*. [12] may be because FA was used as the ligand, which is soluble across a wider pH range than HA. U has been shown to bind more tightly to HA than FA [9], particularly at higher pH [27].

Further experiments would be required here to replicate a system closer to HA:U ratios seen in natural systems (for instance up to 10 000 for the River Enborne). This would induce a larger ADBL to form, however care would be required to ensure that no HA precipitated out of solution. This may then create an artificial barrier to diffusion of the U and HA-U species, which would have the potential to exaggerate any ADBL observed.

9.3.4 Estimating stability constants

The measurement of the stability of a complex is important in determining the influence of the dissociating metal to the flux of metal to the resin layer in the DGT devices. Using the estimates of the kinetic term (g_{kin}^{P}) derived in this chapter, the stability constants of the U-HA complex can be estimated. Warnken *et al*. [11] found that the ADBL increased with decreasing dissociation rate constants (therefore enlarging the zone of dissociation and effectively extending the DBL), and increased with increased stability constants of the metal-organic complex. As expected, if dissociation of the metal-organic complex is fast, then the normal DBL equation (equations 9.3 and 9.4) can be applied and the kinetic term (g_{kin}^{P}) need not be considered. If the Eigen mechanism (that the rate of complex formation is governed by

the rate loss of a water molecule, which is characteristic for each metal cation) applies to a metal-organic system (as described by equations 9.7 and 9.8), then fast association kinetics and small binding constants to the HA will mean fast dissociation constants. Faster dissociation constants and increased lability will mean an increased flux of the metal ion to the resin phase of the DGT device [5]. At the point where full lability is reached then the flux of the metal ion is limited only by the transport and the DGT equation ($C_{DGT}=\frac{M\Delta g}{DtA}$) applies.

The equilibrium constant for a complex under particular conditions can be described using equation 9.3 ($K = c_{ML}/c_M c_L = k_a/k_d$), and the association ($k_a$) and dissociation constants (k_d) calculated (after Warnken *et al*. [11]) using:

$$k_d = \left(D_{ML}^{gel}\right)^2 K c_L / D_{ML}^{gel} {g_{kin}^P}^2 \qquad \text{Equation 9.18}$$

$$k_a = \left(D_{ML}^{gel}\right)^2 K^2 c_L / D_{ML}^{gel} {g_{kin}^P}^2 \qquad \text{Equation 9.19}$$

Table 9.9 below shows the log k_a, k_d and K values derived from the experimental conditions (HA addition and pH). The changing values of the constants with pH demonstrates that this mechanism is in part determined by the diffusion coefficients of the U ion through the gel and the effect that complexation has on the relationship between the diffusion of U through the physical DBL and the diffusive gel (as can be seen from the *P* value, equation 9.15).

Table 9.9 Results of the stability constant calculations for each experimental condition, where k_a and k_d are the association and dissociation constants respectively, and K is the complex stability constant**.** Concentrations of the free metal ion and the ligand concentration were undertaken in Visual Minteq.

pH	**HA:U**	**HA binding sites**	**Log k_d (Equation 9.18)**	**Log k_a (Equation 9.19)**	**Log $K = k_a/k_d$ (Equation 9.8)**
7.8	10:1	All	-0.52	6.33	6.85
	10:1	Phenolic	-1.33	4.82	6.15
	100:1	All	-1.33	5.22	6.45
	100:1	Phenolic	-2.28	3.42	5.70
5	10:1	All	0.53	7.04	6.51
	10:1	Phenolic	-2.77	2.06	4.83
	100:1	All	-0.99	4.63	5.62
	100:1	Phenolic	-2.44	1.71	4.15

The phenolic binding sites have been considered here as a separate case as these are the high affinity sites that the metal becomes bound to preferentially and strongly [11]. 'All' binding sites in Table 9.9 refers to phenolic plus carboxylic. U has been

found to bind very strongly to HA [9] and so both cases were considered. Taking only the 1:1 HA:U complex model, published complexation constants of U (VI) with HA at varying pHs and ionic strengths can be seen in Table 9.10 below. The data presented in Table 9.9 shows that the Eigen mechanism holds because as the stability (log *K*) of a complex increases, the rate of dissociation generally decreases (log k_d).

Table 9.10 Examples of published results on complexation constants of U (VI) with HA where [a] are the constants for weak affinity binding sites, and [b] are the constants for the strong affinity binding sites.

pH	**Ionic strength (M)**	**Log*K* 1:1 complex**	**Refs.**
3.5 - 7	0.1	7.8	[30]
6	0.01	4.72 [a] 6.73 [b]	[28]
4	0.1	5.11	[31]
4.5	0.01	6.5	[32]
3.5 – 4.5	0.1	4.0 – 5.2	[33]
4 - 5	0.1	6.75 – 7.57 4.75 – 5.38 7.59 – 7.64 [b]	[22]

The log*K* results from this study are in line with work from previous studies (Table 9.10). Log*K* figures are specific to each experimental condition, which may account for the differences between studies. These differences include the ratio of the HA:U, ionic strength, pH and temperature. As previously established, the Log*K* value is in part driven by diffusion coefficients. U has a very wide range of diffusion coefficients as described by Hutchins *et al*. [19] with changing pH, making this experimental parameter very important in determining complexation constants.

9.3.5 Implications for in-situ deployments of DGT devices

Measuring U *in-situ* in fluvial environments presents fresh challenges in the presence of complexing organic material. In alkaline situations, dependent on the concentration of DOC, U will preferentially bind with carbonate ions (with a Log*K*'s of ~9 for UO_2CO_3, ~16 for $UO_2(CO_3)_2^{2-}$, and ~21 for $UO_2(CO_3)_3^{4-}$ [34]) in aquatic systems, although this will also depend on the alkalinity and pH. HA has an average log*K* of 6, although this increases with increasing pH, with the presence of carbonates actually increasing the binding efficiency of U to HA.

Zhao *et al*. [9] identified a fully labile fraction of the U-HA complex, which predominates when the HA:U ratio is low (<10). Dissociation rates were in the order of

10^{-3} s^{-1} for the labile fraction (which at pH 8 comprised > 78 % of the HA-U ligand) at the HA:U of 10:1, with the non-labile fraction having dissociation rates of 10^{-5} s^{-1}. When the HA:U ratio was increased, more U was bound to the non-labile fraction of the HA molecule. At HA:U 100:1, at pH 8 only 26 % of the U was bound to the labile fraction of the HA and up to 77% U bound to the non-labile HA group. At HA:U of 1000:1, all the U is bound to the non-labile fraction of the HA. However, when carbonate was added to the system, this promoted U binding to the labile HA component with only ~20% of the U bound to the non-labile fraction. In high pH and alkalinity natural waters, over 90% of the U was bound to the labile fraction of the HA molecule, but the 5-10% of the U bound to the non-labile fraction of the humic substances was inert (i.e the dissociation rates were < 10^{-6} and therefore not distinguishable in the study). The DOC:U ratios in their study were much lower than those in the field sites used in this project (U ~ 0.35 µg L^{-1} and DOC ~1-2 mg L^{-1} and 5-8 mg L^{-1} in the River Lambourn and the River Enborne respectively as seen in Chapter 5). This means that the influence of humic substances cannot be ignored when deploying DGT devices in natural waters due the excess of this ligand. This influence could account for some of the discrepancies observed in Chapter 5 between the grab samples and the DGT measured U concentrations.

Further work would be required to account for binding of U to various other organics, including fulvic acids (due to their prevalence in natural waters and high solubility across a wide pH range) and EDTA (which is a strong organic complexant released into the environment as an industrial waste bi-product).

9.4 Conclusions

The influence of humic acid binding to the uranyl ion on the measurements of uranium were investigated in this chapter at pH 5 and pH 7.8, both representing either an acidic stream, or the pH values of the field sites used in this study. A kinetic parameter was calculated using the ratio of the diffusion coefficients in the water of the over lying DBL to the gel, and accounting for the stability of the U-HA complex. This kinetic parameter (g_{kin}^{P}) represented a physical distance (cm) required for the metal-organic complex to dissociate and contribute to the flux of metal diffusing through the DGT device. If this distance was larger than the physical DBL of ~ 0.025 cm, established in the preliminary experiments, then it likely that there will be some kinetic hindrance on the transfer of U to the DGT devices. Only experiments with a HA:U of 100 at pH 7.8 demonstrated any potential for kinetic limitation, although this could be

quite significant in a field setting as humic compounds can occur in concentrations exceeding 10 000 times the concentration of U. The penetration parameter or the distance into the resin layer that the U:HA complex requires to fully dissociate, increases with decreasing lability factor and increasing kinetic parameter. This is simply a reflection of the lability of the complex and provides some information of the ability of the complex to fully dissociate in the diffusive gel layer. The penetration parameters at pH 5 were negligible, in line with the high lability of the HA:U complex, whilst at pH 7.8, the penetration parameter increases and the lability factor decreases. This study provided initial information on the lability of U in a simple system. More work is required to establish the nature of the binding of U to the HA molecule and to better discriminate the impact of the labile and non-labile components to the flux of U to the DGT, particularly in a complex system, such as high calcium carbonate rivers, where the influence of the carbonate serves not only to encourage complexation of U with HA, but to also act as a competing ligand. Ligand mixtures would also be an area of future investigations in this field as Salvador *et al.* [7] found that the lability of metals that are partially labile are affected by the mixture of ligands in natural waters.

9.5 References

[1] A.L.R. Sekaly, M.H. Back, C.L. Chakrabarti, D.C. Grégoire, J.Y. Lu, W.H. Schroeder, Measurements and analysis of dissociation rate constants of metal–fulvic acid complexes in aqueous solutions: Part I: simulation of decay curves obtained by inductively coupled plasma-mass spectrometry to evaluate a method to measure the distribution of first-order rate constants, Spectrochimica Acta Part B: Atomic Spectroscopy, 53 (1998) 837-846.

[2] S. Lofts, E. Tipping, Assessing WHAM/Model VII against field measurements of free metal ion concentrations: model performance and the role of uncertainty in parameters and inputs, Environmental Chemistry, 8 (2011) 501-516.

[3] I.J. Allan, J. Knutsson, N. Guigues, G.A. Mills, A.M. Fouillac, R. Greenwood, Chemcatcher (R) and DGT passive sampling devices for regulatory monitoring of trace metals in surface water, Journal of Environmental Monitoring, 10 (2008) 821-829.

[4] D.J. Liu, C. Bruggeman, N. Maes, The influence of natural organic matter on the speciation and solubility of Eu in Boom Clay porewater, Radiochimica Acta, 96 (2008) 711-720.

[5] S. Mongin, R. Uribe, J. Puy, J. Cecilia, J. Galceran, H. Zhang, W. Davison, Key Role of the resin layer thickness in the lability of complexes measured by DGT, Environmental Science & Technology, 45 (2011) 4869-4875.

[6] R. Uribe, S. Mongin, J. Puy, J. Cecilia, J. Galceran, H. Zhang, W. Davison, Contribution of partially labile complexes to the DGT metal flux, Environmental Science & Technology, 45 (2011) 5317-5322.

[7] J. Salvador, J.L. Garcés, E. Companys, J. Cecilia, J. Galceran, J. Puy, R.M. Town, Ligand mixture effects in metal complex lability, The Journal of Physical Chemistry A, 111 (2007) 4304-4311.

[8] A.L.R. Sekaly, M.H. Back, C.L. Chakrabarti, D.C. Grégoire, J.Y. Lu, W.H. Schroeder, Measurements and analysis of dissociation rate constants of metal–fulvic acid complexes in aqueous solutions: Part II: measurement of decay rates by inductively-coupled plasma mass spectrometry and determination of rate constants for dissociation, Spectrochimica Acta Part B: Atomic Spectroscopy, 53 (1998) 847-858.

[9] J. Zhao, I.I. Fasfous, J.D. Murimboh, T. Yapici, P. Chakraborty, S. Boca, C.L. Chakrabarti, Kinetic study of uranium speciation in model solutions and in natural waters using Competitive Ligand Exchange Method, Talanta, 77 (2009) 1015-1020.

[10] H. Zhang, W. Davison, Direct *in situ* measurements of labile inorganic and organically bound metal species in synthetic solutions and natural waters using diffusive gradients in thin films, Analytical Chemistry, 72 (2000) 4447-4457.
[11] K.W. Warnken, W. Davison, H. Zhang, J. Galceran, J. Puy, *In situ* measurements of metal complex exchange kinetics in freshwater, Environmental Science & Technology, 41 (2007) 3179-3185.
[12] J.L. Levy, H. Zhang, W. Davison, J. Galceran, J. Puy, Kinetic signatures of metals in the presence of Suwannee River fulvic acid, Environmental Science & Technology, 46 (2012) 3335-3342.
[13] G.R. Choppin, P.J. Wong, The chemistry of actinide behavior in marine systems, Aquatic Geochemistry, 4 (1998) 77-101.
[14] J. Puy, R. Uribe, S. Mongin, J. Galceran, J. Cecilia, J. Levy, H. Zhang, W. Davison, Lability criteria in diffusive gradients in thin films, Journal of Physical Chemistry A, 116 (2012) 6564-6573.
[15] S. Scally, W. Davison, H. Zhang, *In situ* measurements of dissociation kinetics and labilities of metal complexes in solution using DGT, Environmental Science & Technology, 37 (2003) 1379-1384.
[16] K.W. Warnken, H. Zhang, W. Davison, Accuracy of the Diffusive Gradients in Thin-Films Technique: Diffusive Boundary Layer and Effective Sampling Area Considerations, Analytical Chemistry, 78 (2006) 3780-3787.
[17] Ø.A. Garmo, K.R. Naqvi, O. Røyset, E. Steinnes, Estimation of diffusive boundary layer thickness in studies involving diffusive gradients in thin films (DGT), Analytical and Bioanalytical Chemistry, 386 (2006) 2233-2237.
[18] S. Kerisit, C. Liu, Molecular simulation of the diffusion of uranyl carbonate species in aqueous solution, Geochimica Et Cosmochimica Acta, 74 (2010) 4937-4952.
[19] C.M. Hutchins, J.G. Panther, P.R. Teasdale, F. Wang, R.R. Stewart, W.W. Bennett, H. Zhao, Evaluation of a titanium dioxide-based DGT technique for measuring inorganic uranium species in fresh and marine waters, Talanta, 97 (2012) 550-556.
[20] H. Zhang, W. Davison, Diffusional characteristics of hydrogels used in DGT and DET techniques, Analytica Chimica Acta, 398 (1999) 329-340.
[21] Tables of Physical & Chemical Constants in: 2.2.3 Viscosities, Kaye & Laby Online, 2005.
[22] J.J. Lenhart, S.E. Cabaniss, P. MacCarthy, B.D. Honeyman, Uranium(VI) complexation with citric, humic and fulvic acids, Radiochimica Acta, 88 (2000) 345.

[23] J.L. Levy, H. Zhang, W. Davison, J. Puy, J. Galceran, Assessment of trace metal binding kinetics in the resin phase of diffusive gradients in thin films, Analytica Chimica Acta, 717 (2012) 143-150.
[24] J. Levy, H. Zhang, W. Davison, J. Puy, J. Galceran, Does the Chelex resin in DGT devices really act as a perfect planar sink for metals? Kinetic limitations of DGT measurements, Geochimica Et Cosmochimica Acta, 74 (2010) A586-A586.
[25] S. Scally, W. Davison, H. Zhang, Diffusion coefficients of metals and metal complexes in hydrogels used in diffusive gradients in thin films, Analytica Chimica Acta, 558 (2006) 222-229.
[26] J.R. Lead, K. Starchev, K.J. Wilkinson, Diffusion Coefficients of Humic Substances in Agarose Gel and in Water, Environmental Science & Technology, 37 (2003) 482-487.
[27] M.F. Benedetti, C.J. Milne, D.G. Kinniburgh, W.H. Van Riemsdijk, L.K. Koopal, Metal ion binding to humic substances: application of the Non-Ideal Competitive Adsorption Model, Environmental Science & Technology, 29 (1995) 446-457.
[28] W.C. Li, D.M. Victor, C.L. Chakrabarti, Effect of pH and uranium concentration on interaction of uranium(VI) and uranium(IV) with organic ligands in aqueous solutions, Analytical Chemistry, 52 (1980) 520-523.
[29] M. Hiraide, Heavy Metals Complexed with Humic Substances in Fresh, Analytical Sciences, 8 (1992) 453.
[30] B. Kribek, J. Podlaha, The stability constant of the UO_2^{2+} - humic acid complex, Organic Geochemistry, 2 (1980) 93-97.
[31] P.M. Shanbhag, G.R. Choppin, Binding of uranyl by humic acid, Journal of Inorganic and Nuclear Chemistry, 43 (1981) 3369-3372.
[32] J.P. Giesy, R.A. Geiger, N.R. Kevern, UO_2^{2+} -humate interactions in soft, acid, humate rish waters., Journal of Environmental Radioactivity, 4 (1986) 39-64.
[33] C. Munier-Lamy, P.H. Adrian, J. Berthelin, J. Rouiller, Comparison of binding abilities of fulvic and humic acids extracted from recent marine sediments with UO_2^{2+}, Organic Geochemistry, 9 (1986) 285-292.
[34] R. Guillaumont, T. Fanghanel, J. Fuger, I. Grenthe, V. Neck, D.A. Palmer, M.H. Rand, Update on the chemical thermodynamics of uranium, neptunium, plutonium, americium and technitium, in: F.J. Mompean, M. Illemassene, C. Domenech-Orti, K. Ben-Said (Eds.) Chemical Thermodynamics, OECD-Nuclear Energy Agency, Elsevier, Amsterdam, 2003.

[35] L. Yuan-Hui, S. Gregory, Diffusion of ions in sea water and in deep-sea sediments, Geochimica et Cosmochimica Acta, 38 (1974) 703-714.

Appendix

Table A1 Example calculations used to determine g_{kin}^{P} for experiments conducted at pH 7.8. These calculations are based in using the entire HA fraction (carboxylic and phenolic function groups).

$ADBL = \frac{i}{s} = \frac{D_M^{gel}(1+\varepsilon^{gel}K')}{D_M^{w}(1+\varepsilon^{w}K')}\delta + g_{kin}^{P} = P\delta + g_{kin}^{P}$		pH 7.8	pH 7.8
Paramters	Notes	HA:U 100:1	HA:U 10:1
		17°C	17°C
C_{sol} (µg L^{-1})	Metal in solution	103	96
fML: fraction of metal bound to HA	Calculated in Visual Minteq	0.86	0.16
C_{ML} (µg L^{-1})	$C_{ML} = C_{sol}$ x fML	88.10	15.36
Molecular weight (g mol^{-1})	All data needs to be in M	238.03	238.03
C_{ML} (mol L^{-1})	Calculated in Visual Minteq	3.70 x 10^{-7}	6.45 x 10^{-8}
C_M (mol L^{-1})	Calculated in Visual Minteq	6.07 x 10^{-8}	3.53 x 10^{-7}
C_{ML}/C_M	$K' = K_{CL}^{*} = (c_{ML}^{*})/(c_M^{*})$	6.1	0.183
$D_{M\text{-}gel}$ (cm^2 s^{-1})	From Hutchins *et al*. [19] and adjusted for temperature using equation 4.	2.52 x 10^{-6}	2.52 x 10^{-6}
$D_{ML\text{-}gel}$	$D_{M\text{-}gel}$*0.07[25]	1.76 x 10^{-7}	1.76 x 10^{-7}
$D_{M\text{-}water}$	Calculated using Stokes-Einstein equation and the self diffusion value of U in water [18, 20, 35]	4.24 x 10^{-6}	3.08 x 10^{-6}
ε^{gel}	$D_{ML\text{-}gel}$/ $D_{M\text{-}gel}$	0.07	0.07
ε^{water}	$D_{ML\text{-}water}$ /$D_{M\text{-}water}$	0.4	0.4
ADBL: b/m (cm)	From HA:U experiments	0.034	0.024
δ (cm)	From experiments with no HA	0.024	0.025
$D_{M\text{-}gel}(1+\varepsilon^{gel}K')$		3.60 x 10^{-6}	2.55 x 10^{-6}
$D_{M\text{-}water}(1+\varepsilon^{water}K')$		1.46 x 10^{-5}	3.31 x 10^{-5}
P	Equation 13	0.25	0.77
P* δ		0.00616	0.0193
g_{kin}^{P} (cm)	Equation 14	**0.02784**	**0.0047**

Table A2 Example calculations used to determine g_{kin}^{P} for experiments conducted at pH 5. These calculations are based in using the entire HA fraction (carboxylic and phenolic function groups).

$ADBL = \frac{i}{s} = \frac{D_M^{gel}(1+\varepsilon^{gel}K')}{D_M^{w}(1+\varepsilon^{w}K')}\delta + g_{kin}^{P} = P\delta + g_{kin}^{P}$		pH 5	pH 5
Parameter	Notes	HA:U 100:1	HA:U 10:1
		18°C	18°C
C_{sol} (µg L^{-1})	Metal in solution	98.2	73.6
fML: fraction of metal bound to HA	Calculated in Visual Minteq	0.983	0.739
C_{ML} (µg L^{-1})	$C_{ML} = C_{sol}$ x fML	95.6	54.4
Molecular weight (g mol^{-1})	All data needs to be in M	238.03	238.03
C_{ML} (mol L^{-1})	Calculated in Visual Minteq	4.06 x 10^{-7}	2.28 x 10^{-7}
C_M (mol L^{-1})	Calculated in Visual Minteq	6.76 x 10^{-10}	9.68 x 10^{-8}
C_{ML}/C_M	$K' = K_{CL}^{*} = (c_{ML}^{*})/(c_M^{*})$	600	2.36
$D_{M\text{-}gel}$ (cm^2 s^{-1})	From Hutchins *et al*. [19] and adjusted for temperature using equation 4.	2.68 x 10^{-6}	2.68 x 10^{-6}
$D_{ML\text{-}gel}$	$D_{M\text{-}gel}$*0.2	1.88 x 10^{-7}	1.88 x 10^{-7}
$D_{M\text{-}water}$	Calculated using Stokes-Einstein equation and the self diffusion value of U in water [20, 35]	4.61 x 10^{-6}	4.61 x 10^{-6}
ε^{gel}	$D_{ML\text{-}gel}$/ $D_{M\text{-}gel}$	0.07	0.07
ε^{water}	$D_{ML\text{-}water}$ /$D_{M\text{-}water}$	0.4	0.4
ADBL: b/m (cm)	From HA:U experiments	0.009	0.009
δ (cm)	From experiments with no HA	0.023	0.023
$D_{M\text{-}gel}(1+\varepsilon^{gel}K')$		1.15 x 10^{-4}	3.12 x 10^{-6}
$D_{M\text{-}water}(1+\varepsilon^{water}K')$		1.11 x 10^{-3}	8.96 x 10^{-6}
P	Equation 13	0.11	0.35
P* δ		0.00258	0.00867
g_{kin}^{P} (cm)	Equation 14	**0.00661**	**0.00099**

Chapter 10: Conclusions and Future Work

The application of DGT to the measurement of uranium in natural waters was undertaken initially using Chelex-100, Metsorb^{TM} and MnO_2 as the binding layer resins. Under laboratory conditions, all three resins performed well across a wide range of ionic strengths (I = 0.01M to I = 1 M) and pHs (pH 3-10), with uranium uptake only affected at low pH < 4 for the MnO_2 resin, potentially due to a change in oxidation state of the sorbent. All three resins performed well in the presence of environmentally relevant concentrations of inorganic ligands (sulphate, phosphate, calcium and bicarbonate). The sulphate additions did not affect uptake by any of the resins, with the phosphate and calcium only showing an effect at very high concentrations. At 250 mg L^{-1} calcium addition, the uptake of uranium was reduced for all three resins most likely as a result of direct competition with the calcium ion for binding sites. Bicarbonate was found to have the largest effect on uranium uptake, due to the increasingly anionic nature of the solution commensurate with the increased carbonate concentrations. As Metsorb^{TM} is amphoteric, it has the ability to bind both anions and cations to the positively and negatively charged surfaces, which was why it was the least affected by the increased concentrations of bicarbonate. All three resins, when used in DGT devices and deployed in artificial solutions of freshwater, showed linear uptake of uranium over 5 days in line with that predicted by the DGT equation. When deployed in artificial seawater, the MnO_2 and Metsorb^{TM} sorbed uranium in line with the DGT equation for 24 h, whilst Chelex-100 only accumulated the uranium linearly for 4 h.

The freshwater field trials were undertaken in a high pH, calcium carbonate dominated stream. The Chelex-100 in this environment was only able to accumulate uranium linearly for 2 days, the MnO_2 for 4 days and the Metsorb^{TM} for up to 7 days (with a precision of 75%). The marine deployment showed uptake by Metsorb^{TM} and MnO_2 to be linear for 2 days, which is slightly longer than the laboratory deployments (24 h) potentially due to the marine site having a lower salinity than the laboratory made seawater. Further work with these resins would be required to characterise their performance in a neutral or acidic stream.

An important factor in the practical application of DGT was highlighted during this initial study; that the diffusive boundary layer (DBL) in the field is not negligible, despite the fast flow conditions at the freshwater site; and that not considering the DBL resulted in an underestimation of the uranium river concentration by up to 50%. The calculated limits of detection that account for the blank resin measurements, elution

factors and ICP-MS dilution were 1.4, 2.1 and 1.8 ng L^{-1} (or ~ 0.03 Bq L^{-1}) for MnO_2, Metsorb and Chelex-100 resins respectively, which is considerably less than the WHO drinking water limit for U of 30 µg L^{-1},

The importance of the DBL was again highlighted when the Metsorb^{TM} resin was taken forward to a long term environmental monitoring study. Here the uranium concentrations were measured using DGT in two rivers, the River Enborne and the River Lambourn, over a 6 month period, with the DGT samplers changed weekly. These two rivers were chosen because of differences in catchment geology and land use, which in turn affects water chemistry and flow rate. The objective of this study was to ascertain if the DGT devices could be incorporated into a long term regulatory environmental monitoring scheme. The DGT devices worked reasonably well over the six month period, with only occasional instances where the DGT and the grab samples were not in close agreement, although this may have been as a result of natural fluctuations in the dissolved uranium concentration. The DBL was closely coupled to the flow rate in the River Enborne, which due to its clay catchment, had large fluctuations in flow rate and river height. After a precipitation event, the storm flow lag time for the River Enborne is low, meaning the flow rate can change quickly. When the flow rate was high, as per December 2011 and January 2012 from the sampling period, the DBL was small (0.047 – 0.037 cm), and during the deployment on 12th October 2011, the water level was very low, and the measured DBL was 0.141 cm. The DBL was still larger than that found by other works in the field and laboratory, if the sole contributing factor to DBL thickness was flow rate. This implies other processes may affect the thickness of the DBL. One such process was suggested to be the presence of dissolved organics, which at the River Enborne could be significant. Up to 90% of uranium in the River Enborne was complexed with dissolved organic carbon (DOC). This is an area for further research and has to some extend been explored in this thesis.

The DBL in the River Lambourn varied between 0.062 – 0.088 cm. The change in DBL thickness was not related to changing water quality parameters or flow rate. The DBL was potentially found to be related to dissolved organics here, despite the majority of the uranium being complexed as calcium carbonates. The accumulation of macro-flora around the DGT devices, which reduced the water flow past the device sampling area, was also hypothesised here to affect the DBL thickness. Again, this is an area for further research, particularly for the effects of peryphyton growth on the surfaces of the DGT devices. It has been suggested in this thesis that this could add variability to the

DGT results, as the peryphiton, and any microbial mats that may form can act as a both a source and a sink for uranium.

In order to discount sampling technique as an artefact that could be affecting field deployments, a short term study was undertaken to assess the impact on the DBL and DGT accumulated concentrations, of deployment time (3 d and 7 d), deployment site (River Lambourn or Enborne) and deployment technique. Three deployment techniques were trialled that reflect commonly used methods in other studies or as recommended by sampling standards. This included a simple nylon line deployment to which the DGTs were directly attached; the DGT devices suspended in a protective cage; and the DGT devices held between two perspex plates with circular apertures to allow the DGT exposure face direct contact with the water. No statistical significance was found between the different DBLs obtained in each deployment, with most being in agreement with each other within error. The only deployment method that seemed to record the lowest DBL thickness, were the DGT devices attached to the nylon cord in the River Lambourn. This is potentially due to the accumulation of macro-flora around the cage and plate, because of higher surface areas, with the line providing only a small surface area for macro-flora to become entangled. This demonstrates that the deployment technique should be determined on a case by case basis, dependent upon the physical and biological characteristics of the field site.

There were no statistically significant differences in the DBLs measured between the two deployment sites, or when measured over different time scales. This demonstrates that the deployment time chosen for a study should reflect the objectives and requirements of the study i.e. water quality monitoring as part of a regulatory environmental monitoring scheme.

It has been demonstrated thus far in this thesis that the thickness of the DBL should be measured each time a device is deployed in the field as natural systems are complex with several factors always working together to influence the effectiveness of the passive sampling technique.

In order to isolate any effects organic material may have on the uptake of uranium by DGT in natural waters, two studies were undertaken to quantify the lability of the uranyl ion and uranyl humic complexes. The objective was to understand the kinetic limitations (if any) imposed on the uranium by humic acid. Uranium preferentially binds to humic acid over other dissolved organic material such as fulvic acid; and in high pH environments forms strong bidentate bonds with the humic molecule. However, in the presence of carbonates, which are a competing ligand for the

uranium, weaker carboxylic or monodentate bonds are formed between uranium and the humic acid. It was found that in higher pH environments (pH 7.8), in the presence of 0.9 mM carbonate, with the exposure solution equilibrated with atmospheric CO_2, there was a reduction in the lability from a factor of 1 (fully labile) to ~0.7 to 0.8, of the uranium when complexed with humic acid at humic acid:uranium ratio of 100:1. A small area of dissociation was established on the surface of the DGT in the laboratory, which could partly explain why the DBL has been consistently measured in the field to be higher than the 0.25 mm predicted for high flow environments under laboratory conditions. These experiments were conducted using low humic acid:uranium ratios (100:1 was the highest), when in natural system this ratio can exceed 10 000:1. These experiments were only the first step in understanding the impact the complicated uranium-humic acid system has on DGT performance.

It can be seen from this thesis that the complex uranium chemistry in natural systems may have an effect on the uptake by DGT. Future research here could include increasing the humic acid:uranium ratio; testing the lability factor of U with another organic such as fulvic acid, or a mixture of organics; testing any kinetic limitations against deployment time; and also testing the lability of uranyl:organic complexes in the presence of other competing cations, such as calcium.

In order to fully assess whether or not DGT could be used as tool for environmental monitoring of radionuclides, a resin (Diphonix®) which has a high affinity for the tetra- and hexavalent actinides was trialled. The Diphonix® out-performed the MnO_2, Metsorb™ and the Chelex-100 in both laboratory and field trials. The Diphonix® was unaffected by inorganic ligand addition (calcium and bicarbonate), and showed linear uptake in the freshwater field environment up to 7 d, in line with mass uptake predicted by the DGT equation, with ~100 % precision. Seawater deployments did not take up uranium in agreement with the DGT equation past 2 d, and so finding a resin that is capable of sorbing uranium in seawater requires further work. The major drawback to using Diphonix ® is that it has a very high affinity for uranium, making it difficult to back extract the sorbed uranium. This was achieved in this study by using a 1M NaOH/ 1M H_2O_2 solution, in which uranium is soluble. However, other actinides, such as thorium and plutonium, will precipitate out of a sodium hydroxide solution, so this eluent could not be used for any other actinide but uranium. Phosphoric acid is traditionally used to extract the actinides from Diphonix ® and maintains the actinides in the cationic form prior to isotopic separation. This could not be used in this study as the phosphoric acid is highly corrosive to the nickel sampling interface in the

ICP-MS. Further work is required to establish an elution technique that could work across the range of actinides sorbed by Diphonix®, and could also be measured using an instrument with rapid analytical times (such as ICP-MS). The initial work undertaken in this study has shown that there is the possibility of using the DGT technique for actinide environmental monitoring using more specific resins. Diphonix® resin using the methodology described in this thesis had a limit of detection of 0.046 μg L^{-1}, or 0.5 x 10^{-4} Bq L^{-1}.

The DGT devices have been found to be suitable for the monitoring of uranium in natural oxic waters using the resins trialed in this project. The maximum deployment time of the DGT devices in freshwater systems was 7 d, and in marine systems 2 d. The Diphonix® resin demonstrated a more linear uptake of uranium in line with modelled uptake in field deployments, however, the methodology as it is would most likely not work on a wider range of actinides. The disadvantage to this is that additional steps would be required, not only to extract the actinides from the resin, but to clean up the eluent and then separate the isotopes of interest for measurement. One of the advantages of using DGT for environmental monitoring is the reduction of sample handling the ease of deployment, which any further radiochemistry would detract from.

Uncertainties that still surround the technique, such as the effect of the DBL, organic complexes and interfering ions means that for regulatory monitoring grab samples would need to be taken concurrently. However, the DGT technique gives further information about the analyte in the environment than grab sampling; for instance speciation and bioavailability. Other passive samplers described in the literature review do not provide the same level of information (such as speciation and TWA values) that the DGT does, nor do they generally have detection limits suited to environmental monitoring. Auto-sampling is the only other technique that would provide comparable TWA values, however work in other studies has shown that mechanical problems (when and if they arise) can be difficult to overcome, with a high level of maintenance required. Each sampling technique has its own advantages and disadvantages, with some not suitable for particular environments (for instance DGT in measuring marine concentrations of uranium) or time scales (i.e. DGT for more than 1 week in a freshwater environment). The choice of technique is also dependent on the purpose of the sampling, for instance regulatory environmental monitoring requires a low limit of detection, while indicative qualitative sampling methods would not need the same level of accuracy and precision.